Vol. 151 No. 1, July 1, 1983 ISSN 0003-2670

44 0-9 44104

ANALYTICA CHIMICA ACTA

International journal devoted to all branches of analytical chemistry

EDITORS

A. M. G. MACDONALD (Birmingham, Great Britain)
HARRY L. PARDUE (West Lafayette, IN, U.S.A.)
ALAN TOWNSHEND (Hull, Great Britain)
J. T. CLERC (Bern, Switzerland)

Editorial Advisers

F. C. Adams, Antwerp
H. Bergamin F°, Piracicaba
G. den Boef, Amsterdam
A. M. Bond, Waurn Ponds
D. Dyrssen, Göteborg
J. W. Frazer, Livermore, CA
S. Gomišček, Ljubljana
S. R. Heller, Washington, DC
G. M. Hieftje, Bloomington, IN
J. Hoste, Ghent
A. Hulanicki, Warsaw
G. Johansson, Lund
D. C. Johnson, Ames, IA
P. C. Jurs, University Park, PA
D. E. Leyden, Fort Collins, CO
F. E. Lytle, West Lafayette, IN
H. Malissa, Vienna
D. L. Massart, Brussels
A. Mizuike, Nagoya
E. Pungor, Budapest
W. C. Purdy, Montreal
J. P. Riley, Liverpool
J. Růžička, Copenhagen
D. E. Ryan, Halifax, N.S.
S. Sasaki, Toyohashi
J. Savory, Charlottesville, VA
W. D. Shults, Oak Ridge, TN
H. C. Smit, Amsterdam
W. I. Stephen, Birmingham
G. Tölg, Schwäbisch Gmünd, B.R.D.
B. Trémillon, Paris
W. E. van der Linden, Enschede
A. Walsh, Melbourne
H. Weisz, Freiburg i. Br.
H. W. Weiss, Baton Rouge, LA
T. S. West, Aberdeen
J. B. Willis, Melbourne
E. Ziegler, Mülheim
Yu. A. Zolotov, Moscow

ELSEVIER SCIENTIFIC PUBLISHING COMPANY

ANALYTICA CHIMICA ACTA

International journal devoted to all branches of analytical chemistry
Revue internationale consacrée à tous les domaines de la chimie analytique
Internationale Zeitschrift für alle Gebiete der analytischen Chemie

PUBLICATION SCHEDULE FOR 1983

	J	F	M	A	M	J	J	A	S	O	N	D
Analytica Chimica Acta	145	146	147	148	149	150/1 150/2	151/1	151/2	152	153	154	155

Scope. *Analytica Chimica Acta* publishes original papers, short communications, and reviews dealing with every aspect of modern chemical analysis, both fundamental and applied.

Submission of Papers. Manuscripts (three copies) should be submitted as designated below for rapid and efficient handling:

Papers from the Americas to: Professor Harry L. Pardue, Department of Chemistry, Purdue University, West Lafayette, IN 47907, U.S.A.

Papers from all other countries to: Dr. A. M. G. Macdonald, Department of Chemistry, The University, P.O. Box 363, Birmingham B15 2TT, England. Papers dealing particularly with computer techniques to: Professor J. T. Clerc, Universität Bern, Pharmazeutisches Institut, Baltzerstrasse 5, CH-3012 Bern, Switzerland.

Submission of an article is understood to imply that the article is original and unpublished and is not being considered for publication elsewhere. Upon acceptance of an article by the journal, authors resident in the U.S.A. will be asked to transfer the copyright of the article to the publisher. This transfer will ensure the widest dissemination of information under the U.S. Copyright Law.

Information for Authors. Papers in English, French and German are published. There are no page charges. Manuscripts should conform in layout and style to the papers published in this Volume. Authors should consult Vol. 132, p. 239 for detailed information. Reprints of this information are available from the Editors or from: Elsevier Editorial Services Ltd., Mayfield House, 256 Banbury Road, Oxford OX2 7DH (Great Britain).

Reprints. Fifty reprints will be supplied free of charge. Additional reprints (minimum 100) can be ordered. An order form containing price quotations will be sent to the authors together with the proofs of their article.

Advertisements. Advertisement rates are available from the publisher.

Subscriptions. Subscriptions should be sent to: Elsevier Science Publishers B.V., P.O. Box 211, 1000 AE Amsterdam, The Netherlands.

Publication. *Analytica Chimica Acta* appears in 11 volumes in 1983. The subscription for 1983 (Vols. 145–155) is Dfl. 1980.00 plus Dfl. 220.00 (postage) (total approx. U.S. $880.00). Journals are sent automatically by airmail to the U.S.A. and Canada at no extra cost and to Japan, Australia and New Zealand for a small additional postal charge. All earlier volumes (Vols. 1–144) except Vols. 23 and 28 are available at Dfl. 200.00 (U.S. $80.00), plus Dfl. 15.00 (U.S. $6.00) postage and handling, per volume.

Claims for issues not received should be made within three months of publication of the issue, otherwise they cannot be honoured free of charge.

Customers in the U.S.A. and Canada who wish to obtain additional bibliographic information on this and other Elsevier journals should contact Elsevier Science Publishing Company Inc., Journal Information Center, 52 Vanderbilt Avenue, New York, NY 10017. Tel: (212) 867-9040.

ANALYTICA CHIMICA ACTA
VOL. 151 (1983)

ANALYTICA CHIMICA ACTA

International journal devoted to all branches of analytical chemistry

EDITORS

A. M. G. MACDONALD (Birmingham, Great Britain)
HARRY L. PARDUE (West Lafayette, IN, U.S.A.)
ALAN TOWNSHEND (Hull, Great Britain)
J. T. CLERC (Bern, Switzerland)

Editorial Advisers

F. C. Adams, Antwerp
H. Bergamin F°, Piracicaba
G. den Boef, Amsterdam
A. M. Bond, Waurn Ponds
D. Dyrssen, Göteborg
J. W. Frazer, Livermore, CA
S. Gomišček, Ljubljana
S. R. Heller, Washington, DC
G. M. Hieftje, Bloomington, IN
J. Hoste, Ghent
A. Hulanicki, Warsaw
G. Johansson, Lund
D. C. Johnson, Ames, IA
P. C. Jurs, University Park, PA
D. E. Leyden, Fort Collins, CO
F. E. Lytle, West Lafayette, IN
H. Malissa, Vienna
D. L. Massart, Brussels
A. Mizuike, Nagoya
E. Pungor, Budapest
W. C. Purdy, Montreal
J. P. Riley, Liverpool
J. Růžička, Copenhagen
D. E. Ryan, Halifax, N.S.
S. Sasaki, Toyohashi
J. Savory, Charlottesville, VA
W. D. Shults, Oak Ridge, TN
H. C. Smit, Amsterdam
W. I. Stephen, Birmingham
G. Tölg, Schwäbisch Gmünd, B.R.D.
B. Trémillon, Paris
W. E. van der Linden, Enschede
A. Walsh, Melbourne
H. Weisz, Freiburg i. Br.
P. W. West, Baton Rouge, LA
T. S. West, Aberdeen
J. B. Willis, Melbourne
E. Ziegler, Mülheim
Yu. A. Zolotov, Moscow

ELSEVIER Amsterdam–Oxford–New York

Anal. Chim. Acta, Vol. 151 (1983)

ห้องสมุดกรมวิทยาศาสตร์บริการ

© Elsevier Science Publishers B.V., 1983

0003-2670/83/$03.0

All rights reserved. No part of this publication may be reproduced, stored in a retrieval system or transmitted in any forn or by any means, electronic, mechanical, photocopying, recording or otherwise, without the prior written permission o the publisher, Elsevier Science Publishers B.V., P.O. Box 330, 1000 AH Amsterdam, The Netherlands.
Submission of an article for publication implies the transfer of the copyright from the author(s) to the publisher an entails the author(s) irrevocable and exclusive authorization of the publisher to collect any sums or considerations fo copying or reproduction payable by third parties (as mentioned in article 17 paragraph 2 of the Dutch Copyright Act o 1912 and in the Royal Decree of June 20, 1974 (S. 351) pursuant to article 16b of the Dutch Copyright Act of 1912 and/or to act in or out of Court in connection therewith.
Special regulations for readers in the U.S.A. — This journal has been registered with the Copyright Clearance Cente Inc. Consent is given for copying of articles for personal or internal use, or for the personal use of specific clients.
This consent is given on the condition that the copier pay through the Center the per-copy fee stated in the code o the first page of each article for copying beyond that permitted by Sections 107 or 108 of the U.S. Copyright Law. Th appropriate fee should be forwarded with a copy of the first page of the article to the Copyright Clearance Center, Inc 21 Congress Street, Salem, MA 01970, U.S.A. If no code appears in an article, the author has not given broad conser to copy and permission to copy must be obtained directly from the author. All articles published prior to 1980 may b copied for a per-copy fee of US $2.25, also payable through the Center. This consent does not extend to other kinds d copying, such as for general distribution, resale, advertising and promotion purposes, or for creating new collectiv works. Special written permission must be obtained from the publisher for such copying.
Special regulations for authors in the U.S.A. — Upon acceptance of an article by the journal, the author(s) will b asked to transfer copyright of the article to the publisher. This transfer will ensure the widest possible dissemination d information under the U.S. Copyright Law.

Printed in The Netherlands.

Analytica Chimica Acta, 151 (1983) 1—12
Elsevier Science Publishers B.V., Amsterdam — Printed in The Netherlands

A FOURIER-TRANSFORM INFRARED SPECTROMETRIC STUDY OF THE PYROSYNTHESIS OF NICKEL TETRACARBONYL AND IRON PENTACARBONYL BY COMBUSTION OF TOBACCO

A. J. ALEXANDER[a], PETER L. GOGGIN, and MICHAEL COOKE*

Department of Inorganic Chemistry, University of Bristol, Cantock's Close, Bristol BS8 1TS (Gt. Britain)

(Received 2nd December 1982)

SUMMARY

Fourier-transform infrared spectrometry is used to assess the concentration of nickel tetracarbonyl and iron pentacarbonyl in mainstream tobacco smoke. No evidence was found to support the theory that such species are present in mainstream smoke. Moreover, attempts to promote the formation of metal carbonyls during the combustion of tobacco revealed that such compounds, if formed, do not translocate through the filter. Hence loss of metal on combustion of tobacco does not occur via formation of volatile metal carbonyls. The limit of detection for this method was established as 0.1 μl l^{-1} for $Ni(CO)_4$ and 0.05 μl l^{-1} for $Fe(CO)_5$.

The combustion process within a burning cigarette is extremely complex. The vapour-phase constituents of cigarette smoke include a variety of hydrocarbons and volatile oxygen-, sulphur- and nitrogen-containing species [1]. Metals are also transferred into mainstream tobacco smoke during the combustion but the speciation of these metals is uncertain. The metal content of tobacco will be affected by such factors as soil structure and agrochemical treatments, and possibly by translocation during airing, processing, packaging and storing. On combustion of a cigarette (the burning zone temperature ranges from 500 to 900°C), these metals remain largely in the ash unless they are transferred into the smoke stream by vaporization, either as the metal itself or as a volatile metal compound. Amongst the metals present in significant quantities are iron, nickel, arsenic, mercury, cadmium and chromium. Apart from the iron, there is strong epidemiological evidence to implicate compounds of these elements in human carcinogenesis [2]. In view of the potential carcinogenicity of metallic constituents of tobacco, particularly nickel, the fate of these metals during smoking is of considerable interest.

The nickel content of cigarettes ranges from less than 1.0 μg to several micrograms per cigarette [3]. The standard reference cigarette tobacco has 1.1 mg kg^{-1} nickel [3]. Early research [4] suggested relatively high

[a]Present address: Department of Chemistry, University of Alberta, Edmonton, Alberta TG6 2GZ, Canada.

0003-2670/83/$03.00 © 1983 Elsevier Science Publishers B.V.

(140 ppb) concentrations of nickel in mainstream smoke. Subsequently it was considered unlikely that any nickel carbonyl present (produced by reaction with the high concentration of carbon monoxide available) would survive passage down the cigarette to reach the smoker [5]. Later, Stahly and Lard [6, 7] suggested formation of metal carbonyls as the only credible explanation for the volatilization of iron and nickel metals in tobacco smoke. It was thought that the metal had to be present in a low oxidation state for carbonyl formation to occur. Treatment of tobacco with air containing carbon monoxide at various temperatures resulted in loss of iron and nickel from the tobacco. However, no evidence was presented to demonstrate the presence of either $Fe(CO)_5$ or $Ni(CO)_4$ in tobacco smoke.

Numerous nickel salts have been shown to be carcinogenic in both man and animals. This carcinogenic activity is related to the form in which the nickel is administered, being inversely proportional to the solubility of the nickel species in aqueous media [8]; $Ni(CO)_4$ is very toxic and a potent animal carcinogen [9], possibly because of its ready decomposition at lung temperature to atomic nickel [10]. Hence the threshold limit value (TLV) for $Ni(CO)_4$ is 1 ppb [11] compared with 10 ppm for hydrogen cyanide and 50 ppm for carbon monoxide. Teratogenic activity has not been observed [12]. Iron pentacarbonyl is considered to be less toxic than $Ni(CO)_4$ [11]. The relative instability of $Ni(CO)_4$ (it readily decomposes at room temperature) coupled with its low TLV makes routine monitoring for this compound extremely difficult. One technique which can provide the necessary sensitivity, selectivity and stability of analytical conditions is Fourier-transform infrared spectrometry (F.t.i.r.) [13]. This report describes investigations into the formation of $Ni(CO)_4$ and $Fe(CO)_5$ during the combustion of tobacco, using F.t.i.r.

EXPERIMENTAL

Materials

Cigarettes analyzed in this study were taken from commercially available packets and classified according to their stated tar content (high, medium or low tar). An artificial smoking medium was also investigated. The medium-tar, low-tar and artificial cigarettes were filter-tipped. Unfiltered smoke from these cigarettes was examined simply by cutting off the filter.

The following chemicals were used as 1000 mg l^{-1} solutions to spike cigarettes with either nickel or iron: $Ni(NO_3)_2 \cdot 6H_2O$, $(\eta\text{-}C_5H_5NiCO)_2$, and dicyclopentadienyliron (ferrocene). For spiking, the cigarettes were placed in a beaker containing the solution of metal compound such that the ends were just immersed. They were left until the solution had been absorbed up to the filter, then removed, and the solvent was allowed to evaporate before they were "vacuum-smoked". Nickel tetracarbonyl (Matheson Gas Products) and iron pentacarbonyl (Fluka Chemicals) were used as received. Both carbonyls were manipulated by standard vacuum-line techniques.

Instrumentation

A Nicolet Model 7199 high-resolution, rapid-scanning, computer-controlled F.t.i.r. spectrometer with a range capability of 0—7900 cm^{-1} and having nominal resolutions of 16, 8, 4, 2, 1, 0.5, 0.24, 0.12 and 0.06 cm^{-1} was used. This was set up for mid-i.r. operation (400—4000 cm^{-1}) with a germanium-on-KBr beam splitter and a liquid nitrogen-cooled mercury cadmium telluride detector.

Interferograms containing 65536 data points (4-cm path difference) were normally collected, stored (to preserve raw data) and then Fourier-processed using enough data and transform points to give the desired resolution. The advantage of storing the spectral information in the form of a high-resolution interferogram is that equivalent or lower resolution spectra may be generated simply by reducing the number of data points used in the transformation routine. For example, a 65536 point interferogram will transform to give the nominal resolutions shown up to a maximum of 0.24 cm^{-1}, whilst an interferogram with only 8192 data points will give a resolution no better than 2 cm^{-1}. The number of interferograms co-added prior to transforming varied between 50 and 500 depending on the experimental conditions.

The i.r. gas cell was purpose-built, being of the normal cylindrical design, except for the addition of an integral cold-finger trap. Other details were: path length, 10 cm; internal volume, 117 cm^3; NaCl windows. The small path length used was due to the restrictions imposed in fitting the cell into the spectrometer sample compartment.

Sampling

All operations with $Ni(CO)_4$ and $Fe(CO)_5$ were carried out in a closed vacuum system. After the gas cell had been filled to the required pressure with $Ni(CO)_4$ or $Fe(CO)_5$, the residual vapour in the manifold was pumped into the liquid nitrogen cold trap and the line pumped down to $<10^{-3}$ torr before the cell was disconnected. Also, during transfer, the Pirani gauge was switched off to avoid vapour plating the hot element with either nickel or iron.

Reasonably accurate mixtures of $Ni(CO)_4$ and carbon monoxide were prepared by diluting known pressures of $Ni(CO)_4$ with high-purity carbon monoxide and adjusting the final pressure to 76 torr. To illustrate the method, the ≈ 100 $\mu l\ l^{-1}$ $Ni(CO)_4$ standard was obtained by taking 0.8 torr of $Ni(CO)_4$ and diluting to 760 torr with carbon monoxide; 76 torr of this was further diluted to 760 torr with carbon monoxide to give a 1 in 10^4 dilution, i.e., 100 $\mu l\ l^{-1}$ $Ni(CO)_4$. Using 0.8 torr of $Ni(CO)_4$ and appropriate dilution factors, ≈ 10 $\mu l\ l^{-1}$ and ≈ 1 $\mu l\ l^{-1}$ mixtures of $Ni(CO)_4$ in carbon monoxide were similarly prepared. The gas cell was filled to a pressure of 76 torr (i.e., 0.1 atm.) to give equivalent concentrations (at 1 atm.) of approximately 10, 1 and 0.1 $\mu l\ l^{-1}$ $Ni(CO)_4$, respectively.

Mainstream cigarette smoke was sampled by a "vacuum-smoking" technique. Two variations of this technique were used. In the first, the cigarette was connected horizontally to the evacuated gas cell by means of a B14/7 glass adaptor, as shown in Fig. 1, into which it fitted tightly. The cigarette

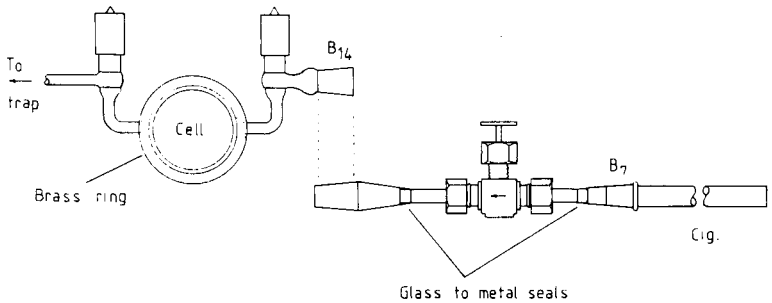

Fig. 1. Cell apparatus for collecting mainstream cigarette smoke. For clarity the NaCl windows, O-ring and retaining plate have been omitted.

was lit with a match and allowed to smoulder for 1—2 min, after which time the tap was opened and the products from the instantaneous surge of combustion were drawn into the gas cell. In the second, a needle valve was inserted between the tap and cigarette. On opening and closing the tap after adjustment of the needle valve, the induced combustion proceeded more gently with the products being drawn into the gas cell intermittently over a period of 2 min. This modification was introduced in an attempt to simulate smoking conditions more closely.

Concentration of the smoke from several cigarettes was achieved as follows. The cell was evacuated and isolated from the vacuum line, and the cold finger was immersed in liquid nitrogen. A cigarette was attached to the cell by means of the reduction valve and lit, and the tap to the cell opened. Air and combustion products were drawn into the cell until the pressure reached atmospheric. During this period, the products of combustion, except carbon monoxide, were progressively trapped out. The cigarette was isolated and the valve to the vacuum line was opened to remove the residual gases such as oxygen. This cycle was repeated to accumulate the less volatile products. The cold finger was allowed to warm to room temperature and the spectrum was recorded.

Reaction between $(\eta\text{-}C_5H_5NiCO)_2$ and carbon monoxide at elevated temperatures

The reaction

$$(\eta\text{-}C_5H_5NiCO)_2 + 2CO \rightarrow (\eta\text{-}C_5H_5)_2Ni + Ni(CO)_4$$

is known to proceed in solution. However, no information is available on the gas-phase reaction. Thus this was investigated to determine the suitability of the nickel complex as a source of $Ni(CO)_4$ when treated with carbon monoxide. Approximately 10 ml of a 1000 mg l^{-1} solution of $(C_5H_5NiCO)_2$ in hexane was transferred to a 12-cm long reaction tube, which was then connected to the vacuum line. The solvent was pumped off under moderate vacuum to leave a dark red film, the colour being characteristic of this complex.

The vacuum line was filled to a pressure of 100 mm with carbon monoxide and the reaction tube was slowly heated by means of a small electric furnace. At about 140°C, a green film was deposited on the cooler part of the tube, the original complex turning light brown by the time the temperature had reached 160°C. At this temperature, a sample of the gas phase was taken by opening the tap to the i.r. cell. At 200°C, no further visible change had occurred, therefore the bottom of the tube was gently heated with a bunsen flame; a nickel mirror deposited immediately. The experiment was repeated twice, the same results being obtained in each case. Analysis of the gas phase (sampled at 160°C) by i.r. clearly showed the presence of $Ni(CO)_4$ even without subtraction of the carbon monoxide spectrum. Furthermore, the formation of a green film is consistent with the above reaction because the other reaction product, $(\eta\text{-}C_5H_5)_2Ni$, is a dark green solid which may be sublimed at 50° C (0.1 torr).

RESULTS AND DISCUSSION

Sensitivity of the detection system

Both $Ni(CO)_4$ and $Fe(CO)_5$ exhibit extremely intense bands in the mid-i.r. region. This has led to the use of F.t.i.r. [14] to overcome the substantial analytical problems posed by monitoring 1 nl l^{-1} or less of $Ni(CO)_4$ to meet TLV requirements. Thus this technique is sufficiently sensitive and selective to permit its use for the study of the gas-phase components of whole smoke.

If $Ni(CO)_4$ is present in tobacco smoke, the concentration could range from 0.1 to 1.3 μl l^{-1}, dependent upon conversion efficiency and the nickel content of the tobacco. Although the iron content of tobacco is considerably higher than that of nickel, $Fe(CO)_5$ is unlikely to be present in significantly greater quantities than $Ni(CO)_4$ because transfer to the mainstream smoke is less efficient [6]. Hence the feasibility of detecting 1 μl l^{-1} $Ni(CO)_4$ and $Fe(CO)_5$ in smoke with a 10-cm gas cell was investigated. (The iron and nickel contents of the standard reference cigarette are 460—506 and 1.1 mg kg^{-1}, respectively [3].) The vibrational spectrum of $Ni(CO)_4$ is dominated by the extremely intense antisymmetric C=O stretching vibration (ν_5). On examination, this was found to consist of a broad band centred at 2057 cm^{-1} (Fig. 2A). The spectrum of $Fe(CO)_5$ was found to exhibit a similar, but even more intense band at 2013 cm^{-1} (Fig. 2B), assigned to the ν_{10} fundamental, together with a second band at 2034.5 cm^{-1}. Another strong band is also present in the spectrum of $Fe(CO)_5$ at 646 cm^{-1}, assigned to the Fe—C—O bending vibration ν_{11}. Owing to their great intensity, the bands at 2057 cm^{-1} and 2013 cm^{-1} are the most useful for monitoring low levels of $Ni(CO)_4$ and $Fe(CO)_5$, respectively. However, from an inspection of the gas-phase i.r. spectrum of whole smoke (Fig. 3), it is clear that the band at 2057 cm^{-1} will be masked by the *P* branch of the carbon monoxide fundamental band. The detection of $Fe(CO)_5$ will not be hampered to the same extent because the overlap from the carbon monoxide rotational fine structure is

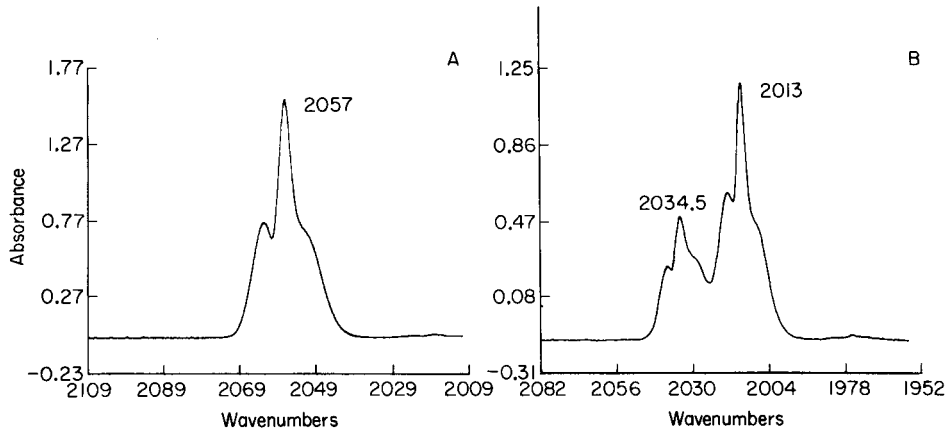

Fig. 2. The i.r. spectrum (carbonyl region) of: (A) $Ni(CO)_4$; (B) $Fe(CO)_5$ (resolution 0.24 cm^{-1}).

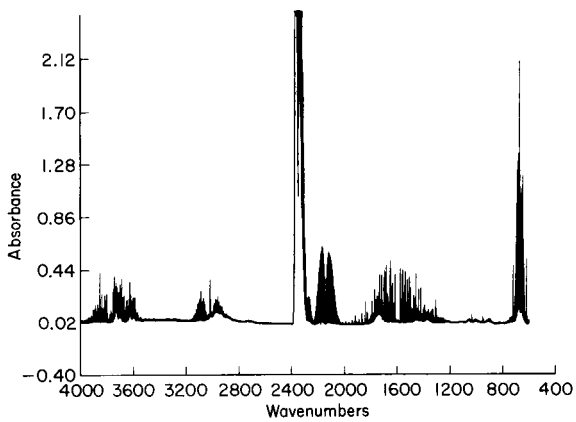

Fig. 3. The gas-phase i.r. spectrum of fresh whole smoke (resolution 0.24 cm^{-1}).

significantly less at 2013 cm^{-1} than at 2057 cm^{-1}, and the band is much more intense than that observed for $Ni(CO)_4$. The rotational line widths for the carbon monoxide fundamental are of the order of 0.5 cm^{-1} and it has been demonstrated [14] that the line-width difference between this and the ν_5 vibration of $Ni(CO)_4$ allows the carbon monoxide spectrum to be removed successfully by absorbance subtraction, permitting detection of the metal carbonyl species at the nl l^{-1} level. Accordingly, the detection limit for $Ni(CO)_4$ using a 10-cm path length gas cell was investigated by using absorbance subtraction.

Nominal 1.0, 10.0 and 100.0 $\mu l\, l^{-1}$ mixtures of $Ni(CO)_4$ in carbon monoxide were introduced consecutively into the gas cell and the final pressure was adjusted to 76 torr to give approximately the same carbon monoxide absorb-

ance as was observed in smoke spectra. (The average carbon monoxide content of cigarette smoke drawn into the evacuated gas cell was found to give approximately the same absorbance as that obtained from pure carbon monoxide at 100 torr.) Thus, the equivalent concentrations of $Ni(CO)_4$ present (at STP) were 0.1, 1.0 and 10.0 $\mu l\ l^{-1}$, respectively. Data were collected and a carbon monoxide reference spectrum was subtracted by means of the interactive absorbance subtraction routine.

The isolation of the $Ni(CO)_4$ band by absorbance subtraction of the carbon monoxide proved to be more difficult than expected. Complete removal of all the carbon monoxide features proved to be impossible, as above a certain reference file scaling factor, "second derivative" line shapes started to form because of spectral mismatching, and further subtraction resulted only in a severely distorted baseline. Figure 4(A—C) illustrates the absorbance spectra of $CO/Ni(CO)_4$ mixtures in the ratios 10^4:1, 10^5:1 and 10^6:1, respectively, with the absolute concentrations of $Ni(CO)_4$ being 10, 1.0 and 0.1 $\mu l\ l^{-1}$ under STP conditions. In each case, the spectrum resulting from the subtraction of carbon monoxide is also shown. The $CO/Ni(CO)_4$ ratio was found to remain constant for 8—12 h after data collection. By zero filling to effect a nominally better resolution by calculating a greater number of spectral points, a significant improvement in the accuracy of the carbon monoxide subtraction was obtained.

From Fig. 4C it is clear that the detection limit for $Ni(CO)_4$ under these conditions (signal = twice the noise level) is 0.1 $\mu l\ l^{-1}$. A conservative estimate for the detection limit of $Fe(CO)_5$ in carbon monoxide, considering the relative intensities of the i.r. bands, would therefore be 0.05 $\mu l\ l^{-1}$.

Analysis of mainstream smoke

The practicality of detecting a nominal concentration of 0.1 mg l^{-1} $Ni(CO)_4$ in a 10^6-fold excess of carbon monoxide having been demonstrated, smoke spectra from high-, medium- and low-tar cigarettes were examined for the presence of nickel or iron carbonyls. The spectra were collected and computed as previously described. A typical gas-phase smoke spectrum at 0.24 cm^{-1} resolution is shown in Fig. 3. Figure 5 shows an expanded plot of the region between 2300 and 1950 cm^{-1}, computed at 2 cm^{-1} resolution, with additional traces showing the resulting spectrum after the subtraction of carbon monoxide and water, respectively. The truncated absorbance is due to $^{12}CO_2$, whilst the adjacent band envelope is from $^{13}CO_2$. After subtraction of carbon monoxide, no broad features at either 2057 or 2013 cm^{-1} were apparent above the residual noise. This was found to be the case for all the cigarettes investigated, irrespective of whether or not the filter was removed, or the smoke was drawn into the cell slowly or instantaneously, or up to 2000 scans were co-added before transforming. The conclusions that can be drawn from these results are that $Ni(CO)_4$ and $Fe(CO)_5$ are not formed in smoke, or if they are, their concentrations are less than 0.1 $\mu l\ l^{-1}$. The latter possibility was investigated (see below).

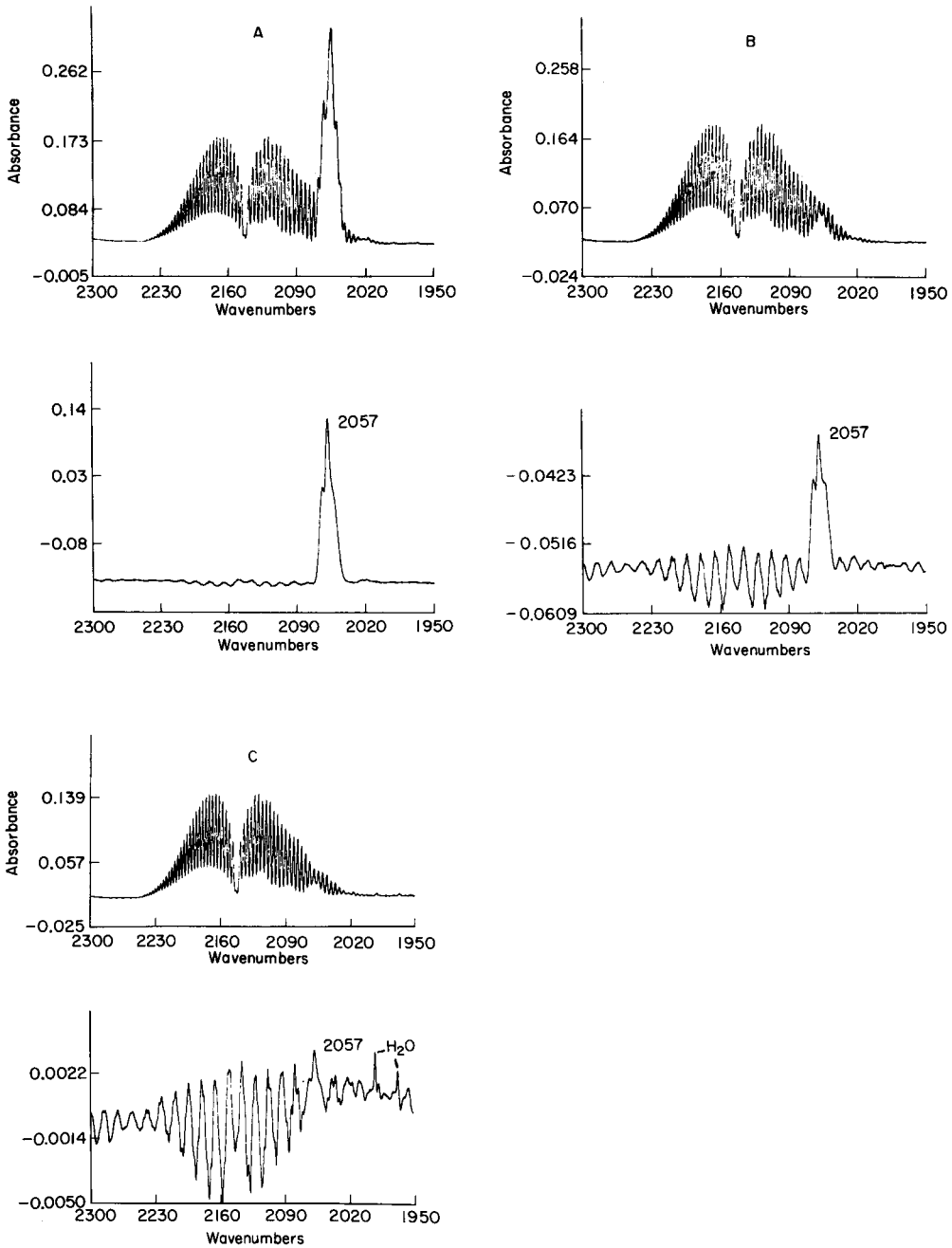

Fig. 4. Absorbance spectra (resolution 2 cm^{-1}) of $Ni(CO)_4/CO$ mixture for an equivalent $Ni(CO)_4$ concentration at STP of: (A) 10; (B) 1.0; (C) 0.1 $\mu l\ l^{-1}$. The lower spectra are those obtained after subtraction.

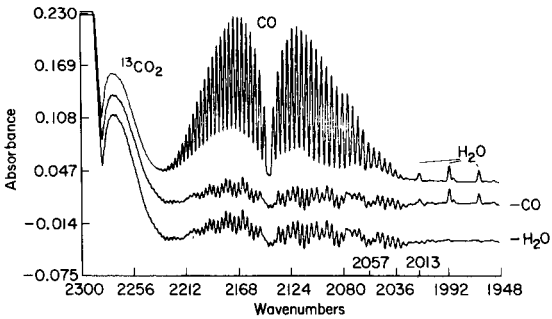

Fig. 5. Expanded plot of the spectrum of whole smoke for the region 2300—1950 cm^{-1} (resolution 2 cm^{-1}), with additional traces showing the resulting spectrum after subtraction of CO and H_2O, respectively.

Detailed examination of the spectrum of whole smoke revealed bands characteristic of methane, carbon monoxide (a dominant species along with water and carbon dioxide), methanol, ethylene, isoprene and hydrogen cyanide. The spectral features of nitrogen monoxide or dioxide were not observed, nor were bands attributable to formic acid or formaldehyde. After subtraction of water, a broad absorbance at ca. 1750 cm^{-1} was apparent but this showed, surprisingly, no *PQR* structure. Acetone and acetaldehyde are produced by combustion of tobacco under normal smoking conditions but both should display *PQR* structure at this resolution. Spectra reported in previous work [15] contain this feature but without comment. Bands indicating the formation of acrolein, nitric acid or chloromethane, all likely products, were not observed.

Spectra obtained from smoke from an artificial smoking medium contained no additional species. Deliveries of water, ethylene, hydrogen cyanide and methanol were less than for conventional cigarettes.

Enrichment experiments

The first approach to confirm whether $Ni(CO)_4$ and/or $Fe(CO)_5$ are formed in concentrations of less than 0.1 $\mu l\ l^{-1}$ was to increase their relative concentrations in the gas phase by concentrating smoke from several cigarettes. For example, two cigarettes containing an artificial smoking medium were vacuum-smoked. This artificial smoking medium contains, on average, 2 μg of nickel per cigarette. This value is approximately double the natural content of tobacco, thus affording an approximately fourfold concentration increase. This procedure allowed a new, lower detection limit of 0.025 $\mu l\ l^{-1}$ to be established for this case. Inspection of the spectra obtained after removal of most of the carbon monoxide and expansion of the relevant spectral regions revealed, besides the greatly increased carbon dioxide absorption, a feature overlapping the *P* band of the residual carbon monoxide fundamental (Fig. 6).

The sharp line at 2076.8 cm^{-1} is the *Q* branch centre of the $11'0 \rightarrow 00^{\circ}0$ transition of carbon dioxide and was only observed because of the high concentration of the gas present. No $Fe(CO)_5$ was detected. A band centred at 2061.6 cm^{-1} was not due to $Ni(CO)_4$, and inhibited its detection at low concentrations. To check on the reproducibility of this very unusual feature, the experiment was repeated, this time with high-tar tobacco cigarettes and removal of all the carbon monoxide produced. The band reproduced exactly. The profile is characteristic of a parallel vibration of a linear or quasi-linear molecule [16]. An isotopic band of carbon dioxide was discounted by comparison with a pure carbon dioxide spectrum obtained at 760 torr. Also, there was no evidence in the spectrum for this being an overtone band. From the resolved rotational structure (Fig. 6), the molecule was estimated to have a minimum *B* value of 0.9 cm^{-1} (27000 MHz). This rules out any molecule that is not essentially diatomic, i.e., a pure diatomic molecule or a triatomic molecule with one atom being hydrogen. The most likely candidate is hydrogen cyanide, which is known to be present, but the observed data do not fit the very accurately known literature values for this molecule. Also the ν_1 fundamental (C≡N) is weak relative to ν_2 (HCN) and ν_3 (C↔H) in the i.r., thus considerably enhanced ν_2 and ν_3 bands would be expected compared with unconcentrated smoke, if hydrogen cyanide were present. There was no evidence for this being so. Thus another species, similar to hydrogen cyanide, is present. An exotic possibility considered was assignment to the N≡C stretch in the isocyanide HNC. However, the values for its ν_1 fundamental, obtained from matrix-isolation studies [17], of 2032 and 2029.2 cm^{-1} are rather too low for this to be realistic. Also the *B* value for HNC is 45 331 MHz; even allowing for a large error in measuring the 2*B* spacing, this value is still too high. A linear fragment Ni—C≡O can also be discounted as it requires a considerably smaller *B* value on account of its necessarily

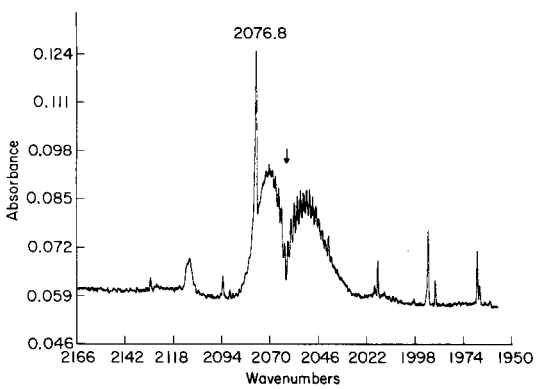

Fig. 6. The i.r. spectrum in the carbonyl region of whole smoke showing the unassigned feature centred at 2061.6 cm^{-1} (arrowed) which will inhibit detection of low levels of $Ni(CO)_4$ (resolution 0.24 cm^{-1}).

higher moment of inertia. Its CO stretching frequency has been evaluated as 1996 cm^{-1} from matrix-isolation studies [18].

The second approach employed was to enhance the natural nickel and iron contents of the tobacco by spiking the cigarettes. However, carbonyl formation is dependent on the amount of metal present in lower oxidation states, as chelates such as amino acid complexes or chlorophyll analogues, and thus the form of the metal used to spike the cigarette is of critical importance. Inorganic salts of iron will not form $Fe(CO)_5$ on treatment with carbon monoxide at atmospheric pressure. However, less is known about the chemistry of nickel in this respect.

In this study, smoke, from cigarettes spiked with 1000 mg l^{-1} nickel as $Ni(NO_3)_2 \cdot 6H_2O$, showed no presence of $Ni(CO)_4$ after subtraction of the carbon monoxide signal. Perhaps the best known organometallic compound of iron is ferrocene, dicyclopentadienyliron. It has the advantage of being very stable, soluble in most organic solvents and easily obtainable. Cigarettes spiked with 1000 mg l^{-1} iron, as ferrocene, showed no presence of $Fe(CO)_5$ in the smoke after subtraction of the carbon monoxide signal. The nickel analogue, nickelocene, unfortunately oxidizes rapidly on exposure to air. However, the π-cyclopentadienylnickel carbonyl complex, $(\eta\text{-}C_5H_5NiCO)_2$, is a purple-red stable solid which when treated with carbon monoxide in solution is known to revert to $Ni(CO)_4$ and $(\eta\text{-}C_5H_5)_2Ni$ [19]. Experiments revealed that $(\eta\text{-}C_5H_5NiCO)_2$, when treated with carbon monoxide below 200°C, reacted to give $Ni(CO)_4$ and nickelocene. It was thus considered to have a suitably low oxidation state for nickel to be used as a probe to ascertain whether the correct conditions existed in a burning cigarette for the pyrosynthesis of $Ni(CO)_4$. A cigarette was spiked with 1000 mg l^{-1} of nickel as $(\eta\text{-}C_5H_5NiCO)_2$ and the cigarette was vacuum-smoked. No new bands appeared in the i.r. spectrum. The expected conversion to $Ni(CO)_4$ was not observed. Hence if $Ni(CO)_4$ was formed, it was present at a level of less than 0.1 $\mu l\ l^{-1}$ from an initial nickel concentration of 1000 mg l^{-1}. The implied conversion efficiency thus is less than 10^{-4}.

CONCLUSIONS

Under the conditions of "vacuum smoking", no $Ni(CO)_4$ or $Fe(CO)_5$ was found in the mainstream smoke from several brands of cigarette. Analysis of concentrated smoke from an artificial smoking medium known to have a higher nickel content than that of an average tobacco yielded the same result. A detection limit of 0.1 $\mu l\ l^{-1}$ was obtained for $Ni(CO)_4$ in a 10^6-fold excess of carbon monoxide, the conditions prevalent in cigarette smoke, whilst that for $Fe(CO)_5$ was estimated as being 0.05 $\mu l\ l^{-1}$.

It was demonstrated that $(\eta\text{-}C_5H_5NiCO)_2$ will form $Ni(CO)_4$ when treated with carbon monoxide between 140 and 200°C. However, no $Ni(CO)_4$ was detected in mainstream smoke from cigarettes spiked with 1000 mg l^{-1} Ni as $(\eta\text{-}C_5H_5NiCO)_2$. Thus any $Ni(CO)_4$ formed must be present in concentra-

tions less than 0.1 μl l^{-1}. Using this result in an order of magnitude calculation (assuming a natural nickel level of 1.0 mg kg^{-1} and a similar efficiency of conversion to the carbonyl in each case) would suggest that $Ni(CO)_4$, if formed under normal smoking conditions, would be present in concentrations of <0.1 nl l^{-1}. This is well below the TLV (8 h industrial exposure). There is no reason to believe that $(\eta\text{-}C_5H_5NiCO)_2$ will not generate $Ni(CO)_4$ during combustion of tobacco, unless the temperature is above 200°C, in which case it will either not form, or if it does, will instantly decompose. It has been assumed that $(\eta\text{-}C_5H_5)_2Fe$ will react, at least partially, with carbon monoxide in a similar manner below 200°C to yield $Fe(CO)_5$. No $Fe(CO)_5$ was detected in cigarettes spiked with 1000 mg l^{-1} iron in the form of ferrocene.

The main assumption made by Stahly [6] was that it is possible to form nickel and iron carbonyls in the cooler parts of the combustion zone at some temperature below 200°C. While the initial formation of $Ni(CO)_4$ and $Fe(CO)_5$ cannot be entirely discounted, the results of this investigation show that this must be followed by almost instant decomposition, and hence translocation through the filter and into the smoker by this mechanism will not occur to any significant extent.

REFERENCES

1 R. J. Phillippe and M. E. Hobbs, Anal. Chem., 28 (1956) 2002.
2 N. J. Birch and P. J. Sadler, Inorganic Elements in Biology and Medicine, Vol. I, Specialist Periodical Reports, The Chemical Society, London, 1979.
3 R. A. Nadkarni, Chem. Ind., (1974) 693, and references therein.
4 F. W. Sunderman and F. W. Sunderman, Jr., Am. J. Clin. Pathol., 35 (1961) 203.
5 E. L. Wynder and D. Hoffman, Science, 162 (1968) 862.
6 E. E. Stahly, Chem. Ind., (1973) 620.
7 E. E. Stahly and E. W. Lard, Chem. Ind., (1977) 85.
8 T. J. Lau, R. L. Hackett and F. W. Sunderman, Jr., Cancer Res., 32 (1972) 2253, and references therein.
9 F. W. Sunderman, Jr., Ann. Clin. Lab. Sci., 7 (1977) 377.
10 A. Oskarsson and H. Tjälve, Brit. J. Ind. Med., 36 (1979) 326, and references therein.
11 N. I. Sax: Dangerous Properties of Industrial Materials, 4th edn., Van Nostrand-Reinhold, New York, 1975.
12 J. S. Warner, Science, 203 (1979) 1194.
13 P. R. Griffiths, H. J. Sloane and R. W. Hannah, Appl. Spectrosc., 31 (1977) 485.
14 A. W. Mantz, Appl. Spectrosc., 30(5) (1976) 539.
15 W. L. Maddox and G. Mamanlov, Anal. Chem., 49(2) (1977) 331.
16 R. E. Dodd, Chemical Spectroscopy, Elsevier, New York, 1962, p. 206.
17 B. M. Chadwick and H. G. M. Edwards, Molecular Spectroscopy, Vol. 1, Specialist Periodical Reports, The Chemical Society, London, 1973, Ch. 8.
18 R. L. De Kock, Inorg. Chem., 10 (1971) 1205.
19 P. W. Jolly and G. Wilke, The Organic Chemistry of Nickel, Vol. 1, Academic Press, London, 1974.

Analytica Chimica Acta, 151 (1983) 13—18
Elsevier Science Publishers B.V., Amsterdam — Printed in The Netherlands

THE DETERMINATION OF UREA BY USING AN ENZYME REACTOR AND SECOND-DERIVATIVE SPECTROPHOTOMETRY

KUNIO NAGASHIMA* and SHIGETAKA SUZUKI

Department of Industrial Chemistry, Faculty of Technology, Tokyo Metropolitan University, Setagaya-ku, Tokyo 158 (Japan)

(Received 25th October 1982)

SUMMARY

A urease reactor, gas—liquid separation and a second derivative spectrophotometer are used. The sample is pumped at 4 ml min^{-1} through a reactor containing urease chemically immobilized on glass beads. The effluent is mixed with 50% (w/w) sodium hydroxide (4 ml min^{-1}) and fed through a gas—liquid separator (80° C). Ammonium ions produced from urea release ammonia which is purged by nitrogen (150 ml min^{-1}) into a heated optical cell (175° C), where the second-derivative absorbance at 201.2 nm is recorded. The conversion of urea to ammonia gas is quantitative for $<10^{-3}$ M urea. Urea and ammonia can be determined separately, and the sample throughput is 20 h^{-1}. The method has a detection limit of 3×10^{-7} M urea, and is applied to human urine.

The most widely used routine methods for the determination of urea are based on the formation of ammonia in the presence of urease. The ammonia may be measured with a pH electrode [1—6] or by formation of colored compounds with hypochlorite and phenol. The latter are susceptible to interference by heavy metals and colored organic species present in the sample solution [7, 8]. An ammonium ion-sensitive glass electrode [9] can be used to detect the ammonium ions formed, but it also responds to sodium and potassium ions, which are commonly present in serum and urine (serum contains ca. 5×10^{-3} M urea, 5×10^{-3} M potassium and 0.14 M sodium). The problem of sodium and potassium interference can be overcome by using an enzyme-coated stirrer and an air-gap pH electrode [10], but the general method then loses operational simplicity. Worse still, the methods based on a pH electrode cannot determine $<5 \times 10^{-5}$ M urea.

Cresser [11] utilized the characteristic u.v. absorption bands of gaseous ammonia for its determination in solutions. This paper describes the continuous determination of urea based on an enzyme reactor [1, 12] in which urease is immobilized on glass beads, evolution of ammonia from the ammonium ions produced and second-derivative spectrophotometric determination of ammonia in the gas phase [13].

0003-2670/83/$03.00 © 1983 Elsevier Science Publishers B.V.

EXPERIMENTAL

Apparatus

A second-derivative spectrophotometer (Model UO-1; Yanaco, Kyoto, Japan) was used for gas-phase absorbance measurements. A deuterium lamp was used as radiation source. A quartz absorption cell (25 cm long, 2 cm i.d., 78.5 ml) was used. It was kept at a constant temperature of 175° C. Atto Co. proportioning pumps, enzyme reactor, heating tubes (55 cm long, 0.4 cm i.d.) and gas—liquid separator (18 cm long, 0.6 cm i.d.) were used to construct the flow system. The gas—liquid separator and the heating tube were kept at 80° C. A precision flow meter was used to control the nitrogen carrier gas flow rate at 150 ml min^{-1}. A schematic diagram of the instrumental setup is shown in Fig. 1.

Reagents

All chemicals used were of guaranteed grade. Sodium hydroxide was used as an aqueous 50% (w/w) solution. Stock 10^{-3} M urea and 10^{-3} M ammonia standards were prepared by dissolving 15.0 mg of urea and 13.4 mg of ammonium chloride in water and making each up to 250 ml. Calibration standards were prepared by serial dilution in aqueous 2 mM EDTA. Purified compressed nitrogen was used as a carrier gas for the ammonia evolved.

Enzyme reactor

The urease was covalently bound to glass via glutaraldehyde coupling, as has been done previously for an enzyme reactor [5]. The CPG 00700 controlled-pore glass (10 ml, 120/200 mesh, mean pore diameter 72.9 nm ± 6.4%, pore volume 0.77 cm^3 g^{-1}, surface area 24.9 m^2 g^{-1}; Electro-Nucleonics, N.J.) was boiled in 150 ml of 5% nitric acid for 45 min. The glass beads were washed with about 1 l of water on a porosity G3 glass filter and dried in an

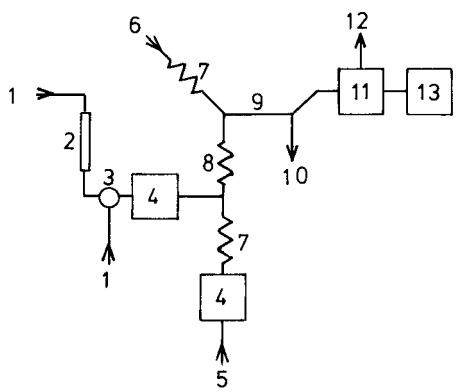

Fig. 1. Schematic diagram of the flow system for the determination of urea. (1) Sample or blank; (2) enzyme reactor, (3) three-way cock; (4) peristaltic pump; (5) sodium hydroxide; (6) nitrogen; (7) pre-heating tube; (8) heating tube; (9) gas—liquid separator; (10) liquid waste; (11) second-derivative spectrophotometer; (12) gas waste; (13) recorder.

oven at 95° C. 3-Aminopropyltriethoxysilane (5 g) was added to 45 ml of water and the pH was very carefully adjusted to 3.3 with 5 M hydrochloric acid. The dried glass was added and the mixture was kept at 75° C on a water bath for 165 min. The flask was swirled every 15 min. The mixture was filtered, washed and dried as described above. The alkylamino glass could be stored in this condition until needed. A buffer (0.1 M sodium phosphate, pH 7.0, 2.5% in glutaraldehyde) was prepared by adding the aldehyde from a 25% stock solution just before use. Alkylamino glass (1 g) was added to 5 g of the glutaraldehyde-containing buffer. The reaction was allowed to proceed for 1 h at room temperature, the first 30 min at reduced pressure to decrease the oxygen partial pressure. The activated glass was washed well with distilled water.

Urease (100 mg, Sigma Type III, 3900 U g^{-1} was dissolved in 3 ml of cold (4° C) 0.1 M sodium phosphate (pH 6.0) and the activated glass was added. The solution was kept between 4 and 10° C for 150 min, the first 30 min being at reduced pressure and the lower temperature. The glass beads were washed with 250 ml of the cold buffer and 500 ml of cold water and stored moist at 4° C. About 0.24 ml of the glass beads on which urease was immobilized were packed in a glass tube (0.4 cm i.d., 4 cm long). Silica wool was packed at the bottom of the tube to support the beads.

Procedure

The operating parameters not stated elsewhere are shown in Table 1. It took 1 h to reach equilibrium temperature conditions in the absorption cell, heating tube and gas-liquid separator. Until a stable base-line was established on the recorder, only sodium hydroxide and water were pumped. The different standard samples and the blank solution were pumped alternately without introducing air. The concentrations of the sample pumped were in the range 10^{-3}—10^{-7} M. The enzyme column was stored in a refrigerator (4° C) overnight and could be used for about 7 weeks without any appreciable loss of activity.

RESULTS AND DISCUSSION

The flow system

The operation of the gas—liquid separator and spectrophotometer were checked with standard ammonia solutions. The sample stream and the sodium hydroxide stream merge on leaving the pump. The resulting mixture at this point contains 37% (w/v) sodium hydroxide. The response signal (peak height) obtained by using 10% (w/w) sodium hydroxide solution was 2.7 times less than that obtained from a 50% solution.

Condensed water vapor in the optical cell absorbs ammonia and obstructs the smooth flow of gases, thus causing base-line drift, peak distortion and tailing. A cell temperature of 175° C overcame this problem.

TABLE 1

Operating conditions

Second-derivative spectrophotometer	
wavelength	201.2 nm
mode	second derivative absorption
attenuator	1/5
time constant	3
Recorder sensitivity	10 and 50 mV full scale
Chart speed	24 cm h^{-1}
Proportioning pump	
sampling, washing	3 min each
Enzyme reactor temperature	20—25° C

Figure 2 shows the second-derivative absorption spectrum of ammonia, evolved from an ammonium chloride solution. Sharp second-derivative absorption bands are seen at 197.8, 201.2, 204.7 and 208.7 nm. The spectrum of the nitrogen carrier gas is also shown. Gases other than ammonia absorb strongly below 195.0 nm. For this work, 201.2 nm was chosen

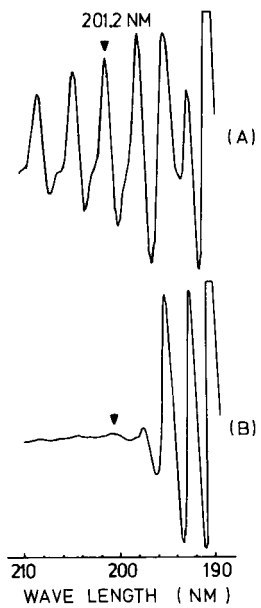

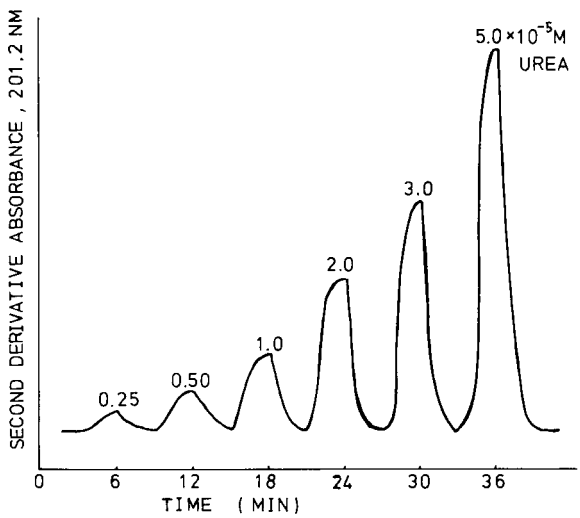

Fig. 2. Second-derivative absorption spectra of: (A) nitrogen with ammonia; (B) nitrogen alone.

Fig. 3. Second-derivative absorbance peaks of urea calibration standards (12-ml samples).

TABLE 2

Effect of concentration of sodium phosphate buffer (pH 7) on the response of urea (4.1×10^{-5} M)

Buffer conc. (M)	0	4×10^{-3}	1×10^{-2}	2×10^{-2}
Relative response	100	93	90	88

because it was sufficiently sensitive, and avoided any nitrogen peaks. Calibration was achieved with ammonium chloride or urea solutions.

The column containing urease immobilized on glass proved to be very efficient. At 4 ml min^{-1} the response to urea was linear between 10^{-6} and 10^{-4} M, indicating 100% conversion to ammonia over this range. Variations in the temperature of the reactor or in the enzyme activity did not affect the response.

Figure 3 shows recordings from successive alternate introduction of urea and water. Equilibrium response was reached within 2.0—2.5 min. Under these conditions, up to 20 samples could be run per hour. The base line is stable enough to allow a 5-fold signal expansion for low concentrations. The relative standard deviations (n = 6) were 1.9 and 6.1% for 5×10^{-5} M and 5×10^{-6} M urea, respectively. The detection limit for urea was about 3×10^{-7} M (S/N = 3). The sensitivity of the proposed method is 10—100 times greater than those previously reported [1—6, 9—13].

When both urea and ammonia are present in the sample, the response is produced by their combined effect. When the sample is not passed through the enzyme reactor, the response is due only to the ammonia present in the sample. Urea can therefore be determined by measuring the difference between the responses with and without the enzyme reactor.

Sample preparation and interference

The pH of the sample to be tested has to be ca. pH 7. Although tris-(hydroxymethyl)aminomethane (Tris) is often used as a buffer solution,

TABLE 3

Determination of urea and ammonia in human urine

Sample	Std. soln. added (M)	Enzyme reactor	NH_3 found (M)
Urine[a]	—	no	2.53×10^{-5}
Urine[a]	ammonia (2.16×10^{-5})	no	4.72×10^{-5}
Urine[b]	—	yes	3.57×10^{-5}
Urine[b]	urea (0.98×10^{-5})	yes	5.59×10^{-5}
None	urea (1.24×10^{-4})	no	$< 6 \times 10^{-7}$

[a] Sample diluted 10^3-fold with 0.2 mM EDTA. [b] Sample diluted 10^4-fold with 0.2 mM EDTA.

0.2 M of this buffer showed a response similar to that of 10^{-5} M ammonia. The response slightly decreased in sodium phosphate buffer (pH 7), as shown in Table 2. Thus, neither Tris nor sodium phosphate buffer should be used. If necessary, the pH of the sample should be adjusted with sodium hydroxide or hydrochloric acid to 6.5—7.5 (optimal activity at pH 7.0).

Volatile organic compounds such as ethanol and acetic acid interfere by absorbing u.v. radiation. Vacuum boiling of the acidified sample solution prior to analysis completely removes this interference.

Table 3 gives the results obtained for human urine by the present method. The results show that urea is not converted to ammonia without use of the enzyme reactor under the conditions used (80°C, 37% sodium hydroxide, reaction time ca. 1 min), so that ammonia and urea can be determined in urine samples.

REFERENCES

1 H. H. Weetall and L. S. Hersh, Biochim. Biophys. Acta, 185 (1969) 464.
2 G. G. Guilbault and M. Tarp, Anal. Chim. Acta, 73 (1974) 355.
3 E. H. Hansen and J. Růžička, Anal. Chim. Acta, 72 (1974) 353.
4 D. S. Papastathopoulos and G. A. Rechnitz, Anal. Chim. Acta, 79 (1975) 17.
5 G. Johansson and L. Ogren, Anal. Chim. Acta, 84 (1976) 23.
6 P. M. Vadgama and G. M. M. Alberti, Anal. Chim. Acta, 136 (1982) 403.
7 T. T. Ngo, A. H. Phan, C. F. Yam and H. M. Lenhoff, Anal. Chem., 54 (1982) 46.
8 K. Nagashima and S. Suzuki, Bunseki Kagaku, 31 (1982) 724.
9 G. G. Guilbault, R. K. Smith and J. G. Montalvo, Anal. Chem., 41 (1969) 600.
10 G. G. Guilbault and W. Stockbro, Anal. Chim. Acta, 76 (1975) 237.
11 M. S. Cresser, Anal. Chim. Acta, 85 (1976) 253; Analyst, 102 (1977) 99.
12 L. D. Bowers and P. W. Carr, Anal. Chem., 48 (1976) 545A.
13 R. N. Hager, Anal. Chem., 45 (1973) 1131A.

Analytica Chimica Acta, 151 (1983) 19—27
Elsevier Science Publishers B.V., Amsterdam — Printed in The Netherlands

DETERMINATION OF POLYNUCLEAR AROMATIC HYDROCARBONS IN VAPOR PHASES BY LASER-INDUCED MOLECULAR FLUORESCENCE

LOUIS J. JANDRIS and R. KEN FORCÉ*
Department of Chemistry, University of Rhode Island, Kingston, RI 02881 (U.S.A.)
(Received 26th October 1982)

SUMMARY

Laser-induced molecular fluorescence (l.i.m.f.) is shown to be a highly sensitive and selective technique for the dynamic quantitation of polynuclear aromatic hydrocarbons (PAH) in the vapor phase. A plot of log (fluorescence intensity × temperature) vs $1/T$ for anthracene is linear over five orders of magnitude; fluoranthene exhibits a linear dependence over four orders of magnitude. The vapor pressures of anthracene and fluoranthene were determined from 25 to 150°C and 25 to 105°C, respectively. The vapor pressures of anthracene and fluoranthene were 9.10×10^{-9} atm and 3.55×10^{-8} atm, respectively, at 25°C. It is feasible to quantify anthracene and fluoranthene in a mixture by using the time delay and emission wavelength selectivity of l.i.m.f.

Polynuclear aromatic hydrocarbons (PAH) are multi-aromatic ring systems that are produced at high temperatures by the incomplete combustion of fossil fuels [1—3]. Certain PAH, such as benzo[a]pyrene, possess mutagenic or carcinogenic properties [4, 5]. Reports on the concentration of atmospheric PAH have indicated that they are adsorbed onto the surfaces of particulate matter [6]. Recently, however, it has been seen that some PAH in the presence of a weak air flow evaporate at room temperature, suggesting that the PAH may be present in the vapor phase as well as adsorbed on particles [7—9]. It has also been reported that some PAH such as phenanthrene and pyrene may exist in higher concentrations in the vapor phase than on particles [10]. To investigate this possibility further, a sensitive method was used to quantify the vapor pressures of PAH over a wide range of temperatures similar to those in the environment.

In this study, the gas-phase fluorescence intensities and vapor pressures of anthracene and fluoranthene were monitored directly over a wide range of temperatures by laser-induced molecular fluorescence (l.i.m.f.). Anthracene and fluoranthene were chosen for this study because of their noncarcinogenicity and resultant ease of handling. The technique of l.i.m.f. was chosen as the method of detection over conventional techniques for PAH determination such as gas chromatography [11], gas chromatography/mass spectrometry [12], and high-performance liquid chromatography (h.p.l.c.)

0003-2670/83/$03.00 © 1983 Elsevier Science Publishers B.V.

[13], because it is the only technique that will allow the dynamic measurement of the PAH while they are in the vapor phase. In addition, l.i.m.f. has been shown to be a more sensitive technique for quantifying PAH than any of the techniques mentioned above [14, 15].

Because most PAH compounds exhibit substantially different fluorescence emission spectra, spectral interference from other PAH present can be minimized through careful selection of emission wavelengths. Also because most PAH possess a characteristic fluorescence lifetime (τ), spectral interference in the system can be minimized by monitoring carefully selected time frames for each PAH. Therefore, by utilizing the wavelength and time selectivity of l.i.m.f., spectral interference in many cases can be substantially minimized. This will allow the determination over a wide temperature range of an individual PAH present in a mixture of PAH compounds. In comparison, effusion techniques permit the vapor pressure determination of only pure PAHs, usually over limited temperature ranges.

Recently the l.i.m.f. of certain PAHs in the vapor phase has been reported [15, 16]. One paper reported only on the limits of detection in both a heated cell and in a flame environment at relatively high temperatures. Others have reported the determination of pyrene vapor pressure over a wide temperature range. Here, a sensitive and selective method is reported for the direct determination of PAH vapor pressures over a wide temperature range (25° C—150° C) by l.i.m.f. Also it is possible, using the time- and wavelength-selectivity possessed by l.i.m.f., to determine, over a wide temperature range, individual PAHs in a PAH mixture.

EXPERIMENTAL

Samples

Reagent-grade anthracene (MC & B) and fluoranthene (Aldrich) were used without further purification. Liquid chromatography was used to examine both compounds for impurities with conditions previously reported [17]. The anthracene was found to be essentially free of impurities (less than 0.1%). However, the fluoranthene was found to contain two impurities each comprising about 0.1% of the total sample by weight. One of the impurities, anthracene, did not influence the fluoranthene results because of the minimal fluorescence intensity of anthracene at 460 nm. The second impurity is suspected to be either phenanthrene or fluorene, neither of which would influence the fluoranthene results because neither exhibits any significant fluorescence at 460 nm.

Instrumentation

Figure 1 shows a diagram of the laser fluorimeter used. The excitation source was a laboratory constructed pulsed nitrogen laser which has output at 337.1 nm. The laser was operated with an average power of 4 mW and a pulse rate of 10 pulses per s; the nominal pulse width is 14 ns (full width

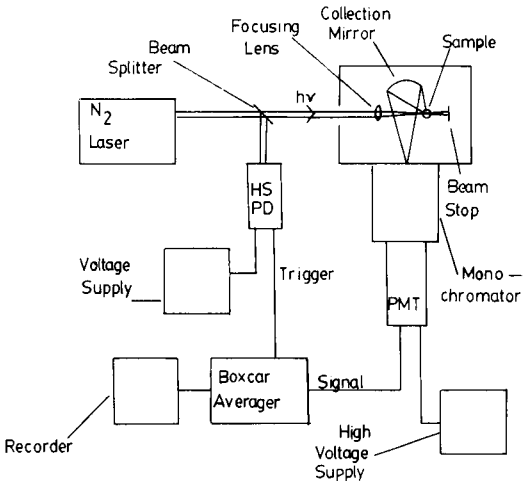

Fig. 1. Schematic diagram of the laser fluorimeter used.

half maximum). The laser beam was focused onto the fluorescence cell by using a 4-cm diameter fused silica lens with a focal length of 12.5 cm. The fluorescence signal was collected at 90° to the laser beam with a 7.5-cm diameter *f*/1.4 spherical mirror and focused onto the entrance slit of an ISA Model H-20 monochromator and detected by an RCA-1P28 photomultiplier tube (PMT). For all fluorescence measurements, 8-nm bandpass slits were used. The PMT was wired for fast pulse response as recommended by the manufacturer. The output from the PMT was passed through a 160-ns RG-58A coaxial cable delay line, processed by a PAR model 162/164/165 boxcar averager, and displayed on a Heath-Schlumberger strip chart recorder. A small portion (about 10%) of the laser output was split off with a microscope slide and routed to a fast photodiode to provide a triggering pulse for the boxcar averager. Unless indicated otherwise, a 50-ns aperture on the boxcar averager was used.

The fluorescence cell consisted of a 5.00 × 3.80 × 1.91-cm aluminum block with glass windows covering the three openings of the cell cavity. The cell was constructed so that the laser beam passed through the entire 1.91-cm pathlength of the cell. The fluorescence signal emerged through an opening in the cell cavity situated at 90° to the incident laser beam. An opening at the top of the cell cavity provided a connection to a vacuum pump so that the pressure could be held constant. The fluorescence cell was heated throughout the experiment by a laboratory constructed tube furnace and the temperature was measured to ±1°C with a copper—constantan thermocouple.

Procedures

Approximately 0.2 g of anthracene was placed into the bottom of the fluorescence cell which was then evacuated and kept at a constant pressure of about three torr. The fluorescence spectrum of the vapor-phase anthra-

cene was then scanned from 340 nm to 600 nm. Fluorescence wavelength maxima were observed at 365 nm and 390 nm and were of approximately equal intensity. The anthracene fluorescence was then monitored at 390 nm as a function of temperature from 25 to 150° C. The same procedure was followed for fluoranthene except that the temperature dependence was monitored from 25 to 105° C. The fluorescence wavelength maximum for fluoranthene was found to be at 459 nm. Because of the relatively long lifetime (τ) of fluoranthene, a 30-ns aperture delay was used on the boxcar averager to optimize signal to noise for fluoranthene as well as minimize spectral interference from contaminants with short lifetime.

Another experiment was run to test the feasibility of quantifying a mixture of anthracene and fluoranthene in the vapor phase. Approximately 0.1-g portions of each solid PAH were thoroughly mixed together and placed into the fluorescence cell. All experimental conditions were the same as previously described, except that a 5-ns aperture was utilized to minimize temporal interference. For the determination of anthracene, a Schott UG-11 bandpass filter was placed in front of the monochromator. The bandpass filter allowed only energy from 300 to 400 nm to pass, thus effectively preventing any fluorescence interference from the fluoranthene from reaching the detector. However, this also reduced the anthracene fluorescence at 390 nm, so an alternative emission wavelength of 365 nm was utilized for the detection of anthracene. The anthracene fluorescence was monitored at 365 nm as a function of temperature from 40 to 90° C in the presence of an approximately equal portion of fluoranthene. The fluoranthene fluorescence was monitored at 459 nm as a function of temperature from 40 to 90° C in the presence of an approximately equal portion of anthracene.

The vapor phase molar absorptivity (ϵ) of fluoranthene was determined by using a 10-cm gas cell in a Cary model 210 ultraviolet/visible spectrophotometer. This was done because of the lack of reliable data for the vapor pressure of fluoranthene. The gas cell consisted of a 1-l round-bottom flask with a 20-cm glass tube attached at the bottom of the flask. Attached horizontally to the bottom of the 20-cm glass tube was a 10-cm absorption cell. Both the glass tube and the absorption cell had an internal diameter of 2.0 cm. Two stopcocks at the top of the gas cell provided a connection to a vacuum pump so that the cell could be evacuated. The entire gas cell was wrapped in insulated resistance wire and aluminum foil so that it could be uniformly heated, and the temperature was monitored at the top and bottom with copper—constantan thermocouples.

Fluoranthene was placed into the gas cell by depositing 100 μl of a 9.547×10^{-3} M solution of fluoranthene dissolved in hexane into the cell. The smallest spectral band-pass available on the spectrophotometer, 0.25 nm, was used for all measurements. The cell was then evacuated at room temperature and placed into the sample chamber of the spectrophotometer and the baseline was set against air. It was assumed that the absorbance was negligible at room temperature. The cell was then heated to a temperature

sufficiently high to ensure sublimation of all the fluoranthene. After a two-hour equilibration, the gas phase absorbance was determined at 337.1 nm and the molar absorptivity, determined from Beer's Law, was found to be 9100 l mol^{-1} cm^{-1}. The absorbance around 337.1 nm is relatively flat and shows little evidence of vibrational fine structure at a spectral bandpass of 0.25 nm.

RESULTS AND DISCUSSION

Equation (1) describes the variation of fluorescence intensity (F) with concentration,

$$F = I\phi_f K[1 - \exp(-\epsilon bC)] \quad (1)$$

where I is the power of the excitation source, ϕ_f is the fluorescence quantum efficiency, K is an instrumental factor, ϵ is the molar absorptivity, b is the cell pathlength, and C is the concentration (mol l^{-1}). If the term ϵbC is <0.05, then Eqn. (1) reduces to $F \approx I\phi_f K\epsilon bC \approx K'C$, where $K' = I\phi_f K\epsilon b$. This equation indicates that at low concentration the fluorescence intensity should be directly proportional to the concentration. Therefore, assuming ideal gas behavior, the fluorescence intensity should also directly depend on the vapor pressure.

The Clausius—Clapeyron equation describes the variation of vapor pressure with temperature: $\log P_{(atm)} = A - B/T$. A plot of $\log P_{(atm)}$ vs. $1/T$ (K^{-1}) should yield a straight line of slope B and intercept A. Because the fluorescence intensity should have a direct dependence on the vapor pressure, a plot of log(fluorescence intensity × temperature) vs. $1/T$ should also yield a straight line. These plots are shown for anthracene and fluoranthene in Fig. 2. The dependence is linear over 4—6 orders of magnitude.

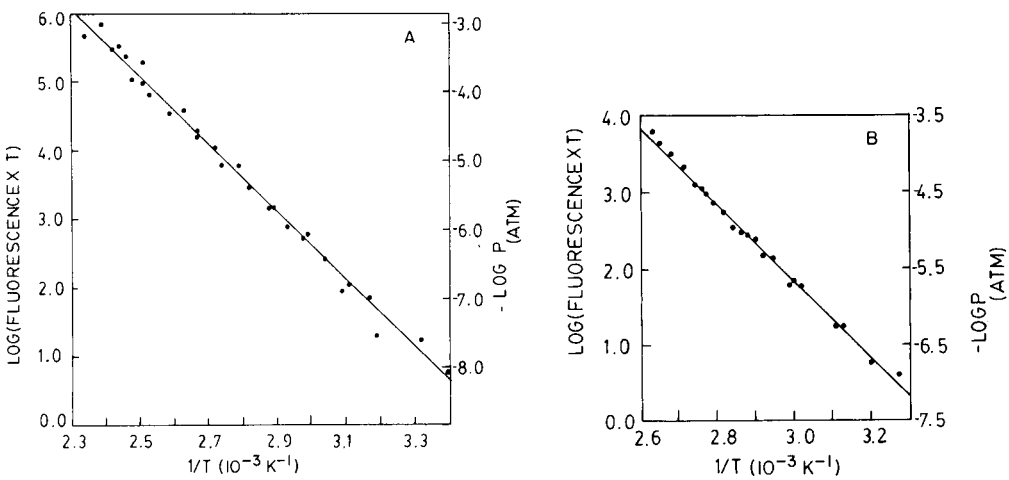

Fig. 2. Plots of log (fluorescence intensity × temperature) vs. $1/T$ (K^{-1}): A, anthracene; B, fluoranthene. The right-hand axes are for plots of $-\log P_{(atm)}$ vs. $1/T$ (K^{-1}).

The fluorescence intensities of anthracene obtained from 25 to 150°C were converted to vapor pressure by calculating the vapor pressure at a single temperature within the experimental temperature range. In this work, the vapor pressure of anthracene was determined at 101°C by using a form of the Clausius—Clapeyron equation described in the literature [18]. Once the vapor pressure is known at one temperature, the vapor pressures throughout the entire temperature range can be determined. A least-squares fit of log $P_{(atm)}$ vs. $1/T$ for anthracene yields a B value of 4944 ± 85 and an A value of 8.64 ± 0.24. The uncertainties quoted are one standard deviation.

Table 1 compares the present results to various anthracene results available in the literature [18—20]. This work describes the vapor pressure of anthracene over a wide temperature range, at relatively low temperatures, and at relatively low vapor pressure. In comparison, the literature values shown encompass limited temperature ranges. Also it was shown that the anthracene vapor pressure at room temperature is directly measurable with the laser fluorimeter; it was found to be 9.10×10^{-9} atm. This corresponds to approximately 3×10^{9} molecules of anthracene, assuming a focused laser beam area of about 1 mm^2.

The vapor pressure of fluoranthene was determined at 82°C in this laboratory rather than calculated by using the Clausius—Clapeyron equation. The absorbance of the fluoranthene in the gas phase was determined at 82°C by measuring the power of the nitrogen laser before and after passing through the fluorescence cell. The concentration of the fluoranthene in the vapor phase was then calculated by using Beer's Law. The gas phase concentration of fluoranthene at 82°C was found to be 5.80×10^{-7} M which yields a vapor pressure of 1.69×10^{-5} atm assuming ideal gas behavior. All vapor pressures of fluoranthene within our experimental temperature range were then calculated assuming ideal gas behavior. A least-squares fit of log $P_{(atm)}$ vs. $1/T$ for fluoranthene, over a temperature range from 306 to 378 K, yields a B value of 5003 ± 79 and an A value of 9.34 ± 0.23. This yields a vapor pressure for fluoranthene of 3.55×10^{-8} atm at 25°C.

TABLE 1

Comparison of Clausius—Clapeyron coefficients for anthracene: log $P_{(atm)} = A - B/T$ (K^{-1})

Temperature range (K)	A	B	Ref.	Technique
378—398	9.12	5102	18	Rodebush gauge
342—359	9.19	5145	19	Effusion
338.7—353.4	9.76	5320	20	Effusion
294—427	8.64 ± 0.24[a]	4944 ± 85[a]	This work	Fluorescence

[a]Uncertainty quoted is one standard deviation.

In a second experiment, the separate vapor-phase fluorescence signals of anthracene and fluoranthene were measured in the presence of one another over a wide temperature range. The major problem encountered in this experiment was isolating the anthracene signal from the fluoranthene signal and vice versa. This was accomplished by utilizing the wavelength- and time-selectivity features of l.i.m.f. Figure 3A, B shows the vapor-phase fluorescence spectra of pure anthracene and fluoranthene. A comparison of these fluorescence spectra reveals that at the maximum emission wavelength of anthracene (390 nm), there is also a considerable amount of fluoranthene signal present. To keep the fluoranthene signal from interfering with the anthracene signal in this experiment, a Schott UG-11 bandpass filter was placed in front of the monochromator which effectively eliminated the fluoranthene signal interference as well as reducing the anthracene signal at 390 nm. However, it can also be seen in Fig. 3A that anthracene possesses a large fluorescence signal at 365 nm. Therefore by monitoring at 365 nm with the UG-11 filter in place, the vapor-phase anthracene signal was measured over a wide range of temperatures in the presence of vapor-phase fluoranthene without significant spectral interference from the fluoranthene. Figure 3C shows the observed vapor-phase spectrum of anthracene in the presence of fluoranthene when the UG-11 filter was in place. A least-squares fit of log (fluorescence intensity × temperature) vs. $1/T$ for anthracene, in the presence of fluoranthene, yields a slope of 4856 ± 81. Converting to log $P_{(atm)}$ vs. $1/T$ yields a B value of 4856 ± 81 and an A value of 8.56 ± 0.23. This result is in excellent agreement with the result already obtained for pure anthracene.

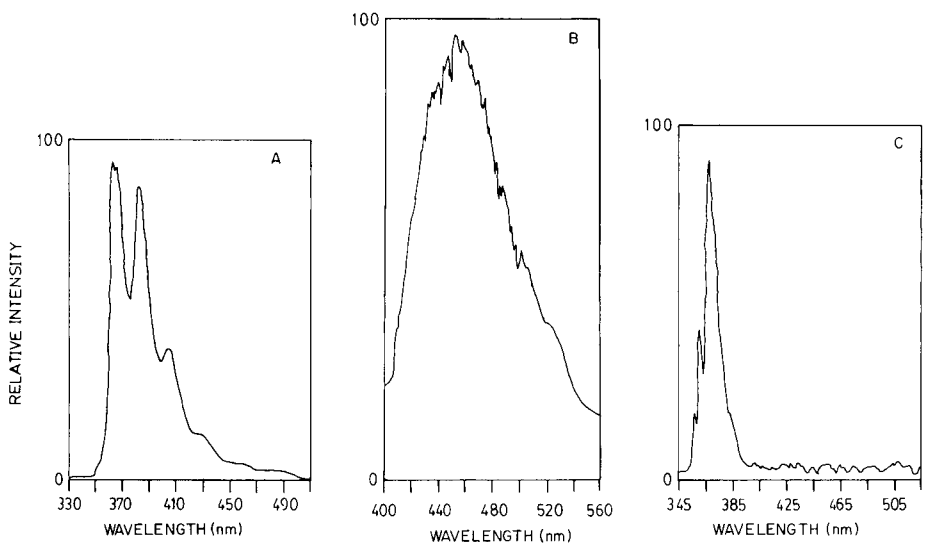

Fig. 3. Vapor-phase fluorescence spectra: A, anthracene; B, fluoranthene; C, anthracene in the presence of fluoranthene. For spectrum C, a Schott UG-11 bandpass filter was placed in front of the monochromator.

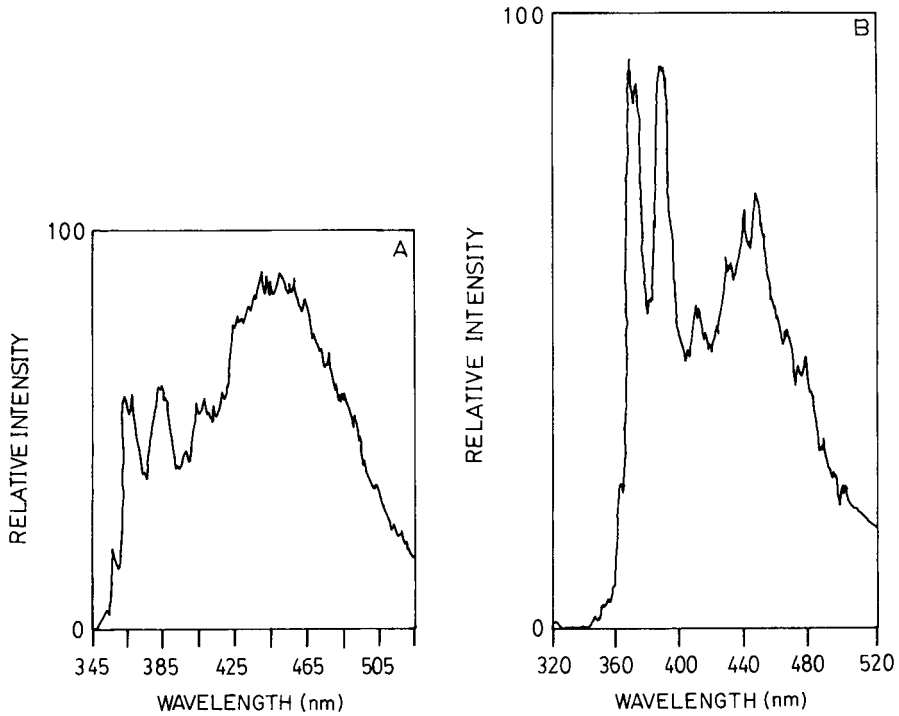

Fig. 4. Vapor phase fluorescence spectra of fluoranthene in the presence of anthracene: A, with a 30-ns aperture delay; B, with no aperture delay.

A comparison of spectra A and B in Fig. 3 also shows that at the maximum emission wavelength of fluoranthene there would also be some anthracene signal present. However, because of the long fluorescence lifetime of fluoranthene, the fluoranthene signal can be monitored after a 30-ns delay. By utilizing the 30-ns delay, the anthracene exhibits little fluorescence signal at 459 nm. Figure 4A illustrates a vapor-phase spectrum of fluoranthene in the presence of vapor phase anthracene when a 30-ns aperture delay is used. Figure 4B illustrates the same conditions but with zero delay. A comparison of these spectra indicates that the fluoranthene signal can be monitored at 459 nm without any interference from anthracene. A least-squares fit of log (fluorescence intensity × temperature) vs. $1/T$ for fluoranthene in the presence of anthracene, yielded a slope of 4842 ± 140. Converting to log $P_{(atm)}$ vs. $1/T$ yielded a B value of 4842 ± 140 and an A value of 8.89 ± 0.41. This result is also in excellent agreement with the results already obtained for pure fluoranthene.

Work is presently underway to examine the spectroscopy of various PAH adsorbed onto fixed supports and onto aerosols.

REFERENCES

1 A. Bjorseth, Anal. Chim. Acta, 94 (1977) 21.
2 J. C. Means, S. G. Wood, J. J. Hassett and W. L. Banwart, Environ. Sci. Technol., 14 (1980) 1524.
3 J. J. Murray, R. F. Pottie and C. Pupp, Can. J. Chem., 52 (1974) 557.
4 D. Hoffman and E. Wynder, in A. C. Stern (Ed.), Air Pollution, Academic Press, New York, 1968, Vol. 2, pp. 187—247.
5 D. Hoffman and E. Wynder, in C. E. Searle (Ed.), Chemical Carcinogens, ACS, Washington, DC, 1976, Monograph 173.
6 A. H. Miguel, in P. W. Jones and P. Leber (Eds.), Polynuclear Aromatic Hydrocarbons, 3rd Int. Symp. on Chemistry and Biology—Carcinogens and Mutagens, Ann Arbor Science, Ann Arbor, MI, 1979, Vol. 3, pp. 383—393.
7 J. Konig, W. Funcke, F. Balfanze, B. Grosch and F. Pott, Atmos. Environ., 14 (1980) 609.
8 C. Pupp, R. Lao, J. J. Murray and R. F. Pottie, Atmos. Environ., 8 (1974) 915.
9 J. Peters and B. Seifert, Atmos. Environ., 14 (1980) 117.
10 C. K. Dettmer and T. F. Bidleman, Pittsburgh Conf. Exp. Anal. Chem. Appl. Spectrosc., (1982), 701.
11 R. A. Greinke and I. C. Lewis, Anal. Chem., 47 (1975) 2151.
12 R. W. Serth and T. W. Hughes, Environ. Sci. Technol., 14 (1980) 2981.
13 B. S. Das and G. H. Thomas, Anal. Chem., 50 (1978) 967.
14 J. H. Richardson and M. E. Ando, Anal. Chem., 49 (1977) 955.
15 T. J. Whitaker and B. A. Bushaw, J. Phys. Chem., 85 (1981) 2180.
16 D. S. Coe and J. I. Steinfeld, Laser Probes for Combustion Chemistry, Am. Chem. Soc. Symp. Ser. No. 134, (1980) 159.
17 A. M. Krstulovic, D. M. Rosie and P. R. Brown, Anal. Chem., 48 (1976) 1383.
18 G. W. Sears and E. R. Hopke, J. Am. Chem. Soc., 71 (1949) 1632.
19 J. D. Kelley and F. O. Rice, J. Phys. Chem., 68 (1964) 3794.
20 R. S. Bradley and T. G. Cleasby, J. Chem. Soc., (1953) 1690.

Analytica Chimica Acta, 151 (1983) 29—38
Elsevier Science Publishers B.V., Amsterdam — Printed in The Netherlands

STUDIES ON MOLYBDOPHOSPHATES CONTAINING A GROUP 4A METAL ION BY LASER RAMAN SPECTROSCOPY
Interference of Group 4A Metal Ions in the Determination of Phosphorus

KATSUO MURATA* and SHIGERO IKEDA

Department of Chemistry, Faculty of Science, Osaka University, Toyonaka, Osaka 560 (Japan)

(Received 7th December 1982)

SUMMARY

The interference of group 4A metal ions in the determination of phosphorus (as phosphate) was investigated by means of laser Raman spectroscopy. Raman spectra and elemental analysis showed that 12-molybdophosphoric acid is transformed to 11-molybdometalophosphoric acid (a ternary heteropolymolybdate containing the group 4A element) in the presence of the group 4A metal ions. The 12-molybdophosphoric acid has an intense Raman line at 996 cm^{-1}, whereas the 11-molybdometalophosphoric acid gives a line shifted by 10—16 cm^{-1} towards a lower wavenumber. This difference makes it possible to estimate the formation constant of the ternary heteropolymolybdate from 12-molybdophosphoric acid. Ternary heteropolymolybdates containing the group 4A element are stable in aqueous solution, but are less readily extracted than the 12-molybdo compound. This is why the group 4A metal ions interfere in the determination of phosphorus.

The presence of a group 4A element (Ti, Zr, and Hf) always leads to errors in the determination of phosphorus by means of a heteropoly acid [1, 2]. Such interfering side-reactions were particularly apparent for solutions containing a group 4A element and 12-molybdophosphoric acid. In previous work [3], the spectrophotometric determination of titanium(IV), zirconium(IV), and thorium(IV) by means of this reaction was examined. The additive production of a ternary heteropolymolybdate has been proposed for this reaction [4], but the existence of the ternary heteropolymolybdate was not readily distinguished in the aqueous solution because the ultraviolet absorption band of the ternary heteropolymolybdate was similar to that of 12-molybdophosphoric acid. The existence of this complex in the aqueous solution can, however, be established by using laser Raman spectroscopy. The purpose of this study is to clarify the reason for the interference in the determination of phosphorus and to estimate the stabilities of the ternary heteropolymolybdate complexes by laser Raman spectroscopy.

0003-2670/83/$03.00 © 1983 Elsevier Science Publishers B.V.

EXPERIMENTAL

Reagents

A molybdate solution was prepared from sodium molybdate ($Na_2MoO_4 \cdot 2H_2O$; analytical-reagent grade) and standardized gravimetrically as its 8-quinolinolate [5]. Polynuclear molybdate complexes were produced by acidification of this molybdate solution. Solutions of phosphate, zirconium(IV), and hafnium(IV) were prepared from potassium dihydrogenphosphate, zirconium oxychloride octahydrate, and hafnium oxychloride octahydrate (all analytical-reagent grade), respectively. A solution of titanium(IV) was prepared by dissolving titanium metal (99.9%) in dilute sulfuric acid and then oxidizing with a small amount of nitric acid. The group 4A metal ions were stored as 2 M perchloric or hydrochloric acid solutions to avoid hydrolysis. Each solution of Ti(IV), Zr(IV), and Hf(IV) was standardized gravimetrically by ignition of the precipitate with cupferron [6].

A solution of molybdophosphate was prepared by acidifying mixed solutions of molybdate and phosphate. A solution of ternary heteropolymolybdate was prepared by acidifying mixed solution of molybdate, phosphate, and the group 4A metal ion. In this case, the order in the addition of each component may be important because the combination of a group 4A ion and phosphate (or molybdate) may cause the precipitation of the group 4A metal phosphate (or molybdate). In order to prepare a solution of ternary heteropolymolybdate, therefore, the mixed solution of molybdate and phosphate is acidified so that molybdophosphate is produced, and then the group 4A metal ion is added. This order favors rapid formation of the ternary heteropolymolybdate. Otherwise, 50 min may be needed to dissolve the precipitate of the group 4A metal molybdate and then to form ternary heteropolymolybdate.

Equipment

Raman spectra were measured with a JASCO R750 triple monochromator and JASCO R800; a 514.5-nm Ar^+ laser was used as the excitation source. Sample solutions of 1-ml volume were used for measurements. It was difficult to measure the molybdate solutions below 10^{-3} M, and a molybdate concentration of 0.12 M was used to obtain better Raman spectra at lower wavenumbers. In order to measure quantitatively the intensity of Raman lines, an internal standard was used. Raman lines of molybdate compounds appear at wavenumbers below 1000 cm^{-1}. The intense and sharp line of nitrate is observed at 1049 cm^{-1}; sodium nitrate of constant concentration (0.08 M) was therefore used as an internal standard, added to each sample solution. This nitrate addition did not affect the Raman spectra of the molybdate solutions. The Raman lines observed were calibrated against those of indene [7].

RESULTS AND DISCUSSION

The formation mechanism of molybdophosphate complexes in weakly acidic solutions has recently been examined by laser Raman spectroscopy [8, 9]; hexamolybdate, $Mo_6O_{19}^{2-}$, and dodecamolybdate, $Mo_{12}O_{37}^{2-}$, were found in weakly acidic molybdate solutions ($Z > 1.5$). It was shown that dodecamolybdate is closely correlated with the formation of 12-molybdophosphoric acid and that 12-molybdophosphoric acid is in equilibrium with 11-molybdophosphoric acid.

Further investigations on heteropolymolybdates indicated that the vibrational spectra of ternary heteropolymolybdate are different from that of molybdophosphate. Figure 1 shows polarized Raman spectra of three ternary heteropolymolybdates and 12-molybdophosphoric acid solutions. The intense Raman lines observed at the highest wavenumber (996, 986, 980 and 980 cm^{-1}) in every heteropolymolybdate disappear for measurements perpendicular to the excitation. These polarization measurements support the idea that the Raman lines of 12-molybdophosphoric (996 cm^{-1}), molybdotitanophosphoric (986 cm^{-1}), molybdozirconophosphoric (980 cm^{-1}), and molybdohafnophosphoric (980 cm^{-1}) acid are all ν_1 lines, i.e., symmetric stretching of Mo=O. Thus a shift of the ν_1 line towards lower wavenumber is observed in the case of ternary heteropolymolybdates, and the intense ν_1 line of each ternary heteropolymolybdate is readily distinguished from that of 12-molybdophosphoric acid. The intense sharp ν_1 line is suitable for the evaluation of each species [8], thus the Raman measurements discussed here were mainly concerned with the ν_1 line observed over 900—1000 cm^{-1}.

Figure 2 shows the influence of titanium(IV) concentration on the Raman spectra of 12-molybdophosphoric acid solution. These spectra clearly indicate the conversion of 12-molybdophosphoric acid to molybdotitanophosphoric acid. The peak intensity at 996 cm^{-1} decreases while a peak appears at 986 cm^{-1} and its intensity increases in proportion to the concentration of titanium(IV). The relative intensities of the peaks at 996 cm^{-1} and 986 cm^{-1} are plotted against the concentration of titanium(IV) in Fig. 3. It can be seen that the increasing intensity at 986 cm^{-1} is closely related to the decreasing intensity at 996 cm^{-1}, i.e., molybdotitanophosphoric acid is produced, while 12-molybdophosphoric acid disappears as the concentration of Ti(IV) increases. Although the intensity at 996 cm^{-1} indicates only the 12-molybdophosphoric acid, the intensity at 986 cm^{-1} always contains not only the contribution of molybdotitanophosphoric acid but also that of 12-molybdophosphoric acid. The contribution of 12-molybdophosphoric acid to curve D (Fig. 3) can be estimated from curve B and the calibration curves of Fig. 4, so that the formation curve (C) for molybdotitanophosphoric acid alone can be plotted by subtracting curve D from curve A.

Similar features were observed in the case of molybdozirconophosphoric acid and molybdohafnophosphoric acid. The influence of the zirconium(IV) concentration on the Raman spectra of 12-molybdophosphoric acid is shown

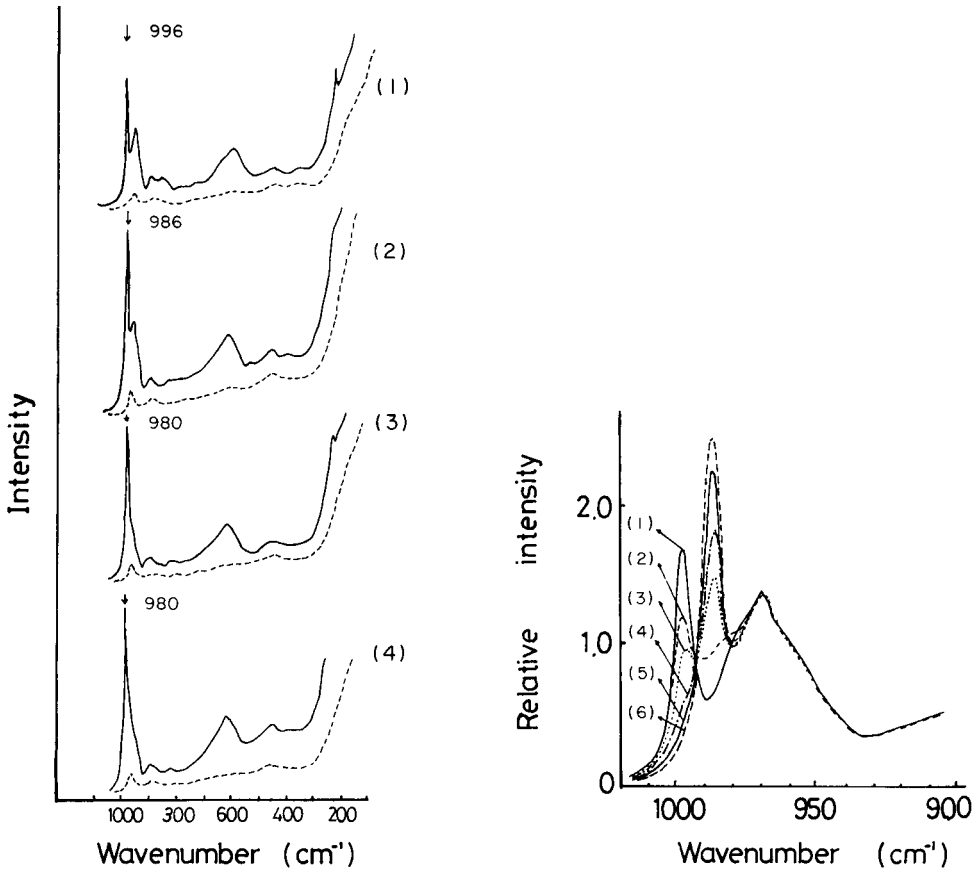

Fig. 1. Polarized Raman spectra of aqueous solutions of binary and ternary heteropoly acids: (1) 12-molybdophosphoric; (2) molybdotitanophosphoric; (3) molybdozirconophosphoric; (4) molybdohafnophosphoric acid. (—) Raman radiation parallel to excitation; (---) Raman radiation perpendicular to excitation. ([Mo] = 1.2×10^{-1} M, [P] = 1.0×10^{-2} M, [Me] = 1.0×10^{-2} M, pH 1).

Fig. 2. Influence of titanium(IV) concentration on the Raman spectra of 12-molybdophosphoric acid solution. Titanium(IV) concentration: (1) 0; (2) 0.2×10^{-2} M; (3) 0.4×10^{-2} M; (4) 0.6×10^{-2} M; (5) 0.8×10^{-2} M; (6) 1.0×10^{-2} M. ([P] = 1.0×10^{-2} M, [Mo] = 1.2×10^{-1} M, [NO_3^-] = 8.0×10^{-2} M, pH 1.0).

in Fig. 5. The relative intensities are plotted against the concentration of Zr(IV) or Hf(IV) in Figs. 6 and 7. The ν_1 lines of both molybdozircono- and molybdohafnophosphoric acid appear at 980 cm^{-1}. The addition of Zr(IV) or Hf(IV) to the solution of 12-molybdophosphoric acid produces molybdozirconophosphoric or molybdohafnophosphoric acid. The formation of ternary heteropolymolybdate is considered as follows.

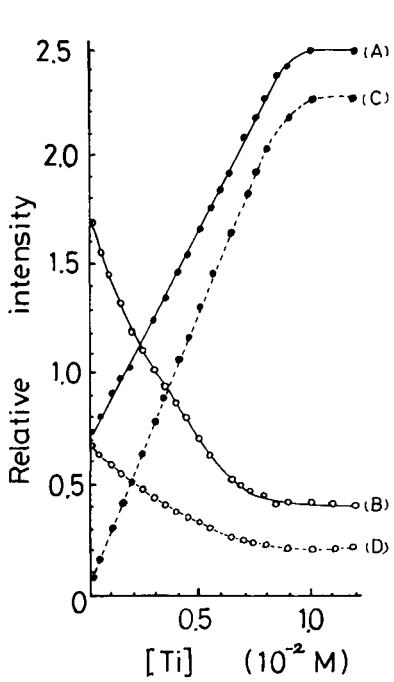

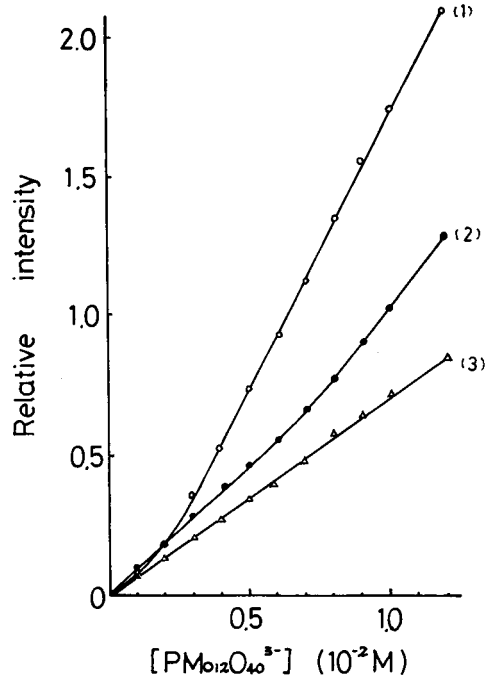

Fig. 3. Formation curve of molybdotitanophosphoric acid estimated from the two Raman lines observed. (A) Intensity at 986 cm^{-1} (observed); (B) intensity at 996 cm^{-1} (observed); (C) intensity at 986 cm^{-1} (estimated by A—D); (D) intensity of 12-molybdophosphoric acid at 986 cm^{-1} (estimated from calibration curve).

Fig. 4. Calibration curves for 12-molybdophosphoric acid: (1) 996 cm^{-1}; (2) 980 cm^{-1}; (3) 986 cm^{-1}.

Mechanisms

It has already been shown [9] that 12-molybdophosphoric acid is in equilibrium with 11-molybdophosphoric acid in solutions at pH 1—2. The latter species has a peak at 975 cm^{-1}, which decreases with increasing acidity, but some 11-molybdophosphoric acid remains at pH 1. 11-Molybdophosphoric acid has a "defect" Keggin structure, missing one of MoO_3 unit, so that there is a hole surrounded by oxygen atoms [10]. The anion can then behave as a ligand to take up a metal ion in this hole [10, 11]. Therefore 11-molybdophosphoric acid is more labile than 12-molybdophosphoric acid. When the group 4A metal ion is added to the solution of 11- and 12-molybdophosphoric acid in equilibrium, the metal ion reacts with 11-molybdophosphoric acid to produce ternary heteropolymolybdate; the consumed 11-molybdophosphoric acid is then replaced by conversion of 12-molybdophosphoric acid. Finally, the 12-molybdophosphoric acid is virtually converted to the ternary heteropolymolybdate.

The elemental results for the tetraethylammonium salts obtained from a

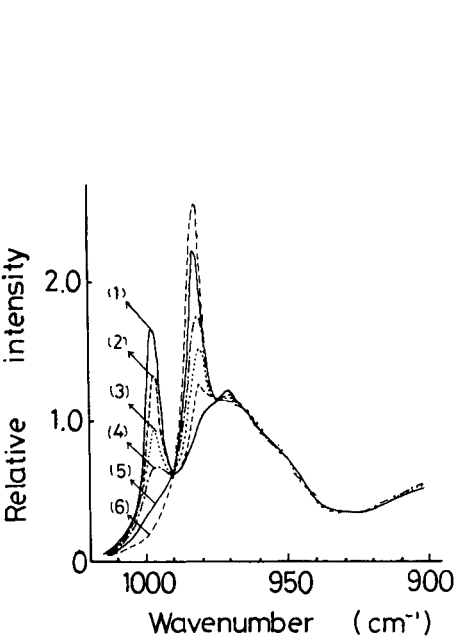

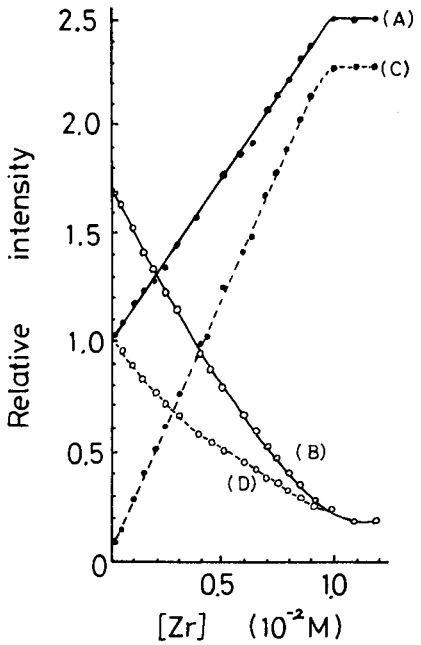

Fig. 5. Influence of zirconium(IV) concentration on the Raman spectra of 12-molybdophosphoric acid solution. Zirconium concentration: (1) 0; (2) 0.2×10^{-2} M; (3) 0.4×10^{-2} M; (4) 0.6×10^{-2} M; (5) 0.8×10^{-2} M; (6) 1.0×10^{-2} M. Other conditions as for Fig. 2.

Fig. 6. Formation curve of molybdozirconophosphoric acid estimated from the two Raman lines observed. (A) Intensity at 980 cm^{-1} (observed); (B) intensity at 996 cm^{-1} (observed); (C) intensity at 980 cm^{-1} (estimated by A—D); (D) intensity of 12-molybdophosphoric acid at 980 cm^{-1} (estimated from calibration curve).

TABLE 1

Elemental results for tetraethylammonium ternary heteropolymolybdate salts
(All results are given as percentages)

	Molybdotitanophosphate			Molybdozirconophosphate			Molybdohafnophosphate		
	Calc[a]	Found	Calc[b]	Calc[a]	Found	Calc[b]	Calc[a]	Found	Calc[b]
C	13.3	14.7	12.5	13.0	11.9	12.3	12.5	12.2	11.8
H	2.9	3.2	2.7	2.8	2.7	2.6	2.7	2.7	2.5
N	1.9	2.2	1.8	1.9	1.75	1.8	1.8	1.8	1.7
Me	2.2	2.2	2.1	4.1	4.9	3.9	7.8	7.0	7.3
P	1.4	1.3	1.3	1.4	1.35	1.3	1.35	1.3	1.3
Mo	48.7	47.2	49.8	47.8	48.0	49.3	45.95	46.8	47.2

[a]Calculated for $[(C_2H_5)_4N]_3PMo_{11}MeO_{39}H_2O$, where Me = Ti, Zr or Hf. [b]Calculated for $[(C_2H_5)_4N]_3MePMo_{12}O_{42}H_2O$, where Me = Ti, Zr or Hf.

solution at pH 1 (Table 1) tend to support reaction (a):

$$PMo_{11}O_{37}^{3-} + MeO^{2+} + 2H_2O \rightleftharpoons PMo_{11}MeO_{40}^{5-} + 4H^+ \quad (a)$$

$$PMo_{12}O_{40}^{3-} + MeO^{2+} + H_2O \rightleftharpoons PMo_{12}O_{42}Me^{3-} + 2H^+ \quad (b)$$

with formation of 11-molybdometalophosphates, $PMo_{11}MeO_{40}^{5-}$, rather than 12-molybdometalophosphates $PMo_{12}O_{42}Me^{3-}$. Previously [3], it was wrongly concluded that the ternary heteropolymolybdate was formed via reaction (b); this might be attributed to the fact that the amounts of ternary heteropolymolybdate formed could not be estimated accurately because of the similarity of the near-ultraviolet spectra of binary and ternary heteropolymolybdates. The present Raman measurements, which can estimate only the ternary heteropolymolybdate, and the elemental analysis of ternary heteropolymolybdate salts support reaction (a).

Estimation of the formation constant

In the solutions relevant to reaction (a), only $PMo_{12}O_{40}^{3-}$, $PMo_{11}O_{37}^{3-}$, and $PMo_{11}MeO_{40}^{5-}$ species are active in Raman spectroscopy. The Ti(IV), Zr(IV), and Hf(IV) species have no Raman lines in the same region. The simple spectrometric estimation of the formation constant, K, for the reaction

$$\underset{(a-x)}{A} + \underset{(b-x)}{B} \rightleftharpoons \underset{x}{C}$$

is based on $K = x/(a-x)(b-x)$, where a and b are the initial concentrations of A and B, respectively, and, x is the equilibrium concentration of C. If d is the absorbance and β is the molar absorptivity, then

$$d = \beta_A(a-x) + \beta_B(b-x) + \beta_C x = (\beta_A a + \beta_B b) + (\beta_C - \beta_A - \beta_B)x \quad (1)$$

Combination of Eqn. 1 and the expression for K yields

$$1/K = [(d-d_0)/(\beta_C - \beta_A - \beta_B)] - a - b + [ab(\beta_C - \beta_A - \beta_B)/(d-d_0)] \quad (2)$$

where $d_0 = (\beta_A a + \beta_B b)$. When B does not absorb, $\beta_B = 0$, and Eqn. (2) is simplified. The resulting plot is called the Rose—Drago plot [12]. When $\beta_A = \beta_B = 0$, Eqn. (2) becomes even simpler:

$$1/K = (d/\beta_C) - a - b + (ab\beta_C/d) \quad (3)$$

When the value of $1/K$ is plotted against the arbitrary β_C for several sets of the initial concentration of A and B, the probable value of $1/K$ is obtainable as the intersection point of several straight lines. This procedure was tested for application with the Raman measurements. The actual formation curve (C) of molybdotitanophosphoric acid in Fig. 3 is well suited to the conditions of the simplified Eqn. (3). The sets of $1/K$ and β_C for molybdotitanophosphoric acid are plotted in Fig. 8. The sets of $1/K$ and β_C for other ternary heteropolymolybdates are given in Tables 2 and 3. The formation constants of the ternary heteropolymolybdates from 12-molybdophosphoric acid were found from these plots to be $5.4 \pm 0.1 \times 10^3$ for molybdotitanophosphoric acid, $2.8 \pm 0.3 \times 10^4$ for molybdozirconophosphoric acid and $1.1 \pm 0.2 \times 10^4$ for molybdohafnophosphoric acid.

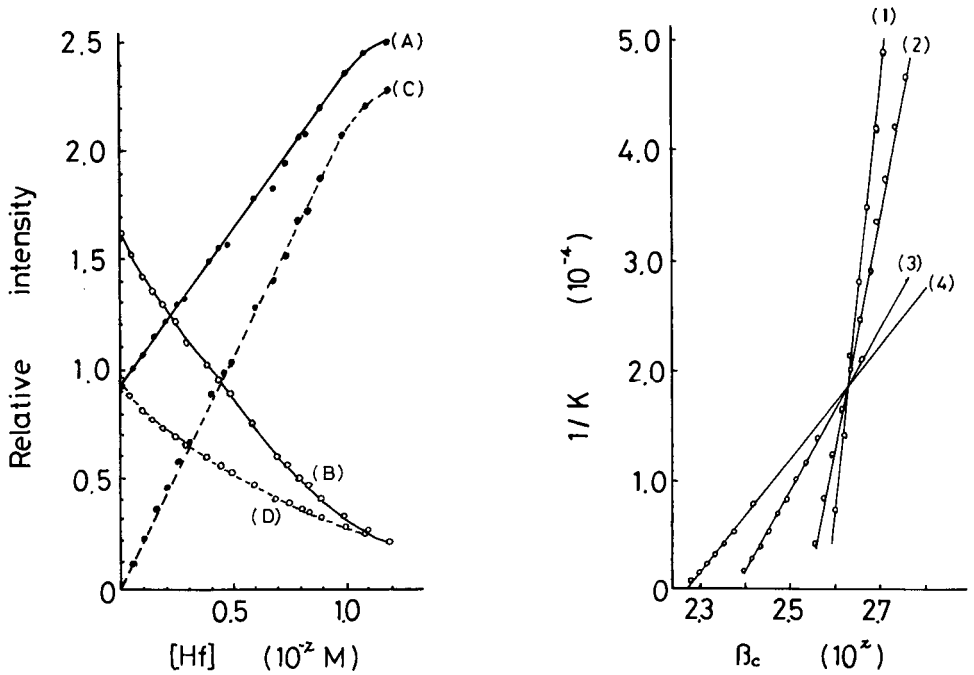

Fig. 7. Formation curve of molybdohafnophosphoric acid estimated from the two Raman lines observed. Curves A—D as for Fig. 6.

Fig. 8. Rose—Drago plot for the formation of molybdotitanophosphoric acid. Titanium-(IV) concentration: (1) 0.1×10^{-2} M; (2) 0.5×10^{-2} M; (3) 0.9×10^{-2} M; (4) 1.0×10^{-2} M. Other conditions as for Fig. 2.

TABLE 2

The sets of $1/K$ and β_C for molybdozirconophosphoric acid

	a = 1.0×10^{-2} *M*, b = 0.4×10^{-2} *M*				
β_C	2.355	2.360	2.365	2.370	2.380×10^2
$1/K$	0.66	1.89	3.21	4.44	7.10×10^{-5}
	a = 1.0×10^{-2} *M*, b = 0.9×10^{-2} *M*				
β_C	2.32	2.34	2.36	2.38	2.40×10^2
$1/K$	0.90	1.99	3.19	4.48	5.98×10^{-5}
	a = 1.0×10^{-2} *M*, b = 0.95×10^{-2} *M*				
β_C	2.30	2.32	2.34	2.36	2.38×10^2
$1/K$	0.64	1.33	2.11	3.10	4.19×10^{-5}
	a = 1.0×10^{-2} *M*, b = 1.0×10^{-2} *M*				
β_C	2.24	2.26	2.28	2.30	2.32×10^2
$1/K$	0.18	0.52	0.97	1.62	2.37×10^{-5}

TABLE 3

The sets of $1/K$ and β_C for molybdohafnophosphoric acid

	a = 1.0×10^{-2} *M*, b = 0.086×10^{-2} *M*							
β_C	2.48	2.49	2.50	2.51	2.52	2.53	2.54	2.55×10^2
$1/K$	0.12	0.48	0.85	1.22	1.59	1.96	2.34	2.71×10^{-4}
	a = 1.0×10^{-2} *M*, b = 0.518×10^{-2} *M*							
β_C	2.44	2.46	2.48	2.50	2.52	2.54	2.56	2.58×10^2
$1/K$	0.11	0.51	0.92	1.33	1.76	2.19	2.62	3.05×10^{-4}
	a = 1.0×10^{-2} *M*, b = 0.864×10^{-2} *M*							
β_C	2.40	2.42	2.44	2.46	2.48	2.50	2.52	2.54×10^2
$1/K$	0.19	0.33	0.48	0.64	0.82	1.00	1.19	1.34×10^{-4}
	a = 1.0×10^{-2} *M*, b = 0.950×10^{-2} *M*							
β_C	2.34	2.36	2.38	2.40	2.42	2.44	2.46	2.48×10^2
$1/K$	0.13	0.21	0.30	0.42	0.54	0.67	0.81	0.96×10^{-4}

Assignment of Raman lines

The Raman lines were initially assigned for the mononuclear species MoO_4^{2-} by Busey and Keller [13]. The ν_1, ν_3, and ν_4 Raman lines are observed at 897, 841, and 318 cm^{-1}, respectively. The present authors also observed three Raman lines and confirmed that the Raman line at 897 cm^{-1} is a totally symmetric vibration by polarization measurements. On acidification of the mononuclear molybdate solution, the Raman spectra change drastically. The ν_3 and ν_4 lines disappear. The ν_1 line decreases greatly but a new ν_1 line appears at the higher wavenumber of 940 cm^{-1}; this was also confirmed to be a totally symmetric vibration by polarization measurements [8]. For isopolymolybdates, Griffith and Lesniak [14] assigned bands above 900 cm^{-1} to Mo=O stretching and those near 350 cm^{-1} to Mo=O bending; 840—750 cm^{-1} bands were assigned to asymmetric Mo—O—Mo stretching and those near 200 cm^{-1} to Mo—O—Mo deformations [14]. The present authors observed that the ν_1 line of Mo=O stretching shifts towards higher wavenumber as condensation proceeds: $Mo_7O_{24}^{6-}$, at 940 cm^{-1}; $Mo_8O_{26}^{4-}$, at 970 cm^{-1}; and $Mo_6O_{19}^{2-}$, at 980 cm^{-1}. These intense Raman lines were also confirmed to be totally symmetric vibrations by polarization measurements [8]. Raman lines below 900 cm^{-1} are very faint in the isopolymolybdate solutions. Only bending of Mo=O is observed at 365 cm^{-1}. Deformations of Mo—O—Mo at 220 cm^{-1} overlaps with strong Rayleigh scattering, and this line is observable only for high concentrations of molybdate (1.2 M). Stretching of Mo—O—Mo near 600 cm^{-1} is not obvious in the isopolymolybdate spectra, but binary and ternary heteropolymolybdates show a characteristic broad Raman peak near 620 cm^{-1}. Although hexamolybdate also has this Raman band near 600 cm^{-1}, isopolymolybdate solutions containing hexamolybdate do not give the band because of small amounts of $Mo_6O_{19}^{2-}$ [15]. Some Raman lines of 12-molybdophosphoric acid were discussed by Franck and co-workers [16],

who assigned the Raman line at 996 cm^{-1} to the totally symmetric stretching of $Mo{=}O_t$. In the present work, the conversion of 12-molybdophosphoric acid to the ternary heteropolymolybdate containing the group 4A element was followed by careful observation of the ν_1 line. The ν_1 line of the ternary heteropolymolybdate was observed with a shift of 10—16 cm^{-1}. Lynhamn et al. attempted to estimate force constants for 12-molybdophosphoric acid [17]. The shift towards lower wavenumber in the ternary heteropolymolybdates may reflect a decrease in the force constant (Mo=O) caused by replacement of a molybdenum atom with a group 4A element. Within the isopoly- and heteropoly-molybdates, 12-molybdophosphoric acid, having the best symmetry, provides the ν_1 line at the highest wavenumber (996 cm^{-1}).

As shown above, the reaction of the group 4A metal ions with 12-molybdophosphoric acid produces ternary heteropolymolybdates containing the group 4A element. These complexes are more stable than 12-molybdophosphoric acid in the aqueous solution, but they are less extractable. Therefore the presence of the group 4A elements causes interference in the determination of phosphorus by extraction of the heteropoly acid. More basic solvents such as cyclohexanone and tributylphosphate, however, can extract the ternary heteropolymolybdates without interference. As previously reported, spectrophotometric determinations of the group 4A metal ions are possible by using the formation of ternary heteropolymolybdates [3].

REFERENCES

1 P. Pakalns, Anal. Chim. Acta, 40 (1968) 1.
2 M. Ishibashi and M. Tabushi, Bunseki Kagaku, 8 (1959) 588.
3 K. Murata, Y. Yokoyama and S. Ikeda, Anal. Chim. Acta, 48 (1969) 349.
4 A. K. Babko and Y. F. Shkaravskii, Zh. Neorg. Khim., 6 (1961) 2091.
5 M. Borrel and R. Paris, Anal. Chim. Acta, 4 (1950) 267.
6 P. J. Elving and E. C. Olson, Anal. Chem., 27 (1955) 1817.
7 P. J. Hendra and E. J. Loader, Chem. Ind., (1968) 718.
8 K. Murata and S. Ikeda, Spectrochim. Acta, Part A, 39 (1983) in press.
9 K. Murata and S. Ikeda, Polyhedron, 2 (1983) in press.
10 C. Rocchiccioli-Deltcheff and R. Thouvenot, J. Chem. Research (S), (1977) 46.
11 F. Umland, A. Janssen, D. Thierig and G. Wünsch, Theorie und Praktische Anwendung von Komplexbildenern, Akademische Verlagsgesellschaft, Frankfurt, 1971, p. 42—43.
12 N. J. Rose and R. S. Drago, J. Am. Chem. Soc., 81 (1959) 6138.
13 R. H. Busey and D. L. Keller, Jr., J. Chem. Phys., 41 (1961) 215.
14 W. P. Griffith and P. J. B. Lesniak, J. Chem. Soc., Sect. A, (1969) 1066.
15 K. Murata, E. Yamamoto and S. Ikeda, Bull. Chem. Soc. Jpn., 56 (3) (1983) 941.
16 C. Rocchiccioli-Deltcheff, R. Thouvenot and R. Franck, Spectrochim. Acta, Part A, 32 (1976) 587.
17 L. Lyhamn, S. J. Cyvin, B. N. Cyvin and J. Brunvoll, Z. Naturforsch., Teil A, 31 (1976) 1589.

Analytica Chimica Acta, 151 (1983) 39—48
Elsevier Science Publishers B.V., Amsterdam — Printed in The Netherlands

ZONE TRAPPING IN FLOW INJECTION ANALYSIS
Spectrophotometric Determination of Low Levels of Ammonium Ion in Natural Waters

F. J. KRUG*, B. F. REIS, M. F. GINÉ and E. A. G. ZAGATTO
Centro de Energia Nuclear na Agricultura (CENA-USP), 13400 Piracicaba (Brasil)
J. R. FERREIRA
Instituto de Pesca, Sec. da Agricultura, Sao Paulo (Brasil)
A. O. JACINTHO
Escola Superior de Agricultura, "Luiz de Queiróz"-USP, 13400 Piracicaba (Brasil)
(Received 23rd December 1982)

SUMMARY

In flow injection analysis, a selected portion of a processed sample zone can be removed and, after a predetermined period of time reintroduced into the same carrier stream. This zone-trapping technique, easily applied, is suitable for methods based on relatively slow chemical reactions in which sensitivity or sampling rate is critical. It has some advantages over the stopped-flow and intermittent-flow approaches. The technique was studied for a model system without chemical reaction, and was then applied in a sensitive spectrophotometric method for the determination of ammonium ion in natural waters, based on a modified Berthelot reaction. In zone trapping, the main portion of the reacting sample zone is retained in a 38°C water bath so that about 80% complete reaction is achieved without limiting the sampling rate. The proposed method is suitable for 90—100 measurements per hour with a relative standard deviation of 0.5% for a typical sample (0.15 mg l^{-1} ammonium). Beer's law is followed up to 1 mg l^{-1} and the detection limit is 5 $\mu g\ l^{-1}$. Interferences of metals are overcome with EDTA. The results for waters agree well with those obtained by a standard manual procedure.

The zone-sampling technique in flow injection analysis was proposed recently [1] and some of its potentialities have already been exploited [1—3]. This technique involves sampling of a small portion from a dispersed zone and introduction of this aliquot into a second carrier stream. Zone trapping can be regarded as a variation of this process: the central portion of a processed sample zone is selected, removed from the analytical path, allowed to stand for a pre-established period of time under defined conditions, and later reintroduced into the same carrier stream. During the trapping period, the sample can participate in slow chemical reactions without undergoing significant dispersion which could reduce sampling frequency. This technique, an improvement of the parallel analyzer proposed by Růžička and Hansen [4], is therefore an alternative to flow injection methods based on

0003-2670/83/$03.00 © 1983 Elsevier Science Publishers B.V.

slow chemistry in which sensitivity and/or sampling rate are limited. The advantages over the stopped-flow [5] and the intermittent-flow [6, 7] approaches are discussed later.

The feasibility of the technique is demonstrated in developing a modified Berthelot method for ammonium determination in natural waters at the $\mu g\ l^{-1}$ level. The zone-trapping process allows the more concentrated portion of the processed sample to remain inside a warm water bath without significant loss in sampling frequency. Thus more complete development of the chemical reaction, with consequent increase in sensitivity, is achieved without stoppage of the peristaltic pump, and without special valves, parallel coils, or cumbersome pre-concentration steps.

EXPERIMENTAL

Instrumentation

An Ismatec mp-13 GJ-4 peristaltic pump was used with a Varian 634-S spectrophotometer provided with a 178-OS Hellma flow cell and connected to a REC-61 recorder with a REA-112 high sensitivity unit (Radiometer). Perspex connectors (Y-shaped) and polyethylene tubing (i.d. 0.8 mm) were used to build up the manifold. The tubing became yellowish-brown after several weeks of routine use, but it was not replaced by tubing of other material because the results were unaffected. In the earlier stages of the research, a stainless steel heating coil was used, but replacement by a polyethylene coil was necessary after a few weeks because corrosion was observed.

Two commutation sections of the electronically operated [1, 8] injector-commutator [8, 9] were employed. The purpose-built water bath, with a NTC sensor, was thermostated to $\pm 0.1^{\circ}C$.

Reagents, standards and samples

All chemicals, except for sodium hypochlorite, were of analytical grade; freshly distilled—deionized water was always used.

The central zone-trapping technique was first studied in a model system (Fig. 1A); the sample was a coloured solution (0.25% w/v ammonium thiocyanate with 10 mg Fe l^{-1}, as iron(III) nitrate, in 0.01 M hydrochloric acid) and the carrier stream was 0.01 M hydrochloric acid.

For the ammonium method, the following solutions were used. The phenol stock solution contained 4% (w/v) phenol in water; this solution was stable for several weeks if stored in a refrigerator and was filtered before use if any turbidity was observed. The aqueous sodium nitrosopentacyanoferrate-(III) (sodium nitroprusside) stock solution contained 10% (w/v) of the reagent as its dihydrate; it was stable when stored in an amber glass bottle. The sodium hypochlorite stock solution (about 2% in active chlorine) was prepared from a domestic bleach solution. When its alkalinity was evaluated by titration, 18.5 ml of 1 M hydrochloric acid was enough to neutralize 100 ml of the bleach solution. The solutions actually pumped were as follows. The alkaline

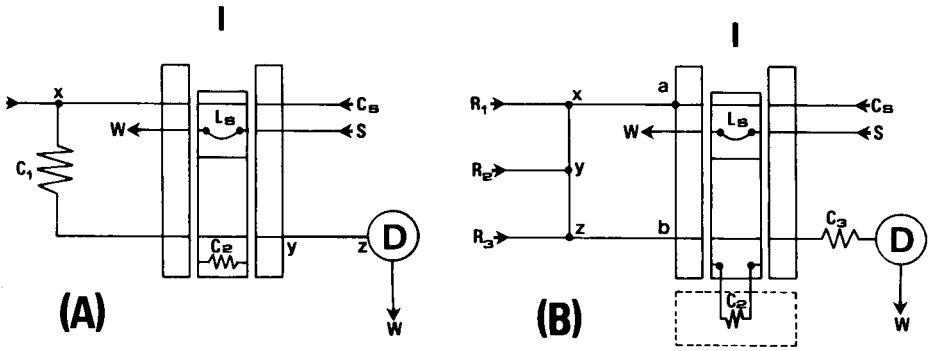

Fig. 1. Flow diagrams of (A) the model system and (B) the system proposed for low-level ammonium determination in natural waters. I represents the injector-commutator, and S is the sample being pumped (4.0 ml min^{-1}), which fills the sample loop (L_S) and then goes to waste (W). In system A: C_S, sample carrier stream (0.01 M HCl solution) at 8.8 ml min^{-1}; C_1, mixing coil (100 cm); C_2, trapping coil (150 cm); *yz*, transmission line (45 cm); D, spectrophotometric detector (480 nm). In system B: L_S, injected volume (100 μl); C_S, sample carrier stream (water) at 6.0 ml min^{-1}; R_1, R_2 and R_3, masking alkaline, phenate and hypochlorite reagents, all pumped at 0.8 ml min^{-1}; *ax*, *xy*, *yz* and *zb*, transmission lines (10, 20, 10 and 5 cm, respectively); C_2, heating coil (150 cm) placed in a 38°C water bath (dashed lines); C_3, transmission coil (150 cm); D, detector set at 695 nm. For this system, Δt_1 = 14 s and Δt_2 = 26 s. For details, see text.

masking reagent (R_1, Fig. 1B) was 2.5% (w/v) Na_2EDTA in 0.5 M sodium hydroxide. The phenate reagent (R_2) contained 2% (w/v) phenol and 1% (w/v) sodium nitroprusside in water; this was stable for only a few days, even in a refrigerator. The hypochlorite reagent (R_3) was prepared daily by tenfold dilution of the corresponding stock with water. The sample carrier stream (C_S) was water.

Working standards ranging from 0 to 500 μg l^{-1} ammonium ion were prepared by dilutions of a 1000 mg l^{-1} stock solution (3.6708 g l^{-1} ammonium sulfate) with water.

Natural water samples from the Piracicaba river were collected, filtered through 0.45-μm Millipore filters and processed the same day, so that no preservation was necessary.

The model system

The flow diagram of the model system used to investigate the main characteristics of the zone-trapping technique is shown in Fig. 1A, with the injector-commutator (I) in the sampling position. The sample (S) feeds the sample loop (L) which defines the injected volume, its excess going to waste (W). When the injector is switched to the other position, the sample is introduced into its carrier stream (C_S) and the C_2 coil is placed in the analytical path. The chemical reactions involved are initiated in the C_1 coil after addition of reagents at point *x*. After a time interval, Δt_1, while the central portion of the sample zone is passing through coil C_2, the commutator is switched back to the sampling position, trapping the more concentrated portion of the

sample zone inside the C_2 coil for a period, Δt_2. In the meantime, the next sample is pumped. More complete development of the hypothetical slow reactions is then attained without increase in sample dispersion. As the outer portions of the sample zone are not trapped, the sampling rate is not reduced. When the next commutation takes place, the second sample is injected and the trapped zone is introduced into the same carrier stream, being transported towards detection. The second sample is similarly processed, trapped, and so on.

The dimensions of the model system were selected on the basis of the following considerations. With this process, slow pumping rates are not imperative, in spite of the relatively slow chemical reactions, thus a high pumping rate (8.8 ml min^{-1}) was chosen for the sample carrier stream. The C_1 coil length was fixed as 100 cm (ca. 500 μl) which allows the replacement of the zone trapped inside the C_2 coil without carry-over troubles; the actual size of the single C_1 coil is not vital in this model system. The length of the C_2 trapping coil was chosen as 150 cm (ca. 750 μl). Larger values are not recommended because the trapping coil would then remove almost the entire sample zone, eliminating one of the advantages of this process over the stopped-flow approach. Modifications in the measured peak shapes caused by sample dispersion after the trapping coil are minimized by using a transmission line yz just long enough to connect the C_2 coil and the detector unit. Because this technique presupposes that sensitivity is critical, large sample volumes (500 μl and 1000 μl) were tested.

The ammonium system

The flow diagram of the ammonium system is shown in Fig. 1B, its operation being similar to that described above. Following sample injection into a water carrier stream (6.0 ml min^{-1}), the sample zone reaches successively the confluence points x, y and z where the alkaline masking, phenate and hypochlorite reagents (all pumped at 0.8 ml min^{-1}) are added. The central portion of the sample zone is trapped for the development of the modified Berthelot reaction with heating. Full descriptions of the reactions have been given elsewhere [10, 11]. After the trapping period Δt_2, the coloured species is reintroduced into the carrier stream, being transported via the C_3 coil to the detector. Under these conditions, the wavelength for maximum absorbance is shifted to 695 nm. Spectra recorded at 28° C and 42° C indicated that this shift is temperature-independent.

This system was designed to provide limited sample dispersion [4] with a 1000-μl sample volume. Lines ax, xy, yz and zb were as short as possible and the flow rates were chosen to minimize sample dilution at the confluence points. Three confluence points in the analytical path are required, because when R_1 and R_2 are mixed before addition to the sample zone, deterioration of the phenate reagent under alkaline conditions starts earlier, leading to a higher blank value. The C_2 and C_3 coils were both 150 cm long. If C_3 is too short (40 cm), the baseline is "noisy", probably because of a

refractive index effect [12] caused by the temperature gradient along the sample zone; if it is too large, the untrapped portions of the sample zone could also produce significant amounts of the species to be detected, thus increasing carry-over.

The utilization of intermittent flows instead of the zone-trapping process was tried in the initial stages of this research without success. When the washing stream was stopped, irregular baseline readings caused by refractive index effects reduced sensitivity.

Preliminary tests and procedures

Model system. The effect of Δt_1 in the zone-trapping technique was investigated for the model system (Fig. 1A) with Δt_1 in the range 3—30 s. For Δt_1 values of 7, 9, 11, 14 and 20 s, peak profiles corresponding to two consecutive cycles were recorded for 500- and 1000-μl sample volumes (Fig. 2). The Δt_2 value was changed appropriately, to maintain a constant period ($\Delta t_1 + \Delta t_2$) of 40 s. The effect of the trapping period was verified by using Δt_2 values of 30—180 s and Δt_1 of 14 s.

Ammonium system. The order of addition of reagents and the concentrations for the ammonium system were defined in preliminary tests at 37°C, involving different concentrations of phenol (1—4%, w/v), sodium nitroprusside (0—1%, w/v), sodium hydroxide (0.25—2.0 M) and sodium hypochlorite (0.01—1% in active chlorine). The use of sodium tetraborate, as recommended in an earlier flow injection procedure [11] was also tested. The recommended concentrations are as outlined above for R_1, R_2 and R_3 (see Fig. 1B).

The optimal Δt_1 value was 16 s for Δt_2 = 26 s; these times were used in all later tests.

The influence of the water bath temperature in the 25—45°C range was studied with the system of Fig. 1B for ammonium standards of 250 and 500 μg l^{-1}. The R_2 reagent was a 0.5 M sodium hydroxide solution. Higher

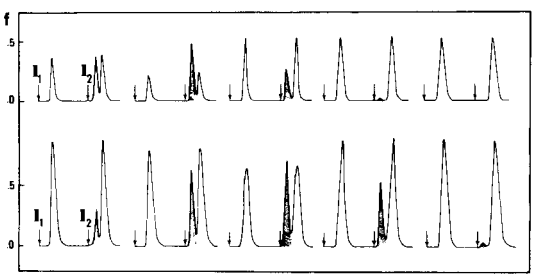

Fig. 2. Effect of the injected volume and the Δt_1 value in the zone-trapping technique. The recorded peaks correspond to two consecutive cycles, I_1 and I_2 being the instants of sample injection ($I_2 - I_1$ = 40 s). The twin peaks refer to the untrapped portions of the sample zone and the dashed areas represent the trapped portions. The upper recorded peaks are for 500-μl samples and the lower peaks for 1000-μl samples. From left to right, the corresponding Δt values are 7, 9, 11, 14 and 20 s. The ordinate f is the dispersion factor [9].

temperatures were not employed, to avoid formation of air bubbles. A temperature of 38° C was selected.

Interfering ions were studied with a system similar to that of Fig. 1B. The main carrier stream was replaced by two equivalent (3.0 ml min^{-1}) water merging streams, into which 500 μl of the ammonium standard and an equal volume of the solution with a potential interferent were introduced. The merging of sample and interfering ion zones provided reproducible addition of the diverse ion to the sample [13, 14]. Ammonium standards of 0, 400 and 1000 $\mu g\ l^{-1}$, corresponding to effective concentrations of 0, 200 and 500 $\mu g\ l^{-1}$ in the proposed system, were tested. Metal concentrations higher than those usually found in natural waters [15] were investigated separately (10 ppm K, 10 ppm Mg, 5 ppm Mn, 10 ppm Fe, 10 ppm Al and 50 ppm Si, as chlorides, 5 ppm Cu and 50 ppm Ca, as nitrates). Several classical masking agents (1—5% w/v sodium tartrate, 1% w/v potassium cyanate, 1% w/v sodium citrate and 1—5% w/v disodium EDTA) were tested by adding them separately in the R_1 reagent (Fig. 1B). If organic interferences are likely to occur at significant levels, a prior distillation is recommended.

RESULTS AND DISCUSSION

Studies with the model system

The effect of Δt_1 in the zone-trapping technique is analogous to that of Δt in the zone-sampling technique (i.e., it selects the portion of the sample zone to be removed). In the model system, trapping was examined for 5 s $< \Delta t_1 <$ 25 s (for sample volumes of 500 μl); for low Δt_1 the sample zone by-passed the trapping coil C_2, whereas at high Δt_1, the zone flowed through C_2 before the commutator was switched. In the latter situation, two undistorted peaks corresponding to two consecutive injections were recorded (Fig. 2, sample volume = 500 μl, Δt_1 = 20 s). Obviously, Δt_1 must be chosen carefully. As can be seen from Fig. 2, if the zone trapping technique occurs, the peak recorded for the untrapped portions of the sample zone is distorted, and the trapped amount originates a new peak (Fig. 2, dashed areas) near the following recorded peak. In real systems involving slow reactions, the outer untrapped portions of the sample zone are almost undetectable, considering the mean sample residence time of untrapped portions in the model system (ca. 13 s). Thus the carry-over between consecutive original and trapped zones, apparent in Fig. 2, is not usually relevant in real applications. The sample throughput depends more on the mean residence time of the trapped amounts (ca. 45 s in the model systems) than on the recorded peak shape which is the limiting factor on sampling rate for flow injection stopped flow systems. For any given flow injection system with zone trapping, there is an optimal Δt_1 value which corresponds to the highest volume of sample selected. In the model systems, ideal Δt_1 values were ca. 9 and 11 s for 500- and 1000-μl injected volumes, respectively, compensating for the delay of the central portion of the sample volume caused by the increased injected volume.

With regard to the sample volume and the trapping volume, it is good practice to choose first the trapping volume (length of C_2 coil, Fig. 1) in order to achieve limited dispersion before detection, and then to adjust the injected volume (length of L_S loop). This must be large enough to minimize dispersion inside C_1 and C_2, avoiding pronounced concentration gradients along the trapped zone. As the detector is not actually used during most of the entire cycle, the sampling rate can be doubled without reducing the available reaction time, by using a 3:4:3 commutation section [16] to inject samples into a system with two parallel equivalent C_2 coils. Also, the transmission line *yz* can be longer without affecting sampling rate.

The Δt_2 value defines the storage period of the sample zone within the C_2 coil. In the model system, variations in Δt_2 had no effect; peak broadening was not observed even when Δt_2 was 5 min and the injected volume was only 100 μl. This confirms the general assumption that ion diffusion is not an important factor in sample dispersion.

The ammonium system

First, the Δt_1 value was adjusted to select the portion of the sample zone corresponding to maximum peak height for Δt_2 = 30 s for injection of a 250 $\mu g\ l^{-1}$ ammonium standard with heating at 38°C. The best Δt_1 value was 16 s for the ammonium system in Fig. 1B. The injected volume was then chosen as 1000 μl because the peak heights were then 97% of those obtained with an infinite volume configuration [17]. With the zone-trapping technique, replacement of the sample carrier stream by the sample (situation of infinite volume) did not produce the usual recorded plateau, but sequential identical peaks corresponding to the successive trapping processes.

In the ammonium system (Fig. 1B), both the sample and blank signals increase with increasing temperature or reaction time (Fig. 3). Increase in the analytical signal is due to the more complete development of the modified Berthelot reaction, while increase in the blank value is caused by varying

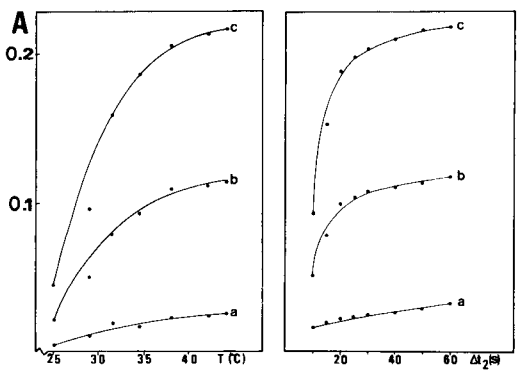

Fig. 3. Effect of the temperature (left) and the Δt_2 value (right) in the proposed method. Curves *a*, *b* and *c* refer to 0, 250 and 500 $\mu g\ l^{-1}$ ammonium standards, respectively, and *A* indicates peak-height measurements, as absorbance.

degrees of deterioration of the phenol/sodium nitroprusside/sodium hydroxide mixture and by the thermal and ionic refractive index effects. The experimental data for the temperature variation are scattered from the hypothetical curve, probably because thermal equilibrium was not fully achieved. A temperature of 38° C was chosen for the water bath as the best compromise between the ratio of the analytical and blank signals, the possibility of air bubble formation at higher temperatures, and the $\Delta A/\Delta T$ relationship. In fact, this relationship is so small at 38° C (Fig. 3) that strict temperature control is not really needed. The effect of changing Δt_2 was examined over the range 15—60 s. The Δt_2 value was chosen as 26 s, enough for the attainment of about 80% complete reaction (cf. the asymptotic tendency of the curves in Fig. 3). This was confirmed in tests with stoppage of the peristaltic pump. Lower Δt_2 values can be employed to improve the sampling rate in analyses of waters with high ammonium contents.

Comparison of the proposed system with a normal flow injection system without the zone-trapping facility (Δt_1 being 30 s) indicated that a four-fold increase in sensitivity was attained by including zone trapping.

Without any masking agent in the R_2 reagent, the proposed method was not affected by Al, K and Si for the concentrations investigated; however, Cu, Mn, Fe, Ca and Mg affected the peak heights corresponding to 200 and 500 $\mu g\ l^{-1}$ ammonium by approximately 12, 10, 1, −1 and 2%, respectively. Also the blank values were increased in presence of these metals. Tartrate was inadequate for masking copper and iron, and citrate did not prevent completely the iron interference. When a 2.5% EDTA solution was used, all the above interferences were reduced to less than 1%. Higher EDTA concentrations cannot be used; when a 5% (w/v) EDTA concentration was tested, the measured signals underwent a 30% reduction.

The proposed system is remarkably stable. The measured peak heights for a sample containing about 150 $\mu g\ l^{-1}$ ammonium ion showed only slight variations (ca. 3%) after four hours of continuous operation, involving about 400 measurements. Baseline drift, which in extreme cases can reach an absorbance increase of about 0.02 per hour, was observed in the analyses of some batches (see also Fig. 4). This drift, probably caused by the accumulation of micro air bubbles in the flow cell, depends on the quality of the water utilized and may be avoided by employing lower temperatures (35 or 36° C) accompanied by increased Δt_2 values to preserve sensitivity. The precision of measurement, around 0.2% (r.s.d. of peak heights), is better than that of other flow injection procedures based on this reaction [11, 16]. A graphical result of part of a routine run for the determination of ammonium ions in river waters (Fig. 4) indicates the stability of the system, as well as the precision, the linearity of the calibration plot (Beer's law followed up to 1 mg l^{-1}), the detection limit (about 5 $\mu g\ l^{-1}$) and the sampling rate (90 h^{-1}). The accuracy of the method can be assessed by considering the data in Table 1. No statistical difference at the 99% level was found between the proposed method and the manual reference method [15] based on the same reactions.

TABLE 1

Comparison of procedures for the determination of ammonium ion in river waters (Results expressed as μg ammonium l^{-1})

Sample	Ammonium ion found ($\mu g\ l^{-1}$)		Sample	Ammonium ion found ($\mu g\ l^{-1}$)	
	Proposed method	Reference method [15]		Proposed method	Reference method [15]
1	123	111	6	50	51
2	20	20	7	108	114
3	256	234	8	51	55
4	43	42	9	27	29
5	239	244			

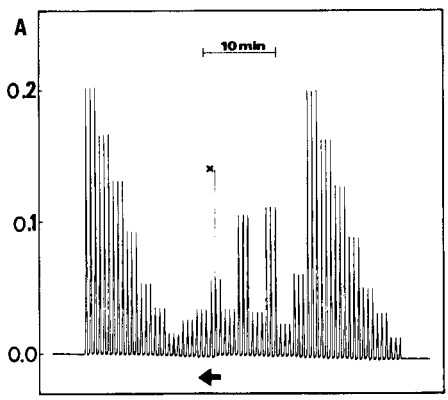

Fig. 4. Routine determination of ammonium ion in river water samples with the system shown in Fig. 1B. From right to left, the blank, six standards (50, 100, 200, 300, 400 and 500 $\mu g\ l^{-1}$), nine samples and the standards again, with all measurements in triplicate. The peak marked x is caused by a spurious air bubble formed inside the system, easily distinguished by the very abrupt change in absorbance.

Partial support from the Conselho Nacional de Desenvolvimento Cientifico e Tecnológico and the Financiadadora de Estudos e Projetos is greatly appreciated. The authors thank M. Pinta, P. B. Vose and R. E. Bruns for their help with the original manuscript and O. Matsumoto and O. Bahia F° for critical comments.

REFERENCES

1 B. F. Reis, A. D. Jacintho, J. Mortatti, F. J. Krug, E. A. G. Zagatto, H. Bergamin F° and L. C. R. Pessenda, Anal. Chim. Acta, 123 (1981) 221.
2 E. A. G. Zagatto, A. O. Jacintho, L. C. R. Pessenda, F. J. Krug, B. F. Reis and H. Bergamin F°, Anal. Chim. Acta, 125 (1981) 37.
3 A. O. Jacintho, E. A. G. Zagatto, B. F. Reis, L. C. R. Pessenda and F. J. Krug, Anal. Chim. Acta, 130 (1981) 361.

4 J. Růžička and E. H. Hansen, Flow Injection Analysis, Wiley, New York, 1981.
5 J. Růžička and E. H. Hansen, Anal. Chim. Acta, 106 (1979) 207.
6 J. Růžička and E. H. Hansen, Anal. Chim. Acta, 114 (1980) 19.
7 E. A. G. Zagatto, A. O. Jacintho, J. Mortatti and H. Bergamin F°, Anal. Chim. Acta, 120 (1980) 399.
8 H. Bergamin F°, B. F. Reis, A. O. Jacintho and E. A. G. Zagatto, Anal. Chim. Acta, 117 (1980) 81.
9 A. O. Jacintho, E. A. G. Zagatto, H. Bergamin F°, F. J. Krug, B. F. Reis, R. E. Bruns and B. R. Kowalski, Anal. Chim. Acta, 130 (1981) 243.
10 P. Blanchard, C. Madec and J. Courtot-Coupez, Analysis, 10 (1982) 155.
11 J. W. B. Stewart, J. Růžička, H. Bergamin F° and E. A. G. Zagatto, Anal. Chim. Acta, 81 (1976) 371.
12 H. Bergamin F°, B. F. Reis and E. A. G. Zagatto, Anal. Chim. Acta, 97 (1978) 427.
13 E. A. G. Zagatto, A. O. Jacintho, F. J. Krug, B. F. Reis, R. E. Bruns and M. C. U. Araujo, Anal. Chim. Acta, 145 (1983) 169.
14 E. H. Hansen, J. Růžička, F. J. Krug and E. A. G. Zagatto, Anal. Chim. Acta, 148 (1983) 111.
15 American Public Health Association, American Water Works Association and Water Pollution Control Federation, Standard Methods for the Examination of Water and Wastewater, 14th edn., American Public Health Association, New York, 1975, p. 412.
16 B. F. Reis, E. A. G. Zagatto, A. O. Jacintho, F. J. Krug and H. Bergamin F°, Anal. Chim. Acta, 119 (1980) 305.
17 M. F. Giné, H. Bergamin F°, E. A. G. Zagatto and B. F. Reis, Anal. Chim. Acta, 114 (1980) 191.

Analytica Chimica Acta, 151 (1983) 49—63
Elsevier Science Publishers B.V., Amsterdam — Printed in The Netherlands

AUTOMATIC POTENTIOMETRIC TWO-PHASE TITRATION IN PHARMACEUTICAL ANALYSIS
Part 2. Determination of Amine Salts, Amines and Related Compounds[a]

PER-ARNE JOHANSSON*, ULF STEFANSSON and GUN HOFFMANN
Astra Pharmaceutical Production AB, Analytical Control, S-151 85 Södertälje (Sweden)

(Received 7th December 1982)

SUMMARY

Acid—base equilibria for amines, A, in liquid—liquid two-phase systems are discussed on the basis of conditional acidity constants, K^*_{HA}. The K^*_{HA} value can be regulated by utilizing different distribution equilibria such as base extraction of A and ion-pair extraction of HA^+. Differentiating titrations and leveling of the acid—base strength in a two-phase system are also discussed. The presence of hydrophobic anions or cations in the aqueous phase reduced the background noise in the electrode signal and automatic titrators could therefore be used in all two-phase titrations. Amine salts, amines and some related compounds were titrated in different samples (reaction mixtures, bulk drug substances and preparations) with sodium hydroxide or sulphuric acid, either directly or after liquid—liquid extraction of the amine. The results were in agreement with theoretical calculations based on the titration error as well as with results obtained by other methods.

Amine salts and related compounds (salts of alkaloids or heterocyclic nitrogen compounds) used as drugs are mostly determined by non-aqueous acid—base titration with perchloric acid [1, 2] or by two-phase titration with lipophilic anions such as dioctyl sulphosuccinate [3, 4], dodecyl sulphate [5, 6], picrate [7, 8], and tetraphenylborate [9] as titrants. These methods are based on quite different properties, i.e., the acid—base strength of the amine and the lipophilic character of the ammonium ion, and so they will have different selectivity. Two-phase titration makes it possible to determine one of the amines in a mixture of homologues [5] while non-aqueous titration will only give the sum of the amines.

Titration methods where both the acid—base and the lipophilic properties of the amine (or the related compound) are utilized have also been reported. The determination of an amine salt may illustrate the principle. The salt is dissolved in water and an immiscible organic solvent is added. The two-phase system is then titrated, during vigorous shaking or stirring, with sodium hydroxide, to a visual [10—14] or potentiometric [15—17] end-point.

[a]This work was presented in part at Euroanalysis III (Dublin 1978), Euroanalysis IV (Helsinki 1981) and at the Analytical Days (Lund 1982).

0003-2670/83/$03.00 © 1983 Elsevier Science Publishers B.V.

Amines can be titrated in an analogous manner with hydrochloric or sulphuric acid [18, 19]. One drawback of most two-phase titration methods, however, is that they are rather time-consuming because it is often necessary to wait for the phases to separate between the additions of titrant. This may also explain why most two-phase titrations have been done manually; the use of automatic titrators seems to have been very limited so far.

One of the aims of the present paper is to demonstrate that potentiometric two-phase titrations can be done automatically. The background noise from the electrodes can be reduced if hydrophobic anions or cations are present in the aqueous phase. These ions also affect the acid—base equilibrium by extracting the sample ions as ion-pairs into the organic phase. The latter is very important because it offers an opportunity to manipulate the conditional acidity constant ("apparent K_a value") in a suitable direction so that selective titrations become possible.

THEORY

The symbols and definitions are basically the same as those used in Part 1 of this series [20]; additions and alterations are given in Table 1. In the treatment below the distribution of the amine as base or ion-pair into the micellar phase has been omitted. The error introduced by the simplification is assumed to be negligible for the compounds and organic phases used in the present work [20].

In most amine salts the ammonium ion, HA^+, is too weak an acid to be titrated in aqueous solution with sodium hydroxide. The equilibrium $HA^+ + H_2O = H_3O^+ + A$ can, however, be displaced to the right if the base, A, is

TABLE 1

Symbols used[a]

A and D	Amines in unprotonated form
X^-	Aprotic anion
HZ^-	Ampholytic anion
Q^+	Aprotic cation
$[A]$ and $[A]_o$	Molar concentrations of A in aqueous and organic phase, respectively.
$[OH^-]_{eq}$ and $[OH^-]_{end}$	Molar concentration of OH^- at the equivalence point and end-point, respectively.
$C'_{HA,eq}$ and $C'_{HA,end}$	Molar concentration of C'_{HA} at the equivalence point and end-point, respectively.
$\Delta pH = \log [OH^-]_{end} - \log [OH^-]_{eq}$	Error in locating the equivalence point of the titration.
$K_{ex(HAX)} = [HAX]_o ([HA^+] [X^-])^{-1}$	Extraction constant for HAX.
e_{rel}	Relative titration error.
r	Volume of organic to aqueous phase (phase ratio).

[a] Additions or alterations to those given in Part 1 of this series.

extracted to an organic phase [14]. If an aprotic anion, X^-, is present, ion-pair extraction according to $HA^+ + X^- = HAX_o$ may also take place. Consequently, two opposing reactions must be considered for the protolysis of HA^+ in a two-phase system.

A convenient way of treating this quantitatively is to use a conditional acidity constant:

$$K^*_{HA} = K'_{HA}\alpha_A/\alpha_{HA} \quad (1)$$

where $\alpha_A = 1 + rK_{D(A)}$ (2)

and $\alpha_{HA} = 1 + rK_{ex(HAX)}[X^-]$ (3)

According to Eqn. (1), HA^+ will become an apparently stronger acid in the two-phase system if $\alpha_A/\alpha_{HA} > 1$ and an apparently weaker acid if $\alpha_A/\alpha_{HA} < 1$. Thus by varying r, $K_{D(A)}$, $K_{ex(HAX)}$, and $[X^-]$, it should be possible to regulate K^*_{HA} within relatively wide limits so that optimal conditions for the titration of HA^+ or A are obtained.

Leveling of the acid—base strength

When $rK_{D(A)} \gg 1$ and $rK_{ex(HAX)}[X^-] \gg 1$ in Eqns. (2) and (3), the α_A/α_{HA} ratio will assume the form

$$\alpha_A/\alpha_{HA} = K_{D(A)}/(K_{ex(HAX)}[X^-]) \quad (4)$$

Because the $K_{D(A)}$ and $K_{ex(HAX)}$ values increase by about 0.6 log units for each CH_2 group introduced into the amine [21, 22] there will be no further increase in the K^*_{HA} value with increasing number of CH_2 groups in the amine, as long as Eqn. (4) is valid and $[X^-]$ is constant.

When X^- in the salt HAX is lipophilic this "leveling effect" can be suppressed by adding an aprotic cation, Q^+, to the system. The reaction $Q^+ + X^- = QX_o$ will then take place and $[X^-]$ will be lowered, which means that the condition $rK_{ex(HAX)}[X^-] \gg 1$ will no longer be valid (cf. Eqn. 3). It should be pointed out that the anion of the Q^+ salt added to the aqueous phase (e.g., chloride) can also be extracted into the organic phase as ion-pairs with HA^+. The effects of the addition of the QCl salt on the α_{HA} value can therefore be illustrated by the equation

$$\alpha_{HA} = 1 + rK_{ex(HACl)}[Cl^-] + rK_{ex(HAX)}[QX]_o/(K_{ex(QX)}[Q^+]) \quad (5)$$

which was obtained from Eqn. (3) by substituting $[X^-] = [QX]_o/(K_{ex(QX)}[Q^+])$ and including the $K_{ex(HACl)}[Cl^-]$ term. Because α_{HA} decreases with increasing $[Q^+]$ but increases with increasing $[Cl^-]$, this means that the $K_{ex(HACl)}[Cl^-]$ term may dominate over the last term in Eqn. (5) at high concentrations of QCl. Accordingly, it is not certain that $\alpha_{HA} = 1$, even though the extraction of HAX has been counteracted.

Titration error

The titration error can be derived by using the Ringbom—Wänninen approach [23, 24], which is illustrated below for the titration of the amine salt, HAX, with sodium hydroxide in a liquid—liquid two-phase system.

At the equivalence point, EP, the condition $C^0_{HA} = C_{OH^-}$ is valid. After combination with the total concentration of HA^+, $C^0_{HA} = C'_{HA} + C'_A$ and the proton balance expression $[H_3O^+] + C_{OH^-} = C'_A + [OH^-]$, this condition assumes the form

$$[H_3O^+] + C'_{HA} = [OH^-] \tag{6}$$

For the situation when $C'_{HA} \gg [H_3O^+]$ in Eqn. (6) the relative titration error, e_{rel}, is given by

$$e_{rel} = ([OH^-]_{end} - C'_{HA,end})/C^0_{HA} \tag{7}$$

where $[OH^-]_{end}$ and $C'_{HA,end}$ denote the concentrations of OH^- and $HA^+ + HAX_o$ at the end-point of the titration. By using the approximations $a_{H^+} = [H_3O^+]$ and $C^0_{HA} = C'_{A,eq}$, Eqn. (7) can be transformed [23] to

$$e_{rel} = 4.6\Delta pH(K^c_w)^{1/2}\,(K^*_{HA}C^0_{HA})^{-1/2} \tag{8}$$

which is valid for $\Delta pH \leqslant 0.4$.

A similar equation is obtained for the case in which $C'_{HA} \ll [H_3O^+]$ in Eqn. (6) and is given in Table 2. The relative titration errors for some other titrations of amine salts and amines were also derived and are included in the table. The magnitude of K^*_{HA} necessary for a titration error $<0.1\%$ is shown in Table 3 for some different titrations. According to the table, a pK^*_{HA} value of less than 7.1 is needed in order to titrate an amine salt with sodium hydroxide under the specified conditions.

EXPERIMENTAL

Apparatus

The following automatic titrators were used in the two-phase titrations: TTT60/REC61/ABU13/PHM61 (Radiometer A/S) with a modified stirrer [25], MemoTitrator DL40 (Mettler Instruments AG), and Titroprocessor 636/Rod Stirrer 622 (Metrohm AG).

The instruments were provided with the usual glass and calomel electrodes for aqueous titrations (G202B/K401, DG11 and EA121H, respectively). In some titrations the saturated KCl solution in the salt bridge (K401) was replaced by 0.1 M NaCl in order to avoid the potential shifts that can occur when these electrodes are used in surfactant solutions [20]. A Cary 219 (Varian) spectrophotometer was used for the spectrophotometric measurements.

Chemicals and reagents

The amine and alkaloid salts and lidocaine were of pharmacopoeial grade. Hexadecylpyridinium chloride (HPC) and sodium dodecyl sulphate (SDS) were obtained from different sources (Fluka, Merck and Serva). The salts should be free from protolytic impurities (e.g., pyridinium hydrochloride); this was checked by acid—base titration before use. Sodium octyl, decyl and

TABLE 2

Relative titration errors for different titrations of amine salts and amines
(The e_{rel} expressions were derived according to the same principles as those leading to Eqns. (6—8), assuming that $pK^*_{HD} > pK^*_{HA}$)

Species titrated	Species present	EP condition (cf. Eqn. 6)	$e_{rel} \times (4.6 \times \Delta pH)^{-1}$
HA^{+a}	—	$C'_{HA} = [OH^-]$	$(K^c_w)^{1/2}(K^*_{HA}C^0_{HA})^{-1/2}$
HA^{+a}	—	$[H_3O^+] = [OH^-]$	$(K^c_w)^{1/2}(C^0_{HA})^{-1}$
HA^{+a}	HD^+	$C'_{HA} = C'_D$	$(K^*_{HD}C^0_{HD})^{1/2}(K^*_{HA}C^0_{HA})^{-1/2}$
HA^{+a}	HD^+	$[H_3O^+] = C'_D$	$(K^*_{HD}C^0_{HD})^{1/2}(C^0_{HA})^{-1}$
H_3O^{+b}	HA^+	$[H_3O^+] = C'_A$	$(K^*_{HA}C^0_{HA})^{1/2}(C^0_{H_3O^+})^{-1}$
D[c]	—	$C'_D = [H_3O^+]$	$(K^*_{HD})^{1/2}(C^0_{HD})^{-1/2}$
D[c]	—	$[H_3O^+] = [OH^-]$	$(K^c_w)^{1/2}(C^0_{HD})^{-1}$
D[c]	A	$C'_D = C'_{HA}$	$(K^*_{HD}C^0_{HD})^{1/2}(K^*_{HA}C^0_{HA})^{-1/2}$
D[c]	A	$[OH^-] = C'_{HA}$	$(K^c_wC^0_{HA})^{1/2}(K^*_{HA})^{-1/2}(C^0_{HD})^{-1}$
OH^{-b}	D	$C'_{HD} = [OH^-]$	$(K^c_wC^0_{HD})^{1/2}(K^*_{HD})^{-1/2}(C^0_{OH^-})^{-1}$

[a] $HA^+ + HAX_o$. [b] Back-titration of A and HD^+, respectively. [c] $D + D_o$.

tetradecyl sulphate (for tenside test, Merck) were used as obtained. Deionized water which had been deaerated with a stream of nitrogen was used in the preparation of the solutions of the surfactants and the quaternary ammonium compounds.

Chloroform (p.a.) was washed with several portions of water before use in order to remove ethanol. 4-Methyl-2-pentanone (MIBK; p.a.) was shaken with 1 M sodium carbonate and then several times with water in order to remove any acidic impurity. Tri-n-hexyl- and tri-n-octylamine (Fluka) were both of "pract." quality; all other chemicals and reagents were of analytical grade.

TABLE 3

Limiting values of the constants giving a relative titration error $\leqslant 0.1\%$
(The values were calculated by using the equations given in Table 2 and the following assumptions: $pK^*_{HD} > pK^*_{HA}$, $pK^c_w = 13.9$, $C^0_{HA} = C^0_{HD} = 0.03$, $C^0_{H_3O^+} = C^0_{OH^-} = 0.01$, and $\Delta pH = 0.1$)

Species titrated	Species present	Limiting value of			
		pK^*_w	pK^*_{HA}	pK^*_{HD}	$pK^*_{HD} - pK^*_{HA}$
H_3O^+ or OH^-	—	$\geqslant 8.37$	—	—	—
HA^+	—	—	$\leqslant 7.05$	—	—
HA^+	HD^+	—	—	$\geqslant 6.85$	$\geqslant 5.33$
H_3O^{+a}	HA^+	—	$\geqslant 7.80$	—	—
D	—	—	—	$\geqslant 6.85$	—
D	A	—	$\leqslant 7.05$	—	$\geqslant 5.33$
OH^{-a}	D	—	—	$\leqslant 6.10$	—

[a] Back-titration of A and HD^+, respectively.

Determination of equilibrium constants

The conditional acidity constants (pK^*_{HA} — values) were determined by potentiometric titrations as described earlier [25]. The pH values were measured in the emulsions during vigorous stirring when surfactants were present. The drift of the electrode system amounted to 0.03—0.07 pH during these titrations, even though 0.1 M NaCl was used in the salt bridge [20].

The conditional extraction constant and critical micelle concentration (c.m.c.) for HPC were determined as described earlier [21, 26] using $C^0_Q = C^0_{Cl} = 2 \times 10^{-5}$—0.1 M. The concentration of HPC in the organic phase (dichloromethane) was measured by spectrophotometry.

Titration procedures for 1:1 amine salts

Use a 2.5—10 ml burette and titrate during vigorous stirring. Protect the two-phase system from atmospheric carbon dioxide by blowing a very gentle stream of nitrogen over the emulsion.

Bulk drug substances. Weigh (2—8) $\times 10^{-4}$ mole of the sample into the titration vessel. Add 20.0 ml of aqueous phase (0.05 M HPC) and 20.0 ml of organic phase (dichloromethane). Titrate with 0.1 M sodium hydroxide.

Preparations. Weigh tablet powder, whole tablets, or sample solution corresponding to (3—12) $\times 10^{-4}$ mole of the amine salt into a 50-ml centrifuge tube. Add 30.00 ml of dichloromethane and 10.0 ml of 0.2 M sodium hydroxide. Shake mechanically for 2—20 min; use the longer extraction time for whole tablets or Durules powder. Separate the phases by centrifugation or by the use of a hydrophobic filter paper (Whatman 1PS). Transfer 20.00 ml of the organic phase to the titration vessel and add 20.0 ml of aqueous phase (0.05 M SDS). Titrate with 0.1 M hydrochloric acid or 0.05 M sulphuric acid.

RESULTS AND DISCUSSION

Regulation of the K^*_{HA} value

The K^*_{HA} value can be changed by varying either α_A or α_{HA} whilst the other factor in the α_A/α_{HA} ratio is kept constant (cf. Eqn. 1). Examples of the regulation of K^*_{HA} by changing α_A are shown in Figs. 1 and 2; Figs. 3—6 give some examples of the regulation of K^*_{HA} through α_{HA}.

The α_A value. According to Eqn. (2), α_A is a function of $K_{D(A)}$ and r, and α_A will therefore depend on both the nature and the volume of the organic phase. Figure 1 shows that relatively large changes of K^*_{HA} can be obtained simply by choosing a different organic phase. It can also be seen that the presence of a micellar phase decreases the pK^*_{HA} value (curve B) but the effect on K^*_{HA} is much larger with an organic phase (Curves C—G). In addition to the organic phases shown in Fig. 1, two-phase titrations were also examined with n-butyl acetate, chloroform, MIBK, and n-octanol. Smooth titration curves were obtained in all cases with the exception of the titrations with the n-alcohols (Fig. 1, Curve F).

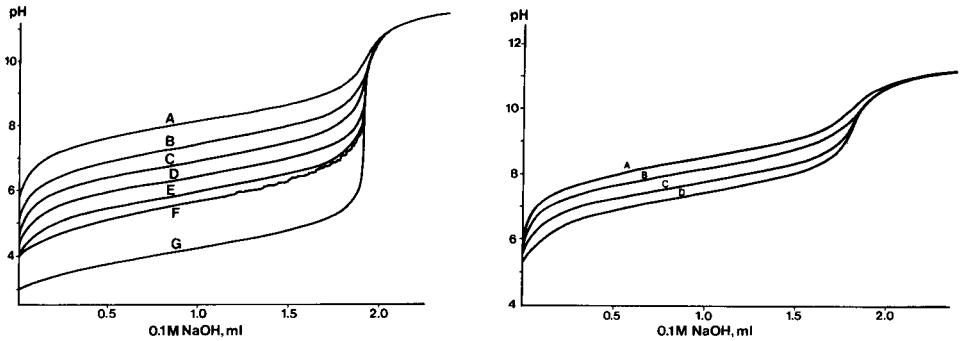

Fig. 1. Titration of lidocaine hydrochloride in the presence of different organic phases. Organic phase: (A) none; (B) 0.05 M HPC (micellar phase); (C) cyclohexane; (D) diethyl ether; (E) toluene; (F) n-pentanol; (G) dichloromethane. Aqueous phase: (A) water; (B–G) 0.05 M HPC.

Fig. 2. Titration of metoprolol tartrate at different phase ratios. Dichloromethane phase: (A) 3; (B) 6; (C) 15; (D) 30 ml. Aqueous phase: 30 ml of 0.05 M HPC.

The influence of r on K^*_{HA} is demonstrated in Fig. 2; a tenfold change in the volume of the organic phase gave a change of pK^*_{HA} with one log unit, which is in agreement with that predicted when $\alpha_{HA} = 1$ (Eqns. 1 and 2). For cases in which $rK_{D(A)} \gg 1$ and $rK_{ex(HAX)}[X^-] \gg 1$, however, K^*_{HA} will become independent of r (Eqns. 1 and 4). Phase ratios greater than unity were not used in the present work in order to avoid unstable pH meter readings [16].

The α_{HA} value. Equation (3) shows that α_{HA} is a function of r, $K_{ex(HAX)}$ and $[X^-]$; α_{HA} will therefore depend on the kind and concentration of X^-.

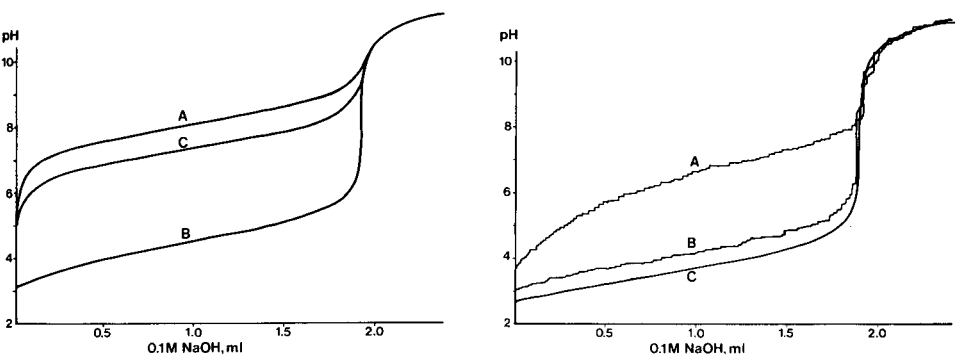

Fig. 3. Titration of lidocaine hydrochloride in the presence of different aqueous phases. Organic phase: (A) none; (B) and (C) dichloromethane. Aqueous phase: (A) water; (B) 0.05 M HPC; (C) 0.05 M SDS.

Fig. 4. Titration of dextropropoxyphene napsylate in the presence of different hydrophobic cations (Q^+) in the aqueous phase. Organic phase: dichloromethane. Aqueous phase: (A) no Q^+ salt present; (B) 0.1 M tetra-n-butylammonium chloride; (C) 0.1 M HPC.

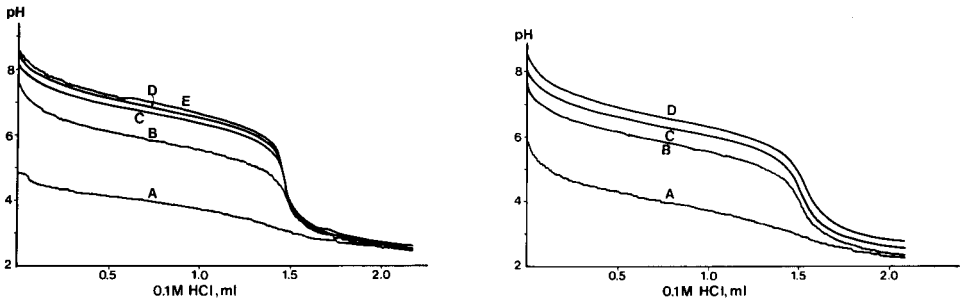

Fig. 5. Titration of lidocaine in the presence of different n-alkyl sulphates. Organic phase: dichloromethane. Aqueous phase: (A) no alkyl sulphate present; (B) octyl; (C) decyl; (D) dodecyl; (E) tetradecyl sulphate, all as 0.05 M sodium salts.

Fig. 6. Titration of lidocaine in the presence of different concentrations of octyl sulphate. Organic phase: dichloromethane. Aqueous phase: (A) 0; (B) 0.05; (C) 0.20; (D) 0.50 M sodium octyl sulphate (c.m.c. = 0.13 M [27]).

The use of r in the α_{HA} equation for the regulation of K^*_{HA} appears to be fairly limited, however, as this presupposes that $\alpha_A = 1$ (Eqns. 1—4). Figure 3 illustrates the effect of the $K_{ex(HAX)}[X^-]$ term on the α_{HA} and K^*_{HA} values; an increase in the pK^*_{HA} value of about 3 log units was obtained simply by changing the aqueous phase (Curves B and C). The increase in the pK^*_{HA} value is due to the extraction of lidocaine (HA^+) as an ion-pair with dodecyl sulphate (X^-) into the organic phase.

In certain titrations, it may be of interest to decrease the α_{HA} value. Figure 4 shows such a case; the interference of an extractable ion was counteracted by adding a lipophilic aprotic cation, Q^+, to the aqueous phase. In this case, the $rK_{ex(HAX)}[X^-]$ term in Eqn. (3) assumes a smaller value because $[X^-]$ has decreased owing to the reaction $Q^+ + X^- = QX_o$, as mentioned above under Theory.

Figures 5 and 6 show that α_{HA}, and thus K^*_{HA} also, can be varied by $K_{ex(HAX)}$ and $[X^-]$. Because log $K_{ex(HAX)}$ increases by about 0.6 log units per CH_2 group in HA^+ or X^- [21, 22], it might be expected that the titration curves in the presence of the C_8—C_{14} alkyl sulphates in Fig. 5 should be approximately 1 pH unit apart. This seems to be valid only for the C_8 and C_{10} alkyl sulphates (Curves B and C); for the higher alkyl sulphates (Curves C—E) the difference in the pK^*_{HA} values was much smaller. A likely explanation is that $[X^-]$ decreases with increasing number of alkyl groups owing to micelle formation; the c.m.c. values for the C_{12} and C_{14} alkyl sulphates (8×10^{-3} and 2×10^{-3} M, respectively [27]) are much lower than C^o_X (i.e., 0.05 M). It should be mentioned that some undissolved sodium tetradecyl sulphate was present during the titration (Curve E) and this may have affected the shape of the titration curve.

Figure 6 demonstrates that α_{HA} increases (K^*_{HA} decreases) with increasing $[X^-]$ (Curves A and B), and that $[X^-] \approx$ c.m.c. $\approx$ constant, when $C^o_X \gg$ c.m.c.

(Curves C and D). The fact that the titration curves do not coincide after the EP is probably due to the formation of octyl sulphuric acid [20].

Leveling effect and differentiating titrations

Some examples of the leveling of the acid—base strength in a two-phase system are shown in Table 4 and in Fig. 7. According to the pK^*_{HA} values in Table 4, it should be possible to determine both amines in an equimolar mixture of triethylamine and tri-n-butylamine when 0.025 M chloride is present. Such a determination cannot be made, however, if 0.025 M picrate is also present unless special titration techniques and evaluation procedures are used. The greater leveling effect obtained in the presence of picrate is due to its higher lipophilicity; the log $K_{ex(HAX)}$ values for tri-n-butyl ammonium chloride and picrate are 0.75 [25] and 6.51 [21], respectively.

The differentiating ability of a liquid—liquid two-phase system is demonstrated in Fig. 8. Two distinctive breaks are obtained in the two-phase system although the ammonium ions have nearly the same pK'_{HA} values. A further example is given in Fig. 9 which shows the determination of diethylamine and lidocaine in a reaction mixture. When a non-aqueous titration in a toluene/acetic acid medium was done, only the sum of the amines could be determined. With a two-phase system of toluene and 0.05 M SDS, however, breaks in the titration curves were obtained for each amine.

Most of the pharmacopoeial methods for the assay of amine and alkaloid salts are based on non-aqueous titration with perchloric acid and measure the sum of HA^+ and A. This is due to the fact that HA^+ is usually converted to A before the titration, either by the addition of mercury(II) acetate [1] or by solvent extraction from an alkaline aqueous phase. The sum of HA^+ and A can also be measured by a single titration in a two-phase system (Fig. 10). In this case the titration is done in the presence of an excess of strong acid

TABLE 4

Leveling of acid—base strength by ion-pair extraction
(Temperature 20°C, ionic strength 0.1)

Amine	pK'_{HA}[a]	pK^*_{HA}		
		Dichloromethane		Toluene
		$X^- = Cl^-$[b]	X^- = picrate[b]	$X^- = Cl^-$[c]
Triethyl-	10.98	9.54	11.31	—
Tri-n-propyl-	10.93	7.42	10.74	—
Tri-n-butyl-	10.20	5.91	10.76	—
Tri-n-hexyl-	10.2[d]	5.0[d]	10.7[d]	3.8
Tri-n-octyl-	10.2[d]	5.0[d]	10.7[d]	3.8

[a]Calculated from pK_a at 25°C [28] as described by Perrin et al. [29]. [b]From [21], $[X^-] = 0.025$ M. [c]From [30], $[X^-] = 1$ M, room temperature, ionic strength 1. [d]Estimated [21, 29] by using the K'_{HA}, $K_{D(A)}$ and $K_{ex(HAX)}$ values for tri-n-butylamine.

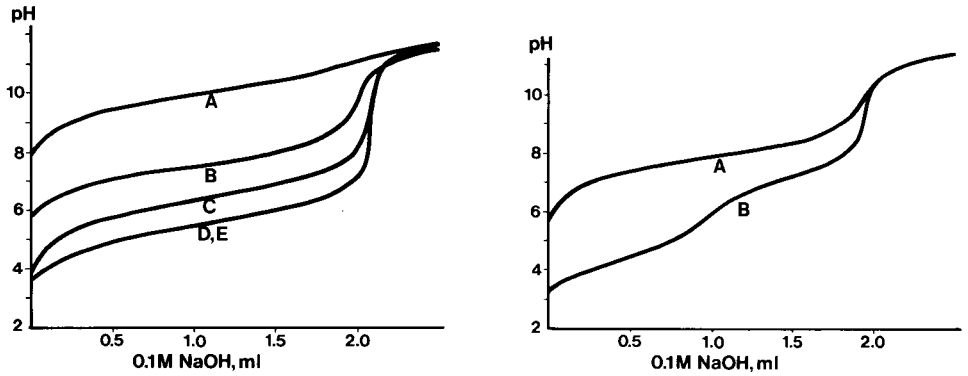

Fig. 7. Leveling of acid—base strength in a two-phase system illustrated by the titration of some tri-n-alkylamine hydrochlorides. Organic phase: dichloromethane. Aqueous phase 0.05 M HPC. (A) triethyl-, (B) tripropyl-, (C) tributyl-, (D) trihexyl-, (E) trioctylamine hydrochloride.

Fig. 8. Titration of an equimolar mixture of lidocaine hydrochloride and tocainide hydrochloride. (A) Aqueous solution, pK'_{HA} = 7.84 and 7.75; (B) Two-phase system (dichloromethane/0.05 M HPC), pK^*_{HA} = 4.27 and 6.94.

(e.g., hydrochloric acid) which will convert A to HA^+ (Curve B), and the difference between the two breaks is thus a measure of HA^+ + A. The dotted curves in Fig. 10 are from titrations of mixtures of HA^+ and A, and the solid curves are from titrations of HA^+ only (in the same total amount).

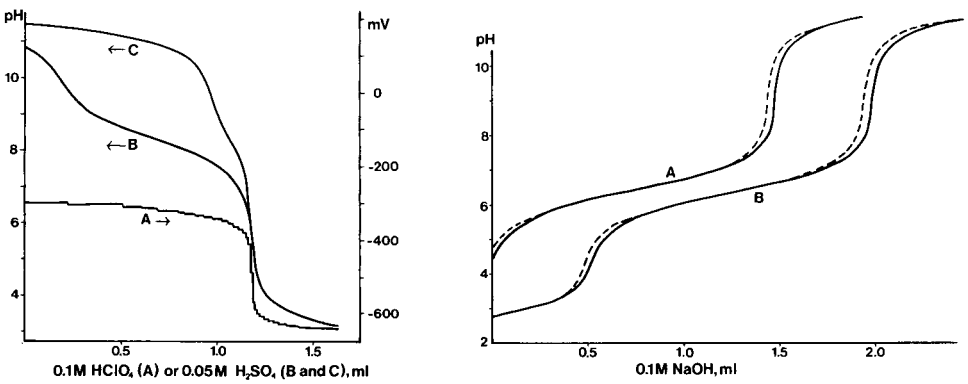

Fig. 9. Titration of mixtures of diethylamine and lidocaine in toluene. (A) Non-aqueous titration (1:1 toluene/anhydrous acetic acid) of 1.0×10^{-3} M diethylamine and 4.8×10^{-3} M lidocaine. (B) Two-phase titration (toluene/0.05 M SDS) of 1.0×10^{-3} M diethylamine and 4.8×10^{-3} M lidocaine. (C) As for (B) but 4.8×10^{-3} M diethylamine and 1.1×10^{-3} M lidocaine.

Fig. 10. Determination of the sum of lidocaine hydrochloride and lidocaine base. Organic phase: diethyl ether. Aqueous phase: (A) 0.05 M HPC; (B) 0.05 M HPC + HCl (2.5×10^{-3} M). Dotted lines: 3% of the hydrochloride converted to base (with NaOH) before titration.

Conditional acidity constants and titration errors

A comparison of some calculated and experimentally measured pK^*_{HA} values is given in Table 5. The good agreement between the two values indicates that the presence of the surfactants does not significantly affect the equilibria involved and that batch extraction data can be used in the estimation of K^*_{HA} values. A large number of pK^*_{HA} values is already available in the literature in the form of the composite constant, $\log K'_{HA}K_{D(A)}$ (see e.g. [21, 32]). This constant represents the situation when $\alpha_{HA} = 1$ and $\alpha_A = K_{D(A)}$ (Eqns. 1–3). Otherwise the pK^*_{HA} values can be calculated from available or estimated pK_a [29, 34], $K_{D(A)}$ [35, 36] and $K_{ex(HAX)}$ [37] values.

The equilibrium constants and relative titration errors for ten of the amine salts that were assayed in this work are given in Table 6. Some salts containing two or more acidic groups are also included in the table. The e_{rel} values for these salts were calculated according to the same principles as for the 1:1 or 2:1 salts; which of the K_{HZ}, K'_{HA}, and K^*_{HA} values that should be used in the calculations of e_{rel} was established from a $\log C^0_{HA}$ versus pH diagram [25, 40]. According to the e_{rel} values, it should be possible to determine the amine salts with an error of 0.3% or less by two-phase titration with sodium hydroxide as titrant.

The properties of Q^+ and X^- and the background noise of the electrodes

The addition of a Q^+ salt or a X^- salt to the two-phase system serves two purposes in most cases. First, they are used to form ion-pairs for manipulation of the K^*_{HA} value; secondly, some of these salts reduce the noise in the electrode signal during the titrations (see Figs. 4–6).

The influence of some Q^+ salts on the noise was studied in the following way: 0.01 M lidocaine hydrochloride was titrated, as described under Experimental, in the presence of 0.1, 0.01 and 10^{-3} M solutions of the aprotic salts in Table 7. Smooth titration curves were obtained in four of the

TABLE 5

Calculation of conditional acidity constants
(Organic phase: dichloromethane or chloroform. Aqueous phase: 0.05 M HPC or SDS. Temperature 25°C; ionic strength 0.01–0.1)

Amine	Phases	$-\log (K'_{HA} K_{D(A)})$	$\log K_{ex(HAX)}$		pK^*_{HA}	
			$X^- = Cl^-$	$X^- = DS$	Calc.[a]	Found
Hyoscyamine	SDS, $CHCl_3$	7.34[b]	—	5.34 [5]	10.38	10.41
Lidocaine	SDS, $CHCl_3$	3.95 [32]	−1.47 [32]	5.4 [5]	7.0	6.78
	SDS, CH_2Cl_2	4.12 [33]	—	—	—	6.92
	HPC, CH_2Cl_2	4.12 [33]	—	—	4.12	4.08
Metoprolol	HPC, CH_2Cl_2	7.12 [33]	—	—	7.12	7.16

[a]By use of Eqns. (1–3) and the $K'_{HA}K_{D(A)}$ and $K_{ex(HAX)}$ values, and $[X^-] = 0.045$ M (chloride) or 5×10^{-3} M (dodecyl sulphate [31]). [b]This work, cf. [25].

TABLE 6

Conditional acidity constants and relative titration errors for some amine salts
(Organic phase: dichloromethane; temperature 20 or 25°C; ionic strength 0.01—0.1)

Amine, A, and stoichiometry of the salt	X^- or HZ^-	pK_{H_2Z}	pK_{HZ}	pK'_{H_2A}	pK'_{HA}	pK^*_{HA}[a]	e_{rel}[b] (%)
Alprenolol (1:1)	Chloride	—	—	—	9.55 [38]	6.26 [25]	4.0×10^{-2}
Brompheniramine (1:1)	Hydrogenmaleate	1.92 [39]	6.23 [39]	3.93 [40]	9.31 [40]	5.15 [40]	3.8×10^{-2}[c]
Chloroquine (1:2)	Dihydrogenphosphate	2.15 [39]	7.20 [39]	8.1 [41]	10.8 [41]	6.2 [41]	0.11[c]
Dextrometorphan (1:1)	Bromide	—	—	—	7.98 [42]	4.50[d] [42]	5.3×10^{-3}[d]
Dextropropoxyphene (1:1)	Napsylate	—	—	—	—	3.20 [43]	1.2×10^{-3}
Hyoscyamine (2:1)	Sulphate	—	1.96 [39]	—	9.68 [34]	7.97 [33]	0.29
Lidocaine (1:1)	Chloride	—	—	—	7.84 [44]	4.27 [33]	4.1×10^{-3}
Metoprolol (2:1)	Tartrate	3.03 [39]	4.37 [39]	—	9.68 [33]	7.27 [33]	0.13
Tocainide (1:1)	Chloride	—	—	—	7.75 [44]	6.94 [44]	8.8×10^{-2}
Zimelidine (1:2)	Chloride	—	—	3.84 [40]	8.74 [40]	4.41 [40]	4.8×10^{-3}

[a]Calculated from the K'_{HA} and $K_{D(A)}$ values, given in the references, for $r = 0.7$. [b]Calculated (Table 2) using $pK^c_w = 13.9$, $C^0_{HA} + C^0_{HZ}$ or $2C^0_{HA} + C^0_{HZ} = 0.03$ M at the EP. [c]K^*_{HA} replaced by K_{HZ} in the calculations. [d]Organic phase, chloroform.

TABLE 7

Extraction constants, critical micelle concentrations and equilibrium concentrations of some aprotic salts in the aqueous phase
(Organic phase: dichloromethane)

Aprotic salt (QX)	log $K_{ex(QX)}$	c.m.c.	$[Q^+]^a$
Tetrabutylammonium chloride	−0.46 [45]	—	9.68×10^{-2}
Tetrapentylammonium chloride	2.18 [45]	—	2.26×10^{-2}
Tetrapentylammonium iodide	4.84 [45]	—	1.20×10^{-3}
Hexadecylpyridinium chloride	3.90[b]	5.7×10^{-4}[b]	≈c.m.c.
Decyltrimethylammonium bromide	0.33[c] [46]	6.5×10^{-2} [27]	≈c.m.c.
Hexadecyltrimethylammonium bromide	3.85[c] [46]	9.2×10^{-4} [27]	≈c.m.c.

[a]When $C_Q^0 = C_X^0 = 0.1$. [b]This work: earlier value for c.m.c. is 9×10^{-4} [27]. [c]Organic phase: 1,2-dichloroethane.

cases in which $C_Q^0 = 0.1$; exceptions were tetrabutylammonium chloride and tetrapentylammonium iodide. At $C_Q^0 = 10^{-3}$ M, all of the curves were "noisy" and at $C_Q^0 = 0.01$ M only hexadecyltrimethylammonium bromide gave smooth titration curves.

A high concentration of Q^+ in the aqueous phase is also favourable for the titration of amine salts which contain hydrophobic anions (Eqn. 5). This limits the suitable Q^+ salts to chloride or bromide salts because iodide extracts Q^+ more readily to the organic phase, cf. the $[Q^+]$ values in Table 7. The surfactant salts are less suitable as reagents because they form micelles in the aqueous phase, which reduces $[Q^+]$ to c.m.c. (approximately). Thus HPC

TABLE 8

Determination of amine salts in bulk
(Titrant: 0.1 M sodium hydroxide. Aqueous phase: 0.05 M HPC. Organic phase: dichloromethane)

Amine salt	Assay (%)	
	2-phase titn.	Other titn.[a]
Alprenolol HCl	99.8, 99.7	99.6, 99.6
Brompheniramine maleate	100.3, 100.6	100.3, 100.2
Chloroquine phosphate	97.9, 98.4	97.5, 97.6
Dextrometorphan HBr	100.1, 99.8	100.1, 100.0
Dextropropoxyphene napsylate	99.8, 99.7	99.2, 99.1
Hyoscyamine sulphate	97.8, 97.9	97.5, 97.1
Lidocaine HCl	99.9, 100.0	100.0, 100.0
Metoprolol tartrate	99.8, 99.9	99.8, 99.7
Tocainide HCl	100.1, 100.2	99.6, 99.7
Zimelidine 2HCl	99.9, 99.6	100.2, 100.3

[a]Non-aqueous titration ($HClO_4$) in most cases.

TABLE 9

Determination of amines and amine salts in different preparations
(Titrant: 0.05 M sulphuric acid, Aqueous phase: 0.05 M SDS. Organic phase; dichloromethane. The amine salts were converted to the amines by solvent extraction before the titrations)

Preparation	Amine or amine salt	Nominal content[a]	Assay[a]	
			2-phase titn.	Other method[b]
Durules	Metoprolol tartrate	200	200, 201	191, 196
Injections	Mepivacaine HCl	20	19.8, 19.6	20.9
Ointment	Lidocaine	50	49.8, 49.6	49.7, 49.9
Tablets	Chloroquine phosphate	160	157, 156	151, 149
Tablets	Metoprolol tartrate	50	50.4, 50.5	50.2, 50.3
Tablets	Metoprolol tartrate	100	98.7, 98.6	98.8, 99.1
Viscous solution	Lidocaine HCl	20	20.3, 20.3	19.3, 19.7

[a]Mg g^{-1}, mg ml^{-1} or mg/tablet. [b]Non-aqueous titration ($HClO_4$) or spectrophotometry.

and SDS are not ideal for forming ion-pairs but were chosen as reagents because they are commercially available in a very pure form and at low cost.

Applications

The two-phase titration technique was applied to the determination of amines and amine salts in reaction mixtures (Fig. 9), bulk drug substances (Table 8), and pharmaceutical preparations (Table 9). In addition to the amine salts in Table 8, the following compounds were also titrated successfully: disopyramide phosphate, quinidine bisulphate and the hydrochlorides of bromhexine, bupivacaine, etidocaine, hydroxizine, mepivacaine, metixene, prilocaine, promethazine and protipendyl.

A paired comparison test [47] using the results from 59 duplicate determinations (21 different amine salts, 1—8 batches titrated for each amine salt) indicated that there is no systematic difference between the two-phase titration and the commonly used methods. The precision of the two-phase titration method also seems to be of the same order as that of the other methods; a variance ratio test [47] indicated that there is no difference in the variances of the methods. The variances of the methods correspond to a relative standard deviation of ±0.2%. The results are thus in agreement with the calculated values ($\leqslant$0.3%, Table 6), indicating that the e_{rel} calculations can be useful in the selection of titration conditions.

REFERENCES

1 C. W. Pifer and E. G. Wollish, Anal. Chem., 24 (1952) 300.
2 O. Budevsky, Foundations of Chemical Analysis, Wiley, New York, 1979, Ch. 7.
3 C. A. Johnson and R. E. King, J. Pharm. Pharmacol., 15 (1963) 584.
4 F. Pellerin, J.-A. Gautier and D. Demay, Ann. Pharm. Fr., 24 (1966) 675.

5 S. O. Jansson, R. Modin and G. Schill, Talanta, 21 (1974) 905.
6 J. Novotná and J. Šubert, Farm. Obz., 47 (1978) 201.
7 I. A. Gur'ev and T. S. Vyatchanina, Zh. Anal. Khim., 34 (1979) 976.
8 H. Y. Mohammed and F. F. Cantwell, Anal. Chem., 51 (1979) 1006.
9 M. Tsubouchi, H. Mitsushio, N. Yamasaki and Y. Matsuoka, J. Pharm. Sci., 70 (1981) 1286.
10 A. B. Lyons, J. Am. Pharm. Assoc., 1 (1912) 525.
11 F. Reimers, Dan. Tidsskr. Farm., 5 (1931) 42.
12 F. A. Rotondaro, Am. J. Pharm., 107 (1935) 237.
13 R. H. Robinson and R. P. Tansey, J. Am. Pharm. Assoc., Sci. Ed., 39 (1950) 389.
14 T. Higuchi and J. I. Bodin, in T. Higuchi and E. Brochmann-Hanssen (Eds.), Pharmaceutical Analysis, Interscience, New York, 1961, Ch. 8.
15 K. Gustavii, P.-A. Johansson and A. Brändström, Acta Pharm. Suec., 13 (1976) 391.
16 A. Brändström, Acta Chem. Scand., B33 (1979) 731.
17 R. A. Hux, S. Puon and F. F. Cantwell, Anal. Chem., 52 (1980) 2388.
18 I. A. Gur'ev, G. M. Lizunova and I. M. Korenman, Fiz.-Khim. Metody Anal., 1 (1976) 78; Chem. Abstr., 88 (1978) 15573.
19 R. Jones and G. Marnham, J. Pharm. Pharmacol., 32 (1980) 820.
20 P.-A. Johansson, G. Hoffmann and U. Stefansson, Anal. Chim. Acta, 140 (1982) 77.
21 K. Gustavii, Acta Pharm. Suec., 4 (1967) 233.
22 K. C. Yeh and W. I. Higuchi, J. Pharm. Sci., 61 (1972) 1648.
23 A. Ringbom and E. Wänninen, in Treatise on Analytical Chemistry, I. M. Kolthoff and P. J. Elving (Eds.), Part 1, Vol. 2, 2nd edn., Wiley, New York, 1979, pp. 483—485.
24 E. Wänninen, Talanta, 27 (1980) 29.
25 P.-A. Johansson and K. Gustavii, Acta Pharm. Suec., 13 (1976) 407.
26 J. Czapkiewicz and B. Czapkiewicz-Tutaj, J. Colloid Interface Sci., 62 (1977) 524.
27 P. Mukerjee and K. J. Mysels, Critical Micelle Concentrations of Aqueous Surfactant Systems, Nat. Std. Ref. Data Ser., U.S. Nat. Bur. Std., 36 (1971).
28 F. M. Jones, III and E. M. Arnett, in A. Streitwieser, Jr. and R. W. Taft (Eds.), Progress in Physical Organic Chemistry, Vol. 11, Wiley, New York, 1974, p. 263.
29 D. D. Perrin, B. Dempsey and E. P. Serjeant, pK_a Prediction for Organic Acids and Bases, Chapman and Hall, London, 1981.
30 R. R. Grinstead in D. Dyrssen, J.-O. Liljenzin and J. Rydberg (Eds.), Solvent Extraction Chemistry, North Holland, Amsterdam, 1967, p. 426.
31 T. Sasaki, M. Hattori, J. Sasaki and K. Nukina, Bull. Chem. Soc. Jpn., 48 (1975) 1397.
32 G. Schill, R. Modin and B. A. Persson, Acta Pharm. Suec., 2 (1965) 119.
33 P.-A. Johansson and K. Gustavii, Acta Pharm. Suec., 14 (1977) 1.
34 D. D. Perrin, Dissociation Constants of Organic Bases in Aqueous Solution, Butterworths, London, 1965.
35 C. Hansch and A. J. Leo, Substituent Constants for Correlation Analysis in Chemistry and Biology, Wiley—Interscience, New York, 1979.
36 R. F. Rekker, The Hydrophobic Fragmental Constant, Elsevier, Amsterdam, 1977.
37 G. Schill, in J. A. Marinsky and Y. Marcus (Eds.), Ion Exchange and Solvent Extraction, Vol. 6, M. Dekker, New York, 1974, Ch. 1.
38 A. Brodin and M.-I. Nilsson, Acta Pharm. Suec., 10 (1973) 187.
39 A. Albert and E. P. Serjeant, The Determination of Ionization Constants, Chapman and Hall, London, 1971.
40 P.-A. Johansson, Acta Pharm. Suec., 14 (1977) 363.
41 G. Schill, Acta Pharm. Suec., 2 (1965) 13.
42 A. Michaelis and T. Higuchi, J. Pharm. Sci., 58 (1969) 201.
43 K. O. Borg, H. Holgersson and P. O. Lagerström, J. Pharm. Pharmacol., 22 (1970) 507.
44 P.-A. Johansson, Acta Pharm. Suec., 19 (1982) 137.
45 K. Gustavii and G. Schill, Acta Pharm. Suec., 3 (1966) 259.
46 B. Czapkiewicz-Tutaj and J. Czapkiewicz, Rocz. Chem., 49 (1975) 1353.
47 W. W. Daniel, Biostatistics: A Foundation for Analysis in the Health Sciences, Wiley, New York, 1974, Ch. 6.

Analytica Chimica Acta, 151 (1983) 65—75
Elsevier Science Publishers B.V., Amsterdam — Printed in The Netherlands

DETERMINATION OF CITRATE BY POTENTIOMETRIC TITRATION WITH COPPER(II) AND A COPPER ION-SELECTIVE ELECTRODE

ÅKE OLIN and BO WALLÉN*

Department of Analytical Chemistry, University of Uppsala, P.O. Box 531, S-751 21 Uppsala (Sweden)

(Received 1st April 1982)

SUMMARY

The potentiometric titration of citrate with copper(II) solution was studied at controlled pH in the concentration range 0.002—0.010 M. From measurements with a copper-selective electrode, it is concluded that the main reaction is $2\ Cu^{2+} + 2HCit^{3-} \rightleftharpoons Cu_2(Cit)_2^{4-} + 2\ H^+$ with $\log \beta_{2-22} = 5.2 \pm 0.1$ when the titration is done at pH 6—8. The appropriate Gran function was derived and used to obtain equivalence volumes that agreed within 0.2—0.4% with the theoretical values. Visual evaluation of the equivalence point from the titration curve gave less precise results; an automatic evaluation procedure (Metrohm Titroprocessor) gave results similar to those obtained with the Gran function. The influence of other complexing agents on the method was studied. A method for calibrating metal ion-selective electrodes is presented.

Titrimetric methods for the determination of citric acid and citrate have been based on complex formation between copper ion and citrate ion [1—3] in buffered solutions (boric acid/borate [1] or sodium hydrogencarbonate [2, 3]). The equivalence point has been established with an indicator [1] or from potentiometric titration curves obtained with a copper [2] or a silicone rubber-based copper(II)-selective [3] indicator electrode. The best reported precision was about 0.9%. In this paper, a titrimetric method employing a copper-selective electrode is described. In the titrations, equal increments of copper(II) solution were added stepwise and the sample solution was kept at constant pH by simultaneously running a pH-stat addition. Titration curves obtained at constant pH can be linearized as described by Gran [4], which considerably increases the precision of the results. As is also shown, the titration procedure, data acquisition and data processing can readily be automated.

THEORY

The copper citrate system

The various species that may be formed in mixtures of copper(II) and citrate ions and the differing values of the stability constants, illustrated by Table 1, give a confusing picture of this system. For some of the proposed

0003-2670/83/$03.00 © 1983 Elsevier Science Publishers B.V.

TABLE 1

Compilation of proposed copper citrate complexes, $Cu_pH_qL_r$, and their stability constants, log β_{pqr}($L^{3-} \equiv HCit^{3-}$)

β_{111}	β_{101}	β_{1-11}	β_{202}	$\beta_{2-2,2}$	Other β		Temp. (°C)	Medium (M)	Ref.
—	5.2	—	12.8	6.0	—		20	1 $NaClO_4$	5
—	—	—	13.2	5.2	—		25	1 KNO_3	6
9.1	5.9	1.6	—	—	β_{201}	8.1		0.1 $NaClO_4$	7
					β_{2-11}	5.0	20		
					β_{121}	12.3			
—	6.5	2.15	—	—	β_{121}	12.5	30	0.1 $NaNO_3$	8
—	3.09	—	—	—	—	—	—	0.2 $NaNO_3$	9
	3.95								
9.7	6.3	1.8	—	—	—		32	0.25 KNO_3	10
—	6.03	—	—	—	β_{102}	10.43	25	0.1 $NaClO_4$	11
9.31	—	1.61	14.72	—	—		25	0.1 KNO_3	12
9.27		1.64	15.03						
8.68	5.94	2.16	—	—	β_{102}	8.09	—	0.5 $NaNO_3$	13
					β_{121}	11.34			
—	4.40	—	—	5.30	β_{121}	11.20	25	2 M $NaClO_4$	14
					β_{102}	7.28			
					β_{112}	11.78			
					β_{122}	16.00			
					β_{132}	19.35			
					β_{142}	22.00			
					β_{2-21}	1.90			

equilibrium models, the corresponding distributions of added copper among the predominant complexes during a titration of 2×10^{-3} M citrate are presented in Table 2. The computations were done for the pH range 6—8 used in the complexiметric titrations. As some of the models are based on data obtained at lower pH values, the calculations in those cases involved an extrapolation. It can be concluded, however, that the following stoichiometries could form the basis for the citrate determination:

TABLE 2

Percentages of copper bound in the predominant complexes during the titration of a 2×10^{-3} M citrate solution at pH 6—8 according to various equilibrium models

CuL	CuL ($-H^+$)	Cu_2L_2	Cu_2L ($-H^+$)	Cu_2L ($-2H^+$)	Cu_2L_2 ($-2H^+$)	Ref.
—	—	—	—	—	100—99.9	6
2.1	97.9—97.0	—	0—0.7	—	—	7
	100—99.9	0—0.1	—	—	—	12
0.6	99.3—99.4	—	—	—	—	13
—	—	—	—	19.6—53.0	79.6—46.9	14

$$Cu^{2+} + HCit^{3-} \rightleftharpoons CuCit^{2-} + H^+ \quad (I)$$

$$2\,Cu^{2+} + 2\,HCit^{3-} \rightleftharpoons Cu_2(Cit)_2^{4-} + 2\,H^+ \quad (II)$$

The corresponding linearized titration curves (Gran functions) are derived below. Citric acid is denoted by H_3L. Reactions I and II both have a 1:1 combining ratio between copper and citrate, and liberate 1 mol of hydrogen ion per mole of copper(II) added, as stated by Ringbom [15].

The Gran functions valid before the equivalence point

For convenience, charges are dropped from ionic symbols. In the model, V_o ml of a citrate solution, of concentration C_o mol l^{-1} and kept at a constant pH 6—8 by addition of sodium hydroxide, is titrated with a copper solution of concentration C mol l^{-1}.

Case I. Mononuclear complex formation with the ratio Cu:L = 1:1. The mass-balance equations are

$$[Cu]^* = [Cu] + \sum [Cu\,H_x\,L] \quad (1)$$

$$[L]^* = \sum_{j=0}^{3} [H_j\,L] + \sum [Cu\,H_x\,L] \quad (2)$$

where the asterisks denote the total concentration of the species. Before the equivalence point, the concentration of free copper ion can be neglected. Above pH 6 the approximation $\Sigma [H_j\,L] \approx [L]\,(1 + K_1\,h)$ is valid, where h is the hydrogen ion concentration and $K_1 = [HL]/h\,[L]$. Accordingly, Eqn. (2) can be reduced to

$$[L] = ([L]^* - [Cu]^*)/(1 + K_1\,h) \quad (3)$$

Introduction of the expressions for the concentrations of the copper citrate complexes and insertion of [L] from Eqn. (3) allows the total concentration of copper ion to be described by

$$[Cu]^* = [Cu]\,([L]^* - [Cu]^*)\,k \quad (4)$$

where $k = \Sigma\beta_{1x1}h^x/(1 + K_1h)$ is a constant at constant pH. However, $[Cu]^* = VC/(V_o + V)$ and $[L]^* = V_oC_o/(V_o + V) = V_eC/(V_o + V)$, where V_e is the equivalence volume. Thus Eqn. (4) becomes

$$VC/(V_o + V) = k\,[Cu]\,(V_eC - VC)/(V_o + V) \quad (5)$$

Rearrangement of this equation yields

$$y = V/[Cu] = k\,(V_e - V) \quad (6)$$

A plot of $V \exp(-E/g)\,(\alpha y)$ vs. V should be linear and intercept the volume axis at $V = V_e$; E and g are the potential and the slope of the copper-selective electrode, respectively.

Case II. Binuclear complexes with the ratio Cu:L = 1. From the mass-balance equations

$$[Cu]^* = 2\Sigma[Cu_2H_xL_2] = VC/(V_o + V) \quad (7)$$

$$[L]^* = [L](1 + K_1h) + 2\Sigma[Cu_2H_xL_2] = V_eC/(V_o + V) \quad (8)$$

the following expressions can be derived in a fashion analogous to case *I*:

$$y = \{V(V_o + V)\}^{1/2}/[Cu] = k'(V_e - V) \quad (9)$$

where $k' = (2\Sigma\beta_{2x2}h^xC)^{1/2}/(1 + K_1h)$ is a constant. If only complexes of the assumed composition are formed, a plot of $\{V(V_o + V)\}^{1/2} \exp(-E/g)(\alpha y)$ should be linear and intercept the volume axis at $V_e = V$.

Calibration of the indicator electrode

When the Gran method is used to calculate the equivalence volumes in potentiometric titrations, the functional relationship between the measured e.m.f. and concentration must be known, and preferably Nernstian. Metal standard solutions (e.g., pCu 1—5) and metal buffers based on nitrilotriacetic acid (NTA) and EDTA as ligands (e.g., pCu 6—18) [16] have frequently been recommended for calibration of ion-selective electrodes. Direct potentiometry or standard additions can be used. The stability constants of the metal complexes and the relevant side-reaction coefficients must be known in the ionic medium used in order to establish the pCu scale. Still [17] has described a calibration procedure based on Gran's first method [18] for testing the response of the copper-selective Selectrode. This method does not assume knowledge of the stability constants and side-reaction coefficients as long as these are invariant during the procedure.

In the work described here, the response of the copper-selective indicator electrode was tested against a copper amalgam electrode, which was assumed to obey the Nernst equation. Metal buffer solutions covering the pCu range 4—9.5 were obtained by adjusting a solution of Cu(II) and NTA to different pH values and were used for the calibration. Unfortunately, the two copper electrodes cannot be placed together in the same solution, thus making a direct comparison impossible; some species dissolves from the amalgam and affects the copper-selective electrode despite rigorous exclusion of oxygen. Thus two separate runs were done: the e.m.f. values were measured in separate aliquots of the metal buffer solutions with the copper amalgam electrode or the Selectrode. The metal buffer solution also contained some acetate and hydrogenphosphate to increase the acid—base buffer capacity and so facilitate the necessary adjustment of pH.

EXPERIMENTAL

Reagents

All reagents were of analytical grade. A stock copper(II) solution (0.1 M) was prepared from copper(II) nitrate trihydrate and made slightly acidic with nitric acid. The stock solution was standardized by electrogravimetry and by complexiметric titration with EDTA. A stock solution of sodium

citrate (0.02 M) was prepared by weighing trisodium citrate dihydrate. All subsequent solutions of copper(II) and citrate were prepared by dilution of the stock solutions. A solution 5.00×10^{-3} M in nitric acid, and 2.50×10^{-3} M in copper(II) nitrate in the ionic medium was used for the E^0 determinations.

All solutions that were used in the titrations were made 0.50 M in nitrate by adding sodium nitrate.

Copper amalgam containing about 2% copper was prepared by electrolyzing a copper(II) sulphate solution with a mercury pool as cathode [19]. The amalgam was washed several times with 0.1 M perchloric acid under a nitrogen atmosphere and was finally stored in a round-bottomed flask (50 ml) under 0.1 M perchloric acid in a nitrogen atmosphere.

Apparatus

The e.m.f. values were measured with two digital voltmeters (Radiometer PHM 64) with a resolution of ±0.1 mV.

For the citrate titrations, the measuring system was based on the two digital voltmeters, a control unit (Radiometer TTT-60), two burets (Radiometer ABU-13 and Metrohm Dosimat), data communication units (Serdex Analog Device) and a desk calculator (Hewlett-Packard 9810) as an over-all control and data acquisition unit. The layout of the titration system is shown in Fig. 1. An Ingold saturated calomel electrode with a liquid junction tube filled with 0.50 M sodium nitrate was used as a reference electrode. The indicator electrodes were an Ingold glass electrode 401, a copper amalgam electrode and a copper-selective Selectrode (Radiometer). The copper amalgam electrode consisted of a pool of the amalgam on the bottom of the titration vessel with electrical contact established by a platinum wire. The surface of the Selectrode was prepared as described by Hansen et al. [16]. When not in use, the Selectrode was stored in 0.1 M EDTA. All measurements were made in a thermostatted room at 25 ± 0.5° C. The titration vessel was a

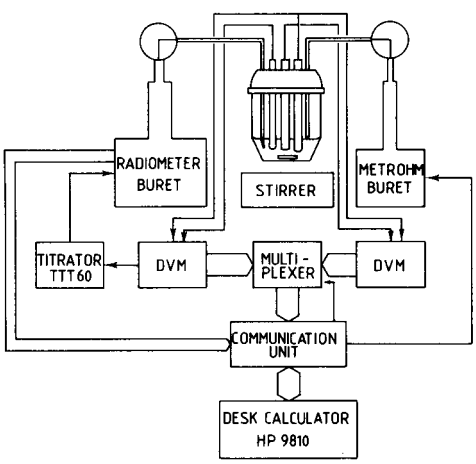

Fig. 1. The computer-controlled titration system.

Metrohm 50-ml glass vessel with a cover having seven holes for electrodes, burets and gas tubes. The solutions were mixed by bubbling with nitrogen and/or with a magnetic stirrer.

Procedures

Standardization. The $E^{0\prime}$ values of the electrodes were measured for the cell

SCE || 5.00×10^{-3} M H^+, 2.50×10^{-3} M Cu^{2+}, 0.50 M $(Na)NO_3$| Glass, Cu(Hg)

$E_{glass} = E^{0\prime}_{glass} + 59.16 \log h + E_j$; $E_{Cu(Hg)} = E^{0\prime}_{Cu(Hg)} - 29.58 \log [Cu^{2+}]$

Before the amalgam was added, the solution was bubbled with oxygen-free nitrogen. The e.m.f.'s were measured when the readings did not change during 15 min by more than 0.05 mV; this usually occurred after 30—40 min.

Calibration. An aliquot of a starting solution (see Table 3) was placed in the cell compartment. The glass and reference electrodes were immersed in the solution, which was then flushed with nitrogen before the amalgam was added. Oxygen-free copper buffer solution (Table 3) was added incrementally from a buret and the e.m.f.'s were measured when they were stable within ±0.1 mV for 5 min. The size of the copper buffer additions was controlled so that three additions covered about one pH unit (about 60 mV). The procedure was repeated with another aliquot of the starting solution and with the copper Selectrode instead of the copper amalgam electrode. Extreme care was exercised to reproduce the potentials of the glass electrode from the preceding titration.

Titration of citrate. The sample solution (25 ml) containing 10—50 mg of citrate was transferred to a titration vessel. The Selectrode, the glass

TABLE 3

Measurements with a Cu(Hg) electrode and a glass electrode [Starting solution: 2.625×10^{-3} M Cu^{2+}, 5.250×10^{-3} M NTA, 0.010 M sodium acetate, 0.010 M HPO_4^{2-}, 0.500 M NO_3^-. V_o = 25.04 ml. Copper buffer solution: 0.1006 M H^+, 2.625×10^{-3} M Cu^{2+}, 5.250×10^{-3} M NTA, 0.500 M NO_3^-. $E^{0\prime}_{glass}$ = 281.1 mV and $E^{0\prime}_{Cu(Hg)}$ = −77.0 mV]

E_{glass} (mV)	p*h*	$E_{Cu(Hg)}$ (mV)	pCu
−96.3	6.380	203.2	9.471
−73.4	5.993	191.4	9.072
−45.3	5.518	177.2	8.594
−3.9	4.818	156.6	7.896
23.3	4.358	143.0	7.436
44.5	4.000	132.2	7.071
73.5	3.510	117.4	6.570
102.0	3.029	102.0	6.053
118.9	2.745	92.2	5.720
129.6	2.566	85.4	5.489
143.3	2.338	75.6	5.161
164.0	1.999	58.8	4.589
186.7	1.640	38.4	3.903

electrode, the reference electrode and the buret tip from the ABU-13, containing a dilute sodium hydroxide solution, were immersed in the sample solution. If necessary, the pH of the sample solution was adjusted to an arbitrary pH value of 6—6.2 with dilute nitric acid. The tip from the buret containing the copper(II) titrant, was not allowed to dip into the sample solution (Fig. 1). The pH-stat, adjusted to some fixed pH value 6.2—6.5, was started and then the titration with the copper(II) solution was initiated from the desk calculator (HP 9810). The copper(II) solution was added automatically in 1.0-ml increments. After each addition, the system was allowed to attain equilibrium before the e.m.f. values and the titrant volumes were recorded.

RESULTS AND DISCUSSION

Calibration of the Selectrode

Representative e.m.f. data are given in the first and third columns in Tables 3 and 4. The compositions of the starting solution and the copper buffer solution were chosen so that the total concentration of Cu^{2+} and NTA were kept constant. The p*h* and pCu values given in Tables 3 and 4 were calculated from the above expressions for E_{glass} and $E_{Cu(Hg)}$. The p*h* values are included in the tables to indicate the p*h* range used and to show the differences in p*h* between the amalgam and Selectrode procedures. Before the slope of the calibration curve for the copper-selective electrode can be calculated, allowance must be made for these differences. The corrected e.m.f. of the electrode, E^*_{CuS}, was calculated from

$$E^*_{CuS} = E_{CuS} - 29.58 \log [h'(1 + K_2h' + K_2K_3h'^2)(1 + K^H_{CuHX}h) / h(1 + K_2h + K_2K_3h^2)(1 + K^H_{CuHX}h')] \quad (10)$$

TABLE 4

Measurements with a copper-selective Selectrode and a glass electrode. [Starting and copper buffer solutions are the same as in Table 3. $E^{o\prime}_{glass}$ = 280.6 mV and $E^{o\prime}_{CuS}$ = −363.4 mV.]

E_{glass} (mV)	p*h*	E_{CuS} (mV)	E^*_{CuS} (mV)	pCu
−96.5	6.375	−85.4	−85.2	9.471
−73.4	5.984	−96.8	−96.6	9.072
−45.4	5.511	−110.6	−110.4	8.594
−3.9	4.809	−131.2	−131.0	7.896
23.2	4.351	−145.0	−144.8	7.436
44.6	3.990	−156.0	−155.6	7.071
73.8	3.497	−171.2	−170.4	6.570
102.0	3.021	−186.6	−185.9	6.053
118.8	2.739	−196.4	−195.8	5.720
129.5	2.560	−203.2	−202.6	5.489
143.3	2.330	−212.6	−211.9	5.161
164.0	1.991	−229.4	−228.8	4.589
186.5	1.635	−250.3	−250.0	3.903

K_2 and K_3 are the second and third stepwise protonation constants of NTA (=X); K^H_{CuHX} is the protolytic stability constant of the acid complex CuHNTA; h and h' are the corresponding hydrogen ion concentrations in the Selectrode and amalgam procedures, respectively. The adjusted e.m.f. values of the Selectrode are entered in Table 4. A plot of E^*_{CuS} versus pCu gives a straight line. Linear regression yields a slope of 29.59 ± 0.05 mV/pCu and an intercept of 364.9 ± 0.3 mV.

The proposed method is well suited for a calibration over a wide range in pM and the results are only slightly affected by errors in stability constant values or solution composition. Liquid junction effects are also eliminated. The method is, however, more demanding and more time-consuming than the established procedure [16].

Titration of citrate

When the titration data (E_{CuS}, V) were inserted into Eqns. (6) and (9), respectively, only Eqn. (9) provided a linear plot and equivalence volumes close to the expected values. Therefore, it may be concluded that the main reaction during the titration of citrate with copper(II) at pH 6—8 occurs according to reaction II. The formation of a 1:1 $CuCit^{2-}$ complex as the main species is certainly not consistent with the present data.

Bottari [14] suggested two concurrent main reactions. As a test of this reaction scheme, theoretical titration data were generated by computer calculations based on Bottari's equilibrium constants. When these data were inserted into Eqns. (6) and (9), straight lines were not obtained and the equivalence volumes produced were far from the correct value. It can therefore be concluded that Bottari's model cannot be fitted to Eqn. (6) or (9).

Table 5 summarizes results obtained when Eqn. (9) was used to evaluate the citrate content of test solutions. The relative standard deviation (RSD) was 0.2% or better. A typical plot is shown in Fig. 2. All titrations were evaluated from titration data obtained in the V/V_e range 0.2—0.9. The time for a titration comprising nine points was about 60 min. There is a systematic trend to higher recoveries with increasing citrate concentrations. This might indicate that species other than $Cu_2(Cit)_2^{4-}$ are present in minor amounts.

TABLE 5

Determinations of citrate

Taken (mg)	Found[a] (mg)	Error (%)	RSD (%)
9.525	9.540	+0.16	0.2
23.97	24.05	+0.33	0.1
47.43	47.64	+0.44	0.1

[a] Average of five determinations.

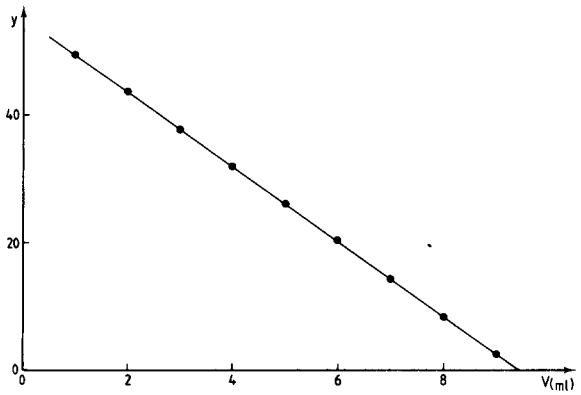

Fig. 2. The Gran function, $\{V(V_0 + V)\}^{1/2} \exp(-E/g)$, against V for the titration of a 2×10^{-3} M solution of citrate with 5×10^{-3} M Cu(II).

Interferences

The influence of other complexing agents in the sample on the accuracy of the citrate titration can be estimated from computer-simulated titration data in conjunction with Eqn. (9). For this purpose, the equilibrium constant of reaction II was evaluated from measurements with a copper-selective electrode at pH 6—8 and citrate concentrations of 0.002—0.010 M in 0.5 M sodium nitrate. On the assumption that only $Cu_2(Cit)_2^{4-}$ is formed, $\log \beta_{2-22} = 5.2 \pm 0.1$ was obtained. This value agrees well with the result of Rajan and Martell, who found $\log \beta_{2-22} = 5.2$ [6].

The error caused by a second ligand is a function of its concentration and stability constants and solution pH. This is illustrated in Table 6; the equivalence volumes were calculated in exactly the same way as for experimental data. Titrations of samples 2×10^{-3} M in citrate and 2×10^{-3} M in acetate ($\log \beta_1 \approx 1.8$), succinate ($\log \beta_1 \approx 2.6$) or oxalate ($\log \beta_2 \approx 5.6$) qualitatively corroborated the values in Table 6. At pH 6.2, acetate did not interfere and

TABLE 6

Calculated errors (%) for the titration of a solution that is 2.00×10^{-3} M in both citrate and a foreign anion X, with 5.00×10^{-3} M Cu(II) at different pH and for different stability constants of the CuX complex

$\log \beta_{CuX}$	Error (%)		
	At pH 6.0	At pH 7.0	At pH 8.0
1	+0.04	—	—
2	+0.02	—	—
3	+0.1	—	—
4	+0.7	+0.06	+0.01
5	+4.4	+0.6	+0.06
6	+22.0	+3.9	+0.5

the influence from succinate was just perceptible; oxalate caused an error of about 20%. The error dropped to 10% when the pH was raised to 7.2. At an oxalate concentration of 2×10^{-4} M, the error was 1% at pH 6.2. These measurements indicate that calculations based on the assumption that $Cu_2(Cit)_2^{4-}$ (with $\log \beta_{2-22} = 5.2$) is formed during the titration can adequately predict interferences from other complexing components.

Although the interferences decreased with increasing pH, titrations were generally done in the pH interval 6–6.5. At higher pH, the buffering capacity of the citrate solution is very low which makes titrations at constant pH difficult. Addition of an extra buffer would solve this problem but would probably cause competing reactions that would affect the accuracy when the Gran functions are used to determine equivalence volumes.

Determination of the equivalence volume from the titration curve

Citrate solutions (0.02—0.005 M) buffered to pH 8.0 with 0.1 M sodium hydrogencarbonate were also titrated. The equivalence volume was evaluated by estimation of the inflection point of the usual titration curve drawn manually or recorded automatically (Radiometer TTT-60/PHM 64, REC-61, ABU-13). Because of the drawn-out curves obtained, especially for concentrations below 0.01 M (cf. [3]), there was uncertainty in the location of the inflection point. The best precision obtained was about 1%.

When this work was almost complete, a Metrohm Titroprocessor E636 became available. This automatic titrator both records and evaluates titration curves. Titrations according to the procedure outlined above with this instrument gave a relative standard deviation of 0.1% for 5 titrations each of 0.02, 0.01 and 0.005 M citrate; the results were 0.3—0.4% higher than expected.

The authors thank Dr. R. Danielsson and G. Wikmark for constructing the titration system and for help with programming.

REFERENCES

1 G. Graffman, H. Domels and M. L. Sträler, Fette, Seifen, Anstrichmittel, 76 (1974) 218.
2 M. Hamon, A. Hoppenot and M. Guernet, Ann. Pharm. Fr., 30 (1972) 595.
3 M. F. El-Taras and E. Pungor, Anal. Chim. Acta, 82 (1976) 285.
4 G. Gran, Analyst, 77 (1952) 661.
5 J. Lefebvre, J. Chim. Phys., 54 (1957) 581.
6 K. S. Rajan and A. E. Martell, J. Inorg. Nucl. Chem., 29 (1967) 463.
7 E. Campi, G. Ostacoli, M. Meirone and G. Saini, J. Inorg. Nucl. Chem., 26 (1964) 553.
8 R. C. Warner and I. Weber, J. Am. Chem. Soc., 75 (1953) 5086.
9 C. Heitner and I. Eliezer, Bull. Soc. Chim. Fr., (1956) 574.
10 R. Das, R. K. Patnaik and S. Panit, J. Indian. Chem. Soc., 37 (1960) 59.
11 S. Ramamoorthy, P. G. Manning and C. Guarnaschelli, J. Inorg. Nucl. Chem., 34 (1972) 3443.
12 T. B. Field, J. L. McCourt and W. A. E. McBryde, Can. J. Chem., 52 (1974) 3119.
13 M. M. Petit-Ramel and I. Khalil, Bull. Soc. Chim. Fr., (1974) 1255.

14 E. Bottari, Ann. Chim. (Rome), 65 (1975) 375.
15 A. Ringbom, Complexation in Analytical Chemistry, Interscience, New York, 1963, p. 190.
16 E. H. Hansen, C. G. Lamm and J. Růžička, Anal. Chim. Acta, 59 (1972) 403.
17 E. Still, Anal. Chim. Acta, 107 (1979) 377.
18 G. Gran, Acta Chem. Scand., 4 (1950) 559.
19 S. Ahrland and J. Rawsthorne, Acta Chem. Scand., 24 (1970) 157.

Analytica Chimica Acta, 151 (1983) 77—84
Elsevier Science Publishers B.V., Amsterdam — Printed in The Netherlands

POTENTIOMETRIC FLOW-INJECTION DETERMINATION OF CHLORIDE

MAREK TROJANOWICZ* and WOJCIECH MATUSZEWSKI
Department of Chemistry, University of Warsaw, 02-093 Warsaw (Poland)
(Received 8th June 1982)

SUMMARY

Potentiometric detection of chloride with a silver/silver chloride electrode can be applied in flow-injection systems in the Nernstian range of electrode response and below it. In the low range, the usual logarithmic relationship is replaced by direct proportionality between the electrode potential and the chloride concentration. In the Nernstian region, the dispersion in the flow system influences the lower limit of linear detection whereas in the sub-Nernstian region it influences the slope of the electrode characteristics. The method is applicable to river water.

Flow-injection procedures for the determination of chloride have been based on displacement of thiocyanate ion from its mercury complex by chloride [1—3]. The released thiocyanate forms coloured complexes with iron(III) so that chloride can be determined spectrophotometrically. A disadvantage of the method is its poor limit of detection (about 5 ppm chloride). Slanina et al. [4] improved this method, determining chloride photometrically in rain waters in the range 0.2—15 ppm in a three-channel computerized flow-injection system. In a different computerized system, Slanina et al. [5] determined chloride in rain waters potentiometrically, but it was necessary to use a discrete analyzer technique.

The purpose of this investigation was to examine the usefulness of potentiometric detection in a flow-injection system for chloride in the Nernstian range as well as in the lower chloride concentration range, where there is a direct, rather than logarithmic, relationship between electrode potential and chloride concentration.

EXPERIMENTAL

A schematic diagram of the manifold is shown in Fig. 1. The injection valve and measuring flow cell were the same as previously described [6]. The carrier solution was pumped at a flow rate of 5 ml min^{-1} with a peristaltic pump (MP13-GJ4, Ismatec). The signals were recorded with a Potentiograph (E-436, Metrohm). The chloride-selective electrode was a second-kind silver/silver chloride electrode, prepared by surface oxidation of silver metal in

0003-2670/83/$03.00 © 1983 Elsevier Science Publishers B.V.

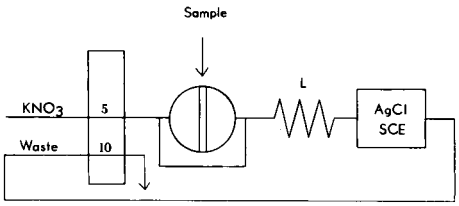

Fig. 1. Schematic diagram of the flow-injection system used in measurements.

0.5 M iron(III) chloride solution. This preparation is simpler and more efficient than the conventional anodic oxidation. A double-junction saturated calomel electrode (Activion, England) with 1 M ammonium nitrate in the electrolytic bridge served as reference. All the reagents were of analytical grade, and solutions were prepared with triply distilled water from a quartz still.

RESULTS AND DISCUSSION

Selectivity of the chloride electrode

In the case of solid-state electrodes, the interference caused by ions that have exchange reaction constants greater than unity, is governed to a significant degree by diffusion processes [7]. The extent of the exchange reaction depends on the interaction time between the membrane and solution. Thus in flow-injection measurements where the sample remains in contact with the electrode for a short time only, the selectivity should be different from that found in batch or flow equilibrium conditions. Comparison of the chloride electrode response in equilibrium and non-equilibrium measurements confirms this statement (Fig. 2). In batch measurements, the time needed to attain stable readings for chloride in the presence of 10^{-4} M bromide or iodide was at least 5 min. In the flow-injection system with dispersion D = 5.2, the residence time of the sample in the electrode compartment was estimated as 1.2 s. For both systems, the solution conditions were close to those in which the diffusion layer model is valid and the establishment of total equilibrium would need a much longer time. The calculated effective selectivity coefficients were found to be 2.9 and 1.9 for bromide and 6.6 and 1.8 for iodide in batch and flow-injection measurements, respectively.

In batch measurements, the presence of the interfering ions shifts the calibration curve for chloride ions towards less positive potentials; this is clearly visible in the concentration range above 10^{-3} M chloride (Fig. 2) and can be ascribed to an additional exchange reaction at the electrode surface. The effect was much smaller in flow-injection measurements and was observed as a shift of the base-line when the injected solution contained 10^{-4} M bromide (Fig. 3). When the chloride concentration was evaluated on the basis of peak height (i.e., the potential difference between the base-line and peak maximum), this shift had no influence on the calibration curve (Fig. 2a).

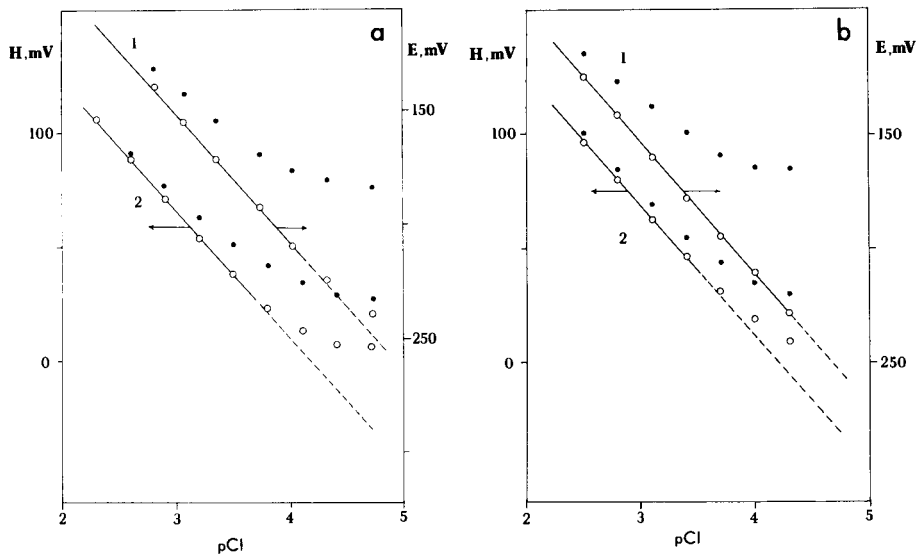

Fig. 2. Effect of the presence of 10^{-4} M bromide (a) and 10^{-4} M iodide (b) on the response of the chloride electrode in batch (curves 1) and flow-injection (curves 2) measurements. (○) Measurements without interfering ions; (●) measurements in the presence of interfering ions. Conditions: L = 25 cm, sample volume (V_s) 60 µl, D = 5.2.

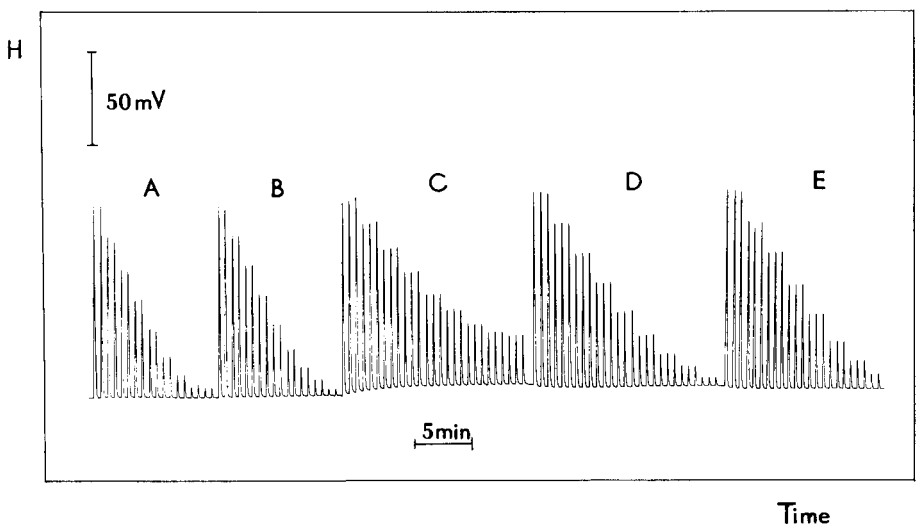

Fig. 3. Calibration of the chloride electrode in the flow-injection system: (A, E) in the absence of bromide; (B, D) in the presence of 10^{-5} M bromide; (C) in the presence of 10^{-4} M bromide. Concentrations of chloride standard solutions for each run were 5.12×10^{-3}, 2.56×10^{-3}, 1.28×10^{-3}, 6.40×10^{-4}, 3.20×10^{-4}, 1.60×10^{-4}, 8.00×10^{-5}, 4.00×10^{-5} and 2.00×10^{-5} M.

Similar conclusions about the improved selectivity of the chloride electrode in flow-injection measurements can be drawn from results obtained in the presence of sulphide (Table 1). In batch measurements or continuous equilibrium measurements in an air-segmented stream, the influence of sulphide must be eliminated by adding hydrogen peroxide [8] whereas in the flow-injection system at high dispersion, the effect is quite small because of the short contact time with the electrode surface. These observations are of practical importance, as the flow-injection conditions can be selected such that the contact time of interfering species with the electrode surface is minimized.

Detection limit in the flow-injection method for chloride

The range of linear response of potentiometric detectors in flow-injection systems depends significantly on dispersion [6]. Optimization of the dispersion value for routine analyses involves at least two opposing factors; lower dispersion in the system provides lower detection limits, but usually requires larger sample volumes, resulting in lower sampling rates for the same flow rate and tubing diameter. These relationships for the present system (Fig. 1) are illustrated in Fig. 4 for two different dispersions, $D = 2$ (curve 2) and $D = 3.7$ (curve 1). The lower limits of linear response are 4.0 and 3.7 pCl (3.5 and 7.0 μg Cl^- ml^{-1}), respectively; the maximum sampling rates, S_{max}, are 100 and 250 h^{-1}, respectively, the former being adequate for most practical purposes.

Another problem is the possibility of potentiometric measurements of low chloride concentration in the sub-Nernstian range of electrode response [9]. For a solid-state membrane composed of a 1:1 sparingly soluble salt with solubility product K_{so}, the equation given by Bardin [10] may be converted to

$$E = E^0 + k \ln [0.5C + K_{so}^{1/2} (1 + C^2/4K_{so})^{1/2}] \quad (1)$$

where k is the slope factor and C is the concentration of the analyte. When $C^2 << 4K_{so}$, and after some simplifications [11], the equation expressing a

TABLE 1

Errors (%) in chloride measurements in the presence of 10^{-5} M sulphide

Chloride concentration ($mg\ l^{-1}$)	Equilibrium method[a]		Flow injection without H_2O_2	
	Without H_2O_2	With H_2O_2	$D = 2.0$[b]	$D = 3.7$[c]
7	+26	+12	+20	+3.1
18	+15	+4.7	+15	+4.1
25	+17.5	+4.7	+7.2	+3.0

[a]In an air-segmented stream. [b]100-cm coil, 300-μl sample. [c]25-cm coil, 60-μl sample.

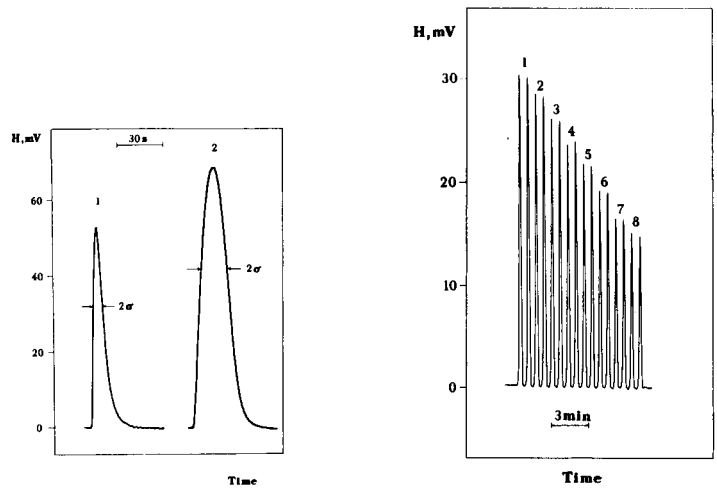

Fig. 4. Peaks recorded to estimate sampling rate for the chloride determination: (1) V_s = 60 µl, L = 25 cm, $S_{max} \approx 250$ h^{-1}; (2) V_s = 300 µl, L = 100 cm, $S_{max} \approx 100$ h^{-1}. σ is the standard deviation of the peak.

Fig. 5. Recording for calibration of the chloride electrode in the sub-Nernstian range at D = 1.9 (V_s = 300 µl, L = 25 cm). Concentrations of chloride standard solutions were: (1) 5.0 × 10^{-5}; (2) 4.5 × 10^{-5}; (3) 4.0 × 10^{-5}; (4) 3.5 × 10^{-5}; (5) 3.0 × 10^{-5}; (6) 2.5 × 10^{-5}; (7) 2.0 × 10^{-5}; (8) 1.5 × 10^{-5} M.

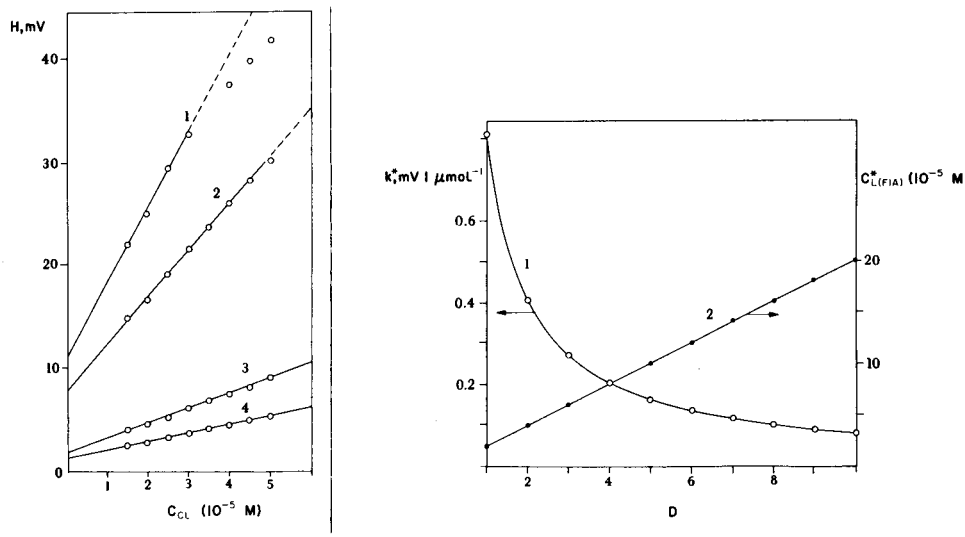

Fig. 6. Calibration graphs for the flow-injection system in the sub-Nernstian range obtained at different dispersions: (1) 1 (equilibrium measurement in the flow system); (2) 1.9; (3) 7.2; (4) 12.2.

Fig. 7. The dependence of calculated values of k^* (curve 1) and $C^*_{L(FIA)}$ (curve 2) on dispersion in flow-injection measurements of chloride.

linear dependence of potential on concentration is

$$E = \text{const.} + (k/2K_{so}^{1/2})C \quad (2)$$

This equation is taken as the basis for considering electrode response in the sub-Nernstian range. In a flow-injection system, the limiting concentration, $C_{L(\text{FIA})}$, for Nernstian response is given by the limiting concentration for equilibrium measurements, C_L, multiplied by the dispersion D [6]. If C^0 is the concentration of the sample injected, the actual concentration reaching the detector will be $C_{\text{FIA}} = C^0/D$. Thus from Eqn. (2)

$$E = \text{const.} + (k/2DK_{so}^{1/2})C^0 = \text{const.} + k^*C^0 \quad (3)$$

where k^* is constant for a particular system. It is obvious from the derivation of Eqn. (3) that it is valid only for $(C^0/D)^2 << 4K_{so}$.

In order to prove the correctness of these considerations, flow-injection measurements of chloride at concentrations of 1.5×10^{-5}—5×10^{-5} M (0.51—1.7 mg l^{-1}) were made at different dispersions obtained by injecting sample volumes of 30—300 μl (Fig. 6). The recorded peaks at D = 1.9 shown in Fig. 5 were used to plot one calibration graph (curve 2, Fig. 6). All the calibration plots in Fig. 6 are linear as should follow from Eqn. (3), and their slopes vary with dispersion. In Table 2 the experimental slopes are compared with those calculated from Eqn. (3); the agreement is satisfactory. The dependence of the sub-Nernstian slope k^* on dispersion D, calculated from Eqn. (3) is shown in Fig. 7 (curve 1).

The concentration range over which these slopes are constant is broader than should follow from the condition $(C^0/D)^2 << 4K_{so}$. Exact computations based on Eqn. (1) without simplifications were done for chloride concentrations of 1×10^{-5}—2.5×10^{-4} M, C being replaced by C^0D^{-1}, to establish the chloride concentrations giving a 1-mV deviation at the upper limit of linear response at different dispersions. The dependence of these calculated upper limits, $C^*_{L(\text{FIA})}$, on dispersion is shown in Fig. 7, curve 2. With increasing dispersion, the linear range of the electrode response expands, but the slope of the calibration graphs decreases. For dispersion 1.9, and with a sensitive recorder, doubling the chloride concentration at the 0.3 mg l^{-1} level gives a potential change of about 5 mV, which seems satisfactory.

The lower limit of the direct linear range is determined by the smallest peak height which can be measured at given background level and noise amplitude in the conditions used. In the ideal case, when the carrier solution

TABLE 2

The effect of dispersion, D, in potentiometric flow-injection measurements on the slope k^* (mV l μmol^{-1}) of the calibration graph in the sub-Nernstian range

D	1.0	1.7	1.9	5.2	7.2	9.1
k^* found	0.76	0.46	0.45	0.17	0.14	0.10
k^* calc.[a]	0.81	0.48	0.42	0.16	0.11	0.09

[a]From Eqn. (3) for $pK_{so} = 9.6$.

does not contain chloride, the calibration graphs shown on Fig. 6 should pass through the origin of the coordinates. Usually, however, the carrier solution contains a trace of chloride, C_{cs}. In such a system, the electrode potential expressed by Eqn. (3) becomes

$$E = \text{const.} + k(C^0 + C_{cs})/2K_{so}^{1/2}D \qquad (4)$$

Subtraction of Eqn. (3) from Eqn. (4) gives an expression describing the shift of the intercept as a function of contamination: $\Delta E_{cs} = kC_{cs}/2K_{so}^{1/2}D$. For dispersions of 1, 1.9, 7.2 and 12.2, and ΔE_{cs} values were 11.2, 7.6, 1.6 and 1.2 mV, respectively (Fig. 6), corresponding to C_{cs} values of 1.41×10^{-5}, 1.76×10^{-5}, 1.42×10^{-5} and 1.80×10^{-5} M, respectively. The agreement of these C_{cs} values confirms the validity of the above outline.

Determination of chloride in waters

This flow-injection determination of chloride was applied to surface waters which contained enough chloride for measurements in the Nernstian range. The calibration plot with 300-μl injections is shown in Fig. 8. Water samples were injected into 0.1 M potassium nitrate carrier solution without pretreatment. The data in Table 3 were obtained over five successive days; each sample was titrated potentiometrically with silver nitrate solution in 33% acetic acid medium and chloride was also determined daily by the flow-

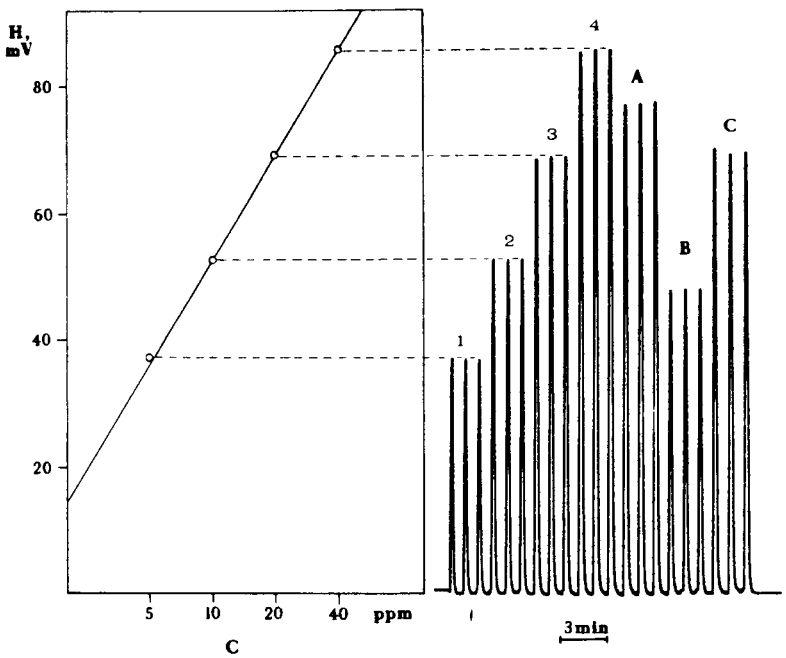

Fig. 8. Calibration and measurements of chloride in water samples. Chloride standards: (1) 5.0; (2) 10.0; (3) 20.0; (4) 40.0 mg l^{-1}. (A, B, C) River water samples. (L = 100 cm, V_s = 300 μl.)

TABLE 3

The results of flow-injection chloride determinations in surface water samples. For details see text

Sample	Chloride found (mg l^{-1})		Flow-injection method	
	Titration	Flow injection	Error (%)	Standard deviation (mg l^{-1})
1	58.3	57.1	−2.1	1.4
2	44.4	43.6	−1.8	1.3
3	36.6	36.7	+0.3	1.4
4	42.6	42.4	−0.5	1.9

injection method. The results shown are the means of these measurements. The maximal bias of 2.1% is satisfactory, as is the precision of the flow-injection data (<2 mg l^{-1}).

The authors express their gratitude to Professor Adam Hulanicki for valuable discussions and help in the preparation of manuscript.

REFERENCES

1 J. Růžička, J. W. B. Stewart and E. A. Zagatto, Anal. Chim. Acta, 81 (1976) 387.
2 E. H. Hansen and J. Růžička, Anal. Chim. Acta, 87 (1976) 353.
3 J. Růžička, E. H. Hansen, H. Mosbaek and F. J. Krug, Anal. Chem., 49 (1977) 1858.
4 J. Slanina, F. Bakker, A. Bruyn-Hes and J. J. Möls, Anal. Chim. Acta, 113 (1980) 331.
5 J. Slanina, F. Bakker, J. J. Möls, J. E. Ordelman and A. G. M. Bruyn-Hes, Anal. Chim. Acta, 112 (1979) 45.
6 M. Trojanowicz and W. Matuszewski, Anal. Chim. Acta, 138 (1982) 171.
7 A. Hulanicki and A. Lewenstam, Anal. Chem., 53 (1981) 1401.
8 M. Trojanowicz and R. Lewandowski, Fresenius Z. Anal. Chem., 308 (1981) 7.
9 D. Midgley, Ion-Selective Electrode Rev., 3 (1981) 43.
10 V. V. Bardin, Zavod. Lab., 28 (1962) 910.
11 K. Tomlinson and K. Torrance, Analyst, 102 (1977) 1.

Analytica Chimica Acta, 151 (1983) 85—90
Elsevier Science Publishers B.V., Amsterdam — Printed in The Netherlands

INDIRECT POTENTIOMETRIC DETERMINATION OF SULPHIDE WITH A CADMIUM ION-SELECTIVE ELECTRODE

A. C. CALOKERINOS, M. TIMOTHEOU-POTAMIA, E. SARANTONIS and T. P. HADJIIOANNOU*

Laboratory of Analytical Chemistry, University of Athens, Athens (Greece)

(Received 6th December 1982)

SUMMARY

An indirect potentiometric method is described for the determination of sulphide in the range 0.3—300 μg (0.06—60 μg ml^{-1}). A known excess of cadmium(II) is added to the sample and the unreacted cadmium ion is titrated with EDTA using a solid-state cadmium ion-selective electrode. The method is applied successfully for determinations of sulphide in spiked air samples and of sulphur in steels.

The solid-state sulphide ion-selective electrode has been widely used for the direct potentiometric determination of low levels of sulphide in samples such as water [1—4], soils [5] and minerals [5, 6]. The electrode may be calibrated with near-Nernstian response down to ca. 2×10^{-7} M sulphide ions [7, 8] but long response times [1, 7], continuous drift of the electrode potential [9] and fast air oxidation of sulphide [7] limit the use of the electrode for low concentrations of the ion. Alternatively, sulphide can be titrated with silver(I) [10], lead(II) [11, 12] and cadmium(II) [13, 14] using the sulphide-selective electrode as the indicator electrode, but erroneous results may be obtained because of adsorption of sulphide on the precipitate or deviations from stoichiometry [11].

The difficulties associated with the direct potentiometric determination of sulphide by means of the sulphide-selective electrode can be eliminated by indirect methods. Thus, sulphide has been determined by oxidation with an ethanolic solution of iodine and measurement of the resulting iodide with an iodide-selective electrode [15, 16]. Sulphide is removed from interferences by precipitation of cadmium sulphide. The precipitate is then filtered and dissolved in sulphuric acid, and the hydrogen sulphide evolved is collected in the ethanolic solution of iodine.

In this paper, a simple and fast indirect potentiometric method for the determination of sulphide is described. A known excess of cadmium(II) ions is added to the sulphide sample (0.3—300 μg) and the unreacted cadmium ion is titrated with EDTA using a solid-state cadmium ion-selective electrode. The method was applied successfully for the determination of sulphide in spiked air samples and of sulphur in steels.

0003-2670/83/$03.00 © 1983 Elsevier Science Publishers B.V.

EXPERIMENTAL

Apparatus

An Orion Model 94-48 A solid-state cadmium ion-selective electrode was used in conjunction with an Orion Model 90-02-00 double-junction silver—silver chloride reference electrode. The outer chamber of the reference electrode was filled weekly with a 10% (w/v) ammonium nitrate solution. The constant-rate burette and the recording system were the same as previously reported [17]. All measurements were made at ambient temperature in a 50-ml beaker equipped with a magnetic stirrer with a teflon-coated magnetic bar.

If the surface of the cadmium ion-selective electrode turned dim, the electrode was polished with fine-grain diamond paste (DP-Paste, Type C; H. Struers Scientific Instruments, Copenhagen). The electrode was stored in silicone oil and rinsed with distilled water before use. After prolonged storing, the electrode was conditioned in a 10^{-3} M cadmium nitrate solution before use.

Reagents

All solutions were prepared with deionized-distilled water from reagent-grade materials, except where stated.

A 0.01000 M cadmium nitrate standard solution was prepared by dissolving 1.1240 g of cadmium metal (Merck, p.a.) in the minimum volume (3—4 ml) of concentrated nitric acid and diluting with water to 1 l. An aqueous 0.01 M cadmium acetate stock solution was prepared from the dihydrate (Merck, p.a.). More dilute solutions were prepared by dilution just before use.

A 0.01000 M EDTA stock solution was prepared by dissolving 3.722 g of disodium ethylenediaminetetraacetic acid (Titriplex III; Merck) in water and diluting to 1 l. More dilute solutions were prepared by dilution. The exact titre of each EDTA solution used was found by titrating appropriate amounts of the standard cadmium nitrate solution with the cadmium electrode as indicator electrode.

A 0.01 M sodium sulphide stock solution was prepared by dissolving 2.40 g of $Na_2S \cdot 9H_2O$ (Ferak Berlin, p.a.) in water and diluting to 1 l. The exact titre of the stock solution was found iodimetrically. More dilute solutions were prepared by the fewest dilution steps possible. All sulphide solutions were prepared daily with water which had previously been boiled, cooled and deaerated with nitrogen gas.

A 0.1 M ammonia —0.1 M ammonium nitrate buffer solution (pH 9.3) was used.

Procedures

Standardization of EDTA. Fill the burette with 10^{-2} M EDTA solution. Transfer 5.00 ml of 4×10^{-3} M cadmium nitrate standard solution and 25.00

ml of the buffer solution to the titration cell, immerse the electrodes and start stirring. Start the recorder and after about 1 min start the burette (delivery rate = 0.327 ml min^{-1}) to obtain the titration curve. For the greatest accuracy, calibrate the recorder for each titration using the burette reading. Locate the end-point graphically and calculate the molarity (M) of the EDTA titrant. If 10^{-3} M or 5×10^{-4} M EDTA solutions are required as titrants, proceed as above with 5.00 ml of 4×10^{-4} M or 8×10^{-5} M cadmium nitrate standard solution, respectively.

Determination of sulphide in aqueous solutions. Transfer 5.00 ml of the appropriate cadmium acetate solution and 25.00 ml of buffer solution to the titration cell. Titrate the solution as previously described and evaluate the volume (V_i) of EDTA titrant required for cadmium(II) alone. To a clean cell, transfer 5.00 ml of cadmium(II) solution, 5.00 ml of sulphide solution and 20.00 ml of buffer and titrate again. Evaluate the volume (V_f) of EDTA titrant consumed by the unreacted cadmium(II). Calculate the sulphide content (μg S per 5 ml of solution) from $m_{\mu g} = 32000(V_i - V_f)$ M.

Determination of sulphide in spiked air samples. The apparatus used comprises a 100-ml pear-shaped two-necked flask with ground-glass joints, attached to a 125-ml Drechsel bottle and thence to a suction pump. Transfer 5.00 ml of the appropriate cadmium acetate solution and 25.00 ml of buffer solution into the Drechsel bottle. Start the suction pump and adjust the flow of air to 10 l min^{-1}. Transfer 5.00 ml of the sulphide solution into the two-necked flask and inject 0.5 ml of concentrated sulphuric acid. After 15 min, disconnect the Drechsel bottle, transfer the solution quantitatively to the titration cell and titrate the unconsumed cadmium(II).

Determination of sulphur in steels. The apparatus used comprises a 25-ml round-bottomed flask with ground-glass joint, attached to a 30-cm Liebig condenser at an angle of about 45°, which is connected to an angled glass tube, with its end immersed in a titration cell. Transfer 0.1—0.2 g of steel, 0.3 g of zinc powder and 10 ml of 4 M hydrochloric acid to the round-bottomed flask and immediately connect the condenser. Dip the outlet of the angled glass tube into the titration cell which contains 5.00 ml of 4×10^{-3} M cadmium acetate solution and 25.00 ml of buffer solution. Warm the mixture in the flask gently until the steel sample has dissolved (15—30 min) and continue boiling for 15 min. The evolved hydrogen sulphide is collected in the cadmium acetate solution. Titrate the unconsumed cadmium(II) and calculate the sulphur content of the steel sample from $\%S = 3200(V_i - V_f)M/$ mass of sample (mg).

RESULTS AND DISCUSSION

The titration of cadmium(II) ions with EDTA shows large potential changes when an alkaline medium is used. For this reason, Brand et al. [18] used a 0.1 M ammonia—0.1 M ammonium nitrate buffer solution of pH 9.3, which was also adopted in this work.

Automatic potentiometric titrations always show a blank which is a function of titrant concentration, rate of addition, electrode geometry and age, etc. However, because all these factors can be kept constant, the blank is very reproducible under a particular set of experimental conditions. In this method, the blank was compensated because V_f was subtracted from V_i. Typical titration curves for cadmium(II) ions alone and in the presence of precipitated cadmium sulphide are shown in Fig. 1.

The range of sulphide that can be determined with the method described depends on the concentrations of EDTA and cadmium(II), as shown in Table 1 for aqueous solutions of sulphide. The relative standard deviation for 16 μg of sulphide was 0.4% (n = 8) and the corresponding potential change was ca. 100 mV. Because sulphide can be removed from complex samples by evolution from acidic solution, the interferences tested were those ions that normally occur with sulphide and might generate vapours on acidification. No interference was observed from 0.1 M carbonate, sulphite, nitrite or chloride ions on 16 μg of sulphide. Larger concentrations of chloride ions as hydrochloric acid interfered severely by dissolving the CdS precipitate.

The method was used for the determination of sulphide in spiked air samples (Table 2) with an average recovery of 96.4%. The advantage of the procedure is that the titration need not be carried out immediately after collection and formation of the precipitate.

TABLE 1

Results for aqueous sulphide solutions with different concentrations of cadmium(II) and EDTA solutions

EDTA (M)	Cd^{2+} (M)	Sulphide (μg)		Relative error (%)
	Initial (final)	Taken	Found	
5×10^{-4}	8×10^{-5} (1.3×10^{-5})	0.800	0.900	+12.5
		1.600	1.532	−4.2
		2.400	2.502	+4.2
		3.200	3.220	+0.6
		4.800	4.969	+3.5
				Av. 5.0
10^{-3}	4×10^{-4} (6.7×10^{-5})	3.520	3.388	−3.8
		8.80	8.93	+1.5
		17.60	18.02	+2.4
		26.40	26.80	+1.5
		35.20	35.18	−0.1
				Av. 1.9
10^{-2}	4×10^{-3} (6.7×10^{-4})	32.00	32.45	+1.4
		80.0	82.8	+3.5
		160.0	161.0	+0.6
		240.0	230.0	−4.2
		320.0	308.0	−3.8
				Av. 2.7

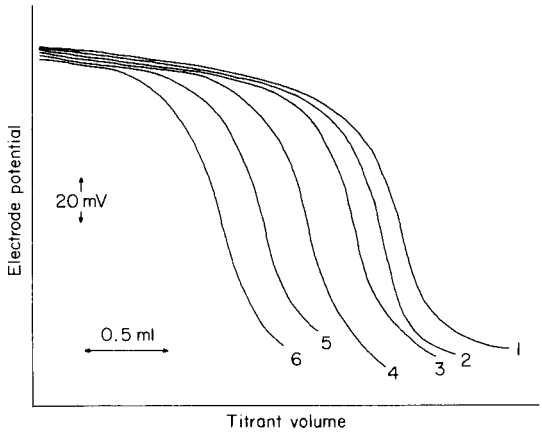

Fig. 1. Titration curves for (1) 5.00 ml of 4.3×10^{-4} M Cd^{2+} with 0.000963 M EDTA in the presence of (2) 3.88 μg, (3) 8.93 μg, (4) 18.02 μg, (5) 26.80 μg, and, (6) 35.18 μg of sulphide.

Sulphur was also determined in steels by the proposed method. Zinc powder and hydrochloric acid ensure complete dissolution of the steel sample and reduction of sulphur to sulphide. Furthermore, the evolution of hydrogen helps the carry-over of hydrogen sulphide from the generation solution into the titration cell. When only hydrochloric acid was used, low results were obtained. The condenser is necessary to condense water vapours and to retain hydrogen chloride fumes which might dissolve CdS if carried over to the titration cell. The results obtained are shown in Table 3.

TABLE 2

Recovery of sulphide from spiked air samples

S^{2-} added (μg)	2.03	3.32	6.15	7.98	8.94	12.66
S^{2-} found (μg)	1.98	3.20	6.00	7.46	8.42	12.55
Recovery (%)	97.5	96.4	97.6	93.5	94.2	99.1

TABLE 3

Determination of sulphur in steels[a]

Sample	Other constituents (%)							Sulphur (%)		Relative error (%)
	C	Mn	Si	P	Ni	Cr	Mo	Expected	Found	
1	0.02	0.05	0.74	0.02	10.41	18.35	—	0.01	0.01	0.0
2	0.37	0.57	0.24	0.011	1.79	0.83	0.25	0.013	0.012	−8.3
3	0.99	0.71	0.86	0.019	—	—	—	0.041	0.041	0.0
4	0.98	0.92	0.92	0.026	—	—	—	0.052	0.050	−3.8

[a]T. Smith Analyzed Standards.

In conclusion, the proposed indirect potentiometric method for the determination of sulphide is simpler and faster than most other available methods. The method can be used easily in connection with any acid evolution system available for generation of hydrogen sulphide.

REFERENCES

1 E. W. Baumann, Anal. Chem., 46 (1974) 1345.
2 E. Mor, V. Scotto, G. Marcenaro and G. Alabiso, Anal. Chim. Acta, 75 (1975) 159.
3 J. Gulens, K. Jessome and C. K. Macneil, Anal. Chim. Acta, 96 (1978) 23.
4 B. L. Wilson, R. R. Schwarzer, C. O. Chukwuenye and J. Cyrous, Microchem. J., 26 (1981) 402.
5 D. L. Sorensen, W. A. Kneib and D. B. Porcella, Anal. Chem., 51 (1979) 1870.
6 H. Bozon and S. Bozon, Analusis, 6 (1978) 243.
7 D. J. Crombie, G. J. Moody and J. D. R. Thomas, Anal. Chim. Acta, 80 (1975) 1.
8 E. J. Duffield, G. J. Moody and J. D. R. Thomas, Anal. Proc., 17 (1980) 507.
9 I. Sekerka and J. F. Lechner, Anal. Chim. Acta, 93 (1977) 139.
10 T. M. Hseu and G. A. Rechnitz, Anal. Chem., 40 (1968) 1054.
11 T. M. Florence and Y. J. Farrar, Anal. Chim. Acta, 116 (1980) 175.
12 E. Lokka, Pap. Puu, 61 (1979) 153.
13 D. L. Ehman, Anal. Chem., 48 (1976) 918.
14 E. J. Green and D. Schnitker, Mar. Chem., 2 (1974) 111.
15 M. Novkirishka and R. Christova, Mikrochim. Acta (Wien), (1978) I, 483.
16 M. Novkirishka, G. Michailov and R. Christova, Fresenius Z. Anal. Chem., 305 (1981) 411.
17 T. P. Hadjiioannou and E. P. Diamandis, Anal. Chim. Acta, 94 (1977) 443.
18 M. J. D. Brand, J. J. Militello and G. A. Rechnitz, Anal. Lett., 2 (1969) 523.

Analytica Chimica Acta, 151 (1983) 91—97
Elsevier Science Publishers B.V., Amsterdam — Printed in The Netherlands

MEMBRANE ELECTRODE-BASED METHOD FOR THE DETERMINATION OF LEUCINE AMINOPEPTIDASE

P. SEEGOPAUL and G. A. RECHNITZ*
Department of Chemistry, University of Delaware, Newark, Delaware 19711 (U.S.A.)
(Received 27th December 1982)

SUMMARY

An ammonia gas-sensing membrane electrode is used as a potentiometric sensor for the assay of leucine aminopeptidase. The method utilizes hydrolysis of L-leucinamide to release ammonia which is detected by the electrode through initial rate measurements and related to the enzymatic activity. A within-run relative imprecision of ±2.5% was established for the method with a working range up to 70 mU ml^{-1} enzyme. Recovery experiments in pooled serum showed an average recovery of 96.6% added enzyme. Good agreement with a spectrophotometric method was obtained for synthetic laboratory samples.

The field of quantitative potentiometry continues to expand with the increasing application of ion-selective electrodes as measurement devices [1]. Gas-sensing membrane electrodes, with their inherent advantages of enhanced selectivity, are particularly suited to clinical enzymology. These sensors monitor enzyme-catalyzed reactions with the catalyst either dissolved in solution or immobilized on the surface of the probe. Recently, the ammonia gas electrode was shown to be useful for the assay of hydrolases [2, 3].

This paper describes a method for the assay of leucine aminopeptidase with the ammonia sensor. Leucine aminopeptidase is a proteolytic enzyme that hydrolyzes the *N*-terminal residues of certain L-peptides, with particular activity towards peptides with *N*-terminal leucine residues. Generally, assay methods for the enzyme are based on the hydrolysis of synthetic substrates. With L-leucinamide as the substrate, liberated leucine was detected by paper chromatography [4] and colorimetry [5], while pH-stat techniques utilized differences in p*K* values of substrate and product [6]. Another procedure titrated the ammonia released with acid after being trapped in a Conway diffusion apparatus [7]. β-Naphthylamine from L-leucine-β-naphthylamine was measured by fluorimetry [8] and spectrophotometry either directly [9] or indirectly following diazotization [10]. Absorbance measurements of nitroaniline from L-leucine-*p*-nitroanilide were also used for enzyme assays [11].

In this work, it is shown that the ammonia gas sensor provides a simple, rapid and convenient method for the determination of leucine aminopeptidase. The procedure is based on the liberation of ammonia resulting from

0003-2670/83/$03.00 © 1983 Elsevier Science Publishers B.V.

the hydrolysis of the substrate, L-leucinamide, in the presence of magnesium ions.

EXPERIMENTAL

Instrumentation

An Orion Model 95-10 ammonia gas sensor connected to a Corning Model 12 Research pH/mV meter was used to make the initial-rate measurements. Potentiometric data were recorded on a Heath-Schlumberger Model SR-255B strip-chart recorder working at a chart speed of 5 mm min^{-1} and a range of 100 mV. Enzymatic reactions proceeded in a 10-ml double-jacketed glass cell thermostated at 30 ± 0.1°C with a Haake Model FM constant temperature circulator. Spectrophotometric measurements were made with a Hitachi Model 100-60 spectrophotometer.

Reagents and Solutions

Solutions were prepared in deionized water from analytical-reagent grade chemicals. Stock substrate solution (1.0 M) was prepared by dissolving 0.83 g of L-leucinamide (Sigma Chemical Co., St. Louis, MO) in 5 ml of water.

Type III-CP (from porcine kidney) leucine aminopeptidase, cytosol (E.C. 3.4.11.1; Sigma) with an activity of 100 units per mg of protein; one unit corresponds to 1.0 μmol of L-leucinamide hydrolyzed to L-leucine and ammonia per minute at pH 8.5 and 25°C. The enzyme was supplied in a solution containing 2.9 M ammonium sulphate and 5 mM magnesium chloride in 0.1 M Tris buffer, pH 8.5. This necessitated the use of dialysis to remove the rather high ammonia background. An aliquot of the enzyme preparation was diluted (1 + 4) and dialyzed for 48—72 h against several changes of 2 l of 0.1 M Tris buffer, pH 8.5, containing 5 mM magnesium chloride. This procedure effectively reduced the ammonia background to below 10^{-5} M. For actual enzyme measurements, the dialyzed enzyme sample was further diluted (1 + 19) with Tris buffer. Both the substrate and enzyme solutions were kept at 4°C when not in use.

Control sera (Ortho Diagnostics Systems) were pooled and dialyzed for recovery experiments. A leucine aminopeptidase assay kit, (No. 251; Sigma) was used for correlation measurements to compare the proposed method with a traditional procedure. The kit methodology is based on spectrophotometric measurement of β-naphthylamine released from L-leucine-β-naphthylamine at 580 nm following the formation of a blue azo dye.

Procedure

For enzyme measurements, 2.8 ml of 0.1 M Tris—HCl buffer, pH 8.5, was added to the thermostated glass cell containing a small teflon-coated stirring bar, and the cell was placed on a magnetic stirrer to obtain continuous and constant mixing. In discrete experiments, various aliquots of enzyme samples were added to the buffer and the electrode was immersed in the mixture.

The base-line potential was allowed to reach a stable reading before the enzymatic reaction was started.

A portion (200 μl) of the stock substrate solution was added to the enzyme solution to initiate the catalytic hydrolysis. Rate curves were recorded and the computed initial rates of potential changes (mV min^{-1}) were plotted as functions of enzyme activities. Blanks in the absence of enzyme were measured under identical conditions and used to correct rate data. The calibration graph provided the values for unknown enzyme activities.

Aqueous and pooled control serum samples were used for recovery studies of added enzyme. The serum was continuously dialyzed for 1 h in a Technicon Basic AutoAnalyzer dialyzer assembly. Aliquots of a standard enzyme solution were added to the serum sample or aqueous solution and the initial rates were determined for each sample. The activity was obtained from the standard calibration graph and compared to the amount added.

RESULTS AND DISCUSSION

Optimization of kinetic parameters

Kinetic parameters influencing the enzyme-catalyzed reaction were studied in order to optimize the procedure. Figure 1 shows a plot of initial rate as a function of substrate concentration at 30°C and pH 8.5 in the presence of magnesium ions. The enzyme (36.2 mU ml^{-1}) was saturated with substrate near 100 mM, and 90 mM substrate was used throughout the remainder of the study. Lower concentrations of substrate decreased the linearity of the calibration curves.

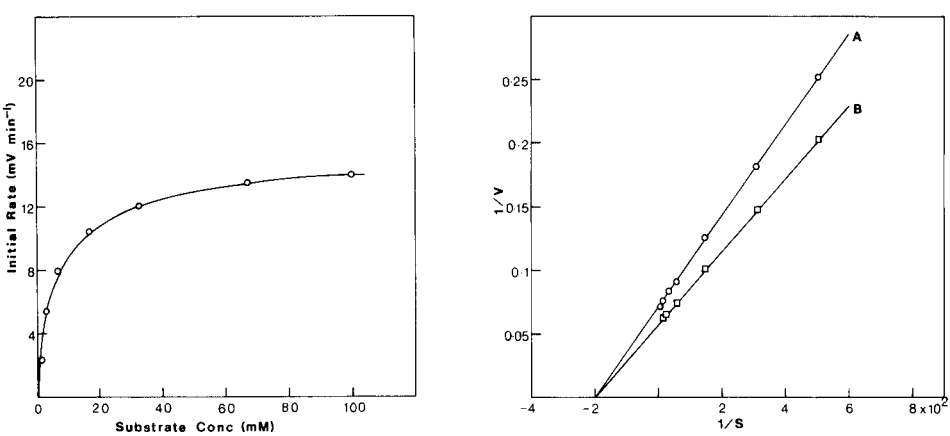

Fig. 1. Effect of L-leucinamide concentration on the rate of the enzyme-catalyzed reaction, using 36.2 mU ml^{-1} enzyme at pH 8.5 and 30°C in the presence of 5 mM $MgCl_2$.

Fig. 2. Lineweaver—Burk plot of the reciprocals of initial rates against substrate concentrations, for (A) 36.2 mU ml^{-1} and (B) 50.6 mU ml^{-1} enzyme activities at pH 8.5 and 30°C in the presence of 5 mM $MgCl_2$.

A Lineweaver—Burk plot of the reciprocals of substrate and initial rates is given in Fig. 2. These data yielded a K_M value of 5.03 mM, indicating good agreement with the previously reported value of 5.21 mM [12]. The choice of working conditions and the source of the enzyme must be considered in comparing the Michaelis constants. Values of K_M for the bovine lens enzyme are generally 2-fold or more higher than for the kidney enzyme [4, 13]. Similarly, values are higher with manganese(II) ions than with magnesium ions [12].

A concentration of 5 mM magnesium chloride proved to be sufficient for optimum enzyme stability and activity. Dissociation of the cation from the enzyme can occur at dilute concentration requiring reactivation. Reactivation is a time-dependent process necessitating incubation of the enzyme with the metal ion prior to measurement [4]. The use of manganese(II) ions gave higher activity, but at high pH the formation of hydroxides is possible. The removal of the ammonia background through dialysis decreased the stability of the diluted enzyme. Working enzyme standards were prepared from the stock solution on a daily basis and were checked frequently for any deterioration of activity.

The effect of pH was studied over the pH range 7.0—9.5. Figure 3 shows the pH profile, indicating an optimum pH range of 8.7—9.0. The observed optimum pH range is well suited for measurements with the ammonia gas-sensor.

Figure 4 shows the temperature effects on the enzyme reaction at pH 8.5

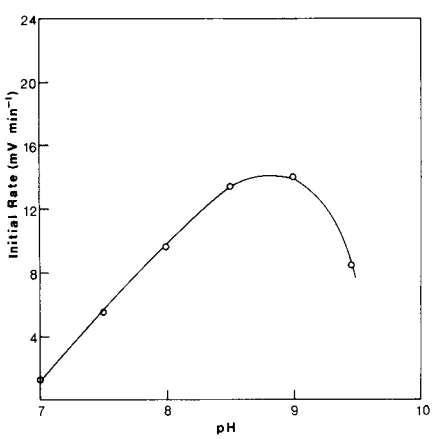

Fig. 3. pH profile of the catalyzed hydrolysis of 90 mM substrate by 36.2 mU ml^{-1} enzyme at 30°C.

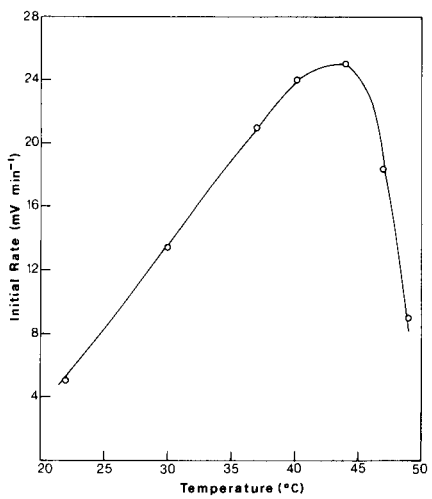

Fig. 4. Effect of temperature on the enzymatic rate with 90 mM substrate and 36.2 mU ml^{-1} enzyme at pH 8.5.

with an incubation time of about 6 min. The rate increased linearly with temperature from 22 to 40°C; some small increase of activity above 40°C is obtained at the expense of enzyme stability. Previous work reported a similar optimum temperature range [13]. The potentiometric method was tested at both 30 and 37°C; potential readings were more reproducible and drift-free at 30°C and this temperature was adopted for enzyme determinations.

Accuracy, precision and recovery studies

Enzyme activities in the range of 2.01—72.3 mU ml^{-1} were quantified in random manner. Table 1 gives the data for random enzyme sampling showing a relative error range of 1.2—3.0%. Data for a within-run precision study, conducted for the same enzyme activity range are also given in Table 1. The percent relative standard deviation (r.s.d.) was based on at least eight measurements for each sample. The relative imprecision ranged from ±1.4% to ±3.9% with an average of ±2.5%.

Results for recovery studies tabulated in Table 2 show average recoveries of 98.4 and 96.6% for aqueous and serum samples, respectively. The good agreement of recovery values from the aqueous and serum samples suggests the possible use of the method for clinical applications.

Determination of leucine aminopeptidase

A plot of enzyme activities against initial rates is shown in Fig. 5; the working range is up to 70 mU ml^{-1}. The method allowed a detection limit of about 1 mU ml^{-1}. Reproducibility data are given in Table 1.

Synthetic aqueous samples were processed by both the electrode method and the Sigma kit spectrophotometric method. Samples were diluted so that the activities were within the working range of the electrode method and processed immediately. For ten samples ranging from 2.2 to 88 mU ml^{-1}, the least-squares equation of data for the potentiometric (y) vs. the photo-

TABLE 1

Precision studies and relative errors in random enzyme assays at pH 9.0 and 30°C with 90 mM substrate

Enzyme activity (mU ml^{-1})		Relative error (%)	Within-run precision[a] (%)
Taken	Found		
2.01	2.07	+3.0	±3.9
4.80	4.92	+2.5	±3.2
14.6	14.4	−1.4	±1.5
36.2	36.9	+1.9	±2.3
50.6	50.0	−1.2	±2.6
72.3	71.0	−1.8	±1.4

[a]R.s.d. calculated from eight determinations.

TABLE 2

Comparative recovery studies of enzyme added to aqueous solution and pooled control sera

Mean enzyme activity added (mU ml^{-1})	Recovery (%)		Mean enzyme activity added (mU ml^{-1})	Recovery (%)	
	Aqueous solution	Pooled sera		Aqueous solution	Pooled sera
2.20	96	95	39.8	99	98
5.80	98	97	50.6	99	96
10.9	97	101	72.3	98	95
25.3	102	94	Average	98.4	96.6

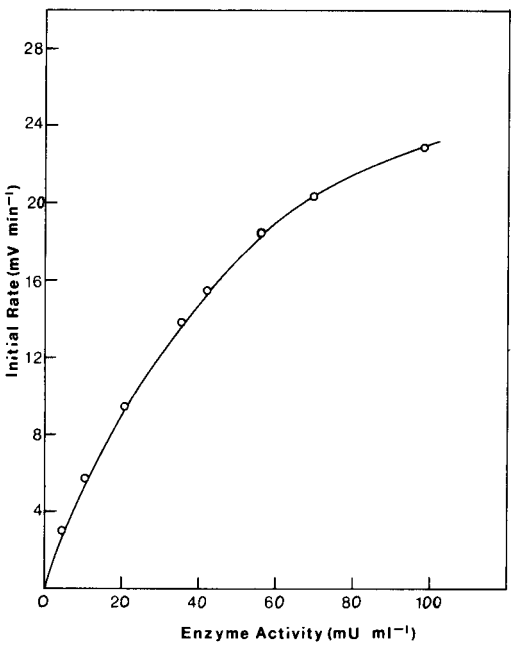

Fig. 5. Calibration curve of leucine aminopeptidase activities against initial rates, with 90 mM substrate at pH 8.5 and 30°C.

metric (x) method was $y = (1.006 \pm 0.02)\,x + 0.2 \pm 1$ with $S_{yx} = 1.8$ and $r = 0.998$. These results indicate favorable comparison between the methods.

The main clinical application of serum leucine aminopeptidase determination is in confirming the diagnosis of hepatobiliary disease [14]. Elevated activities are found in a wide range of pathological conditions, including obstructive jaundice and metastatic disease of the liver [15].

The potentiometric electrode method offers a useful alternative approach for the assay. Spectrophotometric methods suffer from turbidity problems and interferences from native serum compounds, particularly in hemolyzed

samples. The traditional method also involves the compound β-naphthylamine released from leucine-β-naphthylamine, However, β-naphthylamine is believed to be a carcinogen associated with bladder tumors and may represent a laboratory hazard. The method reported here is free from these problems.

We are grateful to the National Institutes of Health (Grant GM-25308) for support of this research.

REFERENCES

1 M. E. Meyerhoff and Y. M. Fraticelli, Anal. Chem., 54 (1982) 27R.
2 P. Seegopaul and G. A. Rechnitz, Anal. Lett., 15 (1982) 709.
3 C. R. Gebauer, M. E. Meyerhoff and G. A. Rechnitz, Anal. Biochem., 45 (1979) 479.
4 H. Hanson and M. Frohne, in S. Colowick and N. Kaplan (Eds.), Methods in Enzymology, Vol. XLV, Part B, Academic Press, New York, 1976, p. 508.
5 F. Brinkley and C. Torres, Arch. Biochem. Biophys., 86 (1960) 201.
6 G. F. Bryce and B. R. Rabin, Biochem. J., 90 (1964) 509.
7 R. J. Haschen, Clin. Chim. Acta, 6 (1961) 322.
8 M. Roth, Clin. Chim. Acta, 9 (1964) 448.
9 H. J. Lee, J. N. LeRue and I. B. Wilson, Anal. Biochem., 41 (1971) 397.
10 M. N. Green, K. C. Tsou, R. Bressler and A. M. Seligman, Arch. Biochem. Biophys., 57 (1955) 458.
11 W. Nagel, F. Willig and F. H. Schimdt, Klin. Wochenschr., 42 (1964) 447.
12 R. J. De Lange and E. L. Smith, in P. D. Boyer (Ed.), The Enzymes, Vol. III, Academic Press, New York, 1971, p. 81.
13 H. Hanson, D. Glaber and H. Kirschke, Hoppe—Seyle Z. Physiol. Chem., 340 (1965) 107.
14 G. A. Fleischer, H. R. Butt and K. A. Huizenga, Proc. Staff Meet. Mayo Clinic, 32 (1957) 410.
15 J. H. Wilkinson, The Principles and Practice of Diagnostic Enzymology, Edward Arnold, London, 1976, p. 156.

Analytica Chimica Acta, 151 (1983) 99—108
Elsevier Science Publishers B.V., Amsterdam — Printed in The Netherlands

CARBON FIBRE MICRO-ELECTRODES IN THE DIFFERENTIAL PULSE VOLTAMMETRY OF COPPER IONS[c]

T. E. EDMONDS*[a] and JI GUOLIANG[b]

Department of Soil Fertility, The Macaulay Institute for Soil Research, Craigiebuckler, Aberdeen AB9 2QJ (Gt. Britain)

(Received 16th December 1982)

SUMMARY

The analytical performance of micro-electrodes manufactured from several types of carbon fibre is investigated. The reduction of copper(II) in a chloride medium is used to assess this performance. Calibration curves in the 10—50 mg l^{-1} range are linear; the relative standard deviation is 4—7% for measurements of 30 mg l^{-1} Cu^{2+}. The effect of electrochemical pretreatment on surface ionizable groups is examined with the aid of pH-stat experiments. This pretreatment increases the sensitivity of the electrodes as well as increasing the number of ionizable groups on the electrode surface. It is suggested that these groups are quinoidal, and that their presence increases the ease with which electrochemical reduction takes place.

Recent publications have demonstrated the analytical utility of microfaradaic electrodes [1—9]. These minute electrodes are fabricated from carbon fibres, the diameters of which are 8—12 μm. There are two prominent features of the electrochemistry attainable at these electrodes: first, their small size results in predominantly diffusion-controlled currents that are time-independent within a very short time of the initial application of potential; secondly, surface conditions can contribute significantly to the electrochemical reactions at the electrode. Hitherto, these electrodes have been used predominantly for oxidations of organic species, and the adjustment of surface conditions has been an empirical matter [2]. In this paper, the analytical utility of carbon fibre electrodes is described for the particular case of the differential pulse voltammetric (d.p.v.) determination of copper(II). In addition, some insight is given into the nature of the surface changes that occur on these electrodes after electrochemical pretreatment.

---

[a]Present address: Department of Chemistry, University of Technology, Loughborough LE11 3TU, England.
[b]Present address: Institute of Soil Science, Nanking, People's Republic of China.
[c]Copyright reserved to the Macaulay Institute for Soil Research.

EXPERIMENTAL

The microfaradaic electrodes were constructed from a variety of carbon fibres (Table 1). Fibres that were epoxy-coated were chosen as well as uncoated fibres, to provide disc-shaped and cylindrical electro-active surfaces. Borosilicate glass capillaries (2.0 mm o.d., 1.16 mm i.d.) were pulled to a tip diameter of 20 μm by a horizontal micro-electrode puller (C. F. Palmer, Ltd.). The carbon fibres were soaked and washed in acetone, dried thoroughly at ambient temperature, then inserted into the capillary tip, and sealed with epoxy resin. The capillary was back-filled with mercury, and electrical contact was established with a platinum wire. Electrodes of varying length (5—20 mm) were made; the entire length of the exposed carbon fibre was immersed in solution during use.

The carbon fibre electrode formed the working electrode of a three-electrode cell; a platinum-wire counter electrode and a Metrohm EA 442 Ag/AgCl reference electrode completed the cell. A PAR 174A polarograph was used for the d.p.v. measurements. A signal generator (Levell TG-200-D) supplied the alternating wave-forms for the electrochemical pretreatment.

All solutions were prepared in distilled—deionized water. The copper standard was made by dissolving copper wire (99.999%) in nitric acid (Aristar, B.D.H.). Hydrochloric acid (Aristar) and citric acid (analytical grade) were used to prepare the background electrolyte (5 M HCl—0.1 M citric acid). Solutions were deaerated with oxygen-free nitrogen.

The pH-stat experiments were done with Radiometer equipment comprising a PHM-64 pH meter, TTT-61 digital titrator, ABU-13 autoburette and TTA-60 titration assembly. The background electrolyte, 0.1 M KCl, was deaerated to constant pH before each experiment. Carbon fibre lengths of ca. 12 mm at masses of 30—90 mg were placed in the titration cell with the electrolyte (10 ml), and were stirred in an atmosphere of oxygen-free nitrogen. When a stable pH value was reached, usually in about 10 min, 10^{-4} M

TABLE 1

Types and properties of the carbon fibres tested

Fibre code	Type[a]	Diameter (μm)	Epoxy-coated	Comments
B	Courtaulds	8	Yes	—
F	Rigilor AG/T	11	No	Phys./chem. treated, high modulus
G	Sigrafil NF12	12	Yes	—
F01	Rigilor AG/F	8	No	Untreated version of AG/T
G01	Sigrafil SFC6	9	No	High modulus
G02	Sigrafil HM12	8	Yes	High modulus

[a]Rigilor fibres are from Le Carbone (France) and Sigrafil fibres from Hoechst (West Germany).

hydrochloric acid was added slowly (0.25 ml min^{-1}) until the initial pH value was restored. To assess the effect of electrochemical pretreatment, brush electrodes were constructed. Approximately 90 mg of 3-cm long fibres were sealed into a disposable plastic pipette-tip, with about 2 cm of the fibres protruding from the tip. The tip was filled with mercury to provide the electrical contact with a platinum wire, and the electrode was incorporated into a three-electrode cell in the titration vessel. The pH-stat measurements were done, as before, on both untreated and electrochemically pretreated brush electrodes.

Metrohm EA-286/1 glassy carbon and EA-287 carbon-paste mini-electrodes were used for comparison purposes. The electrodes were prepared as recommended by the manufacturer. The electrochemical cell was a 50-ml borosilicate glass beaker fitted with a polypropylene stopper through which holes were bored for the electrodes, etc.

RESULTS AND DISCUSSION

Differential pulse voltammetry at untreated carbon fibres

A typical *i*—*E* curve for fibre B in the background electrolyte is shown in Fig. 1 (curve a). In the region +0.5 V to —0.3 V, the curve is flat and featureless but it rises rapidly from around —0.5 V to the hydrogen wave. Most of the carbon fibre electrodes gave similar curves, although a few gave distinct broad peaks at —0.14 V. These peaks appeared on first using the electrodes, and did not reappear in subsequent work.

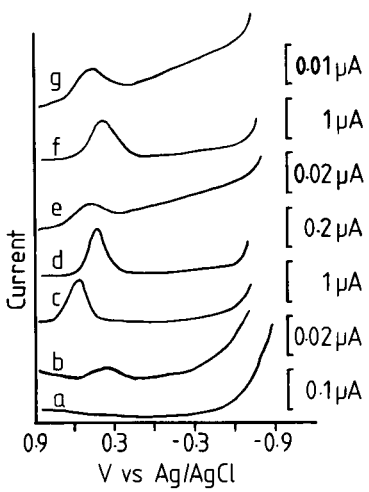

Fig. 1. Background electrolyte scan for fibre B (a), and sample scan (30 mg l^{-1} Cu^{2+}) for fibres B, F, G, F01, G01, G02 (b—g, respectively). All scans run at 5 mV s^{-1}, 50-mV pulse, 0.5-s drop time.

In the presence of 30 mg l^{-1} copper(II) ion, all fibres exhibited a single reduction peak. Both the sensitivities and the peak potentials varied considerably for the different types of fibre (Table 2). Indeed, within a single fibre type there was still variability in the peak potential, although most values were grouped closely around a mean, with a few more divergent values.

Significantly, none of the fibres gave two peaks for Cu^{2+} reduction in the chloride electrolyte. At "normal" electrodes, in electrolytes free of complexing anions, typical E_0 values are +0.521 V for the 1-electron reduction of Cu^+, +0.342 V for the 2-electron reduction of Cu^{2+}, and +0.133 V (vs. SCE) for the 1-electron reduction of Cu^{2+} to Cu^+. A single 2-electron reduction wave is normally observed for Cu^{2+}. However, in chloride solutions, the Cu^+ ion is stabilized and the E_0 values are +0.538 V for $Cu^{2+} + Cl^- + e^- \rightleftharpoons CuCl$, +0.137 V for $CuCl + e^- \rightleftharpoons Cu + Cl^-$, and −0.064 V for $CuCl_2^- + e^- \rightarrow Cu + 2Cl^-$. Thus, electrochemical reductions in chloride media usually give rise to two reduction peaks.

Wightman and co-workers [1, 6] have pointed out that the diffusion zone around a micro-electrode is large compared to its surface area. Consequently, the chemical reaction in an ECE process tends to be masked because of the rapid diffusion of the first electrogenerated species away from the electrode. Accordingly, the copper(I) species generated at the microfaradaic electrode surface may diffuse away from the electrode, preventing further reduction. Differential pulse voltammetry at the carbon paste and glassy carbon electrodes yielded two reduction peaks in this chloride electrolyte. Peak potentials were recorded at +0.60 and +0.35 V, and +0.28 V and −0.38 V, respectively, for the carbon paste and glassy carbon electrodes. The peak potentials at the carbon fibre electrodes generally corresponded to the first peak potential at the carbon paste electrode. Only fibres B and G01 gave peak potentials that tended toward those of the glassy carbon electrode. Undoubtedly, the carbon structure varies both between types of carbon fibre

TABLE 2

Electrochemical properties and surface properties of carbon fibre electrodes

Fibre	Peak potential for Cu^{2+} reduction[a] (V vs. Ag/AgCl)	Typical peak current for Cu^{2+} reduction[b] (μA)	H^+ adsorbed on fibre (μmol g^{-1})
B	+0.32 (+0.51)	7.8×10^{-3}	0.09
F	+0.72 (+0.80—0.70)	2.4×10^{-1}	—
G	+0.65 (+0.79—0.42)	4.8×10^{-1}	0.47
F01	+0.56	2.3×10^{-2}	0.07
G01	+0.42 (+0.49)	1.14	0.7
G02	+0.59 (+0.60—0.49)	8.8×10^{-4}	0.12

[a]Typical value given, plus extreme(s) of range (see text).
[b]Current normalized to 1-cm long electrodes, where appropriate.

and, to some extent, within the type of carbon fibre. These differences are reflected in the peak potential values obtained, which could suggest that fibres F, F01, G and G02 tend to a graphite structure, whereas B and G01 tend to a glassy-carbon structure. This suggestion is, of course, over-simplified, because the degree of electrochemical reversibility depends not only on the carbon type [10], but also on the chemical functional groups on the surface [11]. The latter is an important factor in the electrochemical behaviour of carbon fibre electrodes.

Reduction peaks for copper(II) ion at all fibres are shown in Fig. 1(b—g). Fibres giving the highest current produced the most clearly defined signals, symmetrical peaks superimposed on a flat base line (F, G and G01). In terms of analytical response, fibres G and G01 are the best.

pH-stat experiments

pH-stat experiments indicated that there was a wide range of concentrations of ionizable redox functions on these electrodes (see Table 2). It is assumed that these are associated with the carbon and not with the epoxy coating, and that they are, typically, surface oxide forms such as carboxyl, hydroxyl or quinoidal [12]. The existence of these groups and their effect on the electrochemistry have been established both from studies of carbon or graphite electrodes [5, 6, 12, 13] and from work involving surface-modified electrodes [11].

There is strong evidence from studies on glassy carbon [13] to support the case for quinone-type structures on the carbon surface. The increase in electrolyte pH that occurred when carbon fibres were placed in the 0.1 M KCl solution of the pH-stat experiments could thus be explained on the basis of the classic quinone/quinol redox process. This would help to explain the linear potentiometric pH response of carbon fibres [14, 15].

The number of exposed ionizable groups was calculated for both coated and uncoated electrodes, on the assumption that the former act as flat discs, and the latter as cylindrical rods. This number, when compared with a typical peak current value, indicates proportionality between the number of ionizable groups and sensitivity (see Table 3). It would appear that the very simple pH-stat experiment could give a good indication of the analytical

TABLE 3

Electrochemical properties and surface properties of carbon fibres, compared on an area basis

Fibre	H^+ adsorbed on coated fibre (meq μm^{-2})	Peak current density for Cu^{2+} reduction ($\mu A\ \mu m^{-2}$)
B	3.6×10^{-16}	1.6×10^{-4}
G	1.2×10^{-15}	4.2×10^{-3}
G02	3.2×10^{-16}	1.8×10^{-5}

utility of a particular fibre type. The reasons for increasing current sensitivity with increasing surface redox function concentration are not well understood and several possibilities have been suggested [13].

Differential pulse voltammetry at electrochemically pretreated carbon fibres

Electrochemical pretreatment of carbon fibres by triangular wave or alternating potential programmes has been described [2—4]. The experiments done here were designed to optimize three parameters of the pretreatment, i.e., duration, amplitude and initial potential with respect to sensitivity and reproducibility. The effect of pretreating before each scan or before a series of scans was also investigated. All pretreatments were done at 70 Hz.

Duration of pretreatment. Typical results for the duration of pretreatment for fibre B are shown in Fig. 2. After two minutes of pretreatment, bubbles were observed on the electrode surface; these were removed before analysis. There was no improvement in sensitivity for durations beyond 3.5 min; at longer times, many fibres either broke or provided noisy and erratic reduction peaks.

Amplitude and initial potential. All pretreatments were conducted by setting an initial potential on the polarograph and then adding a sine wave of variable amplitude from the signal generator into the summing amplifier of the polarograph. Results for fibre G02 are shown in Table 4. The two initial potentials (—1.1 V and —0.5 V) were selected to provide starting points on either side of the potential of the hydrogen wave. Increasing the amplitude resulted in a closer approach to the chlorine/oxygen wave in the anodic swing of the pretreatment sine wave. The results in Table 4 show that the greatest improvement in sensitivity is achieved when the pretreatment programme encompasses the chlorine/oxygen wave, but avoids the hydrogen wave. These conditions would be most favourable for the formation and subsequent retention of oxygen at the electrode. Simply holding the electrodes at positive

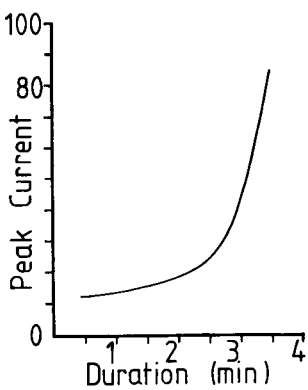

Fig. 2. Effect of duration of pretreatment for fibre B on the peak current (arbitrary units). Pretreatment conditions: amplitude 3 V, initial potential —1.1 V. Other conditions as for Fig. 1.

TABLE 4

Pretreatment conditions and sensitivity for fibre G02

Amplitude (V)	Peak current for Cu^{2+} reduction (arbitrary units)	Amplitude (V)	Peak current for Cu^{2+} reduction (arbitrary units)
Initial potential, −1.1 V vs. Ag/AgCl		*Initial potential, −0.5 V vs. Ag/AgCl*	
3.0	35	1.0	46
1.0	27	1.2	84
1.5	40	1.4	87.5
		1.5	81
		1.8	59

potentials, even for a few seconds, generally damaged the fibres. This underlines the value of applying an alternating current program, in which the potential of the electrode is held at the extreme limits for only a very brief part of the duty cycle.

The optimal pretreatment conditions for sensitivity and reproducibility for the various fibres are shown in Table 5. The improvement in sensitivity after pretreatment is considerable for several of the fibres, most noticeably for those of limited initial sensitivity. In addition to the greater reduction currents obtained, the peak shape was frequently improved. Sharper, more symmetrical peaks were obtained after pretreatment (Fig. 3). In several instances, a shift in peak potential to more positive values was noted. For example, after fifty successive pretreatments and scans, the peak potential for copper(II) reduction at fibre G01 shifted from +0.42 V to +0.57 V.

The overall qualitative effect of pretreatment is not merely an improvement in sensitivity, as would be the case for a simple increase in surface area, but a growing ease with which the electrochemical reduction takes place. This is consistent with the view that the surface functional groups of the electrode are modified by electrochemical pretreatment. If these surface groups are predominantly quinoidal, then the effect of pretreatment is to increase their number. A similar view has been advanced [11] to explain the effect of pretreatment by a radio-frequency plasma discharge in oxygen on pyrolytic graphite electrodes.

Persistence of pretreatment effects. When pretreated carbon fibre electrodes were repeatedly scanned, the sensitivity generally decreased (Fig. 4). A decrease in sensitivity was also noted when the pretreated electrode was left in solution, or in air for >20 min. This decrease was limited to a few percent of the initial value, and soon reached a steady level. Not all fibres showed this simple pattern of decline; fibre F, for example, reached a peak sensitivity some time after pretreatment, and then settled back to a static value. A pretreated fibre usually retained its sensitivity (after the initial decrease) for several hours.

TABLE 5

Optimal pretreatment conditions for carbon fibre electrodes, relative increase in peak current and relative increase in surface groups

Fibre	Pretreatment conditions			Relative increase	
	Amplitude (V)	Initial potential (V vs. Ag/AgCl)	Duration (min)	in peak current	in surface groups
B	3.0	−1.1	2.5	10	5.1
F	1.2	−0.3 V	0.5	1.3	—
G	1.0	−0.5 V	0.5	1.3	1.4
F01	1.2	−0.3 V	0.5	2.3	1.7
G01	1.0	−0.5 V	0.5	1.3	—
G02	1.4	−0.7 V	0.5	5.3	—

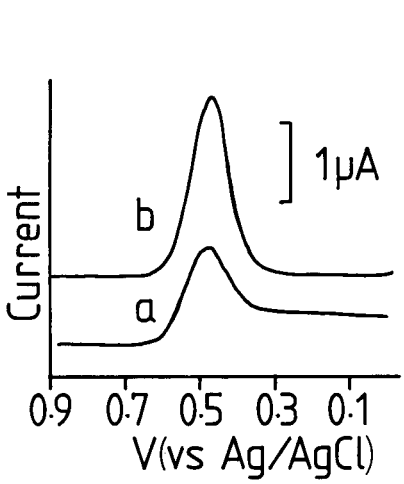

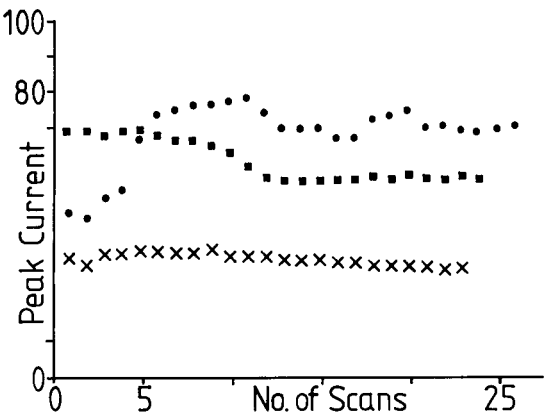

Fig. 3. Reduction peaks for Cu^{2+} (30 mg l^{-1}) at fibre G, before (a) and after (b) electrochemical pretreatment for 30 s. Pretreatment conditions: amplitude 1.0 V, initial potential −0.5 V. Other conditions as for Fig. 1.

Fig. 4. Persistence of pretreatment effects on successive scans: (×) fibre B; (•) fibre F; (▪) fibre G. Pretreatment at scan zero, for the conditions shown in Table 5; other conditions as for Fig. 1. Peak current in arbitrary units.

pH-stat experiments

The change in the number of ionizable surface groups before and after pretreatment was determined, as described, for fibres B, G and F01. The results are shown in Table 5. The relative increase in such groups reflects the relative increase in sensitivity for the three different fibres. This effect agrees well with the proportionality between ionizable groups and peak current for untreated electrodes, and supports the view that electrochemical pretreatment increases the number of surface quinoidal function.

Analytical performance of pretreated fibres

Calibration graphs for the reduction of copper(II) at fibres B, F and G are shown in Fig. 5. The fibres were pretreated before each scan, and the separate curves were recorded over a period of several weeks. Although there are distinct differences in slope between the different types of fibre, different electrodes made from one type of fibre were found to have similar slopes. In this respect the fibres show a broad constancy of response. Over the limited concentration range (0—50 mg l^{-1}), the fibres showed a useful response.

Reproducibility of response for single fibres, pretreated before each scan, was assessed by repetitively scanning 30 mg l^{-1} copper(II) solutions. The relative standard deviations (n = 20) obtained for fibres G, G01, G02, F01, B and F were 5, 4, 5, 4, 7 and 4%, respectively.

Conclusions

In terms of sensitivity and reproducibility, both before and after pretreatment, the high-modulus Sigrafil NF12 and SFC6 fibres are to be preferred to the Rigilor AG/T and AG/F fibres. Perhaps, a truly fair comparison between fibres could best be made by operating the electrodes in the micro-disc configuration [5, 6], but this approach was effectively ruled out by the low currents recorded under such conditions. A suitable preamplifier would be needed to investigate these configurations.

The increase in sensitivity arising from electrochemical pretreatment is thought to be due to surface changes on the electrode. This conclusion is

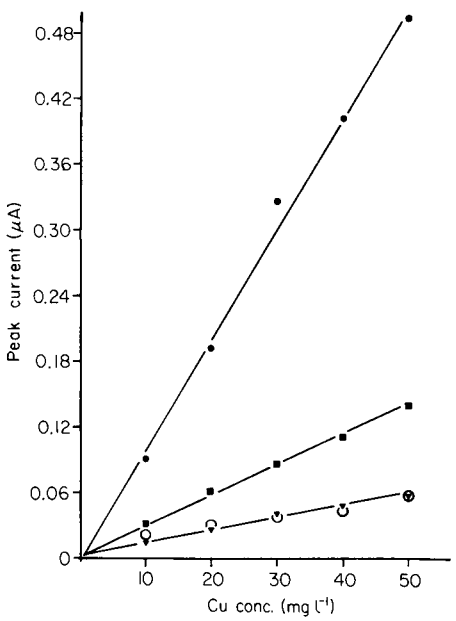

Fig. 5. Calibration graphs for fibres B (▾, ○), F (▪) and G (●). Conditions as for Fig. 1.

supported by the following evidence. First, the sensitivity of untreated fibres appears to be a positive function of the density of ionizable surface groups as determined by the pH-stat experiments, and the increase in sensitivity on pretreatment is matched by a concomitant increase in the number of ionizable surface groups. Secondly, the peak shape and peak potential before and after electrochemical pretreatment reveal a greater ease of electrochemical reduction at the treated electrode surface. Thirdly, the nature of the carbon material and its ready response to pH, as well as comparison with other surface-treated carbons, indicate a quinone/quinhydrone type couple on the surface. Finally, the optimum potential for pretreatment implies the formation of oxygen at the electrode surface, which could enhance the density of oxidized carbon species.

Mr. Ji Guoliang is indebted to the Chinese Academy of Science and the Royal Society for providing financial support. We also thank the Hoechst and Le Carbone companies for their gift of carbon fibres.

REFERENCES

1 R. M. Wightman, Anal. Chem., 53 (1981) 1125A.
2 F. G. Gonon, C. M. Fombarlet, M. J. Buda and J. F. Pujol, Anal. Chem., 53 (1981) 1386.
3 F. G. Gonon, R. Cespuglio, J. L. Ponchon, M. J. Buda, M. Jouvet, R. N. Adams and P. J. F. Pujol, Hebd. Seances Acad. Sci., 286 (1978) 1203.
4 J. L. Ponchon, R. Cespuglio, F. Gonon, M. Jouvet and J. F. Pujol, Anal. Chem., 51 (1979) 1483.
5 M. A. Dayton, J. C. Brown, K. J. Stutts and R. M. Wightman, Anal. Chem., 52 (1980) 946.
6 M. A. Dayton, A. G. Ewing and R. M. Wightman, Anal. Chem., 52 (1980) 2392.
7 M. Armstrong-James, J. Millar and Z. L. Kruk, Nature, 288 (1980) 181.
8 R. S. Robinson and R. L. McCreery, Anal. Chem., 53 (1981) 997.
9 M. R. Cushman, B. G. Bennett and C. W. Anderson, Anal. Chim. Acta, 130 (1981) 323.
10 J. J. Lindquist, J. Electroanal. Chem. Interfacial Electrochem., 52 (1974) 37.
11 J. F. Evans, T. Kuwana, M. T. Henne and G. P. Royer, J. Electroanal. Chem. Interfacial Electrochem., 80 (1977) 409.
12 W. J. Blaedel and R. A. Jenkins, Anal. Chem., 46 (1974) 1952.
13 H. Gunasingham and B. Fleet, Analyst, 107 (1982) 896.
14 V. J. Jennings and P. J. Pearson, Nature, 256 (1978) 31.
15 V. J. Jennings and P. J. Pearson, Anal. Chim. Acta, 82 (1976) 223.

Analytica Chimica Acta, 151 (1983) 109—116
Elsevier Science Publishers B.V., Amsterdam — Printed in The Netherlands

FLOW ELECTROLYSIS AT A POROUS TUBULAR ELECTRODE WITH INTERNAL STIRRING

JOSEPH WANG* and BASSAM A. FREIHA
Department of Chemistry, New Mexico State University, Las Cruces, NM 88003 (U.S.A.)
(Received 29th December 1982)

SUMMARY

The design and characteristics of a porous tubular electrode in which effective mass transport is ensured by a stirrer rotating inside the tube are described. The electrode provides high analytical currents owing to the combination of the high surface area with high mass-transport rates. The dependence of the limiting current and the degree of conversion on stirring rate, flow rate, and electrode length are described. The completeness of the electrolytic process is as high as 100%. A new hydrodynamic modulation mode, based on measuring the current difference while switching the stirring on and off, is used to correct background contributions. Analytical utility of the cell is demonstrated by application to flow injection and continuous flow analyses. Caffeic acid, *p*-acetylaminophenol, dopamine, and hexacyanoferrate(II) were used as test systems to give detection limits at the nanomolar concentration level.

Electrochemical detection in flowing streams is widely used in quantitative chemical analysis. Various flow-through electrodes have been adapted for a variety of flow systems. The most popular cell configurations are those in which the solution flows through a thin-layer channel, onto a wall-jet electrode, or through an open tubular electrode [1]. In addition, various flow-through porous electrodes are being used, aimed mainly at improving the detector response by increasing the electrode surface area [2]. A characteristic common to all of these configurations is that a solution flows past a stationary electrode. Because the limiting current response is dependent on the rate of mass transport at the electrode surface, the sensitivity is determined primarily by the solution flow rate.

Supplementary forced convection, induced independently from the solution flow, has been suggested recently to enhance the sensitivity of electrochemical flow detectors. The additional forced convection can be achieved by moving the electrode in the flow channel (e.g., a rotating disk electrode [3—5]); it can also be obtained with turbulent flow in a tubular electrode [6]. As a result of this supplementary convective transport, high sensitivity is obtainable at low solution flow rates, and under certain conditions the response becomes independent of flow rate.

This paper describes a new flow cell configuration in which a stirrer is rotated inside a porous tubular electrode to provide high rates of mass

0003-2670/83/$03.00 © 1983 Elsevier Science Publishers B.V.

transport to a large surface area. Advantages are obtained when currents are measured with the stirrer on and off to help discriminate against background currents. The porous electrode is made of reticulated vitreous carbon (RVC), a material with many hydrodynamic, electrochemical, and mechanical advantages [7]. Thus, the present design is a hybrid between the turbulent tubular electrode [6] and the rotating RVC electrode [8]. Its characteristics and applications are explored in this study.

EXPERIMENTAL

Apparatus and reagents

A schematic diagram of the cell is shown in Fig. 1. The main body of the cell was machined from a single plexiglas cylinder (5.5 cm long, 2.54-cm diameter). A flow channel (0.85-cm diameter) was drilled through the plexiglass body. The working electrode was composed of a 2xl-100 ppi RVC tube (Fluorocarbon Co.; the production rights were transferred recently to ERG, Oakland, CA). Two RVC tubes (0.45 cm i.d., 0.85 cm o.d.) having different lengths (7 and 11 mm) were evaluated. The tube was held at the lower end of the solution channel by a snug fit. Electrical contact to the RVC was made by pressure to one end of a short glassy carbon rod (2.5 mm diameter). The stirrer was a stainless steel rod (2.8 mm diameter, 6 cm long), machined to screw into the shaft of a commercial rotating disk electrode assembly (Removable End Disk Electrode, Model DDI, Pine Instruments Co., Grove City, PA). The stirrer was centered in the flow channel; care was exercised to align the stirrer and to avoid its contact with the RVC tube. Two holes in the cell wall housed the silver—silver chloride reference (Model RE-1, Bioanalytical Systems) and the platinum wire (0.3 mm diameter) auxiliary electrodes. Solution outflow was maintained through a hole in the cell wall. The three electrodes were connected to a Princeton Applied Research Model 364 polarographic analyzer, the output of which was displayed on a Houston Omniscribe strip-chart recorder.

In all continuous flow experiments, the sample solution was stored in a 400-ml nalgene beaker and solution flowed to the cell by gravity via teflon tubing. For flow injection experiments, samples were introduced with a Rheodyne Model 7010 injection valve with a 200-μl sample loop into the gravity-fed carrier solution. Dispersion of the injected sample plug was kept low by using an 8-cm length of teflon tubing to connect the injection valve to the detector cell. All interconnections were made with 1 mm i.d. teflon tubing and fittings (Pierce Chemical Co.).

Reagents used were as described recently [9], except that millimolar stock solutions of *p*-acetylaminophenol (acetaminophen) and caffeic acid (Sigma Chemical Co.) were prepared daily. Aliquots of the stock solution were added to the supporting electrolyte to give the desired concentration.

Procedure

Daily electrode pretreatment consisted of applying potentials of +0.9 V and −0.9 V alternately over a period of 12 min, allowing 2 min at each potential, and ending with application of the positive potential. During this period the supporting electrolyte solution flowed slowly through the cell. After pretreatment, the desired working potential on the plateau was applied, and transient currents were allowed to decay. Hydrodynamic modulation was provided by switching of the stirrer on and off while maintaining a constant flow rate.

RESULTS AND DISCUSSION

Mass transport

Figure 2 presents the dependence of the limiting current for hexacyanoferrate(II) on the stirring rate for various flow rates and the two lengths of

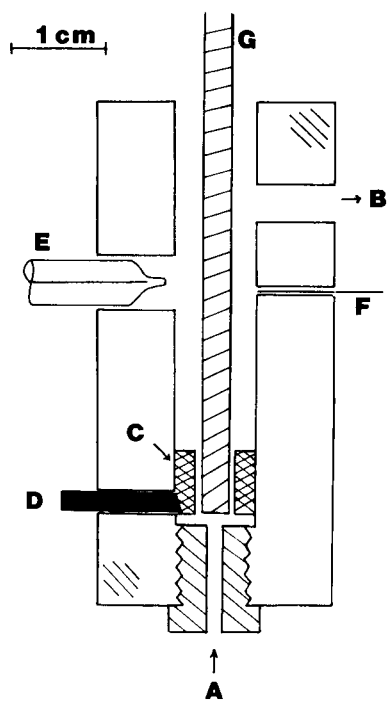

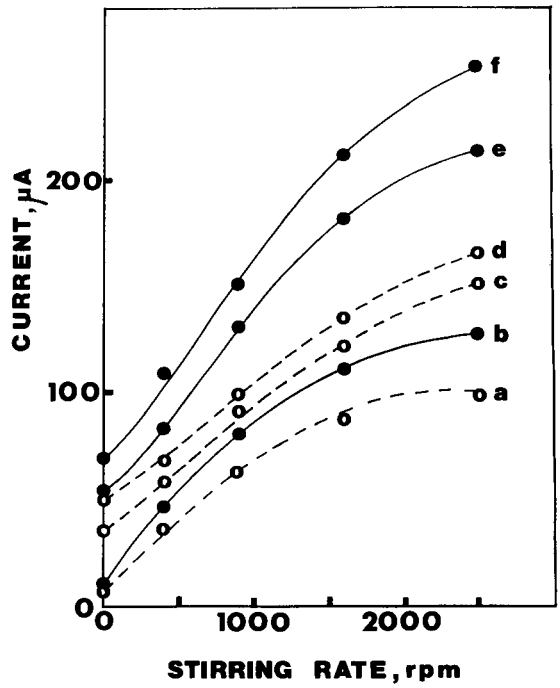

Fig. 1. The flowthrough cell. A, Sample solution inlet; B, sample solution outlet; C, RVC electrode; D, lead to working electrode; E, reference electrode; F, auxiliary electrode; G, stirrer.

Fig. 2. Dependence of limiting current on stirring rate for various flow rates of 50 μM $K_4Fe(CN)_6$ in 0.1 M phosphate buffer. Applied potential, +0.85 V. Flow rates: (a, b) 1.4; (c, e) 5.6; (d, f) 9.5 ml min^{-1}. Dotted curves are for the 7-mm tube, while full curves are for the 11-mm tube.

RVC tube. The response is increased considerably by stirring the solution. For example, with the short tube, the ratios of the limiting currents at 2500 and 0 rpm are 12, 4.5, and 3.3 for flow rates of 1.4, 5.6, and 9.5 ml min^{-1}, respectively. Based on the treatment of Brunt et al. [4] for a flow cell with a rotating disk electrode, the detector response, i_l, depends of the sum of the effects of the stirring rate, w, and flow rate, V:

$$i_l = kC[f(w) + g(V)] \quad (1)$$

where k is a constant, and C is the concentration of the electroactive species. The hydrodynamic pattern inside the electrode is certainly very complex, and a theoretical treatment is complicated because not all the elements of the solution pass through the electrode volume. To examine the power function for $f(w)$, the data of Fig. 2 (short electrode) were replotted on a log–log scale. Straight lines were obtained for stirring rates greater than 400 rpm. The slopes of these plots were 0.44, 0.43, and 0.48 for flow rates of 1.4, 5.6 and 9.5 ml min^{-1}, respectively.

The efficiency of the mass transport can be estimated by calculating the values of the mass-transport coefficient, M, at the electrode surface with the equation $i_l = nFACM$ [10]; n, F and A have their usual meanings. Calculated values of M, obtained from the limiting current data of Fig. 2 are presented in Table 1. With stirring M values are in the range 0.40–2.17 × 10^{-3} cm s^{-1}; without stirring, M values lie in the range 0.09–0.66 × 10^{-3} cm s^{-1}. Values obtained with the additional stirring approach values of 3 × 10^{-3} cm s^{-1}, calculated from data reported for a rotating glassy carbon disk electrode [11]. This indicates that effective mass transport is achieved with the present design.

A parameter of interest, not only from the analytical point of view, but also for applications such as purification or electro-organic synthesis, is the degree of conversion, R. This parameter can be calculated with the equation

TABLE 1

Mass-transport coefficients at the RVC tube with an internal stirrer[a]

Stirring rate (rpm)	Transport coefficient M (10^{-3} cm s^{-1})					
	7-mm tube			11-mm tube		
	Flow rate[a]			Flow rate[a]		
	1.4	5.6	9.5	1.4	5.6	9.5
0	0.11	0.45	0.66	0.09	0.46	0.57
400	0.48	0.74	0.90	0.40	0.68	0.93
900	0.83	1.25	1.31	0.68	1.13	1.24
1600	1.05	1.61	1.77	0.92	1.51	1.72
2500	1.28	1.96	2.17	1.08	1.80	2.13

[a] Conditions as in Fig. 2. Flow rates in ml min^{-1}.

$i_l = nFCVR$ [12]. Table 2 shows the dependence of R on the stirring and the flow rates calculated from the limiting current data in Fig. 2 for both RVC tubes. The parameter R increases as the stirring rate and the tube length increase and as the flow rate decreases. The maximum conversion noted is 100%, which is higher than that reported for a stationary RVC electrode of similar length [13]. Relatively high conversion yields are obtained even at high flow rates (e.g., 47% at 5.6 ml min^{-1}); the yield under these conditions could be improved by further increasing the stirring rate and/or the electrode length. Clearly, the supplementary stirring gives considerably higher conversion yields because of the increased mass transport. For the 11-mm tube operated at flow rates below 1.2 ml min^{-1} and stirring rates higher than 1600 rpm, steady-state limiting currents were not achieved, because the electrolytic depletion exceeded the low rate of supply by the in-flowing solution.

Hydrodynamic modulation

The high currents resulting from electroactive species of interest are accompanied by high background currents that limit the detection of very low concentrations of electroactive species. The detectability can be greatly improved by combining the high sensitivity with techniques that help to correct for the background current. Hydrodynamic modulation voltammetry has been found to be effective in compensating non-convective background currents at solid electrodes [14]. In the approach used here for hydrodynamic modulation, the stirrer is switched on and off while a constant flow rate is maintained, and the resulting current difference is measured. The difference in limiting currents can be described by

$$\Delta i_l = kC[f(w) + g(V)] - kC\,g(V) = kCf(w) \quad (2)$$

The stirring-dependent current is used to obtain the modulated response; this

TABLE 2

Conversion efficiencies at the RVC tube with an internal stirrer[a]

Stirring rate (rpm)	Conversion efficiency, R					
	7-mm tube			11-mm tube		
	Flow rate[a]			Flow rate[a]		
	1.4	5.6	9.5	1.4	5.6	9.5
0	0.07	0.08	0.06	0.10	0.12	0.09
400	0.33	0.12	0.09	0.42	0.18	0.15
900	0.57	0.21	0.13	0.72	0.29	0.19
1600	0.72	0.27	0.18	0.99	0.39	0.27
2500	0.88	0.33	0.22	1.00	0.47	0.33

[a]Conditions as in Fig. 2. Flow rates in ml min^{-1}.

response should reduce effects of non-convective background current contributions. A similar approach has been used in conjunction with a rotating disk electrode-flow cell [5].

Figure 3 shows modulated current—potential curves for the oxidation of 10 μM dopamine. The data were obtained by making 50-mV changes in applied potential and waiting about 20 s before applying the stirring pulse. Potential-independent limiting-current regions are obtainable. As expected, the limiting current increases with an increase in the stirring rate. These data indicate the feasibility of attaining reproducible voltammograms for low concentrations of electroactive species. For mixtures, a derivative approach that yields peak-shaped curves [15] could be advantageous.

A linear correlation was obtained between the modulated current amplitude and the analyte concentration. Six concentration increments from 5 to 30 μM dopamine yielded a linear plot. (Conditions: stirring on, 900 rpm for 10 s, stirring off, 30 s; flow rate, 1.1 ml min^{-1}; applied potential, +0.6 V; 7-mm RVC tube.) Least-squares treatment of these data yielded the equation Δi_l (μA) = (1.97 ± 0.08) C (μM) + 2.46 ± 1.97 μA with r = 0.996 and S_{yx} = 1.86. A 1.0 μM dopamine solution gave a current amplitude of about 8.6 μA, with a noise level of only 30 nA. Thus, defined as a signal-to-noise ratio of 2, the detection limit for dopamine would be about 7 nM. A series of 10 successive modulated measurements with 2 μM dopamine gave an

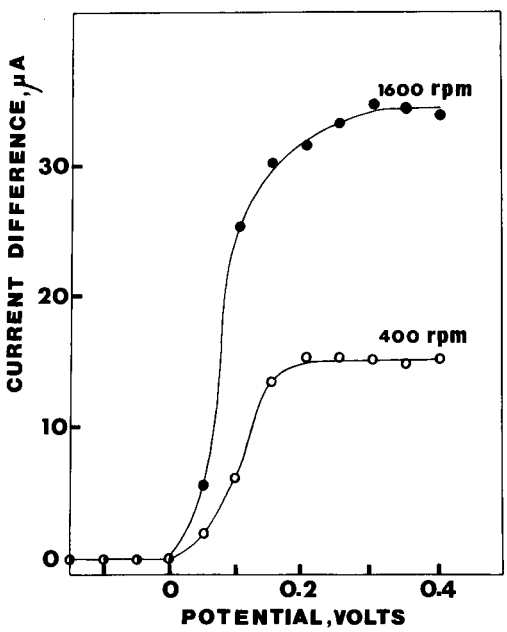

Fig. 3. Hydrodynamic voltammograms for 10 μM dopamine in 0.1 M phosphate buffer. Stop-stirring conditions: 10 s (on, 400 or 1600 rpm), 40 s (off); flow rate, 1.4 ml min^{-1}; 7-mm RVC tube.

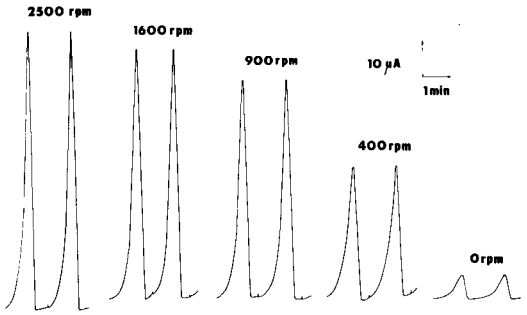

Fig. 4. Response peaks for injected 50 μM acetaminophen solution at different stirring rates. Conditions: flow rate, 1.2 ml min^{-1}; applied potential, +0.7 V; applied potential, +0.4 V; supporting electrolyte, 0.1 M phosphate buffer; 11-mm RVC tube.

average current difference of 5.5 μA with a range of 5.3—5.8 μA and a relative standard deviation of 2%.

Flow injection experiments

The high sensitivity of the present design should be advantageous for flow injection procedures. The unmodulated response was evaluated for flow injection experiments at fixed potentials. Figure 4 shows characteristic response peaks for 0.20-ml volumes of 50 μM acetaminophen solution injected into a flowing stream and measured at different stirring speeds. The peak height without stirring is only 18, 11, 10 and 8% of the response with 400, 900, 1600, and 2500 rpm, respectively. Minimum distortion and tailing of the peaks are observed as a result of the additional stirring.

Data were also obtained for caffeic acid in the 5—15 μM concentration range (0.18—0.54 μg). Peak response increased linearly with concentration (1.7 μA μM^{-1}) with a detection limit near 50 nM (1.8 ng) for the conditions used to obtain Fig. 4 at the highest stirring rate. The time between sample injections was 75 s, and the sampling rate was 48 per hour.

The cell is compatible with continuous flow and flow injection systems. It may be useful for non analytical applications in which high conversion yields are desirable. Miniaturization of the cell may make it applicable to chromatographic detection.

This work was supported by a grant from the U.S. Department of the Interior through the New Mexico Water Resources Research Institute.

REFERENCES

1 R. J. Rucki, Talanta, 27 (1980) 147.
2 A. N. Strohl and D. J. Curran, Anal. Chem., 51 (1979) 354.
3 J. Wang and M. Ariel, Anal. Chim. Acta, 99 (1978) 89.
4 K. Brunt, C. H. P. Bruins, D. A. Doornbos and B. Oosterhuis, Anal. Chim. Acta, 114 (1980) 257.

5 W. J. Blaedel and J. Wang, Anal. Chim. Acta, 116 (1980) 315.
6 W. J. Blaedel and T. W. Schieffer, Anal. Chem., 46 (1974) 1564.
7 J. Wang, Electrochim. Acta, 26 (1981) 1721.
8 W. J. Blaedel and J. Wang. Anal. Chem., 52 (1980) 1697.
9 J. Wang, Anal. Chim. Acta, 129 (1981) 253.
10 J. Jordan and R. A. Javick, Electrochim. Acta, 6 (1962) 23.
11 W. J. Blaedel and R. C. Engstrom, Anal. Chem., 50 (1978) 476.
12 R. E. Sioda, Electrochim. Acta, 15 (1970) 783.
13 W. J. Blaedel and J. Wang, Anal. Chem., 51 (1979) 799.
14 J. Wang, Talanta, 28 (1981) 369.
15 J. Wang, Talanta, 29 (1982) 805.

Analytica Chimica Acta, 151 (1983) 117—122
Elsevier Science Publishers B.V., Amsterdam — Printed in The Netherlands

BIOCHEMICAL DATA PROCESSING WITH MICROCOMPUTERS
Part 1. On-line Data Acquisition from an Amino-Acid Analyser with a Microcomputer

MICHAEL G. GORE and IAN G. GILES*

Department of Biochemistry, University of Southampton, Southampton, SO9 3TU (Gt. Britain)

(Received 4th October 1982)

SUMMARY

A program written in BASIC is described, together with the necessary electronic interfacing, to allow sequential on-line data capture from an automated amino-acid analyser by means of a commercial microcomputer. The data from two concurrent analytical channels can be handled, allowing the measurement of amino acids by spectrophotometry at 440 nm and 570 nm after reaction with ninhydrin. The procedure uses a box-car averaging technique to increase the signal-to-noise ratio, with a concurrent partial integration. This approach preserves area information whilst compressing the data into a manageable number of points for subsequent integration and area apportionment.

The problems associated with collection and handling of data from liquid and gas chromatography are well documented [1—4]. It is many years since it was first suggested that computers could assist in analysing the wealth of information that is provided during a chromatographic separation. Programs to accomplish the overall processing of data yielding information on peak height, retention time and peak area apportionment have evolved, along with the computer hardware available. The first attempts used a low-speed digitising system that created a paper-tape containing the digitised data. This was subsequently processed in the batch-stream of a main-frame computer. There was often considerable delay between data collection, and collection of the processed data; and modification of the integration parameters was a slow process.

A parallel development that had a marked impact was the hardwired dedicated integrator utilizing analog semiconductor technology. For a long time the dedicated integrator was a more cost-effective solution for area apportionment. In spite of its inherent limitations, it did yield answers very quickly for routine chromatograms giving baseline-to-baseline separations. The availability of cheap digital devices, however, now means that the computational approach with a microcomputer is preferred on grounds of both cost and flexibility.

Any on-line system has to collect the data accurately and repetitively

0003-2670/83/$03.00 © 1983 Elsevier Science Publishers B.V.

from the chromatograph output. It should require minimal user intervention for routine separations but should allow the more experienced user access to the full capabilities of the system for unusual and perhaps more complicated samples. Common problems noted when an amino-acid analyser is used (e.g., overlapping peaks, shoulders on the rising or falling edge of a peak, a large ammonia plateau on which other peaks appear, and drifting baselines) all render the simple, inflexible integrator of little value except for well-resolved peaks.

The use of a microcomputer for data processing allows the chromatographer to decide how much user input to the system is required for a particular chromatogram or, indeed, for part of a chromatogram. The collection and processing of the data can logically be divided into two distinct stages: first, data collection and storage; secondly, data retrieval and area evaluation. The separation of data collection from the necessary calculations allows the user to explore the effects caused by changes in the parameters inherent in those calculations. This can be done at any time convenient to the user when the microcomputer is not collecting data. Two linked programs, based on a readily available microcomputer, have been developed here to accomplish the data collection and analysis. The data collection program is reported below, whilst the program used for the area calculations is described in the following paper [5].

EXPERIMENTAL

Equipment

The Rank J180 amino-acid analyser used was equipped with a Vitatron 2-pen recorder. A Commodore PET 3016 microcomputer was interfaced to the analyser via the IEEE port and a 16-channel 8-bit analog-to-digital converter (ADC). Three of the input ports were used: two for data collection from the photometers at 440 nm and 570 nm, and the third to sense when the end of the chromatographic run had occurred. On the Rank analyser, this state can be detected by the PET eavesdropping on the externally controlled chart-recorder mechanism. In normal operation, the analyser switches the recorder off for a short period at the end of each chromatographic run.

The output from the photometers is nominally 10-mV full scale deflection (f.s.d.). This needs to be amplified to the required (0—10 V) range of the ADC. The circuit diagram of the device needed for one photometer is given in Fig. 1. As illustrated, this device gives an output of 7.5 V for an input of 10 mV; thus recorder f.s.d. does not saturate the ADC. Indeed, as the output from the photometer is linear for more than one chart width, this under-amplification means that peaks up to 1.3 times recorder f.s.d. can be sampled and processed. This is a useful feature because analyses are often unpredictable in nature and valuable data can be lost when peak heights exceed the recorder f.s.d. The combined effects of the amplification factor and the resolution of the A/D conversion is to give a minimal digital step equivalent to 0.5% of the recorder f.s.d.

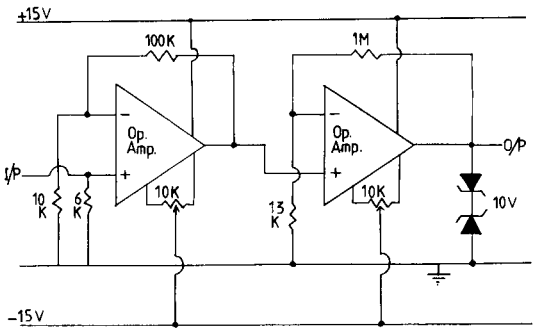

Fig. 1. Circuit diagram of a simple linear operational amplifier of gain 750. This interfaces the 10-mV output from a Rank-Hilger J180 amino-acid analyser to an ADC with an input voltage range of 0—10 V. The × 750 gain allows 1.3 chart widths to be digitised.

Reagents

All solutions used were made from deionised, distilled water and analytical-reagent chemicals (BDH) were used. Typical elution gradients employed on this machine for the separation of amino acids in a protein hydrolysate have been described elsewhere [6].

Program implementation

The general algorithm used is given in Fig. 2. The program was developed for the PET microcomputer by means of the Microsoft BASIC interpreter supplied as standard. The in-built "jiffy" clock was employed for timing. After synchronisation of the computer clock with the start of the chromatographic run, the program monitors the output voltage from the two photometers alternatively as quickly as possible. When the standard PET BASIC is used, approximately 30 samples (15 for each colorimeter) are taken per second. For each channel the digital input is continuously summed over a given sampling window (3 s for a 2-h separation). At the end of the sampling window, the mean value is stored as the representative value of that time slot. Thus in this box-car averaging technique, each point stored is the result of sampling the elution profile of each photometer 45—50 times.

The advantages inherent in this approach are realised when the collected

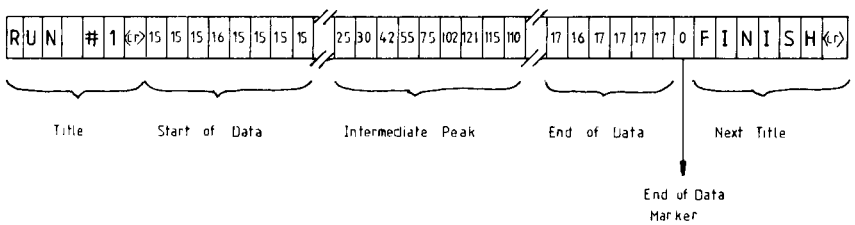

Fig. 2. Storage format of data in the serial output file. Data are stored in the form of one byte per point. The null character (ASCII 0) is used as an end-of-data marker. Therefore the sampled data must fall within the range 1—255. The end-of-file is signalled by the distinctive title "FINISH" following the last data array.

TABLE 1

Algorithm for box-car averaging, and data storage of two channels of an amino-acid analyser

```
INPUT number-of-separations-requested

number-of-runs-completed: = 0
window: = 3                                   (3 second time window)

REPEAT
   wait                                       (for start of next run)
   points-saved: = 0
   zero-clock                                 (set the real-time clock to 0 sec)
   exit-time: = 0

   REPEAT
      exit-time: = exit-time + window
      s(1): = 0                               (zero accumulator for channel 1)
      s(2): = 0                               (  "          "       "     "  2)
      n   : = 0                               (number of samples taken this point)

      REPEAT
         s(1): = s(1) + adc (channel 1)       (sample and add to accumulator)
         s(2): = s(2) + adc (channel 2)
         n: = n + 1                           (increment samples taken by one)
      UNTIL (current-time) > = (exit-time)

      points-saved: = points-saved + 1
      array (1, points-saved): = larger of (rounded value of s(1)/n) and 1
      array (2, points-saved): = larger of (rounded value of s(2)/n) and 1
   UNTIL (end-of-run-flagged)

   output title and data to tape
   number-of-runs-completed: = number-of-runs-completed + 1
UNTIL (number-of-runs-completed) = (number-of-separations-requested)
```

data are subsequently processed by the area apportionment program. During the standard 2-h chromatographic separation, the sampling program initiates some 125 000 A/D conversions for each channel. Obviously it is impractical to process this amount of data in any reasonable time. Some form of data compression is needed, and the box-car technique fulfils two requirements. First, it achieves the data compression without loss of intermediate information; secondly, it has the most desirable side effect of improving the signal-to-noise ratio in the data. The subsequent area apportionment routine was found to behave well when the elution profile is represented by approximately 2500 points. The compression of 125 000 samples to 2500 stored points is associated with an increase in the signal-to-noise ratio of 7, i.e., $(\text{compression factor})^{1/2}$. As the baseline noise-level should be as small as possible for the efficient detection of a peak start, this is highly desirable. If electronic noise is a particular problem, the elution profile can be "cleaned" by taking more samples to represent each time window. This can be achieved by slowing the separation procedure, which means that more points can be taken for the same proportion of the profile. Alternatively, compiled

BASIC can be used in place of the standard BASIC interpreter. Tests showed that up to 10 times more samples can be taken in a given time interval when compiled BASIC is used. This improves the signal-to-noise ratio by a further 3.2.

At the end of each time window, the program monitors the sense line to test if an end of run is being flagged. If it has not ended, then the next time window is begun; if it has ended, then the stored data is off-loaded to magnetic tape (or disc). The format of the serial file is shown in Fig. 2. If another separation is to follow, the program waits for the sense line to indicate the start of the next run, and the sampling is continued.

DISCUSSION

The implementation of this general algorithm for the Rank analyser—PET combination included a few features specific for this combination. First, as the digitisation employs an 8-bit A/D converter, the data for each channel are off-loaded as single byte values followed by a Null (ASCII 0) to signify the end-of-data. This significantly reduces the time taken to store the data to (or retrieve from) cassette tape and allows the output to contain a variable number of data points. Furthermore, because it is usually only the proline peak that is of interest on the 440-nm channel, only the data points in this region of the 440-nm channel are saved (by default). Nevertheless, the user can specify the limits for up to ten time windows of the 440-nm channel to be saved. However, it is our usual practice to save either the proline peak alone or the entire 440-nm elution profile.

One additional criterion must be met before the data are stored, namely, that more than 600 data points have been collected. This criterion was included because the Rank analyser switches the recorder off for approximately 2 min about 15 min (300 stored points) after the amino-acid sample has been taken. This takes into account the delay time of the column and detection system. Therefore, for a period of approximately 15 min after initiation of the first sample, the data coming through to the computer are irrelevant and can be ignored. By ignoring less than 600 data points this spurious start can be ignored, and a means of automatic synchronisation inserted, as the program can be started any time within 30 min of it taking the first sample.

There is an eccentricity of the PET operating system that automatically strips any line-feed characters (ASCII 10) in an output file, as these normally follow a carriage-return character and are redundant in this situation. There are two solutions to this problem. First, any byte containing 10 can be changed to 9 or 11 prior to output. Alternatively, the BASIC subroutine in Table 2 can be called to place the desired value (10) directly into the first cassette buffer of the PET whenever the output byte contains the value 10.

The program as described is the minimum that would suffice in routine use. It can be embellished in several ways within the algorithm described.

TABLE 2

BASIC subroutine to allow output of line-feed character (ASCII 10) by PET operating system

```
10000 REM      Subroutine to output ASCII 10 to PET TAPE unit 1.
10010 REM      Location 187 is the buffer pointer (BASIC 3.0).
10020          LET BP = PEEK (187)
10030 REM    Test to see if first cassette buffer is full. If so
10040 REM    force output to tape, enter 10 and return.
10050          IF (BP = 191) THEN PRINT#1, CHR$(0);: POKE 635, 0: RETURN
10060 REM    Buffer is not full, so enter 10 in next position
10070 REM    and increment pointer by 1.
10080          POKE 635 + BP, 10: POKE 187, BP + 1: RETURN
```

For example, the program permits only one sampling rate. The Rank analyser, however, has standard elution profiles of protein hydrolysates that take 1 or 2 h, whilst physiological samples take 4 h. Alteration of the width of the time window allows the same number of stored points to be collected for the various separation protocols. In each case, the entire elution profile should be stored within 2000—2500 points. Other embellishments are: (1) inclusion of an additional variable to take into account different sensitivity levels used by the two photometers; (2) manual abortion of a set of data points; (3) alteration of the number of samples initially requested once sampling has started; and (4) provision of a scrolling VDU display of the last 20 points sampled on each channel.

REFERENCES

1 A. Fozard, J. J. Franses and A. J. Wyatt, in P. Hepple (Ed.), Applications of Computer Techniques in Chemical Research, Applied Science Publishers, London, (1972) p. 41.
2 R. Taylor and M. G. Davies, Anal. Biochem., 51 (1973) 180.
3 J. E. Fox and J. M. Wilkinson, Anal. Biochem., 76 (1976) 387.
4 G. Schomburg, F. Weeke, B. Weimann and E. Ziegler, Angew. Chem., 11 (1972) 366.
5 I. G. Giles and M. G. Gore, Anal. Chim. Acta, 151 (1983) 123.
6 M. G. Gore and P. M. Jordan, J. Chromatogr., 243 (1982) 323.

Analytica Chimica Acta, 151 (1983) 123—130
Elsevier Science Publishers B.V., Amsterdam — Printed in The Netherlands

BIOCHEMICAL DATA PROCESSING WITH MICROCOMPUTERS
Part 2. A BASIC program for the Detection, Integration and Area Assignment of Chromatographic Elution Profiles

IAN G. GILES* and MICHAEL G. GORE

Department of Biochemistry, University of Southampton, Southampton, SO9 3TU (Gt. Britain)

(Received 4th October 1982)

SUMMARY

A BASIC program which can be used for routine area calculations is summarised. It accommodates most of the problems encountered during peak integration and area assignment, e.g., sloping baselines, overlapping peaks and shoulders on either edge of a major peak. Various levels of user interaction are incorporated so as to permit the parameters used in the calculations of an individual trace to be modified at the discretion of an experienced operator.

The preceding paper [1] reported a data acquisition program suitable for collection, partial processing and storage of information from a chromatographic elution profile, typified by that from an amino-acid analyser. In this paper, an algorithm for the detection of peaks, their integration and area apportionment is described. The methods used obviate manual transfer of data from the analyser to the computer and offer a flexibility that is not possible with a real-time dedicated integrator.

Several programs for such purposes have been described previously but have been written either for a main-frame computer with batch processing [2—7], or for a specific minicomputer in its particular assembly language [8, 9]. The advent of cheap microcomputers and analog-to-digital converters (ADC) means that these are now very attractive alternatives to the dedicated electronic integrator. The programs described here are written in the BASIC language for a Commodore PET microcomputer and should be transferable to other systems with minimal effort.

The integration algorithm described here is applicable to a wide range of chromatographic techniques, as it merely requires a sequential information stream previously stored on a secondary storage medium. The storage of the data in a suitable form was described previously [1]. The only alterations required for a system other than the amino-acid analyser are located in the data acquisition program; they relate to the time window used in the box-car averaging procedure, and possibly to the method of synchronisation used. The area apportionment routines behave stably, whichever chromato-

0003-2670/83/$03.00 © 1983 Elsevier Science Publishers B.V.

graphic method is employed, when each peak is represented by a minimum of 30 points.

In any integration and area apportionment system, whether a dedicated electronic integrator or a computer, several fundamental conditions of the current state of the elution profile need to be identified and acted upon. The important ones are the detection of a peak start from baseline, return of a peak to baseline, and a peak start without return to baseline, i.e., the start of an overlapping peak. In practice, these conditions are tested for by calculating the slope of the elution profile. In a hard-wired integrator, a new peak start is flagged if the slope exceeds a preset minimum value and integration commences, but setting of this threshold is critical. Too small a value results in spurious peak starts caused by baseline noise triggering integration, whilst too large a value results in late triggering with concomitant loss of area. The optimal threshold setting is usually a matter of trial and error, and replicate analyses are needed to establish the optimal value for a given type of separation. There may still be problems, however, because baseline noise may differ from one analysis to another, or indeed between parts of the same chromatogram. The inefficiency of this approach becomes manifest when one considers that a single elution profile from a successful column separation contains all the information required for its correct integration.

In the method advocated in this paper, the entire elution profile is digitised and stored. Subsequent integration of the profile can be effected with unlimited variation in the parameters if required. Furthermore, use of this approach makes it a trivial operation to move from the "current" position on the elution profile to past or future events. For example, sensible integration of a shoulder on the leading edge of a peak can be achieved.

EXPERIMENTAL

The program was written for a Commodore PET 3016 microcomputer using the standard Microsoft BASIC interpreter supplied as standard. Details of the amino-acid analyser and its interfacing to the PET have been reported [1].

PROGRAM IMPLEMENTATION

In any calculation of the area of peaks obtained from experimentally derived data points, adequate precautions must be taken to minimise the effect of random noise superimposed on the baseline signal. It is assumed here that all normal precautions have been taken to avoid unnecessary electronic pick-up, and that the chromatographic apparatus itself is functioning correctly, without, e.g., noise introduced from badly phased, or badly adjusted, peristaltic pumps. In the algorithm presented [1], the box-car averaging used increases the signal-to-noise ratio by approximately 10. As a result, the digitised baseline signals (permitted values 1—255) are essentially constant, varying

by $\leqslant 1$ from the average signal. No further smoothing was found to be required. Other workers have suggested least-squares fitting [10, 11] or group averaging [12] to improve the signal-to-noise ratio despite the potential hazards associated with these techniques [13].

The program is described in algorithmic form in Table 1. In implementing this, several states need to be identified so that the correct action can be taken. Furthermore, the data contain random noise which must be allowed for in the algorithm. The baseline noise level is an important parameter, and in the present system was found to have a value of 1. Use of a 12-bit ADC, or other data collection system may alter this value. The actual value can be measured directly from the elution profile if a pure baseline region can be identified. For example, the standard deviation of the first 50 points can be calculated if it is known that no peaks are present in this region. The baseline noise level can then be set to a given multiple (usually 3) of this standard deviation. The decisions all refer to this baseline noise level and the slope of the profile at the "current" point. The slopes at each point of the stored separation are calculated from the two adjacent points and stored in a

TABLE 1

Algorithm for peak integration and area apportionment
(The points representing the elution profile have previously been stored in an array)

```
Zero peak-area accumulators and Clear warning-flag-array
Form difference array from data array
current-point: = 1
this-peak: = 0

REPEAT

   REPEAT
      current-point: = current-point + 1
   UNTIL (new-peak-start-found) OR (data-exhausted)

   IF (data-exhausted) GOTO EXIT

   REPEAT
      this-peak: = this-peak + 1
      Store start (and finish) parameters of this (and previous) peak

      REPEAT
         accumulate partial area in peak-area (this-peak)
         IF (height = 255) PRINT warning and Set warning-flag (this-peak)
         current-point: = current-point + 1
      UNTIL (peak-end-detected)

   UNTIL (return-to-baseline) OR (data-exhausted)

   IF (return-to-baseline) perform baseline area subtraction
                                                ELSE PRINT warning
   UNTIL (data-exhausted)

EXIT: Output peak identification, retention time & area of peaks
```

difference array. This separate calculation significantly speeds up the final calculation, although it does double the memory required to store the data.

Peak detection

Peak start from baseline. This is detected when a given number of points (preset value = 5) all have positive slopes. This search is conducted in advance (preset value = 3) of the "current" position. If a new peak start is indicated, area accumulation begins at the "current" point to ensure that no area is lost. Increasing the number of successive positive slopes required means that a spurious peak start is less likely. However, there is an increased possibility of failing to recognise a small peak. Obviously, alteration of the baseline noise level parameter can affect the detection of a peak start, especially when a lot of noise is present.

Detection of a peak finish. A peak is deemed finished either when a return to baseline has occurred, or when another peak has started without return to baseline. The algorithm works by first testing for a peak end. If found, secondary tests are applied to establish which of the two possibilities is responsible. A peak end, for whatever reason, is characterised by the current slope being negative, whilst succeeding values (preset value = 6) are zero or positive. (In practice, the program checks whether the values are greater than the negative of the baseline noise.)

Start of an overlapping peak. When this occurs the slope of the profile changes from negative to positive. It is possible to test the slopes of several pairs of points symmetrically disposed about the current point. In this case, all those before should be negative and those after should be positive. In practice, it was found that only one pair of points need be tested.

Return to baseline. This is deemed to occur when consecutive slopes (preset value = 15) are within the baseline noise level. A false baseline can be triggered by one of three situations. A trough between adjacent overlapping peaks can be mistaken for a baseline, as can shoulders on either side of a major peak; increasing the number of consecutive slopes will prevent this. A long tail of a skewed peak (e.g., cysteic acid or ibotenic acid [14]) can also result in erroneous detection of baseline if only slopes are used. A test of absolute height must therefore also be used, i.e., the height of the first and last of the consecutive points should be within the baseline noise limit.

Area calculation

Once a peak has been detected, the area is accumulated using the trapezium rule. This area includes that below the baseline if, as usual, the baseline height is offset from zero. If an overlapping peak is found, the area for the next peak is accumulated separately from the earlier peak, i.e., the perpendicular drop method is used. It has been demonstrated that this approach is satisfactory even for poorly resolved peaks if the two peaks are of similar size [15]. Once a return to baseline has been detected, the actual peak areas are calculated. For a single peak, this merely involves subtracting the area of

the trapezium formed by the points where the peak starts and ends from the accumulated area. This procedure allows for any change in the baseline position caused by drift or changing eluants. If a series of overlapping peaks has occurred, the baseline correction is a little more involved, as the baseline position within the group must be estimated. In this case, a straight line is projected from the start of the first peak to the end of the last and the point where the perpendicular dropped from the trough between adjacent peaks is identified. The area of the trapezium so designated is subtracted from the area accumulated. This correction is applied to each component of the group in turn. As the program is written, up to 50 individual peaks can be accommodated. At all times, the value of the current data point is checked to see whether it corresponds to the maximum value given by the ADC. If saturation has occurred, any area calculated involving that point will be underestimated. To indicate this to the operator, a warning message is given and an internal flag set. Subsequently, an asterisk is appended to the area concerned when the areas are printed out.

The program continues integrating the elution profile until one of two conditions is fulfilled. The first is when all the data points have been scanned and the profile is currently on the baseline; this is the normal finishing condition. The second is when all the input data have been exhausted and the baseline has still not been reached. In this case, no meaningful baseline area, or peak area, can be calculated and so the last peak (or group of peaks) is ignored and a warning message is issued. In either case, the program proceeds to print out the results in terms of retention time of the peak maximum and area accumulated. A menu of options is then offered (Table 2). It is possible at this point to alter any of the integration parameters used and re-integrate.

Tangential skimming. If shoulder peaks occur, the areas obtained by the perpendicular drop method will be in error. A better estimate of the area of the shoulder peak can be obtained by tangential skimming [13]. The difference in areas obtained by this method and the perpendicular drop method is added to the major peak. As the complete elution profile is available, the

TABLE 2

Options available to the user

A — Calculate amounts
C — Continue to next data set
D — Display absorbance factors & parameters
E — Exit program
F — Read in new absorbance factors
P — Alter integration parameters
R — Reprint areas
S — Skim shoulder peak
T — Input data from another tape
Which option?

program can skim shoulders on both the leading and the trailing edge of a main peak.

Peak identification. Although the program is able to identify peaks by the time-window method, coupled to the 570 nm/440 nm ratio, this method is not used routinely because the position of the individual peaks may alter from run to run on account of endogenous salts in the samples. The preferred method is to identify each peak successively from the keyboard and calculate the amount of amino acid in each by reference to a known internal standard (norleucine) by using previously determined absorbance factors. A typical output is shown in Table 3.

DISCUSSION

The reproducibility of this system, when an 8-bit ADC is used, is illustrated in Table 4. The absorbance factors of 17 amino acids relative to norleucine calculated from 12 individual amino-acid analyses are given together with appropriate statistics. In all cases, with the exception of arginine, the perpendicular drop method gave a relative standard deviation that is acceptably low; that for arginine also became acceptable when the tangential skimming routine was used. The difficulty with arginine is associated with the presence of ammonia upon which the arginine peak is superimposed. This can be

TABLE 3

A typical output

The following absorbance factors were found:

ASP 0.909	THR 0.940	SER 1.023	GLU 0.997	GLY 1.053
ALA 0.981	CYS 0.682	VAL 0.943	MET 1.058	ISO 0.926
LEU 1.100	NOR 1.000	TYR 1.066	PHE 1.186	HIS 0.953
LYS 1.034	ARG 0.767			

Data from file DATA SAMPLE NUMBER 1 — 570NM

Peak	Time	Area	AA	Amount
1	31:54	530	ASP	56.12
3	35:06	1345	THR	137.71
4	37:12	1080	SER	101.61
5	44:06	450	GLU	43.40
6	54:36	827	GLY	75.59
7	56:15	120	ALA	11.77
9	59:12	633	CYS	89.33
11	60:18	1532	VAL	156.36
12	63:51	999	MET	90.88
15	69:03	587	ISO	61.01
16	70:54	776	LEU	67.90
18	76:51	231	TYR	20.86
19	79:12	187	PHE	15.18
23	103:21	840	ARG	105.41

TABLE 4

Reproducibility of the complete of amino-acid analyser and integrator system[a]
(The absorbance factors of 17 amino acids in a standard mixture were calculated with respect to norleucine)

Amino acid	Mean	S.d.	R.s.d. (%)
Methionine sulphone	0.452	0.019	4.37
Aspartic acid	0.909	0.044	4.89
Threonine	0.940	0.054	5.83
Serine	1.023	0.051	5.02
Glutamic acid	0.997	0.040	4.01
Glycine	1.053	0.034	3.24
Alanine	0.981	0.038	3.96
Cysteine	0.682	0.028	4.18
Valine	0.943	0.033	3.59
Methionine	1.058	0.040	3.79
Isoleucine	0.926	0.025	2.73
Leucine	1.100	0.025	2.31
Tyrosine	1.066	0.071	6.68
Phenylalanine	1.186	0.077	6.50
Histidine	0.953	0.054	5.69
Lysine	1.034	0.031	3.08
Arginine[b]	0.792	0.144	18.25
Arginine[c]	0.767	0.025	3.26

[a]Mean of 12 replicate runs with standard deviation (s.d.) and relative standard deviation (r.s.d.). [b]Perpendicular drop. [c]Tangential skim.

a particular problem when protein hydrolysates are used, because widely varying amounts of ammonia may be present and make the simpler perpendicular drop method unacceptable.

Several embellishments can be added to the basic program. These include: (1) reading in a time factor so that the correct retention times are output, irrespective of the elution program used; (2) printing only those areas greater than a given minimum; (3) calculating the amount of materials in the 440-nm traces correctly, irrespective of the 570/440 sensitivity ratio used.

Experience has shown that the combination of procedures described above provides an adequate, yet flexible analytical tool. Although complicated curve-fitting and curve-deconvolution techniques have been advocated [16–19], assumptions have to be made regarding the overall shapes of the constituent peaks. An unsatisfactory feature of the programs as implemented is that an integration takes about 2-min calculation time with the BASIC interpreter. This delay can be shortened by compiling the BASIC program. An alternative would be to write the program in another high-level compiled language. This, however, is not without problems as one objective was to obtain a program that would be portable with minimal effort from one machine to another by using a programming language available on any of the

current generation of microcomputers. Compared to the 2—4 hours needed to separate the amino acids, a 2-min calculation is not a significant overhead.

REFERENCES

1 M. G. Gore and I. G. Giles, Anal. Chim. Acta, 151 (1983) 117.
2 M. T. Krithevsky, J. Schwartz and M. Moye, Anal. Biochem., 12 (1964) 94.
3 H. L. Back, P. J. Buttery and V. Greyson, J. Chromatogr., 68 (1972) 103.
4 H. D. Spitz, G. Henyon and J. W. Sivertson, J. Chromatogr., 68 (1972) 111.
5 W. C. Starbuck, C. M. Mauritzen, C. McClimans and H. Busch, Anal. Biochem., 20 (1967) 439.
6 R. Taylor and M. G. Davies, Anal. Biochem., 51 (1973) 180.
7 A. Yonda, D. L. Filmer, H. Pate, N. Alonzo and C. Hirg, Anal. Biochem., 10 (1965) 53.
8 A. Thomas and K. C. Blanchard, Biochem. Soc. Trans., 2 (1974) 66.
9 J. E. Fox and J. M. Wilkinson, Anal. Biochem., 76 (1976) 387.
10 A. Savitsky and M. J. E. Golay, Anal. Chem., 36 (1964) 1627.
11 J. Steiner, Y. Termonia and J. Deltour, Anal. Chem., 44 (1972) 1906.
12 F. Baumann, A. C. Brown and M. B. Mitchell, J. Chromatogr., Sci. 8 (1970) 20.
13 A. Fozard, J. J. Franses and A. J. Wyatt, in P. Hepple (Ed.), Applications of Computer Techniques in Chemical Research, Applied Science Publishers., London, 1972, p. 41.
14 M. G. Gore and P. M. Jordan, J. Chrom., 243 (1982) 323.
15 J. Novak, K. Petrovic and S. Wicar, J. Chromatogr., 55 (1971) 221.
16 A. B. Littlewood, T. C. Gibb and A. H. Anderson, in C. L. A. Harbourn (Ed.), Gas Chromatography 1968, Institute of Petroleum, London, 1969, p. 297.
17 E. Braswell, Anal. Biochem., 44 (1971) 58.
18 A. W. Boyne and W. R. H. Duncan, J. Lipid Res., 11 (1970) 293.
19 H. Thomas, Anal. Biochem., 120 (1982) 101.

Analytica Chimica Acta, 151 (1983) 131—141
Elsevier Science Publishers B.V., Amsterdam — Printed in The Netherlands

A CRITICAL EVALUATION OF QUALITY CRITERIA FOR THE OPTIMIZATION OF CHROMATOGRAPHIC MULTICOMPONENT SEPARATIONS

H. J. G. DEBETS*, B. L. BAJEMA and D. A. DOORNBOS

Research Group Optimization, Department of Pharmaceutical and Analytical Chemistry, State University, Antonius Deusinglaan 2, 9713 AW Groningen (The Netherlands)

(Received 3rd August 1982)

SUMMARY

Quality criteria for two-component and multicomponent chromatographic separations are reviewed. The relation of quality criteria to chromatographic resolution, and the usefulness of criteria in expressing the quality of separation in reversed-phase high-performance liquid chromatography are evaluated. It is shown that the quality criteria published in the last twenty years all suffer from severe shortcomings in expressing the quality of multicomponent chromatographic separations.

Ever since the introduction of chromatography, research workers have directed major efforts towards the development of optimum separation methods. In general, however, optimization is still done by methods of trial and error and some luck is necessary to establish a reasonable separation within an acceptable time. Furthermore, the complex interaction of various experimental factors can lead to situations where even experts cannot easily comprehend which parameters are really the most important for an optimum separation. During the past ten years, a systematic approach to the optimization of chromatographic separations has been presented by several authors [1—5], and different experimental optimization techniques have been examined. A necessary, but not sufficient, condition for successful experimental optimization is that the optimization criterion is uniquely related to, or is itself, the quantity that has to become optimal [6]. Therefore, it is necessary to define an objective criterion that can quantify the quality of separation in a chromatogram.

THEORY

A well known measure for the separation of two peaks in a chromatogram is the chromatographic resolution R_s. The value of R_s can be calculated in several ways [7, 8]:

$$R_s = (t_j - t_i)/2(\sigma_j + \sigma_i) \quad (1)$$

0003-2670/83/$03.00 © 1983 Elsevier Science Publishers B.V.

where t_i is the retention time of peak i, and σ_i is the peak width at the point of inflection of the gaussian peak i;

$$R_s = 2(t_j - t_i)/(w_j + w_i) \quad (2)$$

where w_i is the peak width at the base of the gaussian peak i;

$$R_s = \tfrac{1}{4}[(\alpha - 1)/\alpha] \cdot [k'_j/(1 + k'_j)] \cdot N^{1/2} \quad (3)$$

where α is the relative retention or selectivity factor between peak i and peak j (k'_j/k'_i), k'_j is the capacity factor of peak $j[(t_j - t_0)/t_0]$, and N is the plate number of the column.

The relative retention, or selectivity factor, α, is itself a measure of separation between two peaks. However, whether the desired resolution is achieved or not depends strongly on the plate number of the column used. R_s and α are measures of separation based on chromatographic theory, whereas the valley-to-peak ratio, V [9] and the peak separation, P [10] are based on the properties of the output of the chromatographic system, the chromatogram. Therefore, the valley-to-peak ratio and the peak separation are not biased by peak asymmetry. The valley-to-peak ratio, V, is defined as the height of the valley between two peaks divided by the height of the smaller peak (see Fig. 1a). If two peaks overlap totally, the value of V is considered to be one, and if the two peaks are resolved to the baseline, V will have the value zero.

The peak separation, P, is defined as the depth of the valley between two peaks, below a straight line connecting the two adjacent peak maxima, divided by the height of the straight line above the baseline at the position of the valley (see Fig. 1b). The value of P is considered to be zero when the two peaks overlap totally, and one if the peaks are resolved at the baseline. These measures of separation are more or less satisfactory for description of the separation of two peaks. In the past, these criteria have also been used in multicomponent separations to find optimal experimental conditions for resolving all peaks in a chromatogram [11—13]. All these authors calculated the value of the criterion for each pair of adjacent peaks. The chromatographic situation in which the criterion-value of the worst separated pair of peaks was highest was considered as being the situation with optimal separation for all pairs of adjacent peaks.

This approach has been made by using the chromatographic resolution R_s, the selectivity factor α and the peak separation P. The usefulness of the approach in finding the situation with optimal overall separation in a chromatogram is questionable, because the two-component criteria mentioned express only the quality of the separation of two adjacent peaks. Useful information about the separation of other peaks in the chromatogram is completely ignored.

A more convenient approach seems to be a multicomponent criterion such as suggested by Giddings [14]. In these criteria, information pertaining to the separation of all pairs of adjacent peaks is taken into account. The multi-

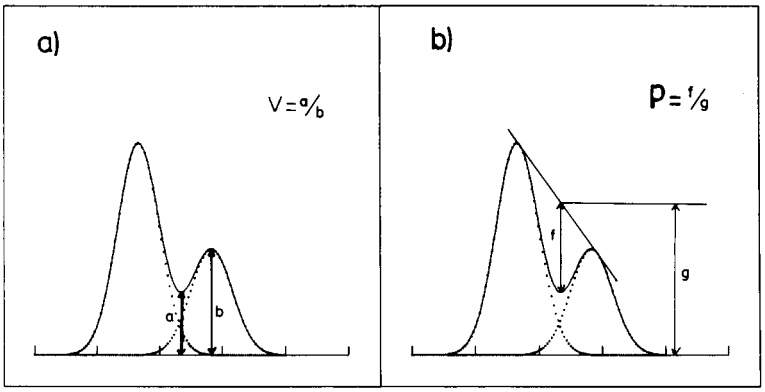

Fig. 1. Illustration of the measurement of (a) valley-to-peak ratio, and (b) peak separation.

component criteria published in the last twenty years are listed in Table 1. Most of them are summations of two-component criteria in such a way that strongly overlapping peaks contribute to a greater extent than reasonably resolved peaks. Modifications of some known criteria have been presented [16, 17, 19]; in these, time for chromatography or a desired value of the measure of separation was used to improve the performance of the criteria. Weighting factors were used to enhance the resolution of certain pairs of adjacent peaks in the chromatogram. A short explanation of the necessary calculations will be given in the later discussion.

The purpose of this work was to investigate the relation of the presented criteria to chromatographic resolution and to test the performance of some useful criteria on computer-simulated chromatograms.

EXPERIMENTAL

The computer used was the Cyber-170/760 computer (CDC) of the Rekencentrum, State University, Groningen, equipped with a 1200-baud CRT terminal (Beehive Electronics) and an electrostatic plotter (Versatec V80). All software was written in Standard Pascal [24]. The compiler used was the Pascal compiler (E.T.H. Zurich/University of Minnesota).

Chromatograms were simulated, assuming gaussian peak shapes, according to the formula

$$Y(x) = A(2\pi\sigma)^{-1/2} \exp[-(x - x_0)^2/2\sigma^2] \quad (4)$$

wherein A is the peak area, x_0 the position of peak maximum, N the plate number of the column, and $\sigma = x_0 N^{-1/2}$, σ being the variance of the gaussian distribution. The total detector response shown in the chromatograms was simply achieved by summing the responses of the individual simulated peaks.

The relation of eight quality criteria to chromatographic resolution was investigated by calculating the criterion responses for chromatograms wherein

TABLE 1

Quality criteria for chromatograms with all published modifications

1. Total overlap [14]	
$\phi = \sum_{i=1}^{k} \exp(-2R_i)$	R_i is the resolution of the ith pair of peaks.
2. Chromatographic response function [15—17]	
(a) $CRF = \sum_{i=1}^{k} \ln(p_i)$	p_i is the peak separation of the ith pair of peaks.
(b) $CRF = \sum_{i=1}^{k} p_i$	
(c) $CRF = 1/t \sum_{i=1}^{k} p_i$	t is the time of chromatography.
(d) $CRF = \sum_{i=1}^{k} w_i \ln(p_i)$	w_i is the weighing factor for the ith pair of peaks.
(e) $CRF = \sum_{i=1}^{k} \ln(p_i/p_0) - \alpha(t_1)$	p_0 is the desired value of the peak separation. t_1 is the retention time of the last peak.
(f) $CRF = \sum_{i=1}^{k} w_i \ln(p_i/p_0) + \beta(t_{max} - t_1)$	t_{max} is the maximal allowed retention time.
3. Chromatographic optimization function [18]	
$COF = \sum_{i=1}^{k} w_i \ln(R_i/R_d) + \beta(t_{max} - t_1)$	R_d is the desired resolution.
4. Informing power [19—21]	
(a) $P_{inf} = \sum_{i=1}^{k} {}^2\log S_i$	$S_i = (\Omega_{i-1,i} + \Omega_{i,i+1})^{-1}$, where $\Omega_{i-1,i}$ is the fractional overlap between peak $i-1$ and peak i.
(b) $P_{inf} = 1/t \sum_{i=1}^{k} {}^2\log S_i$	t is the time of chromatography.
5. Separation number [22]	
$SN = \sum_{n} {}^2\log p_n$	$p_n = x_n(2x_n - y_n)^{-1}$ where x_n is the real value or predicted value, whichever is larger; y_n is then the smaller value.
6. Product resolution [23]	
$\text{Prod.}R_s = \prod_{i=1}^{k} R_i$	R_i is the resolution of the ith pair of peaks.

two peaks were separated step by step from $R_s = 0$ to $R_s = 2$. The responses of the valley-to-peak ratio V, the peak separation P and the multicomponent criteria ϕ, CRF, COF, P_{inf}, SN and Prod.R_s (see Table 1) were plotted against the value of the chromatographic resolution R_s (Fig. 2); R_s was calculated

from Eqn. (3). The responses of the criteria were calculated with known peak parameters for every value of R_s, except the criteria V, P, CRF and SN, which require the simulation of the whole chromatogram. For these four criteria, chromatograms were simulated as described above.

A peak-search routine was used for detecting peaks, valleys and points of inflection. The fractional overlap, necessary for calculating the criterion P_{inf}, was determined by using standard numeric integration routines for gaussian peaks (available from the Rekencentrum, State University, Groningen). In the second example, the criteria were tested on chromatograms with four peaks. The retention times of the four components were assumed to change linearly with change in composition of the solvent as shown in Fig. 3(a). The plate number of the simulated chromatographic column was 2000 and the chromatograms were calculated from Eqn. (4). Typical chromatograms obtained in this example are shown in Fig. 3(b—e) which pertain respectively to the solvent compositions indicated by I, II, III and IV in Fig. 3(a).

The criterion responses were calculated in the following way. The chromatographic resolution (first example) or the solvent composition (second example) was changed in a hundred steps from initial to final value. For each

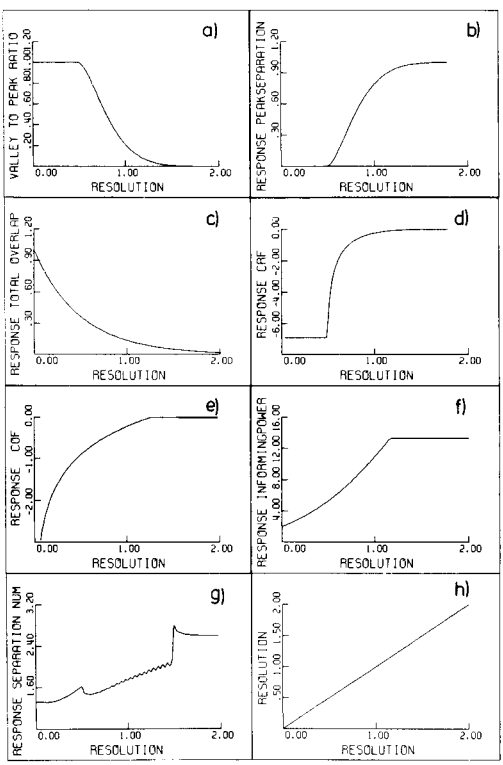

Fig. 2. Quality criteria for chromatograms plotted against chromatographic resolution.

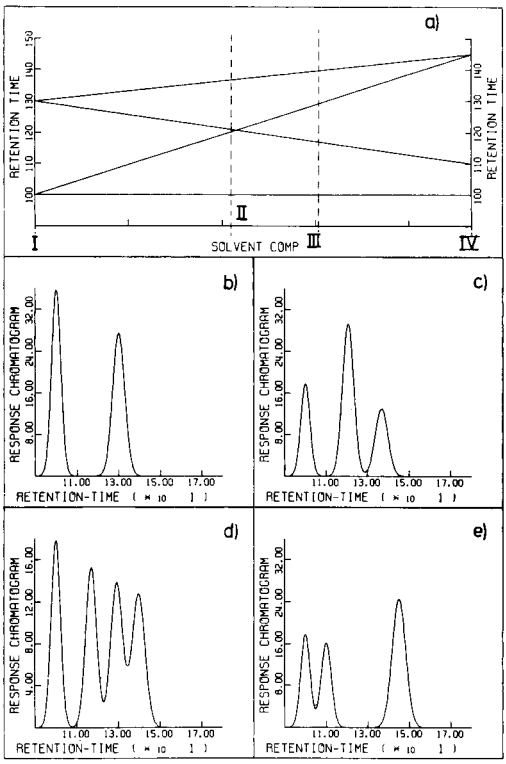

Fig. 3. (a) The change of retention times of the four peaks with solvent composition. (b—e) Chromatograms measured at the four solvent compositions indicated by I, II, III and IV.

value of the resolution or the solvent composition, the peak parameters were established. When necessary, a chromatogram was simulated, from which the positions of peak maxima, valleys and points of inflection were measured with the aid of the peak-search routine. The value of the criterion was then calculated.

RESULTS AND DISCUSSION

Typical diagrams of criterion response against chromatographic resolution are obtained when the valley-to-peak ratio V or the peak separation P are used. When the peak-search routine cannot find two peak maxima, the diagrams show straight lines (Fig. 2a, b). When the peaks become better resolved than $R_s = 0.5$, the criteria improve quickly until baseline resolution is achieved. When the chromatographic resolution increases further, the criteria will keep their final value (Fig. 2a, b).

When the total overlap ϕ is plotted against chromatographic resolution, it is clear that a simple exponential curve results (Fig. 2c). Like the valley-to-

peak ratio V, and the peak separation P, the chromatographic response function will keep its initial value until two peak maxima can be detected. The initial value is due to a constraint applied to the value of the peak separation. This constraint is necessary because the natural logarithm tends to minus infinity when the value of the peak separation is close to zero. Thus, if the value of the peak separation becomes smaller than 0.01, the value of the CRF remains constant. If two peak maxima can be detected, the response of this function changes more quickly when peaks overlap strongly because of the natural logarithm of the peak separation (Fig. 2d).

The chromatographic optimization function used is a simplified one. The parameters w_i, R_d, and β (Table 1 [3]) are chosen in such a way that the simplest form of this function is achieved ($w_i = 1, R_d = 1.25, \beta = 0$). A simple logarithmic curve is obtained until the chromatographic resolution becomes equal to the value of R_d. For $R_s > R_d$, the *COF* value remains constant (Fig. 2e).

The informing power, P_{inf}, gives a maximum value when the two peaks become resolved to the baseline, because the fractional overlap tends to zero. The minimal allowed value of the fractional overlap Ω is 0.01. When the fractional overlap becomes smaller than 0.01, the value of the informing power remains constant (Fig. 2f).

The separation number *SN* behaves quite differently. This criterion is based on the disagreement of a predicted value with the actual value in the chromatogram. Predictions are based on gaussian peak shape, threshold value and previous data [22]. The response of the criterion depends strongly on the way the chromatogram is scanned. Undesired perturbations occur when two peak maxima can be detected in the chromatogram. When the two peaks are baseline-resolved, another spike appears (Fig. 2g). The product resolution function becomes identical to chromatographic resolution in this test where only one pair of peaks is present. A straight line results in the plot (Fig.2h).

To summarize the first test, it appears that the separation number is a multicomponent criterion, the usefulness of which in expressing the quality of the overall chromatographic separation is questionable. That is why, in the second test, only the multicomponent criteria ϕ, *CRF*, *COF*, P_{inf} and Prod.R_s were investigated. The second test is more discriminating because the elution order of the four peaks changes with the solvent composition. Chromatograms with less than four peaks which are better than baseline-resolved will occur (Fig. 3b, c, e). In this test, all the criteria are calculated with parameters from the peak-search routine. This procedure demonstrates clearly the influence of detecting less than four peaks on the criterion responses.

The responses of the multicomponent criteria are plotted against the solvent composition in Fig. 4. When the total overlap, ϕ, is used as the quality criterion, a minimum response indicates optimal overall separation in a chromatogram. If the peak-search routine does not find the correct number

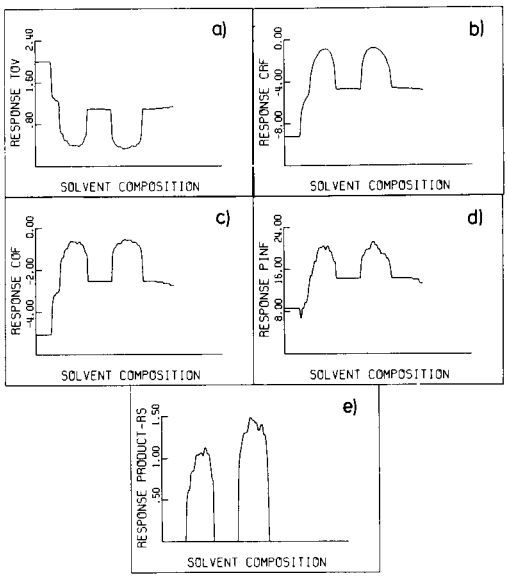

Fig. 4. The criterion response of five quality criteria, in the test illustrated in Fig. 3, plotted against solvent composition.

of peaks, the R_s value of the overlapping pair of peaks is considered to be zero. The response of the total overlap is plotted in Fig. 4(a). It is obvious that for two different solvent compositions, similarly good values of the criterion response are found. As the time for chromatography is not taken into account, the second minimum in the value of the response is the global minimum.

The response of the chromatographic response function (*CRF*) plotted against the solvent composition (Fig. 4b) shows two equally good values indicating optimal overall separation in a chromatogram. The lower values of the response are due to corrections made during calculation when less than four peaks were found in the chromatogram. The value of the peak separation for a pair of strongly overlapping peaks (only one peak maximum can be detected) is arbitrarily chosen as 0.01 (Fig. 4b).

The chromatographic optimization function (*COF*) also needs corrections in calculating the response. If less than four peaks are detected, the R_s value of the strongly overlapping peaks is considered to be 0.1. If the R_s value is smaller than 0.1, the *COF* tends to minus infinity, and therefore the R_s value of strongly overlapping peaks is kept constant at a non-zero value. This correction causes a minimum value of the response when only two peak-maxima can be detected. A maximum value of the *COF* is reached when the chromatographic resolution of all adjacent pairs of peaks exceeds R_d = 1.25. The maximum values shown in the plot of response against solvent composition (Fig. 4c) are not caused by the maximum constraint of R_d = 1.25, but are just the best values of R_s in this test.

The plot of the P_{inf} function against the solvent composition shows the same profile as the other criteria. If less than four peak maxima can be detected, the retention times of strongly overlapping peaks are considered to be identical, and so the response is bad. If a pair of peaks becomes almost baseline-resolved, the fractional overlap becomes very small and thus the response becomes very large. The response is truncated at a value of the fractional overlap of 0.01. In this test, the situation wherein all adjacent pairs of peaks are almost baseline-resolved does not occur, and so there is only one value of the solvent composition where the criterion response is maximal, indicating optimal overall separation (Fig. 4d).

The quality criterion, Prod.R_s, gives zero response when less than four peaks are found in a chromatogram because when two or more peaks overlap strongly, the R_s value of the overlapping peaks is considered as zero. The maximum value of the response indicates optimal overall separation (Fig. 4e).

CONCLUSIONS

All the multicomponent criteria tested on the second example of this study give a worst value of the criterion response when the elution order of two peaks changes. Because of that effect, the plots made in this test all show two local optima in the criterion response. Only one of these is the global optimum. Furthermore, it appears that all the quality criteria presented above need prior information about the number of peaks to be found in a chromatogram. When such information is not available, optimal values of the criterion responses will occur in situations where peaks overlap strongly (Fig. 5).

All the multicomponent criteria tested need constraints or corrections in calculating the values of the responses. When peaks show strong overlap or when they become more than baseline-resolved, mathematical and/or graphical impossibilities and inconveniences may occur.

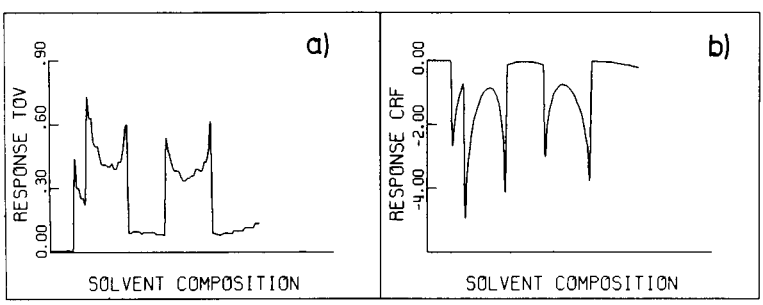

Fig. 5. The criterion response of (a) the total overlap function and (b) the *CRF* plotted against solvent composition. The criterion responses are calculated, without prior information about the number of peaks to be found in the chromatograms, for the test illustrated in Fig. 3.

A severe disadvantage of all the criteria is that they cannot set an unequivocal quantitative value on the overall separation in a chromatogram because a good separation of one pair of peaks can be compensated by a bad separation of some other pair of peaks. Criteria that are modified by taking a desired value of the measure of separation show a better performance than the others, because the measure of separation does not increase further when the desired value is reached or passed.

Weighting factors seem to be useful only if the peaks in a chromatogram can be identified. When the retention times of all peaks change with solvent composition, recognition of peaks is possible only with more sophisticated instruments or with time-consuming extra effort.

All the multicomponent criteria tested on the second example gave responses that looked alike. Sharp changes in the response mark the solvent compositions at which the number of detected peak maxima changes. This behaviour makes the criteria less useful in sequential experimental optimization strategies such as the simplex method [25, 26].

Finally, the multicomponent quality criteria tested are all directly related to chromatographic separation, but lack theoretical bases in information theory or systems theory. They do not give an optimal value of the criterion response when all peaks are baseline-resolved, without prior information about the number of peaks to be found in the chromatogram. They all give intractable responses when the elution order of peaks in a chromatogram changes.

REFERENCES

1 R. P. W. Scott, in J. C. Giddings and R. A. Keller (Eds.), Advances in Chromatography, Vol. 9, M. Dekker, New York, 1970, p. 205.
2 J. L. Glajch, J. J. Kirkland and L. R. Snyder, J. Chromatogr., 238 (1982) 269.
3 J. Holderith, T. Toth and A. Varadi, J. Chromatogr., 119 (1976) 215.
4 S. L. Morgan and S. N. Deming, Sep. Purif. Methods, 5 (1976) 333.
5 J. C. Berridge, J. Chromatogr., 244 (1982) 1.
6 H. N. J. Poulisse and P. L. M. Engelen, Anal. Chim. Acta, submitted.
7 L. R. Snyder and J. J. Kirkland, Introduction to Modern Liquid Chromatography, 2nd edn., Wiley, New York, 1979 p. 34.
8 H. Engelhardt, High Performance Liquid Chromatography, Springer-Verlag, Berlin, 1979, p. 14.
9 A. B. Christophe, Chromatographia, 4 (1971) 455.
10 R. Kaiser, Gas-Chromatographie, Geest und Portig, Leipzig, 1960, p. 33.
11 M. L. Rainey and W. C. Purdy, Anal. Chim. Acta, 93 (1977) 211.
12 R. J. Laub and J. H. Purnell, Anal. Chem., 48 (1976) 1720.
13 S. L. Morgan and Ch. A. Jacques, J. Chromatogr. Sci., 16 (1978) 501.
14 J. C. Giddings, Anal. Chem., 32 (1960) 1707.
15 S. L. Morgan and S. N. Deming, J. Chromatogr., 112 (1975) 267.
16 W. Wegscheider, E. P. Lankmayer and K. W. Budna, paper presented at 8th Int. Microchemical Symp., Graz, 1980.
17 M. W. Watson and P. W. Carr, Anal. Chem., 51 (1979) 1835.
18 J. L. Glajch, J. J. Kirkland, K. M. Squire and J. M. Minor, J. Chromatogr., 199 (1980) 57.
19 R. Smits, C. Vanroelen and D. L. Massart, Fresenius Z. Anal. Chem., 273 (1975) 1.

20 D. L. Massart and R. Smits, Anal. Chem., 46 (1974) 283.
21 D. L. Massart, J. Chromatogr., 79 (1973) 157.
22 W. A. Spencer and L. B. Rogers, Anal. Chem., 52 (1980) 950.
23 A. C. J. H. Drouen, Chromatographia, submitted.
24 K. Jensen and N. Wirth, Pascal User Manual and Report, 2nd edn., Springer Verlag, Berlin, 1978.
25 W. Spendley, G. R. Hext and F. R. Himsworth, Technometrics, 4 (1962) 441.
26 J. A. Nelder and R. Mead, Comput. J., 7 (1965) 308.

Analytica Chimica Acta, 151 (1983) 143—151
Elsevier Science Publishers B.V., Amsterdam — Printed in The Netherlands

DEVELOPMENT OF A MICROPROCESSOR-CONTROLLED COULOMETRIC SYSTEM FOR STABLE pH CONTROL

P. BERGVELD,* B. H. v.d. SCHOOT and J. H. L. ONOKIEWICZ

Department of Electrical Engineering, Twente University of Technology, P.O. Box 217, 7500 AE Enschede (The Netherlands)

(Received 17th January 1983)

SUMMARY

The coulometric pH control system utilizes a programmable coulostat for controlling the pH of a certain volume of unbuffered solution. Based on theoretical considerations, conditions are established which guarantee stable operation with maximum suppression of disturbances from the dissolution of carbon dioxide, for example. It is shown that the dynamic properties of the control system depend greatly on the response time of the pH sensor which measures the actual pH. The best results are therefore obtained by using an ISFET as pH sensor.

The determination of variations in offset and sensitivity of glass pH electrodes and other pH sensors such as ISFET's, necessitates the availability of a certain volume of an aqueous solution, the pH of which can be controlled over a long period and is not affected by external interferences, e.g., by dissolution of carbon dioxide. To keep the pH of a solution constant, a buffer is mostly used. However, drift in the output voltage of a pH sensor can be detected in this way, only as a function of available buffer solutions which are used in succession, while the sensors have to be cleaned thoroughly between measurements. Any initial drifts observed cannot be interpreted in this way, because they depend more on the cleaning procedure than on the previous pH value. A procedure of successively dipping in different buffers with cleaning procedures in between is also unsuitable for the determination of variations in the sensitivity and the response time of pH sensors.

A more appropriate procedure is the addition of acid or base to change the pH of a solution and to control the required pH, which may be constant or variable, by means of a closed-loop control system. In this case, the actual pH of the test solution is continuously measured and compared with a preprogrammed reference pattern. The difference between the measured pH and the required pH is automatically kept at a minimum, e.g., by means of a set of controllable motor burettes which add the correct amount of acid or base. A disadvantage of such a system is that the volume of the test solution constantly increases and thus also the ionic strength, which may affect the response of the sensors under test. A second disadvantage may be a limitation

0003-2670/83/$03.00 © 1983 Elsevier Science Publishers B.V.

of the quantity of acid or base to be added, thus restricting the time of a continuous test.

To eliminate such problems, a pH control system was designed in which pH changes are produced coulometrically and where a microprocessor is applied to control a coulostat. The desired flexibility is obtained by the choice of software in relation to the operational design of the whole system. A block diagram of this system is shown in Fig. 1. Stable and rapid operation of the system requires that the design complies with certain rules. These can be established by applying known control engineering criteria in relation to certain properties of the different blocks given in Fig. 1. Accordingly, these blocks will first be discussed separately.

DESCRIPTION OF THE SYSTEM

The test set-up

The pH of the test solution is changed by coulometric action, in which an electric current generates H^+ or OH^- ions at a platinum electrode in accordance with the chemical reactions:

$$2H_2O \rightarrow 4H^+ + O_2 + 4e^- \quad (1)$$

$$2e^- + 2H_2O \rightarrow H_2 + 2OH^- \quad (2)$$

at the anode and cathode, respectively. In order to avoid other reactions than those given in Eqns. (1) and (2) for a broad pH range, the test solution chosen was 1 M sodium sulphate or 1 M sodium perchlorate (50 ml). In order to avoid neutralization of generated H^+ and OH^- ions, the test solution in which the platinum gauze working electrode was inserted, was connected

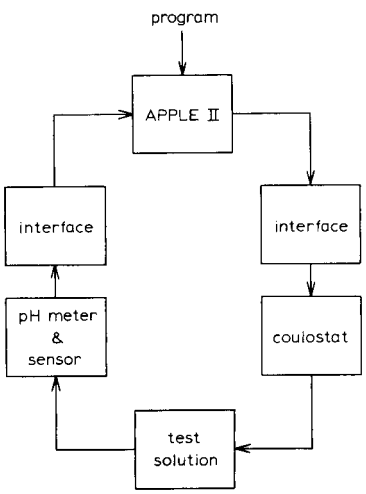

Fig. 1. Block diagram of the pH control system.

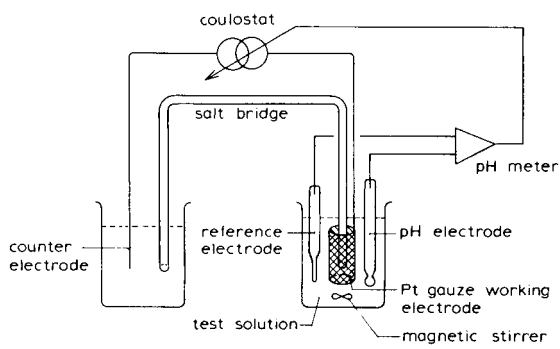

Fig. 2. Experimental set-up of the coulometric control system.

by a salt bridge (containing agar-agar and sodium perchlorate) to a second solution of the same composition provided with a platinum counter electrode. The test solution also contained a pH-measuring electrode and a reference electrode to record the generated pH, as shown in Fig. 2.

To avoid any direct influence of the coulometric current on the pH measurement, the generating electrode in the test solution was a platinum gauze cylinder around the salt bridge contact. Outside this working electrode, the electric field was almost negligible. Further, any effect of a small stray field could be minimized by proper positioning of the pH sensor with respect to its reference electrode. The test solution was thermostated at the required temperature.

The coulostat

The current source used was a Metrohm E524 coulostat, which can deliver preprogrammed currents (I) at floating electrodes during a certain time T. The output is expressed in moles of H^+ or OH^- ions: for $I > 0$, the moles of H^+ generated is $\int_0^T (I\ dt/F)$ and for $I < 0$, the moles of OH^- generated is $\int_0^T (-I\ dt/F)$, where F is the Faraday constant (F = 96 487 C mol^{-1}). The corresponding transfer function in pH mol^{-1} can be described as $H_c(s) = K_1/sF$, where s is the Laplace variable and K_1 is a function of the volume of the test solution, its composition, and the actual pH, caused by the non-linearity of the titration curve.

To keep the current source floating, the coulostat is controlled at its appropriate control input by means of two opto-couplers which are activated by the microprocessor. Because the electronic circuitry for the implementation of opto-couplers is much simpler for digital than for analog application, the required output from the coulostat is obtained by a preprogrammed constant value of the output current during a certain time T which is determined by the microprocessor and corresponds with the desired control program. The direction of the current is also controlled by the microprocessor, by activating one opto-coupler for a positive current and the other for a negative current.

The pH measurement

The actual control of the pH of the test solution is achieved by measuring and comparing it with the required value. Obviously, this measurement of the pH determines the accuracy of the pH control. Any type of pH sensor can be used for this measurement, although they should in principle be better than the pH sensors which have to be tested by means of programmed pH variations of the test solution. This aspect will receive more attention below, in considering the response time of the system.

In general, any pH sensor and its attached amplifier will respond to a variation in the pH with a time constant τ_e. This time constant may be a function of the actual pH of the test solution. For instance, it is known that a glass pH electrode is rather slow around pH 7 but faster at higher and lower

pH values. The transfer function for such an electrode can be written as

$$H_e(s) = 1/(1 + s\tau_e) \tag{3}$$

Of course, the H^+ or OH^- ions generated at the gauze electrode near the pH sensor are not immediately available at the place of measurement. Even when the solution is well stirred, there will always be a certain transportation lag between the working electrode and the sensor, with a corresponding delay time constant τ_d, as well as simultaneously occurring mixing, introducing another time constant τ_m. Both effects result in a transfer function in the system, which can be described as

$$H_d(s) = [\exp(-s\tau_d)]/(1 + s\tau_m) \tag{4}$$

The microprocessor interfaces

As already mentioned, the interface between the microprocessor and the coulostat merely provides a digital signal applied to one of two optocouplers. The interface with the pH meter consists of an A/D converter which samples the analog pH signal with a sampling frequency $1/T_s$. This introduces an additional transfer function

$$H_s(s) = [1 - \exp(-sT_s)]\,[1/sT_s] \tag{5}$$

which can be approximated for low frequencies by

$$H_s(s) = \exp(-sT_s/2) \tag{6}$$

Thus this sampling introduces a delay of $T_s/2$ seconds.

The complete control loop

The separate descriptions of the various blocks given above allow the overall system to be represented as shown in Fig. 3. In this figure, the transfer functions for sampling, coulostat, transport/mixing and pH measurement can be distinguished, while two blocks are added, namely a proportional controller, characterized by K_2 (A/pH) and a block that represents the relation K_1/s between an interfering action (e.g., dissolution of carbon dioxide) and the resulting pH mol^{-1}. This K_1 is the same factor as is used for the coulostat, and so is a function of the test solution and its pH.

The overall transfer function (closed-loop amplification) of the system is

$$H_{\text{closed loop}} = \exp[-s(\tau_d + T_s/2)]/\{\exp[-s(\tau_d + T_s/2)] + [Fs(1 + s\tau_e)(1 + s\tau_m)/K_1K_2]\} \tag{7}$$

which value approaches unity for $s \to 0$.

The suppression of the interference signal is

$$H_{\text{interference}} = (F/K_2)(1 + s\tau_m)/\{\exp[-s(\tau_d + T_s/2)] + [Fs(1 + s\tau_e)(1 + s\tau_m)/K_1K_2]\} \tag{8}$$

which value approaches F/K_2 for $s \to 0$.

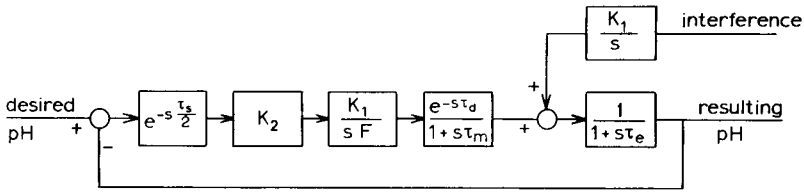

Fig. 3. The pH control loop.

A maximum suppression of interference can thus be expected for a large value of K. The value of K_2, however, is limited by the general control criteria for stable closed-loop systems, which can be determined from the amplitude and the phase diagram (Bode diagrams) [1] of the open-loop amplification as given by

$$H_0(s) = K_1K_2 \exp\left[-s(\tau_d + T_s/2)\right] / \left[sF\,(1 + s\tau_e)(1 + s\tau_m)\right] \tag{9}$$

From Eqn. (9) it follows that

$$|H(j\omega)| = (K_1K_2/F)/\omega\left[\omega^2(\tau_e + \tau_m)^2 + (1 - \omega^2\tau_e\tau_m)^2\right]^{1/2} \tag{10}$$

$$\phi(j\omega) = -\frac{\pi}{2} - \omega\left(\tau_d + \frac{T_s}{2}\right) - \operatorname{arctg}(\tau_e\omega) - \operatorname{arctg}(\tau_m\omega). \tag{11}$$

where ω is the circular frequency ($j\omega = s$).

The control criteria are as follows: for the phase margin, $|H(j\omega)| = 1$ and $\phi(j\omega_1) \leqslant 50°$; and for the gain margin, $\phi(j\omega) = -180°$ and $|H(j\omega_2)| \leqslant 0.5$. Both conditions have to be fulfilled. The tolerable value of K_2 can be calculated from Eqns. (11) and (10) in relation to given values of τ_d, τ_m, T_s, τ_e(pH), and K_1 (pH). The optimal control over a broad pH range requires that the microprocessor contain a preprogrammed table of the K_2 values, which are previously determined experimentally in the given set-up as described in the next section.

DETERMINATION OF THE ESSENTIAL SYSTEM PARAMETERS

In order to guarantee stable operation of the closed-loop system described in the previous section, the essential parameters τ_d, τ_m, τ_e(pH) and K_1(pH) have to be measured or calculated beforehand from that part of the system that fixes these parameters, i.e., the measuring vessel with the working electrode and the pH sensor.

To determine the other parameters, a current pulse I is generated for a certain time T in the experimental set-up, and the resulting ΔpH, which must be small enough for the system to be considered linear, is recorded by the pH sensor. A typical result of such an experiment is shown in Fig. 4.

It was found from these experiments that τ_d is 1.5 seconds. The values of τ_e and τ_m cannot be determined separately because the effects are mixed.

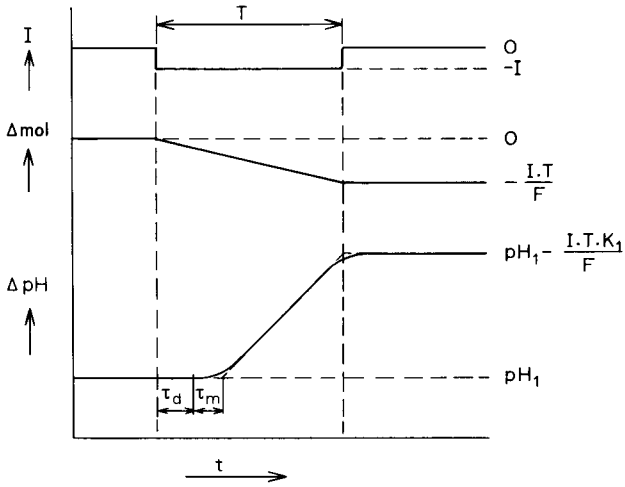

Fig. 4. Experimental result of ΔpH = f(Δmol), measured with an ISFET.

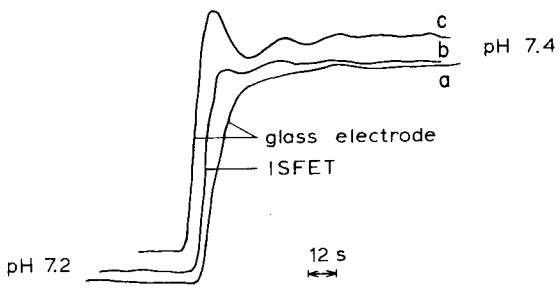

Fig. 5. Programmed stepwise change in the pH of the test solution. Curves: (a) glass electrode with K_2 = 7.9 → 6.1; (b) ISFET with K_2 = 15.8 → 12.3; (c) glass electrode with K_2 = 15.8 → 12.3.

However, if an ISFET is used as the pH sensor, the time constant τ_e will be very small (of the order of ms) [2], and the value of τ_m can be measured. The value found was 0.5 second. Both time constants, τ_d and τ_m, are independent of pH.

When a glass electrode is used as the pH sensor, the value of τ_e must be considered, but it is not possible to measure this value within the above experiment. In order to be certain, the worst case for the τ_e value of 3 seconds around pH 7, known from the literature, is taken into account for the whole pH range.

The values of K_1 (pH mol^{-1}) as a function of pH can be determined from a sequence of experiments as described above. The values of K_1 can also be determined from a titration curve. Table 1 gives the calculated values for K_1, as well as the corresponding maximum values of K_2 for a glass electrode and

TABLE 1

Measured values of K_1 as a function of pH and calculated maximum values of K_2. The control program uses such a table in the pH range 3—11. The values K_2 in brackets give the pulse duration in milliseconds when the coulostat is set at 9.65 mA (0.1 μmol s^{-1}) for an error of 0.01 pH. The values are given for a test volume of 50 ml

pH	K_1(pH μmol^{-1})	K_2(mA/pH)	K_2(mA/pH)
		Glass electrode[a]	ISFET[b]
6.00	0.34	39.8 (41)	80.1 (83)
6.25	0.45	30.1 (31)	60.5 (63)
6.50	0.65	20.8 (21)	41.9 (43)
6.75	0.91	14.9 (15)	29.9 (31)
7.00	1.27	10.7 (11)	21.5 (22)
7.25	1.72	7.9 (8)	15.8 (16)
7.50	2.22	6.1 (6)	12.3 (12)
7.75	2.56	5.3 (5)	10.6 (11)
8.00	2.22	6.1 (6)	12.3 (12)
8.25	1.64	8.2 (8)	16.6 (17)
8.50	1.02	13.3 (13)	26.7 (27)
8.75	0.63	21.5 (22)	43.2 (44)
9.00	0.42	32.2 (33)	64.9 (67)

[a]Conditions: τ_d = 1.5 s; τ_m = 0.5 s; τ_s = 1 s; τ_e = 3 s. [b]Conditions: τ_d = 1.5 s; τ_m = 0.5 s; τ_s = 1 s; τ_e = 0 s.

an ISFET, respectively, calculated on the basis of the control criteria given in the previous section. A value of ω can be calculated for the phase margin $\phi = -130°$ from Eqn. (11). This value is substituted in Eqn. (10) for $|H(j\omega)| = 1$. From this calculation the maximum value of K_2 is found which obeys the phase margin. In the same way, a value of K_2 can be calculated to obey the gain margin ($\phi = -180°$ and $|H(j\omega)| = 0.5$). In order to fulfil both criteria, the smallest value of K_2 is taken in Table 1.

From the table it can be seen that the steepest part of the titration curve is between pH 7.5 and 8. This is due to the fact that the second dissociation of sulphuric acid is weak ($K_a = 1.2 \times 10^{-2}$). Calculation shows that the equivalence point is at approximately pH 7.8. The slope of the titration curve (K_1 values) is influenced by the buffering properties of dissolved impurities and is thus somewhat smaller than would be expected for a pure sodium sulphate solution. Dissolution of carbon dioxide causes the K_1 values to change in time. After some hours in use, however, the titration curve tends to stabilize resulting in the values given in Table 1.

The table is stored on a floppy disk and used in the desired control programs for optimal pH control. Note that the fast response of an ISFET (assumed τ_e = 0 s) results in a larger tolerable value of K_2 which makes the system as a whole faster and more stable.

RESULTS

The pH control system was tested with a stepwise sequence of desired pH values for any desired span of time. The sampling time was set to 1 s and the coulostat output current to 0.1 μmol s^{-1} or 9.65 mA. This means that the microprocessor has to calculate the sign and the duration of the fixed coulostat output current after each measuring sample of the actual pH, in relation to the corresponding system parameters, from the stored table and at the desired pH value. The calculated pulse duration is also given in Table 1 for a minimum $\Delta pH_{min} = 0.01$. The duration is x times this value for a $\Delta pH = x\ \Delta pH_{min}$. The calculated time is entered in a programmable clock circuit which controls the coulostat. After each sample a new calculation is carried out and the clock is reprogrammed. This means that the effective duration of a current pulse is limited to approximately one second. If the calculated time exceeds this value (large value of $\Delta pH = pH_{desired} - pH_{actual}$), the speed of the system becomes limited by the fixed output current from the coulostat, which determines the slope of the titration curve. A comparison between the system response times when a glass electrode or an ISFET is used as the pH sensor is therefore useful only for those cases where no limitation is imposed by the coulostat (pulse width τ (Fig. 4) <1 s).

Figure 5 shows the results of a stepwise sequence in pH when a glass electrode was used as the pH sensor (lower curve), and when an ISFET was used (middle curve). The small fluctuations of ΔpH (± 0.01) are due to the limited resolution of the A/D converter. It can be seen that the use of an ISFET is preferable with regard to the response time, in agreement with the calculated larger values of K_2 as shown in Table 1. The upper curve of Fig. 5 shows the instability of the system when a glass electrode is used and the value of K_2 taken is twice the permitted value.

The control system was developed for the elimination of interferences, e.g., from dissolution of carbon dioxide. To test the effectiveness of the system quantitatively, 0.03 ml of 0.01 M HCl was injected at around pH 7, the most sensitive pH area. The control action is shown in Fig. 6 for a glass elec-

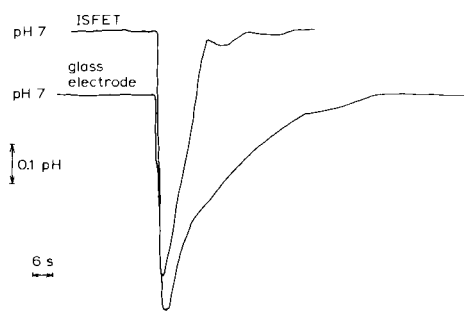

Fig. 6. Recovery of the pH after injection of 0.03 ml of 0.01 M HCl. The upper curve is for the ISFET with $K_2 = 21.5 \rightarrow 41.9 \rightarrow 21.5$; the lower curve is for the glass electrode with $K_2 = 10.7 \rightarrow 20.8 \rightarrow 10.7$.

trode or an ISFET as the pH sensor. Because of the larger value of K_2 in the latter case, the effect of the disturbance is much shorter which is in complete agreement with the theoretical expectation as described by Eqn. (8).

Conclusions

It is shown that a system can be designed and made to control the pH of a certain volume of unbuffered solution. The accuracy and the response time of the system depend on the ion sensor which is used to measure the actual pH of the solution. The faster the response time of this sensor, the larger the open-loop amplification of the system that can be chosen, and the more stable the system will be. Therefore an ISFET as pH sensor is preferable to a glass electrode. It will be clear that other programs can also be implemented in the system. For example, to obtain a linear increase or decrease of pH, the desired pH value is simply programmed as a function of time. The maximum slope of a linear pH change is again a function of the response time of the ion sensor.

The authors thank Dr. M. Bos from the Department of Chemical Technology for his help and useful suggestions.

REFERENCES

1 F. H. Raven, Automatic Control Engineering, 3rd edn., McGraw-Hill, New York, 1978, Ch. 11, 12.
2 L. J. Bousse, P. Bergveld and W. E. van der Linden, Scientific Session on Electrochemical Detection in Flow Analysis, October, 1982, Matrafüred, Hungary.

Analytica Chimica Acta, 151 (1983) 153—160
Elsevier Science Publishers B.V., Amsterdam — Printed in The Netherlands

MASS TRANSFER ACROSS LIQUID—LIQUID INTERFACES

Part 1. A Computer-controlled Apparatus based on the Free-falling Droplet Technique

INGER NAHRINGBAUER* and BO LARSSON

Institute of Inorganic and Physical Chemistry, Faculty of Pharmacy, Biomedical Center, Uppsala University, Box 574, S-751 23 Uppsala (Sweden)

(Received 6th December 1982)

SUMMARY

An automatic apparatus for studying the rate constants for the transport of a drug between immiscible solvents is described. The whole system is on-line with a computer. The contact time between dispersed and continuous phases, the free-fall rates of the droplets, and their mean radius are determined by utilizing the capacity of the computer to measure time. The dispersed phase at a desired pH and solute concentration is prepared automatically.

Partition coefficients between immiscible solvents have been reported for a large number of drugs and related compounds [1, 2]. The relationship between partition coefficient and structure has also been studied extensively. Hansch developed the SAR model (structure—activity relationship) which has attracted much interest over a number of years. The relationship between chemical structure and drug activity is a constant preoccupation of many organic chemists, medicinal chemists, and pharmacologists. In order to design a drug molecule for a specific biological purpose, different approaches to the quantitative structure—activity relationships (QSAR) have been developed [2—4]. The biological activity of a drug depends on its concentration at a certain site in the body, e.g., the receptor compartment. In QSAR approaches, this concentration is predominantly correlated with equilibrium constants (partition and acidity constants). However, theoretically, it seems to be more realistic to correlate concentration with kinetic parameters, such as the rate constants, for the transport of a drug from an aqueous to an organic phase and for the reverse transport.

An investigation on correlation of the rate constants with equilibrium constants of different kinds (e.g., partition coefficients, acidity constants, extraction coefficients, complex constants) should contribute to a better understanding of the complex nature of the QSAR. In order to accelerate the collection of data as well as increase the accuracy of the determinations, the automatic apparatus described in the present paper has been developed.

0003-2670/83/$03.00 © 1983 Elsevier Science Publishers B.V.

THEORY

The process of mass transfer at an interface is generally assumed to consist of three relatively simple steps: diffusion of solute molecules from the bulk of the raffinate phase to the interface, crossing of the interface, and diffusion from it into the bulk of the extract solvent. Several of the earlier investigations on interfacial transport were aimed at identifying the portion of the mass transfer resistance associated with the interface. The interface between two clean immiscible solvents is usually considered to be a two-dimensional boundary between the liquids. As a result of this inability to resolve the interfacial region into a continuum, rate constants are generally assigned to the interface as kinetic parameters, to explain resistances in excess of the solute diffusion to and from the interface.

Brenner and Leal [5] presented a refined kinetic model. They considered the interfacial region to be a microscopic continuum where the resistance associated with the interface is expressed in terms of an energy profile which arises from the influence of the adjacent phase on the diffusion of the solute molecule. In the present paper, we use the formulation of the mass transfer proposed by Shaelwitz and Raterman [6], based on a macroscopic kinetic model for the interface which is consistent with the results of Brenner and Leal. Two sets of forward and reverse rate constants are assumed. One set is associated with the entry of the solute molecule into the interfacial region and the other set is combined with its departure. Thus, this kinetic model corresponds to an energy profile with two maxima and one minimum instead of the single barrier assumed in previous kinetic models.

The flux of mass-transfer exchange between the bulk and the interface can be expressed as the product of the transfer coefficient and the driving force. Within a falling or rising drop, circulation currents are caused by the friction drag of the outer fluid [7—15]. This results in very thin diffusion layers at the interface and, to a good approximation, mass transfer is assumed to be pseudo-steady between the phases. The flux is

$$J = k_{m1}(c_1 - c_1^f) \quad \text{(diffusion)} \tag{1}$$

$$J = k_{a1} c_1^f - k_{d1} c^* \quad \text{(adsorption/desorption)} \tag{2}$$

$$J = k_{d2} c^* - k_{a2} c_2^f \quad \text{(desorption/adsorption)} \tag{3}$$

$$J = k_{m2}(c_2^f - c_2) \quad \text{(diffusion)} \tag{4}$$

where 1 and 2 represent the raffinate and extract phases, respectively. At or very near the interface is denoted by f, and asterisks indicate the part of the interfacial region where the energy profile has its minimum. Bulk mass-transfer coefficients are k_{m1} and k_{m2}, and rate constants for the energy barrier near the interface are k_{a1}, k_{d1} and k_{a2}, k_{d2}, respectively. All constants have the dimension mm s^{-1}.

If all the fluxes (Eqns. 1—4) are combined,

$$J = K_{app}(c_1 - c_2/m) \quad (5)$$

$$\text{where } 1/K_{app} = 1/k_{m1} + 1/k_{a1} + (1/k_{m2} + 1/k_{a2})m^{-1} \quad (6)$$

$$\text{and } m = (1 + a_{H^+}/K_a)^{-1} k_{a1} k_{d1}^{-1} k_{d2} k_{a2}^{-1} \quad (7)$$

provided that the solute is a base and only neutral particles are distributed from the aqueous phase to the organic one. The expression $k_{a1}k_{d1}^{-1}k_{d2}k_{a2}^{-1}$ is the thermodynamic partition coefficient, K_d, if the raffinate phase is water and the extract phase is the organic solvent. For dilute solutions K_d is only a function of the solute and the two solvents if the temperature and pressure are constant. According to the above discussion, the overall mass-transfer coefficient, K_{app}, is dependent on the acidity constant, K_a, the partition coefficient, K_d, and pH.

In the raffinate phase, the overall rate of the mass transfer will be

$$dc_1/dt = -(A/V_1)J \quad (8)$$

The interfacial area is represented by A. The volume of the raffinate phase, V_1, is assumed to be independent of the time as the mass transfer does not cause a significant change of the volume. When sink conditions are applied to the extract phase and the raffinate phase is a droplet, Eqns. (5) and (8) give

$$dc_1/dt = -(3/r)K_{app}c_1 \quad (9)$$

where r denotes the radius of the droplet. If K_{app} is independent of the total time of contact between the droplet and the continuous phase, $\ln c_1$ will be linearly dependent on the contact time.

DESCRIPTION OF THE METHOD

Equipment

The computerized system (Fig. 1) consists of an Alpha LSI-2 computer (48 kbyte memory), an Altema magnetic tape station, a Silent 700 terminal, a Radiometer PHM64 pH meter, a Therm 3240 digital thermometer, five Metrohm motor-driven burettes, a Zeiss DM4 spectrophotometer, a specially-made thermostatted glass tube (height 2.25 m, inner diameter 0.016 m), three Galitron photoelectric cells (Griestrabe Elektronik, Zürich), several valves, and some complementary equipment.

All measuring instruments in the system have a binary coded decimal output which is easily connected to, and understood by, the computer. Very precise time measurement is possible by means of the built-in oscillator of the computer. Each pulse from the oscillator interrupts the computer and causes the execution of a special time-counting routine. An oscillator frequency of 100 Hz corresponds to the smallest measurable time unit of 0.01 s. The longest measurable time without resetting the clock is 32 767 s (about 9 h).

The computer reads the different instruments via 80 bits parallel input and decides the state of the system. The computer controls the system

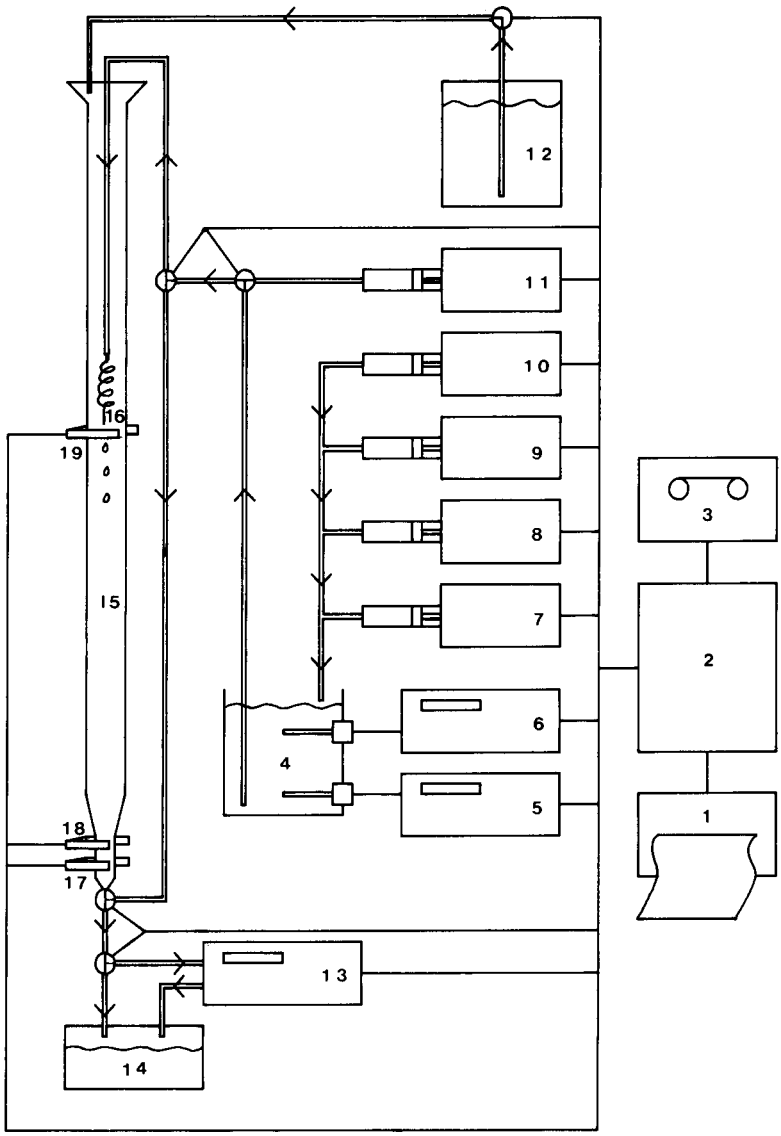

Fig. 1. The computerized measuring system. The different components are: (1) Computer terminal; (2) computer; (3) magnetic tape station; (4) mixing vessel; (5) digital thermometer; (6) pH meter; (7—11) motor-driven burettes; (12) container for organic solvent; (13) spectrophotometer; (14) container for outlet liquids; (15) thermostatted glass tube; (16) drop-forming nozzle; (17—19) photoelectric cells.

via a 16-bit output interface. Each output bit activates or deactivates a special function in the system, e.g., a valve is opened or closed with one bit, a motor-driven burette is started or stopped by another bit. The operator communicates via a terminal. Mass storage of programs is done on magnetic tapes in a cassette station connected to the computer.

The contact time between dispersed and continuous phases

The time of contact is recorded only during the free-fall period of a droplet, i.e., the time from the detachment of the droplet from the nozzle to its arrival at the coalesced layer at the bottom of the tube. A major problem was to design a system of recording this. The thermostatted glass tube in Fig. 1 is in fact composed of two concentric glass tubes. The outer diameter is 0.05 m. Any kind of apparatus chosen to sense the droplets has to be located more than 0.025 m from the fairly small drops (0.002—0.003 m in diameter). Furthermore, there are two glass walls, and two different liquids between the sensing body and the droplet. Another difficulty is the wobbling fall of the droplet which diverges in an irregular way from the central line of the inner tube. The Galitron miniature photoelectric cells were found to be the best solution to these problems. This cell manages to sense very small objects and has a relay or an electronic output suitable for connection to a computer. In addition, an enlarged image of the droplet is observed when the photoelectric cells are placed at a proper distance from, and perpendicularly to, the glass tubes acting as optical lenses. When a very careful adjustment of the position and sensitivity of the photoelectric cell has been made, the system of photoelectric cells works with satisfactory precision.

For the computation of the free-fall time of a droplet, the computer compares two pulse trains, one travelling from the higher, movable photoelectric cell, and the other from the lower, fixed cell. If t'_{h1}, t'_{h2}, t'_{h3}, . . ., t'_{hn} and t'_{k1}, t'_{k2}, t'_{k3}, . . ., t'_{kn} represent the points of time when n drops pass the higher and the lower photoelectric cells, respectively, then the free-fall time of the drop, i, will be $t_i = t'_{ki} - t'_{hi}$. The stored contact time is a mean value based on the free-fall times of the first 20 droplets out of about 200.

The height of droplet free fall

The contact time between dispersed and continuous phases is varied by changing the height of free fall. The nozzle and the movable photoelectric cell (19 in Fig. 1) are attached to the same motor, driving them upwards or downwards at a constant velocity. The time that the motor has been on will be a measure of how far the nozzle and the photoelectric cell have moved. The distance between the two drop-recording photoelectric cells (18 and 19 in Fig. 1) can thus be determined very precisely.

Control of liquid flow and record of added volumes of liquid

The flows of liquids are regulated by opening or closing the appropriate valves. The function of each valve depends on a solenoid controlled by the

computer. Burette pistons, air pressure, and gravity are the driving forces of the different flows of the liquids present in the system. The dispersed phase, consisting of a buffer solution of the desired solute concentration, is prepared in the mixing vessel by the addition of suitable volumes of liquids from four different motor-driven burettes (7—10 in Fig. 1). The contribution from each burette is controlled by the computer counting the pulses of a pulse train signal from each burette. One pulse corresponds to 2×10^{-9} m^3 (0.002 ml).

Process

The necessary data, such as temperature, pH values, number of different heights at each pH, and concentration of the solute, are fed into the computer. The following steps are then processed consecutively.

(1) If there is any solvent in the glass tube, it is let out until the fixed photoelectric cells at the bottom of the tube (17 and 18 in Fig. 1) show that the tube is empty.

(2) A buffer solution is prepared in the mixing vessel. The desired pH is obtained by mixing the buffer components according to a stored table of values.

(3) The glass tube is filled with a fresh organic solvent.

(4) A water/organic liquid interface is formed at the bottom of the glass tube by dropping a few drops of the buffer solution through the continuous organic phase.

(5) Both the cuvettes of the spectrophotometer are filled with the buffer solution. The absorbance is recorded and used as zero adjustment at point 12 (see below).

(6) The desired solute concentration is prepared by the addition of the calculated volume of a stock solution to the buffer solution.

(7) The temperature and the pH value of the dispersed phase in the mixing vessel are measured and printed on the terminal.

(8) The nozzle and the movable photoelectric cell are moved to the desired height.

(9) Droplets of the solution form at the nozzle and fall through the organic solvent.

(10) The time of contact during the free fall is recorded. The mean time of contact and the mean rate of free fall are calculated.

(11) When the coalescence level at the bottom of the tube is above the lowest photoelectric cell (17 in Fig. 1), the aqueous phase is emptied into the sample cuvette of the photometer. The valve is kept open until the interface passes the lowest photoelectric cell and then the valve is closed. In this manner, the coalescence level is maintained by opening and closing the valve.

(12) The absorbance of the solute in the sample cuvette is recorded and stored when 200 drops have fallen through the continuous phase.

(13) The mean radius of the droplet is calculated, based on the number of drops formed and the total volume of water phase used.

(14) The absorbance, the mean time and mean rate of free fall,and the mean radius of the droplet are printed on the terminal.

(15) Points 8—14 are run for the desired number of different heights.
(16) A plot of ln A (A = absorbance) versus free-fall contact time, t, is prepared on the terminal. The overall mass-transfer coefficient is calculated by the linear regression method and printed on the terminal.
(17) Points 1—16 are run for all pH values required.

Test system

As a preliminary test of the apparatus, the mass-transfer rate of L-ephedrine from water drops to a continuous cyclohexane phase was measured at 25.1°C. L-Ephedrine hydrochloride (Pharmacopoeia Nordica quality) was used without further purification. The glass-redistilled water was saturated with cyclohexane (pro analysi quality) and vice versa before they were used. The buffer systems used were composed of phosphate or borate buffer solutions (pro analysi quality). The ionic strength was kept constant at 0.1 in all experiments. The initial concentration of L-ephedrine in the buffer solution was 2.6×10^{-3} M and the absorbance of L-ephedrine was measured at the wavelength of maximum absorbance, 258 nm.

RESULTS

The overall mass-transfer coefficient, $K_{app,1}$, was determined at 25 pH values varying between 8.165 and 11.380 (Fig. 2). Each mass-transfer coefficient was based on extractions done at five different heights of fall of the droplets (0.60, 0.90, 1.20, 1.65, 2.00 m). The contact times between the droplet and the continuous phase varied from 3.5 to 12.8 s. The correlation coefficient of the linear regression for the dependence of ln c_1 on the contact time was as high as 0.998 or more for the determinations of $K_{app} > 10^{-5.3}$ m s^{-1}, and it was never below 0.990 for determinations of $K_{app} < 10^{-5.3}$. The calculations of the latter rate coefficients were based on a difference in absorbance of less than 0.02 between the shortest and longest contact times. This helps to explain the lower precision in the determination of these coefficients.

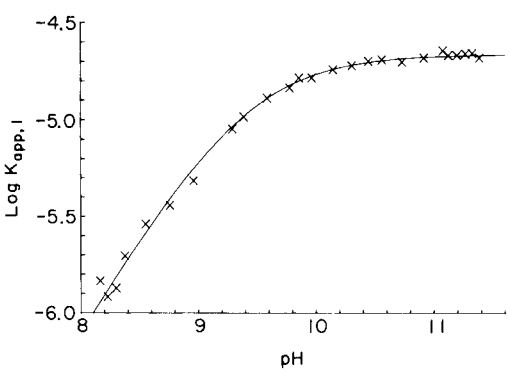

Fig. 2. Plot of log $K_{app,1}$ versus pH for L-ephedrine at 25.1°C.

Equation (6) was applied to the observed $K_{app,1}$ values by refinement of the two parameters $k_1 = (1/k_{m1} + 1/k_{a1})^{-1}$ and $k_2 = (1/k_{m2} + 1/k_{a2})^{-1}$. The refinement was done by a non-linear regression technique, using a modification of the MINUIT program [16]. The best fit to the observed $K_{app,1}$ (see Fig. 2) was obtained for $k_1 = 6.6 \times 10^{-5}$ and $k_2 = 8.9 \times 10^{-5}$ m s^{-1}. The correlation coefficient, R^2, was 0.997 where

$$1 - R^2 = \sum (K_{app,calc} - K_{app,obs})^2 / \sum (K_{app,obs} - K_{app,mean})^2$$

The previously determined acidity constant $K_a = 10^{-9.59}$ [17] and partition coefficient $K_d = 0.36$ [18] were utilized at this refinement.

We wish to express our sincere gratitude to Professor Allan Ågren for helpful discussions and for all the facilities placed at our disposal. Sincere thanks are due to Margrét Haraldsdóttir for the data collection on L-ephedrine. One of us (I.N.) thanks the IF Foundation for Pharmaceutical Research for grants in support of this investigation.

REFERENCES

1 A. Leo, C. Hansch and D. Elkins, Chem. Rev., 71 (1971) 525.
2 R. F. Rekker, The Hydrophobic Fragmental Constants, Elsevier, Amsterdam, 1977.
3 J. A. Keverling Buisman, Biological Activity and Chemical Structure, Elsevier, Amsterdam, 1977.
4 W. P. Purcell, G. E. Bass and J. M. Clayton, Strategy of Drug Design: A Guide to Biological Activity, Wiley, New York, 1973.
5 H. Brenner and L. G. Leal, A.I.Ch.E.J., 24 (1978) 246.
6 J. A. Shaelwitz and K. T. Raterman, Ind. Eng. Chem. Fundam., 21 (1982) 154.
7 V. G. Levich, Physicochemical Hydrodynamics, Prentice-Hall, Englewood Cliffs, 1962, Ch. 8.
8 R. Kronig and J. C. Brink, Appl. Sci. Res., A-2 (1950) 142.
9 A. E. Handlos and T. Baron, A.I.Ch.E. J., 3 (1957) 127.
10 F. H. Garner and P. J. Haycock, Proc. Roy. Soc. (London), 252 (1959) 457.
11 T. J. Horton, T. R. Fritsch and R. C. Kinter, Can. J. Chem. Eng., 43 (1965) 143.
12 B. T. Chao, J. Heat Transfer, (1969) 273.
13 B. T. Chao and J. L. S. Chen, Int. J. Heat Mass Transfer, 13 (1970) 359.
14 H. Brauer, Int. J. Heat Mass Transfer, 21 (1978) 455.
15 J. T. Thornton and T. J. Anderson, Int. J. Heat Mass Transfer, 24 (1981) 1847.
16 F. James and M. Roos, CERN/DD International Report, 75/20 (1976).
17 D. H. Everett and J. B. Hyne, J. Chem. Soc., (1958) 1636.
18 A. Brodin and A. Ågren, Acta Pharm. Suec., 8 (1971) 609.

Analytica Chimica Acta, 151 (1983) 161—166
Elsevier Science Publishers B.V., Amsterdam — Printed in The Netherlands

A COMPARISON OF SOME HIERARCHAL MONOTHETIC DIVISIVE CLUSTERING ALGORITHMS FOR STRUCTURE—PROPERTY CORRELATION

VIVIENNE RUBIN and PETER WILLETT*

Department of Information Studies, University of Sheffield, Western Bank, Sheffield S10 2TN (Gt. Britain)

(Received 19th October 1982)

SUMMARY

Four hierarchal divisive classification procedures were used to cluster eleven sets of compounds characterised by substructural fragments. The effectiveness of the different algorithms for the study of structure—activity relationships was assessed by the use of the resulting classifications for simulated property prediction. No single algorithm was found to be consistently superior to the others, and the effectiveness of all of the algorithms was generally better when homogeneous, rather than heterogeneous, data sets were evaluated.

Automatic classification, or cluster analysis, is a multivariate technique which attempts to group objects on the basis of some similarity relationship between them [1, 2]. Several workers have applied clustering procedures to the classification of chemical compounds, using sets of substructural fragments to characterise the molecules in a data set [3—7]. Such classifications are of value in computer-based information systems for the storage and retrieval of similar structures, and in structure-property correlation where structurally related molecules may be expected to exhibit comparable activities.

A very wide range of clustering algorithms has been described in the literature and Everitt [8] has advocated the comparative testing of different procedures on the same data so as to identify the most suitable algorithms for a given area of application. Adamson and Bawden [6] and Willett [7] have evaluated a range of hierarchal agglomerative algorithms, and have found that several of them, in particular that described by Ward [9], are quite successful in producing clusters of compounds which are not only subjectively reasonable but also contain molecules with similar properties. This paper considers the use of hierarchal monothetic divisive procedures for clustering chemical structures and assesses the effectiveness of the resulting classifications for structure—activity studies by simulated property prediction experiments.

0003-2670/83/$03.00 © 1983 Elsevier Science Publishers B.V.

MONOTHETIC DIVISIVE CLUSTERING

The clustering procedures considered in previous work [6, 7] are agglomerative in character, and build up the final hierarchal classification by fusing individual compounds or clusters to form larger clusters so that, after the final fusion, all of the molecules in a data set are in a single cluster. Divisive clustering works in precisely the opposite manner, with an initial single cluster being progressively broken down into smaller and smaller clusters. Although polythetic divisive algorithms have been described, they are extremely expensive in computational terms, and this paper is therefore restricted to a consideration of the more widely used monothetic methods [1, 2, 10—12]. These methods are based on the division of each cluster into two sub-clusters, membership of which is dependent upon the presence or absence of some chosen substructural feature. All of the compounds in one of the resulting clusters will contain the substructure, while it will be absent from the fragment lists of the compounds in the other new cluster.

Clifford and Stephenson [1] suggest that monothetic divisive methods have several advantages over agglomerative procedures. Firstly, the group definitions are simple and unambiguous, resulting as they do from the presence or absence of a single substructural feature. Secondly, the computational requirements are generally somewhat less than for agglomerative clustering, although still extensive in many cases. Finally, divisive methods should in theory be superior because the initial splits take place on the entire data set where the maximum amount of information about substructural frequencies and co-occurrences is available; in contrast, agglomerative methods start with individual pairs of structures, and thus the final classification is strongly dependent on the characteristics of individual compounds. It may also be noted that many chemistry texts are organised on a monothetic basis with sections devoted to the reactions and properties of individual structural types.

The fragment chosen as the basis for the division will be that which maximises the dissimilarity between the new set of clusters formed, and the four algorithms tested here differ primarily in the criteria used for the selection of the dividing fragment. Association analysis, which was the earliest approach to divisive clustering, involves the selection of that fragment at a given stage in the classification which is least strongly associated with the rest of the fragments, the strength of the association being measured by a modified χ^2 test [10]. A problem with this approach is that, for a data set containing p fragment types, no less than $p(p-1)/2$ χ^2 tables must be created as a precursor to the generation of the classification. An alternative approach, group analysis, again involves the selection of fragments on the basis of a χ^2-like measure called the interaction statistic [11]; however, the individual fragment scores may be calculated by using frequency data obtained from a simple serial scan of the data matrix, thus making the procedure extremely efficient in operation. Information analysis selects at each stage in the

division that fragment which maximises the change in the so-called information content of a cluster when sub-divided into two, information content being a function similar to that used in information theory to measure the capacity of a communication channel [12]. The final algorithm, error sum of squares, involves the selection of that fragment which minimises the separation between each of the molecules and the centroid of its cluster: a similar concept forms the basis of Ward's agglomerative clustering algorithm and many other centroid optimisation techniques. Full details of these procedures are given in the references quoted, and in the books by Clifford and Stephenson [1] and by Sneath and Sokal [13]. All of the algorithms are available as FORTRAN subroutines in the CLUSTAN computer package [14] which was used for the experiments reported below.

DATA SETS AND EXPERIMENTAL DETAILS

The data sets and experimental details are similar to those involved in the earlier experiments [7]. Eleven small collections of compounds for which associated property data were available were selected from the structure—property literature. The data sets include physical, chemical, and biological properties and were as follows:

(A) pI values of 20 naturally occurring amino acids [4],
(B) local anaesthetic activity of 37 diverse structures [15],
(C) inhibition of complement by 105 benzamidines [16],
(D) serum-binding activity of 79 penicillins [17],
(E) tadpole narcosis activity of 34 diverse structures [18],
(F) molar refractivity of 65 aliphatic ethers, amines, alcohols, and halides [19],
(G) chymotrypsin hydrolysis by 72 *N*-acyl esters [20],
(H) mouse toxicity of 25 aliphatic and carbocyclic ethers [21],
(I) antimicrobial activity of 28 phenyl propyl ethers [22],
(J) inhibition of dihydrofolate reductase by 46 quinazolines [23],
(K) heats of vaporisation for 126 alkenes, alcohols, ketones, benzenes, and pyridines [24].

The connection table representing each of the structures in a data set was analysed automatically to identify the substructural fragments present. Two small fragment types were chosen to characterise the molecules, these being the bond-centred octuplet, which consists of an atom—bond—atom triplet together with the immediately adjacent atoms and bonds, and the atom-centred augmented atom, which consists of an atom together with the immediately adjacent atoms and bonds. Each structure was described by a list of the distinct augmented atom or octuplet types contained within it, and these lists comprised the data matrix for the generation of the classifications. These formed the basis for simulated property prediction, by using a "leave-one-out" approach [4, 7]. The property value for each molecule, *i*, in turn within a data set was assumed to be unknown, and the classification was

scanned to identify the smallest cluster containing *i*. The predicted property value for *i* was taken to be the mean of the observed values for the other structures in that cluster. The correlation between the observed and predicted values was then determined by means of the product–moment correlation coefficient.

RESULTS AND DISCUSSION

Table 1 gives the correlation coefficients between the observed and predicted property values for each of the eleven data sets listed above.

The first comment to be made is that no single algorithm is consistently better than the others, with all yielding acceptable results in some cases. In particular, the computationally efficient group analysis algorithm was not noticeably inferior to the other, more time-consuming procedures (however, a limitation of this method, which tends to cause difficulties in the evaluation of the classifications obtained by using it, is that the similarities at which the divisions take place are not monotonically increasing). This result is in marked contrast with earlier work in which agglomerative algorithms were used [6, 7], where one method, that of Ward, gave consistently better results than the others while the simple and efficient single linkage method performed very poorly indeed.

The magnitudes of the coefficients in Table 1 vary considerably from one data set to another. Some data sets, such as the benzamidines or the *N*-acyl esters, exhibit uniformly high correlations while others, such as the amino acids or, most noticeably, the toxic ethers, gave correlations which were not

TABLE 1

Correlation between observed and predicted property values for each of the 11 data sets by using (a) minimum error sum of squares, (b) divisive information analysis, (c) association analysis, and (d) group analysis
(Asterisks denote a statistically non-significant coefficient at the 0.05 level)

Data set	Correlation coefficients							
	Augmented atom				Octuplet			
	(a)	(b)	(c)	(d)	(a)	(b)	(c)	(d)
A	0.54	0.54	*	*	0.22	0.21	0.20	*
B	0.59	0.67	0.59	0.79	0.63	0.74	0.82	0.77
C	0.86	0.85	0.82	0.85	0.87	0.86	0.85	0.86
D	0.67	0.66	0.69	0.67	0.67	0.68	0.70	0.61
E	0.51	0.51	0.64	0.73	0.53	0.58	0.41	0.65
F	0.36	0.36	0.29	0.33	0.46	0.23	0.21	0.41
G	0.86	0.84	0.87	0.88	0.85	0.84	0.89	0.88
H	*	*	*	*	*	*	*	*
I	0.39	0.39	0.29	0.45	0.31	0.31	0.42	0.60
J	0.78	0.78	0.46	0.40	0.79	0.79	0.44	0.81
K	0.84	0.86	0.86	0.81	0.84	0.83	0.84	0.70

statistically significant. Many of the better correlations were obtained with the structurally homogeneous data sets. These consist of a series of analogues in which substructural variation is restricted to some small part of the basic molecule. Accordingly, the various compounds in a data set differ only in a particular substituent or a few substituents, and the monothetic algorithms used here may be expected to be able to reproduce this structure quite accurately in the classifications arising from their use: indeed, for the benzamidines, *N*-acyl esters, and quinazolines, the correlations are comparable with, or even superior to, those obtained with the best of the polythetic agglomerative algorithms. However, as the ethers show clearly, the tendency to better results with homogeneous data does not always hold. Conversely, a monothetic procedure may be expected to give a good correlation with a structurally disparate group of compounds only if it is possible to identify as divisive criteria those fragment types which most strongly influence the chosen property. It is thus not surprising that the correlations observed with the heterogeneous data sets are often noticeably less than those obtained with the polythetic agglomerative algorithms, which appear to be more suitable for the treatment of such data.

Rubin [25] presented additional results obtained for a range of smaller substructural fragment types, and the general trends in the correlations were similar to those reported in Table 1. However, were the techniques to be applied to large data sets, rather than the small ones tested here, it is unlikely that the mere presence or absence of a limited range of small substructural attributes would discriminate sufficiently between groups of molecules in a machine-readable structure file.

Perhaps the main comment which should be made about the results obtained here and in earlier work is to emphasise that classifications which have been generated purely on the basis of inter-molecular structural similarities also reflect similarities in some property types. This finding has potential implications in drug development programs. An important component of such programs is the testing of compounds in biological screens which permit the rapid elimination from further consideration of those molecules which cannot possess some desired biological activity. Apart from structures which have been synthesised specifically for testing against a particular screen, extensive use is also made of random screening in which compounds which have been previously synthesised, or are available for some other reason, are put forward for testing in the hope of some serendipitous find.

A more systematic means of empirical screening would be available if structurally related compounds could be grouped together in a machine-readable file so that when molecules were required for screening, compounds could be systematically selected from each of the groups in turn. This approach has two clear advantages over random screening. Firstly, as each of the groups is considered in turn, all of the main classes of structure within the file will have been screened in the particular test, thus ensuring that no important structural types are omitted from consideration. Secondly, if the

structure selected for testing from a group is found to be inactive, it seems reasonable to transfer attention to other untested clusters while, if the chosen molecule is active, it would be worth investigating the other members of the group from which it was selected.

The experimental results to date show clearly that such groupings of structurally related compounds could indeed be generated by the use of automatic classification techniques. However, most of the clustering methods which have been tested are not applicable to files containing many thousands of compounds because they generally require an amount of computation proportional to N^2, or even greater, for a file of N compounds. Thus these methods are restricted to the processing of relatively small data sets. The clustering of very large files has been extensively studied as a way of grouping documents for information retrieval purposes [26—28], and there are now several algorithms available which are sufficiently efficient in operation to permit the classification of some thousands of objects in an acceptable amount of time. The suitability of some of these procedures for clustering chemical compounds will be tested in the near future.

REFERENCES

1 H. T. Clifford and W. Stephenson, An Introduction to Numerical Classification, Academic Press, New York, 1975.
2 B. Everitt, Cluster Analysis, Heinemann, London, 1980.
3 P. J. Harrison, Appl. Stat., 17 (1968) 226.
4 G. W. Adamson and J. A. Bush, Inform. Stor. Retr., 9 (1973) 561.
5 K. C. Chu, Anal. Chem., 46 (1974) 1181.
6 G. W. Adamson and D. Bawden, J. Chem. Inf. Comput. Sci., 21 (1981) 204.
7 P. Willett, Anal. Chim. Acta, 136 (1982) 29.
8 B. Everitt, Biometrics, 35 (1979) 169.
9 J. H. Ward, J. Am. Stat. Assoc., 58 (1963) 236.
10 W. T. Williams and J. M. Lambert, J. Ecol., 48 (1960) 689.
11 R. M. M. Crawford and D. Wishart, J. Ecol., 55 (1967) 505.
12 G. N. Lance and W. T. Williams, Comput. J., 11 (1968) 195.
13 P. H. A. Sneath and R. R. Sokal, Numerical Taxonomy, W. H. Freeman, San Francisco, 1973.
14 D. Wishart, CLUSTAN 1C User Manual, Edinburgh University, 1978.
15 D. Agin, L. Hersh and D. Holtzman, Proc. Nat. Acad. Sci., 53 (1965) 952.
16 C. Hansch and M. Yoshimoto, J. Med. Chem., 17 (1974) 1160.
17 A. C. Bird and A. C. Marshall, Biochem. Pharmacol., 16 (1967) 2275.
18 L. B. Kier, W. J. Murray and L. H. Hall, J. Med. Chem., 18 (1975) 1272.
19 L. B. Kier and L. H. Hall, J. Pharm. Sci., 65 (1976) 1806.
20 C. Hansch, C. Gricco, C. Silipo and A. Vittoria, J. Med. Chem., 20 (1977) 1420.
21 T. DiPaolo, J. Pharm. Sci., 67 (1978) 565.
22 L. H. Hall and L. B. Kier, J. Pharm. Sci., 67 (1978) 1743.
23 B. K. Chen, C. Horvath and J. R. Bertino, J. Med. Chem., 22 (1979) 483.
24 G. W. Adamson and D. Bawden, J. Chem. Inf. Comput. Sci., 20 (1980) 242.
25 V. Rubin, M.Sc. Dissertation, University of Sheffield, 1982.
26 G. Salton, Dynamic Information and Library Processing, Prentice-Hall, Englewood Cliffs, 1975.
27 W. B. Croft, J. Am. Soc. Inf. Sci., 28 (1977) 341.
28 P. Willett, J. Inf. Sci., 2 (1980) 223.

Analytica Chimica Acta, 151 (1983) 167—178
Elsevier Science Publishers B.V., Amsterdam — Printed in The Netherlands

A CRITICAL ASSESSMENT OF MODELS PREDICTING ALLOYING BEHAVIOUR BY MEANS OF PATTERN RECOGNITION

A. P. M. KENTGENS

Institute for Theoretical Physics, Catholic University, Toernooiveld, 6525 ED Nijmegen (The Netherlands)

F. W. PIJPERS*

Department of Analytical Chemistry, Catholic University, Toernooiveld, 6525 ED Nijmegen (The Netherlands)

G. VERTOGEN

Institute for Theoretical Physics, Catholic University, Toernooiveld, 6525 ED Nijmegen (The Netherlands)

(Received 29th October 1982)

SUMMARY

Pattern recognition techniques are applied in order to investigate the relevance of a large set of physical and chemical parameters for the description of the formation of binary alloys. Only alloys with a well-established sign of the heat of formation are considered. The electronic work function and the electron density at the boundary of the Wigner—Seitz cell, as given by Miedema et al., appear to be the most relevant parameters. A difference between the Miedema scale and the Pauling electronegativity scale is noted. The parameters suggested by Miedema et al. are evaluated.

The possible prediction of the alloying behaviour of two metals has intrigued many people. Several empirical rules have been proposed in order to predict such behaviour. The Hume-Rothery rule is well known [1]; this "15% rule" states that two metals do not form a solid solution if their atomic radii differ by over 15%. Further, the stability of intermetallic compounds increases with increasing difference in electronegativity between the constituent elements, and the concept of "valence" must also be taken into account [1]. Waber et al. [2] showed that the 15% rule, in combination with a second rule stating that the difference in electronegativity must not exceed 0.4 Pauling electronegativity units [3], predicts the mutual solubility of two metals with an accuracy of 77%. It should be noted that alloying refers both to the mutual solubility of two metals (i.e., random distribution of atoms over the crystal lattice in the solid phase) and to the formation of intermetallic compounds (i.e., regular distribution on the crystal lattice). A slightly different approach was given by Mott [4]; combining the Pauling [3] term for ionic bonds with Hildebrandt's solubility parameter, Mott predicted the mutual solubility of two liquid metals with an accuracy of 80%.

0003-2670/83/$03.00 © 1983 Elsevier Science Publishers B.V.

By far the most successful approach is that given by Miedema et al. [5]. Their empirical model, which appears to be related to Mott's model, is based on a "macroscopic atom picture". Its range of validity covers liquid as well as solid alloys of a transition metal with another transition metal, or a noble metal, or an alkali or alkaline-earth metal; the model also covers liquid alloys consisting of two non-transition metals. An exceptional situation arises for alloys of a transition metal with "*p*-type" metals [5] (see Table 2), where additional energy effects occur; such alloys could also be covered by adding an extra term to the model. This type of alloy, however, will not be considered in this paper.

The model of Miedema et al. considers an alloy to consist of atomic (Wigner—Seitz) cells of the individual elements. The basic idea is that contact between Wigner—Seitz cells of two different elements has two effects: first, charge transfer towards the most electronegative cell results in a negative contribution to the energy; second, elimination of the accompanying discontinuity in the electron density at the boundary of the cells contributes positively to the energy.

Sophisticated theories based on quantum mechanics have been presented in order to explain alloying behaviour [6—9]. These theories, however, cannot account for the impressive overall applicability of the semi-empirical model [5]. Even the physical picture proposed by Miedema et al. has been criticized by Williams et al. [10]. Undoubtedly, a fundamental theory should provide a physical understanding of the parameters introduced by Miedema et al. Before such a theory is formulated, it is clearly of interest to know which physical and chemical parameters play a prominent part in alloying, and to assess if the parameters of Miedema et al. are the only relevant ones.

The purpose of this paper is to discuss alloying behaviour from the point of view of pattern recognition [11—13]. This technique selects the relevant parameters from a set of parameters under investigation; the ARTHUR computer program [14] is commonly used. A concise description of the techniques relevant to this paper is given below. This is followed by an argument assuming that the description of the generally accepted electronegativity difference given by Miedema et al. is correct. Replacement of the less well understood term describing the difference in electron density by a more satisfactory physical or chemical parameter is then discussed and the Miedema work function scale and the Pauling electronegativity scale [3] are compared. Miedema et al. [5] describe the charge transfer in an alloy by means of a work function scale for pure metals, specially designed for the purpose. Generally, however, the Pauling electronegativity scale is used for describing the electrochemical effect in an alloy. Finally, it is shown that the Miedema parameters should be used together in order to add up to the best set.

THE PATTERN RECOGNITION TECHNIQUES USED

In pattern recognition, some item, an alloy in the present case, is positioned in a multidimensional feature space, spanned by all physical and chemical data, called features, of that particular item (the parameters given in Table 1). When several items in that feature space cluster together, it is obvious that their chemical and physical behaviour is similar. In pattern recognition, it is assumed that such behaviour not only holds for the known physical and chemical data, but also reflects similar behaviour of properties that have not been measured or cannot be measured without considerable effort.

When a large number of parameters is involved, it is important to obtain an indication about their mutual dependence. This is reflected by the correlation coefficient c_{ij}:

$$c_{ij} = \sum_{k=1}^{n} (x_{i,k} - \bar{x}_i) \cdot (x_{j,k} - \bar{x}_j) \Big/ \left[\sum_{k=1}^{n} (x_{i,k} - \bar{x}_i)^2 \sum_{k=1}^{n} (x_{j,k} - \bar{x}_j)^2 \right]^{1/2} \qquad (1)$$

where $x_{i,k}$ denotes parameter i of item k, and $\bar{x}_i$ the mean value of parameter i over the n items. This can be used to reduce the dimensionality of the feature space by removal of those parameters that are highly correlated to others. Such reduction is advantageous because it simplifies the description of the property investigated for the items (here, the sign of the heat of formation of alloys).

The alloys are divided into two categories on the basis of their known chemical and physical behaviour (positive or negative heat of formation). Then the procedure WEIGHT can be applied in order to investigate which parameters are mainly responsible for the discrimination of the categories. The variance weight (WV) is the ratio of the interclass variance (a measure of the spread of a certain parameter over both categories) to the intraclass variance (a measure of the spread of that parameter within one category):

$$WV_{j,1,2} = \left[\sum_{k=1}^{n_1} \frac{x_{k,1,j}^2}{n_1} + \sum_{k=1}^{n_2} \frac{x_{k,2,j}^2}{n_2} - 2 \frac{\sum_{k=1}^{n_1} x_{k,1,j} \cdot \sum_{k=1}^{n_2} x_{k,2,j}}{n_1 n_2} \right] \Big/$$

$$\times \left[\sum_{k=1}^{n_1} \frac{(x_{k,1,j} - \bar{x}_{1,j})^2}{n_1} + \sum_{k=1}^{n_2} \frac{(x_{k,2,j} - \bar{x}_{2,j})^2}{n_2} \right] \qquad (2)$$

where $WV_{j,1,2}$ denotes the weight of a parameter j for separating category 1 from category 2, $x_{k,1,j}$ is parameter j of the kth item in category 1, and $\bar{x}_{1,j}$ is the mean value of parameter j over the n_1 items in category 1.

The procedure SELECT chooses the parameter with the largest variance weight and consecutively decorrelates all remaining parameters from the selected one by means of some kind of Gram–Schmidt procedure. These decorrelated parameters are then reweighted and so on. A final test for the

separability of the categories is offered by LEAST, that aims to predict the category number by means of a linear combination of the chosen parameters:

$$P_k = b_0 + \sum_{i=1}^{n'} b_i x_{i,k} \tag{3}$$

where P_k denotes the predicted category number of item k, $x_{i,k}$ is the ith parameter of item k, and n' is the number of parameters; b_i are the coefficients of the least-squares multilinear regression. Then the P value is calculated which separates the two categories optimally. The percentage of correctly classified elements is called the predictive ability.

SELECTION OF PARAMETERS

Miedema et al. [5] described the heat of formation of a binary alloy, ΔH, in terms of the expression

$$\Delta H = f(c)[-P(\Delta\phi^*)^2 + Q_0(\Delta n_{ws}^{1/3})^2] \tag{4}$$

where $f(c)$ is a function of the concentration of the metals, ϕ^* and n_{ws} denote the electronic work function of a pure metal and the electron density at the boundary of the Wigner–Seitz cell, respectively, Δ represents the difference between the considered quantities of both models, and P and Q_0 are constants. It follows directly that, in a graphical representation of $\Delta\phi^*$ versus $\Delta n_{ws}^{1/3}$, the alloys with a positive heat of formation, $\Delta H > 0$, are separated from the alloys with a negative heat of formation, $\Delta H < 0$, by the line

$$\Delta n_{ws}^{1/3} = (P/Q_0)^{1/2}\,\Delta\phi^* \tag{5}$$

Plots of $\Delta\phi^*$ versus $\Delta n_{ws}^{1/3}$ are shown in Fig. 1 and 2A.

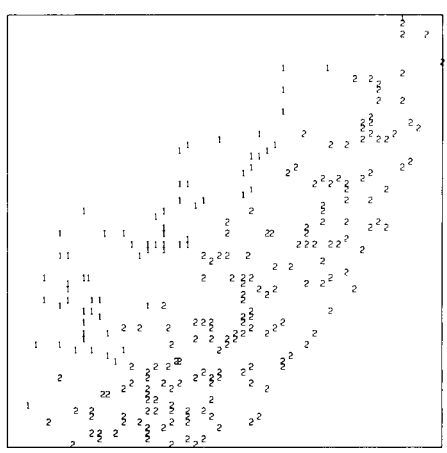

Fig. 1. $\Delta n_{ws}^{1/3}$ (Y) versus $\Delta\phi^*$ (X) for 257 alloys of transition and noble metals. The alloys with positive heat of formation (category 1) are well separated from those with a negative heat of formation (category 2).

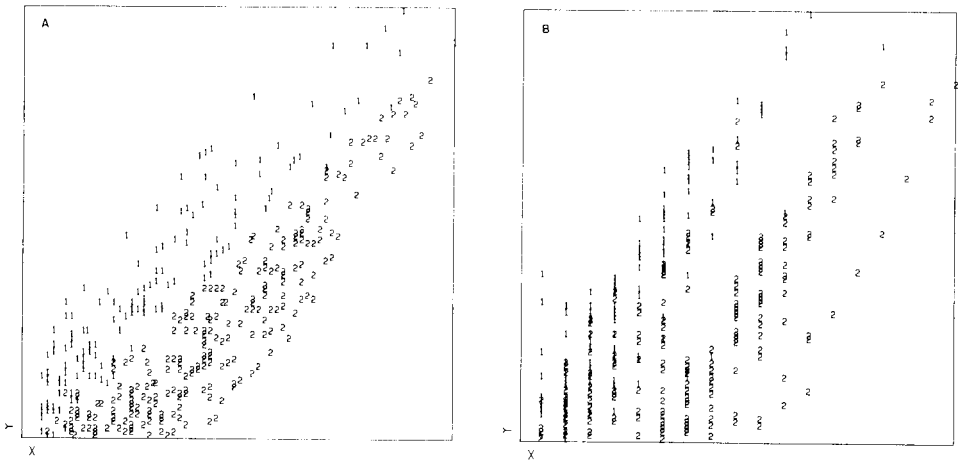

Fig. 2. A, $\Delta n_{ws}^{1/3}$ (Y) versus $\Delta\phi^*$ (X) for all 390 alloys to which Eqn. (4) is applicable; the separation between category 1 ($\Delta H > 0$) and category 2 ($\Delta H < 0$) is convincing. B, $\Delta n_{ws}^{1/3}$ (Y) versus $\Delta\chi_p$ (X), the difference in Pauling electronegativity; the categories overlap.

The ϕ^* values are based on the work function ϕ of the pure metals. They are obtained by slightly changing the original ϕ values in order to enhance the applicability of Eqn. (4). These adjustments are such that they fall within the experimental error of the ϕ values, which themselves represent an average of the measured orientation-dependent work functions.

The numerical value of n_{ws} is less easily obtained. For alkali metals, the value of n_{ws} can be assumed to be equal to the number of valence electrons per atomic volume. For some other elements, its value can be calculated by means of self-consistent calculations of band structure. These n_{ws} values appear to be highly correlated with $(K/V_m)^{-1/2}$ [15], where K and V_m denote the compressibility and the molar volume, respectively. Because of this high correlation, Miedema et al. [15] assumed $(K/V_m)^{-1/2}$ to be the measure for n_{ws} but they allowed small shifts in the resulting value of n_{ws} in order to optimize their model. From a physical point of view, the meaning of a parameter obtained in such a way is rather obscure. Therefore a variety of parameters (Table 1) was tested for 49 pure metals (Table 2) with regard to their relevance to the alloying behaviour of two metals. The same set of parameters was recently tested for its relevance to superconducting behaviour [16]. The parameters describing the alloy are the differences between the corresponding parameters of the two constituting elements.

Information about the sign of ΔH was available for 390 alloys, where Eqn. (4) can be applied. This information was obtained from phase diagrams and from Hultgren et al. [17]; the phase-diagram information was kindly provided by Miedema and Niessen. In the first instance, only alloys consisting of metals in columns 3—11 of Table 2 are considered. The ΔH data of 257 phase diagrams out of the 378 possible combinations in this set were

TABLE 1

Parameters investigated for their predictive ability with respect to alloying behaviour

Parameter	Symbol
1 Electronic work function as given by Miedema et al.	ϕ^*
2 Electron density at the boundary of the Wigner—Seitz cell as given by Miedema et al.	$n_{ws}^{1/3}$
3 Electron density at the boundary of the Wigner—Seitz cell, calculated from compressibility and molar volume	$n_{ws}^{*1/3}$
4 Number of relevant valence electrons as given by Miedema et al. rounded off to integer values	N
5 Specific heat at 25° C	C_p
6 Melting point (° C)	m.p.
7 Boiling point (° C)	b.p.
8 Ionic radius in the commonest oxidation state	IR
9 Bond length in the solid state of the element at 25° C	BL
10 Heat of melting	ΔH_m
11 Heat of sublimation at 25° C	ΔH_s
12 Period number in the periodic system of elements	PER
13 Young modulus	Y
14 Compressibility	K
15 Debye temperature as obtained from electrical resistivity measurements	T_d
16 Linear term in the specific heat	γ
17 Density at 25° C	ρ
19 Electrical resistivity at 20° C (ohm cm)	RHO

available. In pattern recognition, the data are organized in categories. Two categories are distinguished here. The first category contains all phase diagrams with a positive heat of formation; this means that there are no compounds, and the mutual solubility of the constituting metals is less than 10%. The second category contains the phase diagrams relating to compounds

TABLE 2

Metals which are investigated with respect to alloying
(The elements in the last 4 columns are "p-type" metals [5]. The underlined elements are assigned lower electronegativity values by Miedema et al. as is to be expected from the Pauling scale)

	1	2	3	4	5	6	7	8	9	10	11	12	13	14	15
2	Li											Be			
3	Na											Mg	Al		
4	K	Ca	Sc	Ti	V	Cr	Mn	Fe	Co	Ni	Cu	Zn	Ga		
5	Rb	Sr	Y	Zr	Nb	Mo	—	Ru	Rh	Pd	Ag	Cd	In	Sn	Sb
6	Cs	Ba	La	Hf	Ta	W	Re	Os	Ir	Pt	Au	Hg	Tl	Pb	Bi
7			Th		U										

or ordered phases that are stable at low temperatures. These phase diagrams relate to alloys that are assumed to have a negative heat of formation.

The data were processed with the pattern recognition program ARTHUR [14]. Each alloy was represented as a data vector in a multidimensional space spanned by all given parameters. The aim was to look for the minimal set of parameters, which separated both categories. A suitable method of establishing the separability of two categories is offered by the LEAST program [12]. This procedure applies a multilinear least-squares regression to the category number. First, a two-parameter LEAST procedure was considered for the above-mentioned set of 257 alloys. The first parameter was always chosen to be the Miedema $\Delta\phi^*$ value, whereas the second parameter was taken from the set mentioned in Table 1. Moreover, a prediction was given on the basis of $\Delta\phi^*$ only. The results of this evaluation are presented in Table 3.

The parameters of Miedema et al. appear to be superior to all other combinations. Particularly striking is the information that is obtained when only $\Delta\phi^*$ is used. This demonstrates clearly the importance of the electrochemical effect in an alloy. The remaining parameters do not offer significant information concerning the alloying behaviour except for the number of valence electrons (N), the bond length (BL) and the compressibility (K), which contribute somewhat. This is not surprising because of their high correlation with $n_{ws}^{1/3}$ (0.80, −0.80 and −0.84, respectively). The correlation itself follows directly from the definition of n_{ws} as "the electron density at the boundary of the Wigner–Seitz cell" [5]. The predictive ability of the parameter set $\Delta\phi^*$ and $\Delta n_{ws}^{1/3}$ (97.5%) differs considerably from that of the parameter set $\Delta\phi^*$ and $\Delta n_{ws}^{*1/3}$ (88.5%). The parameter n_{ws}^* was calculated from compressibility and molar volume data, as given by Gschneidner [18]. This parameter is the starting value for n_{ws}. Clearly, small alterations of n_{ws} (see Fig. 4) strongly influence the effectiveness of the model. This point is further considered below.

TABLE 3

Predictions of a two-parameter LEAST procedure for 257 alloys of metals from columns 3–11 of Table 2. The first parameter was always $\Delta\phi^*$

2nd parameter	Predictive ability (%)	2nd parameter	Predictive ability (%)
–	80.5	$\Delta(\Delta H_m)$	81.0
$\Delta n_{ws}^{1/3}$	97.5	$\Delta(\Delta H_s)$	78.5
$\Delta n_{ws}^{*1/3}$	88.5	ΔPER	80.0
ΔN	83.0	ΔY	81.0
ΔC_p	80.5	ΔK	85.5
Δm.p.	80.0	$\Delta\gamma$	81.5
Δb.p.	80.0	$\Delta\rho$	81.5
ΔIR	81.5	ΔRHO	80.5
ΔBL	83.5		

The possibility of removing n_{ws} and replacing it by two other parameters was then studied. This appeared to be unfruitful. The best result was obtained with the parameters ΔN and ΔBL together with $\Delta\phi^*$, of course (88.0%). It should be remarked here that when the value of N was increased by one unit for vanadium and chromium and decreased by one unit for uranium the predictive ability could be enhanced to 90.5%. However, this was valid only for the set of 257 alloys. When these changes were extended to the entire data set of 390 alloys, the predictive ability dropped to 82.5%, whereas the parameters of Miedema et al. still gave 96.0% predictive ability.

COMPARISON OF THE MIEDEMA AND PAULING SCALES

It is generally accepted that the stability of an alloy is highly correlated with the difference in electronegativity of the constituent metals. This electronegativity concept, originally introduced by Pauling [3], is well understood in principle, but hard to calculate. Electronegativity is used to estimate the ionic contribution to the heat of formation of a compound. Hodges and Stott [6] developed a theory which bears some resemblance to the model. In this theory, the electrochemical effect in an alloy is ascribed to the difference in Fermi level, μ, of the constituent atomic cells. This Fermi level appears to be correlated with the Pauling electronegativity, χ_p. The concept of electronegativity for the description of alloys is also important for the interpretation of isomer shifts in Mössbauer spectroscopy (Miedema and van der Woude [19]).

Miedema et al. preferred a physically well-defined parameter to describe charge transfer in alloys. For that purpose, an average of the orientation-dependent work functions was chosen as the starting value ϕ for their electronegativity scale. The work function ϕ is strongly correlated with the Pauling electronegativity χ_p [20]. Likewise, ϕ and the Fermi level are correlated [15].

The correlation coefficient for the ϕ^* scale of Miedema et al. with the Pauling χ_p scale is 0.94. In Fig. 3 the relationship between ϕ^* and χ_p is shown. Some elements spoil the linear relationship between the two scales; without these, the correlation coefficient increases to 0.98. In order to verify this observation, the ΔH information was divided into several groups, and the predictive ability for these groups was evaluated by the LEAST procedure using $\Delta\phi^*$ and $\Delta\chi_p$ with and without $\Delta n_{ws}^{1/3}$. The results are given in Table 4.

When the predictive abilities of $\Delta\phi^*$ and $\Delta\chi_p$ alone are compared a difference of 4% is noted for the set of 257 alloys consisting of metals from columns 3—11 of Table 2. When the 75 phase diagrams with Cu, Ag, Au and U are removed from this data set, both predictive abilities become equal. Clearly, the scale of Miedema et al. assigns better values to these four elements. Another striking difference concerns the predictive ability for liquid alloys consisting of "p-type" metals with "p-type", alkali, or alkaline-earth metals.

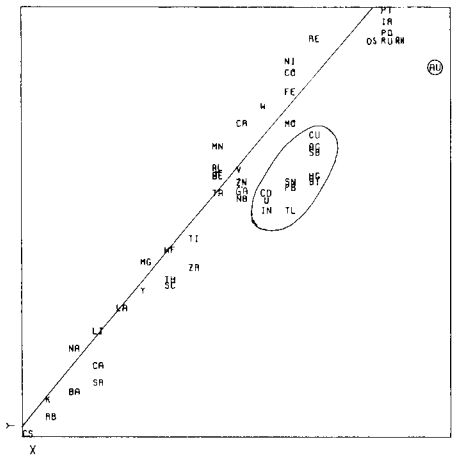

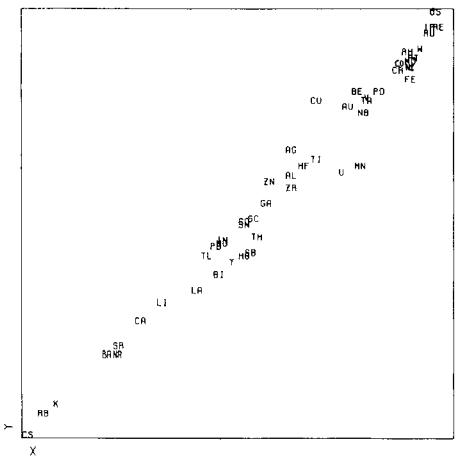

Fig. 3. The electronic work function ϕ^* (Y) for the pure elements versus electronegativity χ_p (X). The encircled elements have a significantly lower value in Miedema's scale compared to Pauling's scale. For the other elements, the least-squares line is represented by $\phi^* = 2.5\,\chi_p + 0.3$.

Fig. 4. $n_{ws}^{*1/3}$ (Y) calculated from compressibility data and molar volume versus Miedema's adjusted $n_{ws}^{1/3}$ (X). The latter hardly differ from their starting values.

Here the charge-transfer term appears to be the only relevant parameter, because $\Delta n_{ws}^{1/3}$ is quite small. This is clearly demonstrated by the LEAST procedure. The inclusion of $\Delta n_{ws}^{1/3}$ does not enhance the predictive ability. The prediction based on $\Delta\phi^*$ is superior to that based on $\Delta\chi_p$.

It is concluded that Miedema et al. assigned lower values to the work functions of the elements Cu, Ag, Au, U, Cd, Hg, In, Tl, Sn, Pb, Sb and Bi than one would expect on the basis of the Pauling scale. These lower values allow a better description of the charge transfer in the underlying alloys. In contrast, alloys of alkali or alkaline-earth metals with metals of columns 3—10 of Table 2 are better described with the aid of the Pauling scale (i.e., on the basis of charge transfer only) so that ϕ^* might be improved. However, in combination with $\Delta n_{ws}^{1/3}$, $\Delta\phi^*$ is distinctly superior to $\Delta\chi_p$. This indicates that ϕ^* and n_{ws} are best used in combination.

The influence of replacing ϕ^* by ϕ in Eqn. (4) was also studied. For several ϕ scales, the predictive ability based on $\Delta\phi$ and $\Delta n_{ws}^{1/3}$ was lower than 80%, which is obviously inferior to the ϕ^* scale. Moreover, it was not clear which ϕ values should be taken.

THE PARAMETERS ϕ^* AND n_{ws}

The decrease in predictive ability when n_{ws}, as given by Miedema et al., was replaced by n_{ws}^* (i.e., the electron density calculated from the compressibility and the molar volume) was shown above. The plot of $n_{ws}^{*1/3}$ versus

TABLE 4

LEAST predictions for one and two parameters applied to different data sets

Data set	Predictive ability (%) for the parameters			
	$\Delta\phi^*$, $\Delta n_{ws}^{1/3}$	$\Delta\chi_p$, $\Delta n_{ws}^{1/3}$	$\Delta\phi^*$	$\Delta\chi_p$
Alloys of metals of columns 3—11[a] (257)	97.5	85.0	80.5	76.5
As above with alloys of Cu, Ag, Au and U removed (182)	99.5	89.5	82.5	82.0
Alloys of alkali and alkaline-earth metals with a metal of columns 3—10[a] (64)	97.0	92.0	81.5	89.0
Liquid alloys of "*p*-type"[a] metals with a "*p*-type", alkali, or alkaline-earth metal (62)	95.0	80.5	95.0	80.5
All alloys for which Eqn. (4) is valid (390)	96.0	83.0	72.5	71.5

[a]See Table 2.

$n_{ws}^{1/3}$ given in Fig. 4 demonstrates that these parameters hardly differ, yet small changes have a significant influence as is shown in Table 5. The influence of replacing $\Delta n_{ws}^{1/3}$ by $\Delta n_{ws}^{*1/3}$ in predictions based on $\Delta\chi_p$ instead of $\Delta\phi^*$ is smaller.

Table 4 shows that, although $\Delta\chi_p$ alone gives predictions equal to or better than $\Delta\phi^*$ alone for some data sets, the combination of $\Delta\phi^*$ with $\Delta n_{ws}^{1/3}$ is always superior for these data sets. This is also demonstrated in Fig. 2.

It must be concluded that the work function ϕ^* and the electron density n_{ws}, as given by Miedema et al., form an optimal set for the description of

TABLE 5

LEAST predictions indicating the influence of replacing $\Delta n_{ws}^{1/3}$ by $\Delta n_{ws}^{*1/3}$

Data set	Predictive ability (%) for the parameters			
	$\Delta\phi^*$, $\Delta n_{ws}^{1/3}$	$\Delta\phi^*$, $\Delta n_{ws}^{*1/3}$	$\Delta\chi_p$, $\Delta n_{ws}^{1/3}$	$\Delta\chi_p$, $\Delta n_{ws}^{*1/3}$
Alloys of metals of columns 3—11[a] (257)	97.5	88.5	85.0	82.0
All alloys for which Eqn. (4) is valid (390)	96.0	87.0	83.0	78.0

[a]See Table 2.

alloying behaviour. It remains to be seen if this set is unique. In this context, the high correlation (0.91) between ϕ^* and $n_{ws}^{1/3}$ is surprising. As shown in Fig. 5, the $n_{ws}^{1/3}$ values are distributed around the line $y = (P/Q_0)^{1/2}\,\Delta\phi^*$. The significant information concerning alloying behaviour is contained in the deviation from this line as noted previously [6, 7]. The relevance of this deviation was demonstrated by application of the parameter selection procedures WEIGHT and SELECT [12].

WEIGHT selects parameters on the basis of their individual importance for the separation of two categories; this is expressed in the so-called variance weight, which is the ratio of the interclass and intraclass variance of the two categories. SELECT chooses the parameter with the highest variance weight as the most important one. The remaining parameters are then decorrelated from the chosen one and reweighted; the decorrelated parameter with the highest variance weight is selected as the second parameter and so on.

According to the WEIGHT procedure, the only important parameter of those investigated (Table 1) is $\Delta\phi^*$. Apart from $\Delta\phi^*$, SELECT assigned a significant weight to the $\Delta n_{ws}^{1/3}$ parameter, after decorrelation from $\Delta\phi^*$. This means that the deviation mentioned above contains the significant information with respect to alloying behaviour.

Conclusions

Evidently the parameters ϕ^* and $n_{ws}^{1/3}$ of Miedema et al. are the most relevant macroscopic parameters for giving a correct description of the alloying behaviour of two metals. These parameters are optimal as a set, but it remains to be seen if their values are uniquely determined for a given metal. Despite the high correlation between the two parameters, n_{ws} still contains additional information.

A comparison between the Pauling and Miedema scales shows that Miedema et al. assign a lower value to several elements than Pauling does. The Pauling

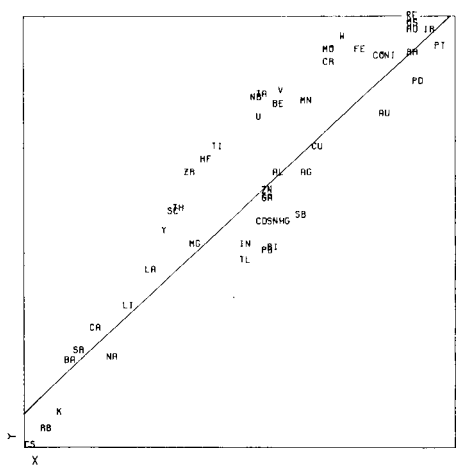

Fig. 5. The $n_{ws}^{1/3}$ value (Y) of Miedema et al. versus their electronic work function ϕ^* (X).

scale appears to be less well suited for situations where metallic (rather than covalent) bonds compete with ionic bonds.

Pattern recognition itself does not provide theories but merely indicates the relevance of certain parameters and can be useful for developing theories. Pattern recognition is advantageous in handling large amounts of information. The influence of certain parameters can be easily studied and the correlation between parameters can be seen at first glance.

The authors thank A. R. Miedema and A. K. Niessen for stimulating and helpful discussions, for generously supplying them with the necessary data, and for critically reading the manuscript. They also thank P. F. A. van der Wiel for his valuable assistance with computer programming and B. R. Kowalski for making the ARTHUR program available.

REFERENCES

1 W. H. Hume-Rothery and G. V. Raynor, The Structure of Metals and Alloys, The Institute of Metals, London, 1962, p. 97.
2 J. T. Waber, K. Gschneidner, A. C. Larson and M. Y. Prince, Trans. Metal. Soc. AIME, 227 (1963) 717.
3 L. Pauling, The Nature of the Chemical Bond, Cornell University Press, Ithaca, 1960.
4 B. W. Mott, J. Mat. Sci., 3 (1968) 424.
5 A. R. Miedema, P. F. de Châtel and F. R. de Boer, Physica, 100 (1980) B1.
6 C. H. Hodges and M. J. Stott, Phil. Mag., 26 (1972) 375.
7 C. H. Hodges, J. Phys., F: Metal Phys., 7 (1977) L247; Phil. Mag., 38 (1978) 205.
8 P. F. de Châtel and G. G. Robinson, J. Phys., F: Metal Phys., 6 (1976) L173.
9 J. R. Chelikowsky and J. C. Phillips, Phys. Rev., 17 (1978) B2453.
10 A. R. Williams, C. D. Gelatt, Jr. and V. L. Moruzzi, Phys. Rev. Lett., 44 (1980) 429.
11 G. Kateman and F. W. Pijpers, Quality Control in Analytical Chemistry, Wiley, New York, 1981, Ch. 4.
12 B. R. Kowalski, Chemometrics: Theory and Application, American Chemical Society, Washington, DC, 1977, Ch. 2.
13 E. R. Malinowsky and D. G. Howery, Factor Analysis in Chemistry, Wiley, New York, 1980.
14 D. L. Duewer, J. R. Koskinen and B. R. Kowalski, ARTHUR Laboratory for Chemometrics, Department of Chemistry BG-10, Univ. of Washington, Seattle.
15 A. R. Miedema, F. R. de Boer and P. F. de Châtel, J. Phys., F: Metal Phys., 3 (1973) 1558.
16 F. W. Pijpers and G. Vertogen, J. Physique, 43 (1982) 97.
17 R. Hultgren, P. D. Desai, D. T. Hawkins, M. Gleiser and K. K. Kelly, Selected Values of the Thermodynamic Properties of Binary Alloys, American Society for Metals, Ohio, 1973.
18 K. A. Gschneidner, in F. Seitz and D. Turnbull (Eds.), Solid State Physics Vol. 16, Academic Press, New York, 1964, p. 275.
19 A. R. Miedema and F. van der Woude, Physica, 100 (1980) B145.
20 W. Gordy and W. J. O. Thomas, J. Chem. Phys., 24 (1956) 439.

Analytica Chimica Acta, 151 (1983) 179—185
Elsevier Science Publishers B.V., Amsterdam — Printed in The Netherlands

DETERMINATION OF ARSENIC IN SOIL, COAL FLY ASH AND BIOLOGICAL SAMPLES BY ELECTROTHERMAL ATOMIC ABSORPTION SPECTROMETRY WITH MATRIX MODIFICATION

SHAN XIAO-QUAN*, NI ZHE-MING and ZHANG LI

Institute of Environmental Chemistry, Academia Sinica, P.O. Box 934, Beijing (People's Republic of China)

(Received 20th September 1982)

SUMMARY

The tolerable charring temperature for samples containing arsenic can be raised to 1300°C when palladium is added as a matrix modifier. In its presence the sensitivity for arsenic is 50% greater than that in the presence of nickel. Digestion with a mixture of sulphuric and perchloric acids and sodium molybdate is used to decompose soil, coal fly ash and biological samples before the direct determination of $\mu g\ g^{-1}$ concentrations of arsenic by graphite-furnace atomic absorption spectrometry. A mixed acid decomposition procedure is also described.

Arsenic compounds are widely used in agriculture and industry as herbicides, pesticides and wood preservatives. Large amounts enter the environment annually, about 70% as inorganic salts, and the remainder as organoarsenicals [1]. Arsenic and its compounds are extremely toxic, and environmental concern has stimulated great interest in the development of analytical methods for arsenic in a variety of samples. Brooks et al. [2] reviewed instrumental methods for the determination of arsenic, and found atomic absorption spectrometry to be the most popular.

In the direct determination of arsenic by graphite-furnace atomic absorption spectrometry (a.a.s.), difficulties arise from severe interferences by large amounts of aluminium, sodium, potassium and sulphate in the samples [3]. Many efforts have been made to minimize or eliminate these interferences; hydride generation and liquid—liquid extraction procedures are widely used. However, very recently there has been great interest in the direct determination of arsenic, antimony and selenium by electrothermal a.a.s. Arsenic is a relatively volatile element, and losses will occur during charring. In order to overcome this difficulty, addition of nickel was suggested [4]. However, erratic readings and accelerated tube deterioration are observed at acidities greater than 2% nitric acid when nickel is used as a matrix modifier. Therefore, Subramanian et al. [5] used a 0.05% solution of nickel in 1% nitric acid. Under these conditions reproducible results were obtained and interferences became minimal. Koreckova et al. [6] discussed the important factors

0003-2670/83/$03.00 © 1983 Elsevier Science Publishers B.V.

affecting the determination of arsenic by graphite-furnace a.a.s. with special emphasis on surface reactions. Radioactive measurements were employed to study losses of arsenic during the preatomization steps, and the penetration of arsenic into the graphite. The mechanisms of the stabilizing effects of nickel and lanthanum were also discussed.

The aim of this study was to develop a method for the determination of arsenic in soil, coal fly ash and biological samples by electrothermal a.a.s. with palladium as a matrix modifier. First the samples were digested with a sulphuric—perchloric acid mixture in the presence of sodium molybdate, or with a nitric—perchloric—hydrofluoric acid mixture.

EXPERIMENTAL

Apparatus and reagents

A Perkin-Elmer model 4000 atomic absorption spectrometer fitted with a model HGA-400 graphite furnace was employed. Signals obtained under argon "stopped flow" and "maximum power" were recorded on a model 056 chart recorder. A Perkin-Elmer arsenic electrodeless discharge lamp was operated at 8 W. Deuterium arc background correction was employed throughout the study. A 20-μl Eppendorf pipette fitted with disposable polypropylene tips was used to introduce sample solutions into the graphite tube.

An arsenic stock solution (1000 μg ml^{-1}) was prepared by dissolving 0.1320 g of arsenic trioxide (analytical-reagent grade; Beijing Chemical Co., Beijing) in 4 ml of 1 M sodium hydroxide followed by the addition of 25 ml of water and 5 ml of 1 M hydrochloric acid and dilution to 100 ml with deionized water. All other working standard solutions were prepared from this stock solution by serial dilution prior to use. Nitric and hydrofluoric acids were redistilled from quartz and platinum apparatus, respectively. Other chemicals used were of analytical-reagent grade.

Procedures

Digestion of soil. Accurately weigh ca. 0.100 g of soil into a 50-ml conical flask. Add about 1 ml of water to moisten the sample thoroughly, followed by 1.5 ml of a (3 + 4) sulphuric—perchloric acid mixture and 3 ml of a 5% (w/v) solution of sodium molybdate dihydrate. Use a short-necked filter funnel as an air condenser head, with the diameter of its top slightly larger than that of the neck of the conical flask, to reduce the evaporation of acids during the digestion. Heat the flask on a hot plate at about 100°C until white fumes of perchloric acid are evolved. Raise the temperature to about 150°C and maintain the flask at this temperature for 15 min. Swirl occasionally until the solution becomes clear and a white residue is obtained. When digestion is complete, remove the flask from the hot plate, cool, and wash down the condenser head with water. Remove the condenser head and wash the interior wall of the flask cautiously with water. Dilute the

cooled solution to about 30 ml with water and reheat on a hot plate until the solution boils. Remove the flask from the hot plate, cool to about 40°C, and filter through fine-porosity filter paper, collecting the filtrate in a 100-ml volumetric flask. Wash the silica residue several times with 0.01 M nitric acid and dilute the solution to the mark with water. A complete digestion requires about 30 min.

Digestion of coal fly ash. Use a procedure similar to that for digestion of soil except that a 3-h digestion at 150°C is necessary.

Digestion of biological samples. Samples such as orchard leaves (NBS SRM 1571) and pepperbush are destroyed easily by acid digestion, thus use only 0.8 ml of the sulphuric—perchloric acid and 2 ml of the molybdate solution. Because the arsenic content of these samples is lower than for the soil and fly ash, use a 25-ml volumetric flask for the collection of the filtrate.

Mixed acid digestion. Transfer an accurately weighed 100-mg sample of soil or coal fly ash to a 30-ml teflon crucible, and add the minimal volume of 0.01 M nitric acid needed to moisten the sample thoroughly, followed by 1 ml of 72% perchloric acid. Cover the crucible with a teflon cover. Heat on a hot-plate at about 120° C for 1 h. Remove the crucible from the hot plate, cool and wash the interior surface of the teflon cover with 1 ml of concentrated nitric acid into the crucible. Reheat on a hot plate at 140°C until the acid volume is decreased to about 0.5 ml. Remove the crucible, wash the interior of the crucible with 2 ml of 0.01 M nitric acid when cool, and add 2 ml of concentrated hydrofluoric acid. Heat at 100° C for 30 min, then raise the temperature to 140° C until complete decomposition of sample is achieved. If it is not complete, add a further 0.2 ml of nitric acid and 0.1 ml of perchloric acid and repeat the above procedure. When sample decomposition is complete, add 5 ml of 0.1 M nitric acid and heat to nearly boiling, until a clear solution is obtained. Transfer the solution to a 100-ml volumetric flask, wash the crucible several times with 0.01 M nitric acid, combine the washings and dilute the solution to the mark with deionized water. If small dark carbon particles are visible, filter the solution.

Determination of arsenic. After appropriate dilution of the solutions prepared as above, inject 20 μl and the same volume of 100 μg ml^{-1} palladium solution into the graphite tube. After drying, char the residue at 1000°C for 30 s, and atomize at 2400°C for 5 s at "maximum power" and "argon gas interrupted". Measure the arsenic absorbance at 193.7 nm. Finally, clean the graphite tube at 2700°C for 4 s.

RESULTS AND DISCUSSION

Matrix modification effect of palladium on arsenic

In previous publications, matrix modification techniques have been applied for the determinations of mercury [7], lead [8], bismuth [9], antimony [10], tellurium [11] and other elements [12] in environmental

samples. In this paper, the stabilizing effect of palladium, zirconium, barium, nickel and molybdenum on arsenic in the graphite furnace is described. The results (Fig. 1) show that molybdenum and nickel stabilize arsenic up to 1400°C, but with zirconium and barium, loss of arsenic occurs above 800°C though the sensitivity for arsenic is apparently improved. It should be noted that in the presence of microgram amounts of palladium, not only is the maximum tolerable charring temperature for arsenic raised to 1300°C but also the sensitivity is 50% better than that in the presence of nickel.

Brooks et al. [13] reported the arsenic peak height was about four times greater if a tantalum-coated graphite tube was used. However, the peak height obtained when such a tube is used is lower than that available with palladium matrix modification. Therefore, palladium was employed in the remainder of this work. The arsenic absorbance increases with increasing palladium concentration. However, the effect becomes constant over the range 50—200 $\mu g\ ml^{-1}$ (Fig. 2). Thus, in all the following experiments, 20 μl of a 100 $\mu g\ ml^{-1}$ palladium solution was added for each determination.

Possible interferences from matrices

Severe interferences have been observed in the determination of arsenic by electrothermal a.a.s. [14]. In order to study possible interferences from sample matrices and from the acid mixtures used for sample digestion, a series of standard arsenic solutions was added to sample digestion solutions from river sediment or coal fly ash (0.4 mg ml^{-1} sample) of known arsenic

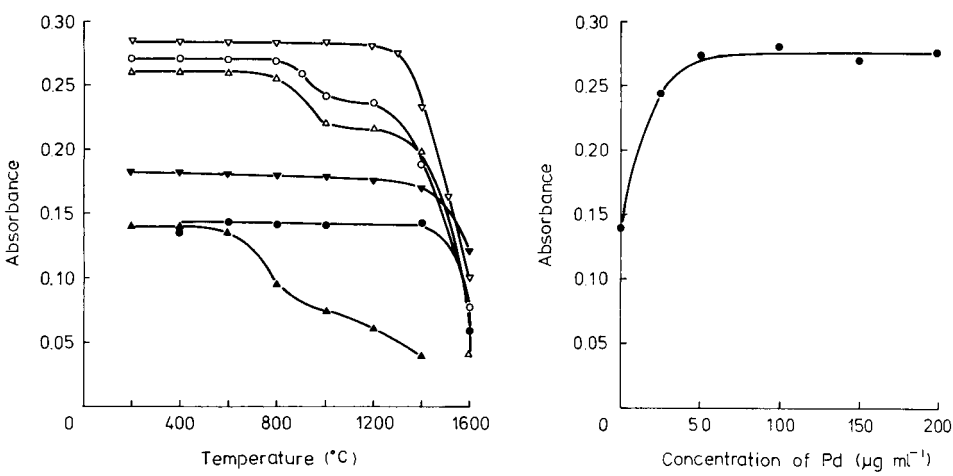

Fig. 1. Effect of ashing temperature on the absorbance of arsenic (0.8 ng) in the presence and absence of matrix modifiers: (▲) alone; (●) +4.8 μg Mo; (▼) +20 μg Ni; (△) +20 μg Ba; (○) +20 μg Zr; (▽) +2 μg Pd.

Fig. 2. Dependence of the absorbance for 0.8 ng of arsenic on the concentration of the palladium solution added (20 μl).

concentration and a peach leaf solution (10 mg ml^{-1}) with no arsenic detected by this method. The recoveries of arsenic are summarized in Table 1. The data indicate that the use of palladium as a matrix modifier prevents interferences from sample matrices and the acid digestion mixture on the determination of arsenic.

Selection of method of sample dissolution

Various acids and acid mixtures have been widely used for dissolution of arsenic from soil [15—17] and biological samples [18—21]. In addition, dry ashing has been used, with magnesium nitrate added as an ashing aid [22]. For samples containing an appreciable amount of silicon and when total arsenic is required, a fusion procedure has been suggested [23]. Compared to the methods for soil and biological samples, there are only a few reports on the digestion of coal; nitric and sulphuric acids [24] or perchloric—periodic acids [25] have been used. Recently a solid sampling technique was applied [26]. In general, the digestion methods are time-consuming. The acid digestion method used for hydride-generation atomic absorption spectrometry is not suitable for preparing solutions for direct injection into the graphite-tube atomizer owing to the relatively high acidity obtained. After consideration of these methods, it was decided to use a sulphuric acid—perchloric acid—sodium molybdate medium to dissolve arsenic in soil,

TABLE 1

Effect of sample composition and reagents on the determination of arsenic with palladium as matrix modifier

Sample	As added (ng ml^{-1})	Net As found (ng ml^{-1})	Recovery (%)
River sediment[a]	8	8	100
(0.4 mg ml^{-1})	16	15	94
	24	24	100
	32	34	106
Coal fly ash[a]	8	8	100
(0.2 mg ml^{-1})	16	14	88
	24	22	92
	32	29	91
Peach leaves	5	5	100
(10 mg ml^{-1})	10	8	80
	15	13	87
0.047 M H_2SO_4 + 0.04 M $HClO_4$ + 0.0025 M $Na_2MoO_4 \cdot 2H_2O$	40	38	95

[a]For identity, see Table 2.

coal fly ash and biological samples. The method is shorter than the above-mentioned procedures. Complete digestion of soil and biological samples requires about 30 min; 3 h is needed for coal fly ash. Thus there is less possibility of contamination, and direct determination is feasible after appropriate dilution of the digest, owing to the small volume of acid mixture used.

The effect of the concentration of acid mixture and sodium molybdate on the recoveries of arsenic from 0.100 g of soil or coal fly ash of known arsenic content was investigated, by otherwise following the recommended procedure. The arsenic concentration was obtained from a calibration graph obtained by direct injection of arsenic standards in dilute nitric acid. The recoveries of arsenic from soil are shown in Fig. 3. Greater than 90% recovery was achieved when 1—1.5 ml of acid mixture and 2—5 ml of the sodium molybdate solution were added. Similar results were obtained for arsenic in coal fly ash. In practice, 1.5 ml of the mixed acids and 3 ml of the molybdate solution were used for soil and coal fly ash, and 0.8 ml of acid mixture and 2 ml of molybdate solution for biological samples. In order to eliminate the suppressive effect caused by the acid mixture, the standard addition method was employed for real samples.

In order to provide a more universal method of sample attack which can be used for samples containing appreciable amounts of silicon, an acid decomposition procedure was also used, involving treatment with hydrofluoric acid.

Application to various samples

The results obtained for soil, fly ash and plant tissue reference materials are given in Table 2. The results obtained by use of the two dissolution procedures are in good agreement, and are also in excellent agreement with the certified values. The relative standard deviations for 10 replicate determinations following the entire procedure were found to be 2.3% and 4.5% for soil and pepperbush samples in which the arsenic contents were 66 and 2.3 $\mu g\ g^{-1}$, respectively.

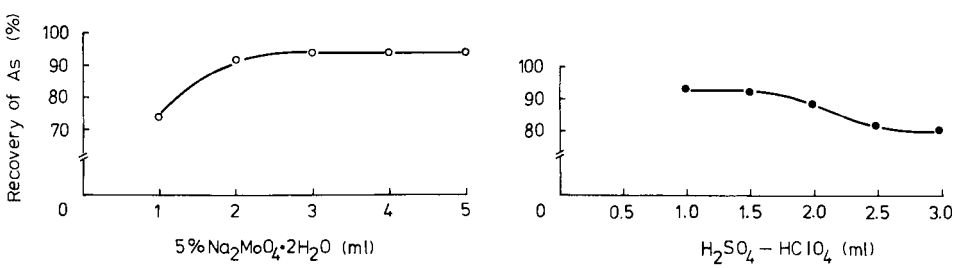

Fig. 3. Effect on the recovery of arsenic from soil of the volume of (•) acid mixture and (○) molybdate solution used for sample digestion.

TABLE 2

Determination of arsenic in soil, coal fly ash and biological standard reference materials

Samples	Arsenic content ($\mu g\ g^{-1}$)		
	Digestion by H_2SO_4—$HClO_4$—Na_2MoO_4	Digestion by HNO_3—$HClO_4$—HF	Certified value
SRM 1645	68	65	66
river sediment[a]	64	65	
SRM 1633a	145	153	145 ± 15
coal fly ash[a]	145	153	
SRM 1571	9.8		10 ± 2
orchard leaves[a]	10		
SRM No. 1	2.1		2.1 ± 0.3
pepperbush[b]	2.3		

[a]U.S. National Bureau of Standards. [b]N.I.E.S. (China).

REFERENCES

1 G. R. Ricci, L. S. Shepard, G. Colovos and N. E. Hester, Anal. Chem., 53 (1981) 610.
2 R. R. Brooks, D. E. Ryan and Hanfei Zhang, Anal. Chim. Acta, 131 (1981) 1.
3 D. Chakraborti, W. De. Jonghe and F. Adams, Anal. Chim. Acta, 119 (1980) 331.
4 R. D. Ediger, At. Absorpt. Newsl., 14 (1975) 127.
5 K. S. Subramanian, P. C. Leung and J. C. Merauger, Int. J. Environ. Anal. Chem., 11 (1982) 121.
6 J. Koreckova, W. Frech, E. Lundberg, J. Persson and A. Cedergren, Anal. Chim. Acta, 130 (1981) 267.
7 Shan Xiao-quan and Ni Zhe-ming, Hua Hsuch Hsuch Pao, 37 (1978) 261; Chem. Abstr., 92, 220474x (1980).
8 Shan Xiao-quan and Ni Zhe-ming, Can. J. Spectrosc., 27 (1982) 75.
9 Jin Long-zhu and Ni Zhe-ming, Can. J. Spectrosc., 26 (1981) 219.
10 Sun Han-wen, Shan Xiao-quan and Ni Zhe-ming, Talanta, 29 (1982) 589.
11 Shan Xiao-quan and Ni Zhe-ming, Acta. Sci. Circum., 1 (1981) 74; Chem. Abstr., 95, 225335z (1981).
12 Shan Xiao-quan and Ni Zhe-ming, Huaxue Xuebao, 6 (1981) 575; Chem. Abstr., 96, 192474j (1982).
13 R. R. Brooks, D. E. Ryan and Hanfei Zhang, At. Spectrosc., 2 (1981) 161.
14 C. W. Fuller, Electrothermal Atomization for Atomic Absorption Spectrometry, The Chemical Society, London, 1977, p. 67.
15 B. J. A. Haring, W. van Delft and C. M. Bom, Fresenius Z. Anal. Chem., 310 (1982) 217.
16 A. J. Thompson and P. A. Thoresby, Analyst, 102 (1977) 9.
17 T. J. Forehand, A. E. Dupuy, Jr., and H. Tai, Anal. Chem., 48 (1976) 999.
18 S. Peats, At. Absorpt. Newsl., 18 (1979) 118.
19 T. Hirayama, Y. Sakazami, M. Nohara and S. Fukui, Bunseki Kagaku, 30 (1981) 279.
20 N. Thieu, J. Assoc. Off. Anal. Chem., 63 (1980) 496.
21 K. Yanagi and M. Ambe, Bunseki Kagaku, 30 (1981) 209.
22 H. Woidich and W. Pfannhauser, Fresenius Z. Anal. Chem., 276 (1975) 61.
23 R. G. Smith and J. C. Van Loon, Anal. Chim. Acta, 93 (1977) 61.
24 P. Aruscavage, J. Res. U.S. Geol. Surv., 5 (1977) 405.
25 G. I. Speielholtz, G. C. Toralballa and R. J. Steinberg, Mikrochim. Acta, 6 (1971) 918.
26 L. Ebdon and W. C. Pearce, Analyst, 107 (1982) 942.

Analytica Chimica Acta, 151 (1983) 187—194
Elsevier Science Publishers B.V., Amsterdam — Printed in The Netherlands

A RAPID METHOD FOR THE DETERMINATION OF ARSENIC, CADMIUM, COPPER, LEAD AND ZINC IN AIRBORNE PARTICULATES BY FLAME ATOMIC ABSORPTION SPECTROMETRY

R. E. BYRNE

Chemical Laboratory, Mount Isa Mines Limited, Mount Isa, Queensland, 4825 (Australia)

(Received 14th December 1982)

SUMMARY

A rapid method for the routine determination of As, Cd, Cu, Pb and Zn in airborne particulates by flame atomic absorption spectrometry is described. NBS-SRM 1648 Urban Particulate Matter is used to validate the procedure. Various types of glass fibre filters normally used in high volume samplers were tested; only one provided low blanks and accurate results. An acid-insoluble residue was examined by both x-ray fluorescence and diffraction to determine its major components.

In most developed countries the sampling and monitoring of airborne particulate matter from industrial areas is mandatory. Many investigations have been done in regions which contain non-ferrous metal smelters [1—5]. Both a lead and a copper smelter are operated at the major mining centre of Mount Isa in Australia. Atmospheric particulates are sampled with high-volume samplers. The total suspended particulate on one half of an exposed glass fibre filter is analysed for arsenic, cadmium, copper, lead and zinc. The other half is sent to the appropriate regulatory authority for analysis, if required.

Numerous instrumental methods have been applied to the determination of elements in the total suspended particulates. Published methods include graphite-furnace atomic absorption spectrometry (g.f.a.a.s.) [6—10], x-ray fluorescence (x.r.f.) spectrometry [11—13], instrumental neutron activation analysis (i.n.a.a.) [14—16], mass spectrometry [17, 18], inductively-coupled plasma emission spectrometry (i.c.p.e.s.) [1, 19], anodic stripping voltammetry [20], atomic emission spectrometry [21], proton-induced x-ray emission [22] and Auger electron spectrometry [23]. In many of these methods it is necessary to matrix-match the standards with the sample. This often involves tedious preparation of standards and the use of different calibration graphs for different sample types. A recent review on advances in the measurement of air contaminants by Katz [24] gives details of, and references to, problems encountered when these various techniques are used.

The aim of this investigation was to evaluate the applicability and accuracy of a rapid method of determining arsenic, cadmium, copper, lead and zinc in

0003-2670/83/$03.00 © 1983 Elsevier Science Publishers B.V.

the total suspended particulates. Conventional flame atomic absorption spectrometry was chosen over other available instrumentation because of its simplicity, speed and adequate sensitivity. The N.B.S. Standard Reference Material (SRM) 1648, Urban Particulate Matter was selected for validation of the method. This environmental SRM was prepared from a large amount of atmospheric particulate matter collected over a period of three years from baghouses at St. Louis. It is considered to be representative of urban dust [25]. The need to use such standard materials has been described by Cali [26]. It was hoped that arsenic could be determined in the same acid digest as the four metals. Low-temperature ashing was not considered because of the danger of arsenic loss [16, 27]. Reasons for the selection of acids and other reagents used in the digestion process are given in the later discussion.

EXPERIMENTAL

Apparatus and chemicals

A Varian-Techtron Model AA6 atomic absorption spectrometer with a hydrogen arc background corrector was used for all measurements. Cadmium, copper, lead and zinc were determined by using an air/acetylene flame and the optimum parameters specified by the manufacturer. Varian hollow-cathode lamps were used and the monochromator was tuned to the most sensitive resonance wavelength for each lamp. A modified Varian Model 65 vapour generation accessory was used for arsenic determination in a nitrogen/hydrogen/entrained air flame. A Westinghouse electrodeless-discharge lamp, run at 7 W, was the source for arsenic determination.

Readings for cadmium, copper, lead and zinc were taken in the absorbance mode and concentrations were determined from six-point standard calibration graphs. Arsenic was determined in the absorbance peak height mode. Stock standard solutions (1000 mg l^{-1}) were prepared from high-purity metals; the arsenic stock was made up from analytical reagent-grade arsenic(III) oxide. Calibration standards were prepared each day by diluting the stock with a solution which was 20% (v/v) in hydrochloric acid and 0.4% (w/v) in disodium—EDTA. Distilled deionized water was used for the preparation of all solutions. Analytical reagent-grade acids and solids were used for all dissolution processes.

Procedure

Half of a glass fibre filter (original dimensions 20 cm × 25 cm) was cut into small pieces and placed in a 150-ml squat beaker. About 100 mg of urban particulate matter (N.B.S. SRM 1648) was accurately weighed into the beaker. Solid potassium chlorate (0.5 g) was added followed by 100 ml of 20% (v/v) nitric acid. The beaker was covered with a watchglass and the contents were allowed to simmer for 15 min on a hot plate. The beaker was then placed to the edge of the hot plate after it had cooled somewhat, and the liquid was evaporated to dryness overnight. The beaker and contents were

cooled and 20.0 ml of concentrated hydrochloric acid was added. The beaker was warmed to about 80°C and 80.0 ml of the 0.4% EDTA solution was added. The mixture was allowed to stand for 30 min and then stirred well with a glass rod. Elemental determinations were made as described above. The procedure was repeated for the reference material without the addition of any filter paper. Acid, reagent and filter paper blanks were carried through the complete procedure.

RESULTS AND DISCUSSION

Elemental analysis of the SRM alone

It is evident from the data presented in Table 1 that the analysis of the SRM by the proposed method gave results which agree well with the NBS certified values. All of the mean values obtained lie within the certified 95% confidence limits. The value obtained for copper appears slightly low but agrees well with the reference values obtained when a wet digestion was used. Duplicate samples of the SRM were digested by the method of Agemian and Chau [32] in a Uniseal decomposition vessel. The mean value for copper, as determined by flame a.a.s., was 588 ± 14 mg kg^{-1} which is not significantly different ($P = 0.95$) from the results obtained with the proposed method.

Analysis in the presence of filter media

Initially three types of glass fibre filter were examined for compatibility with the proposed method. Whatman GF/A was discarded after the early trials for reasons outlined below. The main proportion of the investigation was conducted with Whatman EPM-1000 and Schleicher and Schuell No. 1-HV glass fibre filters. The data in Table 2 indicate that lower mean values were found with the 1-HV paper. Those obtained for copper, lead and zinc were outside of the certified 95% confidence intervals. This trend was consistently

TABLE 1

Values for arsenic, cadmium, copper, lead and zinc in N.B.S. SRM 1648 Urban Particulate Matter (mean value ±95% confidence limits)

Method	Concentration (mg kg^{-1})					Ref.
	As	Cd	Cu	Pb	Zn	
Certified	115 ± 10	75 ± 7	609 ± 27	6550 ± 80	4760 ± 140	28
A.a.s.	112 ± 2	74 ± 2	586 ± 11	6560 ± 100	4670 ± 70	This work[a]
G.f.a.a.s.	—	69 ± 4	586 ± 22	6210 ± 85	4580 ± 60	29
I.n.a.a.	117 ± 5	70 ± 6	—	—	4700 ± 200	30
X.r.f.	—	—	640 ± 60	6900 ± 200	4800 ± 100	12
I.c.p.e.s.	112	73	598	7000	4700	31

[a] $n = 8$.

TABLE 2

Experimental values for arsenic, cadmium, copper, lead and zinc in N.B.S. SRM 1648 Urban Particulate Matter

	Concentration (mg kg^{-1})[a]				
	As	Cd	Cu	Pb	Zn
Original method					
SRM alone	112 ± 2	74 ± 2	586 ± 11	6560 ± 100	4670 ± 70
SRM + EPM-1000 filter	112 ± 4	75 ± 2	582 ± 15	6620 ± 200	4640 ± 80
SRM + 1-HV filter	112 ± 3	74 ± 3	566 ± 15	6440 ± 190	4510 ± 70
Bulking to volume					
SRM alone	111 ± 2	74 ± 1	587 ± 11	6580 ± 90	4660 ± 90
SRM + EPM-1000 filter	110 ± 3	72 ± 3	576 ± 8	6360 ± 110	4580 ± 80
SRM + 1-HV filter	109 ± 2	63 ± 4	535 ± 18	6040 ± 320	4210 ± 90

[a]Results expressed as the mean ±95% confidence interval (n = 4, except for the SRM alone in the original method, where n = 8).

observed in all the trials conducted here. It was also found that the 1-HV paper tended to disintegrate during the recommended procedure. Fine fibres were suspended in the final solution. This presented problems such as clogging of the nebulizer and the production of erratic absorbance readings unless the suspension was centrifuged prior to the a.a.s. measurements. The EPM-1000 paper proved far more tenacious and showed little tendency to break up. Its use was adopted for routine particulate sampling.

Quantitative transfer

It was recognised that one possible source of error in the proposed method was the dual addition of reagent solutions (20.0 ml and 80.0 ml) to give a final volume of 100.0 ml. While it was considered that the error was likely to be insignificant by comparison with the sampling error, it was decided to test the method using a bulking-to-volume finish. The E.P.A.-recommended method for the determination of lead in airborne particulates uses a quantitative transfer and bulking-to-volume procedure; the description stresses that adequate standing time for each addition of diluent to the beaker and filter is essential. A contact time of 30 min is specified, as this period allows the nitric acid "trapped in the filter to diffuse into the rinse water" [33].

After the initial acid attack and reduction to dryness, 20.0 ml of concentrated hydrochloric acid was added to the beaker which was then warmed to 80°C. The EDTA solution (20 ml) was added and the mixture was cooled for 30 min. As much liquid as possible was poured into a 100-ml volumetric flask. A further 20 ml of EDTA solution was added and the procedure was repeated. Further 15-ml additions were made until the volume was made up to 100.0 ml. A total of 100 ml of EDTA solution was required to reach the specified volume indicating that 20 ml of liquid was retained by the filter.

Table 2 also lists the results obtained when the modified method was used. It may be inferred that small amounts of all five elements remain in the solution absorbed by the filter. It is possible that this problem could be rectified by bulking to a larger volume, but this would increase the processing time markedly and decrease the sensitivity of the method.

Blank values for glass fibre filters

The E.P.A. specifies glass fibre filters for the collection of total suspended particulates through the National Air Surveillance Network [15]. The agency's recommended method for the determination of lead in total suspended particulates also involves collection on glass fibre filters [33]. Recently there has been some controversy over the use of glass fibre as opposed to membrane or polymer filters such as cellulose acetate, vinyl chloride and polytetrafluoroethylene [34, 35]. Technological advances in production have made available filters with total metal levels far below those of a decade ago.

Glass fibre filters have been used in all high-volume sampling by the company in Mount Isa on the recommendation of the Air Pollution Council of Queensland. The three types of glass fibre filters used in this investigation have been previously mentioned. Blank values for the acid-extractable portions are given in Table 3. The results were determined on half sheets and the data obtained were doubled to provide full sheet values. The GF/A paper was eliminated from the project at an early stage because of the very high values of acid-extractable zinc. The EPM-1000 paper provided the lowest blanks for all five elements. The values for copper and lead are slightly higher than the manufacturer's specified typical levels of 3 and 10 μg per sheet, respectively. Values obtained for cadmium and zinc are about ten times lower than the specified values of 2 and 100 μg per sheet, respectively. No value for arsenic is listed by the manufacturer.

The E.P.A.-recommended flow rate for sampling of total suspended particulates lies within the range 1.1—1.7 m^3 min^{-1} over a sampling period of 24 h. If it is assumed that air can be sampled at the lowest recommended flow rate and that elemental concentrations can be determined accurately

TABLE 3

Acid-extracted blank values for arsenic, cadmium, copper, lead and zinc in different types of glass fibre filter

	Concentration (μg/sheet)[a]				
	As	Cd	Cu	Pb	Zn
Whatman GF/A[b]	0.78 ± 0.28	0.79 ± 0.12	3.1 ± 1.1	29 ± 2	>30 000
Whatman EPM-1000[c]	0.49 ± 0.11	0.23 ± 0.10	3.3 ± 1.5	12 ± 2	14 ± 1
S. and S. 1-HV[c]	1.4 ± 0.1	0.42 ± 0.15	11 ± 3	15 ± 2	60 ± 8

[a]Results expressed as the mean ± 95% confidence limit. [b]n = 33. [c]n = 21.

when the ratio of blank to sample concentration is 1:3, then the following levels (ng of analyte per m^3 of air) should be determined successfully: As, 0.93; Cd, 0.44; Cu, 6.2; Pb, 23; Zn, 26.

Compatibility of the SRM

Any quantitative procedure provides only an estimate of the true concentration of the element(s) determined. A reliable reference standard should have a similar sample matrix to the unknown being tested. Frauerwieser [36] considered that the SRM 1648 Urban Particulate is the only reliable standard reference material for airborne particulates, after an investigation of the problems of preparing standard reference materials similar to SRM 1648.

The chemical composition of particles found in airborne particulates in the vicinity of lead and copper smelting operations has been described elsewhere [2—4, 14]. Typically, the compounds exist as oxides, sulphides or sulphates. Experience gained in this investigation suggests that SRM 1648 is a far more refractory material than the unknowns routinely processed. The fact that reliable results have been obtained for the SRM does not prove that the same degree of accuracy applies to the unknown samples. It does, however, provide a high degree of confidence in the probable accuracy of the results obtained for the unknown samples. The possibility of preparing a secondary reference material typical of airborne particulate found in Mount Isa has been considered, but the project would be time-consuming and expensive, and the success of a validation program must be doubtful because of the problems described by Frauerwieser [36].

Digestion reagents

A combination of nitric acid and potassium chlorate was used as the digesting medium because of the ability of the mixture to decompose polymetallic copper, lead and zinc ores. Furthermore, digested arsenic is oxidised to arsenic(V) so that the possibility of losses by volatilisation is minimised. It was found in an early trial that arsenic loss was nearly 50% if hydrochloric acid was used for the digestion. The final concentration of 20% (v/v) hydrochloric acid was optimum for the production of arsine in the vapour-generation device. The EDTA was added to complex copper, thus preventing depressive interference in the determination of arsenic by hydride generation. The acid concentration was more than sufficient to take up cadmium, copper, lead and zinc. The addition of EDTA had no effect on the a.a.s. readings for these metals.

Acid-insoluble residue

A large amount of acid-insoluble residue was obtained when the proposed method was applied to the SRM alone. The residue was filtered off, washed thoroughly and dried. A qualitative scan on a Philips PW-1212 sequential x.r.f. spectrometer showed that the residue contained aluminium, calcium, iron, potassium, silicon and titanium. These elements had previously been

shown to be major components of the SRM [29, 30]. No trace of the five elements determined by a.a.s. in this investigation was found. The major phases were identified by x-ray diffraction as α-quartz and feldspar, (CaNaK)-$Al_2Si_2O_8$.

The author thanks D. G. MacDonald for the x.r.f. scan, J. F. Riley for the x-ray diffraction analysis and Mount Isa Mines Limited for permission to publish this work.

REFERENCES

1 A. J. Lynch, N. R. McQuaker and D. F. Brown, J. Air Pollut. Control Assoc., 30 (1980) 257.
2 R. M. Harrison, C. R. Williams and I. K. O'Neill, Environ. Sci. Technol., 15 (1981) 1197.
3 R. L. Foster and P. F. Lott, Environ. Sci. Technol., 14 (1980) 1240.
4 M. Small, M. S. Germani, A. M. Small, W. H. Zoller and J. L. Moyers, Environ. Sci. Technol., 15 (1981) 293.
5 M. S. Germani, M. Small, W. H. Zoller and J. L. Moyers, Environ. Sci. Technol., 15 (1981) 299.
6 B. N. Noller and H. Bloom, Clean Air, 14 (1980) 9.
7 B. N. Noller and H. Bloom, Anal. Chem., 49 (1977) 346.
8 E. M.-M. Sutter and M. J.-F. Leroy, Anal. Chim. Acta, 96 (1978) 243.
9 P. Geladi and F. Adams, Anal. Chim. Acta, 96 (1978) 229.
10 C. J. Pickford and G. Rossi, Analyst, 103 (1978) 341.
11 K. K. Nielson, Anal. Chem., 49 (1977) 641.
12 H. Kingston and P. A. Pella, Anal. Chem., 53 (1981) 223.
13 R. D. Giauque, L. Y. Goda and N. E. Brown, Environ. Sci. Technol., 8 (1974) 436.
14 R. C. Ragaini, H. R. Ralston and N. Roberts, Environ. Sci. Technol., 11 (1977) 773.
15 J. P. Lambert and F. W. Wilshire, Anal. Chem., 51 (1979) 1346.
16 J. F. Walling, G. Evans, T. A. Hinners, J. P. Lambert, S. J. Long and F. W. Wilshire, J. Air Pollut. Control Assoc., 28 (1978) 1134.
17 J. W. Gramlich, L. A. Machlan, T. J. Murphy and J. L. Moore, Trace Subst. Environ. Health, 11 (1977) 376.
18 W. D. Davis, Environ. Sci. Technol., 11 (1977) 593.
19 N. R. McQuaker, D. F. Brown and P. D. Kluckner, Anal. Chem., 51 (1979) 1082.
20 G. Colovos, G. S. Wilson and J. Moyers, Anal. Chim. Acta, 64 (1973) 457.
21 D. R. Scott, W. A. Loseke, L. E. Holboke and R. J. Thompson, Appl. Spectrosc., 30 (1976) 392.
22 K. Kemp and F. Jensen, Nucl. Instrum. Methods, 142 (1977) 101.
23 R. W. Linton, P. Williams, C. A. Evans, Jr., and D. F. Natusch, Anal. Chem., 49 (1977) 1514.
24 M. Katz, J. Air Pollut. Control Assoc., 30 (1980) 528.
25 J. Josephson, Environ. Sci. Technol., 15 (1981) 1408.
26 J. P. Cali, Fresenius Z. Anal. Chem., 297 (1979) 1.
27 P. R. Walsh, J. L. Fasching and R. A. Duce, Anal. Chem., 48 (1976) 1012.
28 J. P. Cali, N.B.S. Certificate of Analysis, Standard Reference Material 1648, November, 1978.
29 J. G. Farmer and M. J. Gibson, At. Spectrosc., 2 (1981) 176.
30 R. R. Greenberg, Anal. Chem., 51 (1979) 2004.
31 M. A. Floyd, V. A. Fassel and A. P. D'Silva, Anal. Chem., 52 (1980) 2168.

32 H. Agemian and A. S. Y. Chau, Anal. Chim. Acta, 80 (1975) 61.
33 Federal Register, 43 (1978) 46246.
34 R. D. Gilbert and R. E. Fornes, Anal. Chem., 52 (1980) 1153.
35 J. P. Lambert and F. W. Wilshire, Anal. Chem., 52 (1980) 1153.
36 G. Frauerwieser, Mikrochim. Acta, II (1982) 55.

Analytica Chimica Acta, 151 (1983) 195—202
Elsevier Science Publishers B.V., Amsterdam — Printed in The Netherlands

DETERMINATION OF SULFUR FORMS IN NATURAL FUEL MATERIALS BY ATOMIC ABSORPTION SPECTROMETRY OF BARIUM

TERRY J. HOCKING[a] and WILSON M. GULICK, Jr.*

Department of Chemistry and Chemical Engineering, Michigan Technological University, Houghton, MI 49931 (U.S.A.)

(Received 12th October 1982)

SUMMARY

Forms of sulfur are converted seriatim to barium sulfate which is metathesized to barium carbonate, dissolved, and quantified by atomic absorption spectrometry. Sulfate is extracted with perchloric acid. Pyritic sulfur is converted by lithium aluminum hydride to hydrogen sulfide which is oxidized with alkaline hydrogen peroxide. Organic sulfur is completely oxidized by using the "liquid fire" reaction. Application of these methods to synthetic samples carefully treated to insure homogeneity resulted in average relative standard deviations of 3.0, 2.7, and 3.2% for sulfate, pyrite, and organic sulfur, respectively. Average absolute errors were less than 0.04% S for the determination of each sulfur form.

Determinations of sulfur forms in coal, oil shale, and related materials are of current interest because these substances are important potential sources of energy if their utilization can be accomplished with appropriate environmental protection. Sulfur is found in these materials principally in three forms. Published research on determination of each form, sulfate [1—3], pyritic sulfur [1, 2, 4—11], and organic sulfur [1, 3, 4, 12], has led to methods currently accepted for their determination: those of ASTM [4, 5, 12], the Laramie Energy Research Center [3, 13], and the U.S. Bureau of Mines [14]. In each method sulfate is determined gravimetrically by precipitation of barium sulfate. In the ASTM and Bureau of Mines pyrite determinations, nitric acid oxidation is used; the former recommends quantitation of liberated Fe(III) by atomic absorption spectrometry, while the latter estimates pyritic iron by titration and also quantifies by gravimetry the sulfur concomitantly oxidized to sulfate. The Laramie pyrite determination involves reduction of pyrite to hydrogen sulfide which is trapped in a cadmium solution; the acid liberated is then titrated. Organic sulfur is determined indirectly in both ASTM and Bureau of Mines methods; total sulfur is determined in a separate sample by the Eschka [12] fusion method and the organic sulfur is taken as equal to total sulfur less sulfate and pyritic sulfur.

[a]Present address: Texas Instruments, Inc., Dallas, TX, U.S.A.

0003-2670/83/$03.00 © 1983 Elsevier Science Publishers B.V.

In the Laramie method, the residue from the first two determinations is used for direct determination of organic sulfur by the Eschka fusion [3].

Modifications of the accepted methods were sought that would meet three criteria: (1) use of a single sample for successive determinations; (2) conversion of all three forms of sulfur to the same chemical species; (3) spectroscopic quantitation of that chemical species without loss of accuracy or precision in comparison to accepted methods. This paper describes a method which has been tested for accuracy and precision with synthetic standards and a small number of natural samples readily available. Results are encouraging and this procedure is recommended to workers who require these determinations frequently. The procedure offers substantial reduction in determination time and such utilization may provide long-term validation.

Because atomic absorption spectrometry of barium is a convenient and well-documented procedure, and barium sulfate affords a ready route to isolation of sulfate, the points for study are whether all three forms of sulfur can be converted conveniently and quantitatively to sulfate under conditions which permit its isolation as barium sulfate, and whether the barium sulfate can subsequently be redissolved for quantitation by atomic absorption spectrometry. Successful resolution of these questions yielded the following scheme. Sulfate is extracted with dilute perchloric acid [3]. Pyrite is reduced to hydrogen sulfide which is trapped in a scrubber containing alkaline hydrogen peroxide [15] which oxidizes it to sulfate. The residue from these procedures is completely oxidized by using the "liquid fire" reaction [16, 17]. Sulfate, isolated from each step as barium sulfate, is redissolved by using the classical method that involves metathesis to barium carbonate [18]. The latter salt is dissolved in hydrochloric acid for quantitation of barium by atomic absorption spectrometry (a.a.s.).

EXPERIMENTAL

Chemicals and equipment

Pyrite, a pure mineral sample ground to —325 mesh, was obtained from the Department of Metallurgical Engineering, Michigan Technological University. Dibenzothiophene (95%), n-octadecylmercaptan (98%), and 5-methyl-2-thiophenecarboxylic acid (99%) were obtained from the Aldrich Chemical Company. All other reagents were available from standard sources.

A Perkin-Elmer 305B atomic absorption spectrometer system was used for all a.a.s. measurements. A Damon/IEC DPR-600 centrifuge equipped with a six place rotor for 50-ml tubes was used.

Samples

Synthetic shale samples were prepared from calcium sulfate dihydrate, pyrite, and approximately equal quantities of three organosulfur compounds (see above) with washed and ignited sand as diluent. Synthetic coal samples were identical except for the addition of decolorizing carbon to simulate the

greater reducing power of coal. Concentrations of each form of sulfur were varied over ranges expected in natural materials. Each sample, of approximately 10-g total mass, was mixed in a jar mill. Natural shale samples were from the Antrim formation of lower Michigan and were well cores identified as Antrim Shale 1, (Well MI-3, 1318—1328 feet) and Antrim Shale 2 (Well MI-1, 1369.5—1370.5 feet). Coal samples were obtained from the Michigan Technological University Institute of Mineral Research and are identified as IMR Coal 5 (Moris Mine, Middle Kittanning Seam, Tioga County, PA) and IMR Coal 3 (Bokoshe Mine, Upper and Lower Hartshorne Seam, Haskell County, OK). The natural samples were ground to —325 mesh. All samples were processed in triplicate.

Isolation of sulfur as barium sulfate

Samples (1 g) were extracted for 30 min with 100 ml of 10% perchloric acid [3] with gentle boiling. The resulting slurry was filtered with suction through No. 42 paper and washed with five portions of hot water. The filtrate and washings were combined and concentrated to 100—125 ml, treated with 20 ml of 10% barium chloride solution, and further concentrated to a final volume of less than 50 ml. The precipitate and supernatant liquid were reserved for subsequent treatment.

The filter paper and solid residue from above were transferred to a round 500-ml two-neck flask and dried at 110°C for 2 h. This flask was then incorporated into an apparatus similar to that described previously [3] to collect hydrogen sulfide. A Claisen-type 3-way parallel side-arm adapter permitted attachment of both a nitrogen inlet and a condenser to one joint of the flask; the second joint was closed with a rubber serum cap. The previous design was modified with an all-glass transfer line equipped with 12/2 ball and socket joints from the condenser to a gas scrubber. All joints were ungreased. A report [19] that hydrogen sulfide dissolves in rubber tubing prompted the all-glass, grease-free system. The gas scrubber, which contained 100 ml of 30% hydrogen peroxide adjusted to pH 10 with 6 M sodium hydroxide, was placed in an ice bath. (The oxidation of hydrogen sulfide by peroxide is exothermic and can lead to vigorous, uncontrolled decomposition of the peroxide solution [20] if the ice bath is omitted.) Lithium aluminum hydride (1 g) dissolved in 50 ml of tetrahydrofuran was added to the flask and a slow purge with nitrogen was begun, assisted by application of aspirator vacuum to the outlet of the gas scrubber. The solution was refluxed with stirring for 30 min and then cooled in an ice bath. Small portions of water were then injected through the serum cap until a total of 50 ml had been added. The ice bath was replaced by a heating mantle, 50 ml of 30% perchloric acid was injected, and the mixture was refluxed with stirring for 30 min to complete evolution of hydrogen sulfide. Completion of the reaction was demonstrated by applying a syringe full of head-space gas to lead acetate paper. The solution in the scrubber was transferred to a beaker, boiled to destroy excess of peroxide, treated with 20 ml of 10% barium

chloride solution, and then evaporated to a final volume of less than 50 ml. This precipitate and supernatant liquid were reserved for the measurement step.

The residue from the preceding step was filtered through No. 42 paper with suction. Paper plus residue were placed in a 500-ml round flask and treated with 20 ml of concentrated nitric acid. After 10 min, 40 ml of concentrated perchloric acid was added and reaction at ambient temperature was allowed to occur for an additional 10 min. The flask was then gradually heated with stirring under partial reflux until a temperature of approximately 200°C was reached. This temperature was maintained until the solution became colorless or only light yellow. The cooled solution was carefully neutralized with 6 M sodium hydroxide and filtered. The filtrate and washings (hot water) were adjusted to pH 5 with 6 M hydrochloric acid, heated to near boiling, and treated with 20 ml of 10% barium chloride solution. This solution was concentrated to a final volume of less than 50 ml and reserved for the measurement step. The validity of each step described above was proved individually and as part of the sequence; however, alternative methods have not been ruled out.

Metathesis

Precipitates and supernatant liquids from the procedures described were transferred to 50-ml centrifuge tubes and centrifuged, and the supernatant liquid was removed by using a micropipet attached to an aspirator. Precipitates were washed with three portions of distilled water with washings removed in the same way and discarded. A solution containing 25 ml of 1.5 M sodium carbonate and 1.5 ml of 6 M sodium hydroxide was added [18] and the centrifuge tubes were heated on a steam bath for 30 min with occasional stirring. These mixtures were centrifuged and the supernatant liquid was discarded. The resulting barium carbonate was washed three times with minimal volumes of a solution prepared from 25 ml of distilled water and 1.5 ml of 6 M sodium hydroxide. The washings were discarded and the precipitate was dissolved in a small volume of 6 M hydrochloric acid and transferred to a volumetric flask for dilution.

Spectrometric measurement of barium

Barium was quantified by a.a.s. at the 553.6-nm line from a reducing nitrous oxide—acetylene flame optimized in the usual way for barium. Sodium chloride at a concentration of 1 mg ml^{-1} was added to all solutions to suppress ionization. Nine standard solutions spanning the range 2--25 mg l^{-1} barium were prepared. Five replicate measurements for each solution established the calibration, a least-squares line with a slope of 0.042 ± 0.001, an intercept of 0 ± 0.3 and a standard error of estimate of 0.03.

Sample solutions were diluted to have barium concentrations within the calibrated range; a minimum of three measurements was made on each sample. Standard solutions were re-examined periodically. Sulfur contents of samples

were calculated from the amount of barium found and the appropriate stoichiometric and dilution factors.

RESULTS AND DISCUSSION

Results for three synthetic shale samples demonstrated that there are no unexpected chemical interferences in this method and that the accuracy, judged by comparison of sulfur taken and found for each form, is encouraging. Scatter was greater than expected, and greater attention was paid to ensuring sample homogeneity in three subsequent synthetic coal samples. Results for these samples are summarized in Table 1. The standard deviations reported are three to five times smaller than those observed for the synthetic shale. Table 2 presents results for real shale and coal samples. The results labeled A are from samples which were ground and stored until used, whereas those designated B are from samples which were carefully reground immediately prior to final processing. Pooled variances for each sulfur form from group A were compared with those from group B by using the *F*-test. In each case, one concludes with at least 90% confidence that the difference is significant. The only factor to which this difference can be attributed is non-uniform settling of the material between grinding and final processing. Sample inhomogeneity [21] has previously been suggested as a major factor causing poor precision.

Although no claim is made that our synthetic samples are true mineral surrogates, an essential proof of any analytical scheme is its ability to give reasonable results on materials of known composition. Table 1 suggests that the method described here meets this criterion. The largest absolute errors occur in the determination of organic sulfur. The standard sulfur compounds were chosen for convenience and similarity to compounds tested by Smith et al. [3], as possible organosulfur species in oil shale, and were not available at the highest purity.

Comparisons of precision can be made with previous work. It has been stated [4] that the results of consecutive determinations done in the same laboratory on the same sample by the same operator using the same apparatus should not differ by more than 0.02% for sulfate sulfur; by more than 0.05%

TABLE 1

Results (% S) for synthetic coal samples

Coal	Sulfate			Pyrite			Organic		
	Taken	Found[a]	Error	Taken	Found[a]	Error	Taken	Found[a]	Error
1	0.500	0.495 ± 0.006	−0.005	1.156	1.13 ± 0.01	−0.030	1.066	1.05 ± 0.05	−0.15
2	0.094	0.097 ± 0.003	+0.003	1.507	1.50 ± 0.02	−0.009	0.508	0.528 ± 0.008	+0.020
3	0.245	0.284 ± 0.004	+0.039	0.689	0.70 ± 0.02	+0.006	1.565	1.65 ± 0.04	+0.084

[a]Mean and standard deviation for three independent determinations.

TABLE 2

Results (% S)[a] for oil shale and coal samples

	Sulfate	Pyrite	Organic
A. Antrim Shale 1	0.11 ± 0.02	1.46 ± 0.07	1.1 ± 0.3
IMR Coal 5	0.10 ± 0.02	0.77 ± 0.03	0.52 ± 0.08
(Total S = 1.22)[b]	(0.07)	(0.69)	(0.46)
B. Antrim shale 2	0.046 ± 0.002	1.03 ± 0.03	0.352 ± 0.009
IMR Coal 3	0.055 ± 0.004	0.42 ± 0.02	0.52 ± 0.03
(Total S = 1.05)[b]	(0.04)	(0.51)	(0.50)

[a]Mean and standard deviation for three independent determinations.
[b]Values in parentheses determined by MTU's Institute of Mineral Research using ASTM Method.

for pyritic sulfur present at $\leqslant 2\%$, or by more than 0.10% for pyritic sulfur present at $>2\%$. The Bureau of Mines [14] specifies similar precision levels for total sulfur. Results in Table 1 and Table 2B are well within these limits. Because organic sulfur is determined by difference, ASTM does not give limits of error; however, Paris [22] reported that Batelle-Columbus Laboratories calculated the imprecision of organic sulfur determinations by the ASTM method as ±25%. Triplicate sulfate results for the two coal samples used in this work were obtained by the MTU Institute of Mineral Research using ASTM Method D2492 (Table 2) and showed relative standard deviations of ±25% and ±10%, respectively. Smith et al. [3] report relative standard deviations of ±1.5% for pyritic sulfur and ±6% for organic sulfur, using the Laramie method. Therefore, the precision of the proposed method seems to compare favorably with established methods.

Data presented here confirm previous work [23] which indicated that organic sulfur is not reduced by lithium aluminum hydride under conditions which reduce pyrite. These data also confirm the report [11] that particle size affects the efficacy of pyrite reduction. Quantitative yields of hydrogen sulfide were not obtained with pure pyrite samples of —65 and —100 mesh and it was for this reason that natural samples and standard pyrite were ground to --325 mesh. Intermediate particle sizes were not investigated.

It should be noted that this method, like previous methods, is not completely species-specific. In initial experiments to authenticate the method for pyrite, resublimed sulfur was selected as a standard material of reliable purity. In the procedure, elemental sulfur is quantitatively converted to hydrogen sulfide and then to sulfate. Although no significant amount of elemental sulfur is thought to be present in coal [3] and related materials, it would be determined as pyritic sulfur if present. Small amounts of elemental sulfur were isolated from one sample of Antrim shale.

Users should be aware that metal sulfides will cause errors in all the methods discussed here. Sulfides of the ammonium sulfide group will dis-

solve in the initial acid leach and remain undetected unless the leach solution is treated with bromine water [3]. The treatment will increase the apparent amount of sulfate sulfur, but because sulfate is environmentally harmless, potential pollutants will be underestimated. This problem can be corrected by extraction of two samples with acid, one with exclusion of air for sulfate, and the second with the addition of bromine water for sulfate plus soluble sulfide. Hydrogen sulfide group sulfides may also dissolve in the first step if the Mott procedure with hydrochloric acid [2] is used because the formation of chloro complexes helps to dissolve many of these sulfides. In the nitric acid decomposition [4] of pyrite, remaining hydrogen sulfide group materials will dissolve [18], but will not be detected by the indirect determination based on iron. In the Laramie method as well as the method presented here, sulfides that are insoluble in 10% perchloric acid will be carried through to the final oxidative step and be quantified as organic sulfur.

In comparison with accepted methods, the procedure outlined here appears to be less time-consuming and of comparable accuracy and precision.

Partial support for this work from the Department of Energy under contract EX 76-C-01-2346 administered by the Dow Chemical Company is gratefully acknowledged. This paper is abstracted from a thesis submitted by T. J. H. in partial fulfilment of the requirements for the M. S. in Chemistry, Michigan Technological University, 1980.

REFERENCES

1 A. A. Powell and W. W. Parr, Eng. Exp. Station Univ. Illinois, Bull., 111 (1919) 66.
2 R. A. Mott, Fuel, 29 (1950) 53.
3 J. W. Smith, N. B. Young and D. L. Lawlor, Anal. Chem., 36 (1964) 618.
4 Am. Soc. Test. Mater., Book ASTM Stand., Pt. 26 (1976) 269.
5 Am. Soc. Test. Mater., Book ASTM Stand., Pt. 26 (1978) 332.
6 W. van Hees and E. Early, Fuel, 38 (1959) 424.
7 M. S. Burns, Fuel, 49 (1970) 126.
8 A. H. Edwards, G. N. Daybell and W. J. Pringle, Fuel, 37 (1958) 47.
9 R. Belcher and C. E. Spooner, Fuel, 20 (1941) 172.
10 W. Radmacher and P. Mohrhauer, Glueckauf, 89 (1953) 503.
11 J. K. Kuhn, L. Kohlenberger and N. F. Shimp, Ill. State Geol. Surv. Environ. Geol. Note, (1973) 66.
12 Am. Soc. Test. Mater., Book ASTM Stand., Pt. 26 (1976) 381.
13 D. L. Lawlor, J. I. Festor and W. E. Robinson, Fuel, 42 (1963) 239.
14 U.S. Bur. Mines Bull., 638 (1967) 11.
15 J. Polcin, Chem. Zvesti, 11 (1957) 494; H. A. C. Van Straten, Anal. Chim. Acta, 14 (1956) 325.
16 G. F. Smith, Anal. Chim. Acta, 8 (1953) 397.
17 H. Diehl and G. F. Smith, Quantitative Analysis, Wiley, New York, 1952, p. 304.
18 E. H. Swift, A System of Chemical Analysis, Freeman, San Francisco, 1938, pp. 362, 202.
19 J. A. Kitchener, A. Liberman and D. A. Spratt, Analyst, 76 (1951) 509.
20 P. J. Durrant and B. Durrant, Introduction to Advanced Inorganic Chemistry, Wiley, New York, 1970, p. 820.

21 J. K. Kuhn, in T. D. Wheelock (Ed.), Coal Desulfurization, ACS Symp. Ser. 64, American Chemical Society, Washington, DC, 1977, p. 16.
22 B. Paris, in T. D. Wheelock (Ed.), Coal Desulfurization, ACS Symp. Ser. 64, American Chemical Society, Washington, DC, 1977, p. 22.
23 N. G. Gaylord, Reduction with Complex Metal Hydrides, Interscience, New York, 1956, p. 832.

Analytica Chimica Acta, 151 (1983) 203—210
Elsevier Science Publishers B.V., Amsterdam — Printed in The Netherlands

AN ELECTROMIGRATION METHOD FOR STUDYING TECHNETIUM IN GROUND WATER UNDER OXIC AND ANOXIC CONDITIONS

A. CHATT[a], G. BIDOGLIO* and A. DE PLANO

Commission of the European Communities, Joint Research Centre, Ispra Establishment, Radiochemistry and Nuclear Chemistry Division, I-21020 Ispra-Varese (Italy)

(Received 20th October 1982)

SUMMARY

A free-liquid electromigration method is described for studying the occurrence of technetium in ground water. Cells made of pyrex glass, teflon and plexiglas were examined for adsorption, diffusion, and electro-osmotic effects. Average mobilities of 5.38×10^{-4} in oxic conditions and 5.15×10^{-4} cm^2 s^{-1} V^{-1} in anoxic conditions were obtained for the pertechnetate ion in ground water (ionic strength 3×10^{-3} M) at 24°C. The effective diffusion coefficient of this ion was calculated as 1.37×10^{-5} cm^2 s^{-1} for oxic conditions.

The migration of radionuclides from vitrified highly active waste (HAW) in a deep geological repository to the biosphere, depends more upon the physicochemical state of the radionuclides than on their total concentrations. Consequently, analytical methods are being developed to investigate the speciation of radionuclides in solutions. A few reliable techniques have been reported for determining the physicochemical states of trace elements. However, these techniques cannot directly be applied to radionuclides for several reasons. For example, the radionuclide concentrations of interest are much lower (10^{-9}—10^{-16} M) than the trace element levels generally studied (10^{-5}—10^{-7} M), which indicates the increased problems of detection, adsorption, losses, etc., that must be dealt with. Further, trace element speciation is normally done in oxic environments whereas anoxic conditions are of primary importance in radionuclide migration studies, and biological hazards associated with the handling of highly toxic radioactive substances must be reduced to a negligible amount. Some of the trace element speciation techniques, such as electromigration and polarography, can still be applied to radionuclides after appropriate modifications of instrument and methodology. Here, the electromigration technique is used in studying technetium species in ground water under oxic and anoxic conditions. Technetium-99 is of interest in radioactive waste management, because it has a very high fission yield, and a long half-life of 2.13×10^5 years. The pertechnetate ion has been reported to be mobile in soil under oxic conditions [1], and partial

[a]Permanent address: Department of Chemistry, Dalhousie University, Halifax, Nova Scotia, B3H 4J1, Canada.

0003-2670/83/$03.00 © 1983 Elsevier Science Publishers B.V.

reduction to and retention of $TcO_2(s)$ have been said to occur in anoxic conditions [2, 3].

Since the discovery of electrophoresis by Reuss [4] in 1809, many books, reviews and papers have been published on its theoretical principles and applications. Makarova and Stepanov [5] have summarized the use of electromigration in radiochemistry. Recently, Benes and coworkers [6, 7] have reported its application to mainly trace element species. In the work discussed here, the principles of the free-liquid tracer electrophoresis method described by Hoyer et al. [8] were applied, and electromigration cells made of pyrex glass, teflon and plexiglas were constructed. Factors such as adsorption, diffusion, and electro-osmotic effects which could influence the mobility of an ion were studied. Details of an electromigration method for measuring the mobility of the pertechnetate ion in a number of solutions are given.

EXPERIMENTAL

In order to evaluate the possibility of applying electrophoresis to determine the mobility of pertechnetate reliably, preliminary experiments were done with paper electrophoresis in a standard cell; Whatman cellulose 3MM and glass fibre GF/A papers were used.

A simple electromigration cell made of pyrex glass, and consisting of two vertical side-arms and a horizontal compartment connected through two 3-way teflon stopcocks, was used during the early stages of studies on free-liquid electrophoresis. As the problem of the electro-osmotic effect in this cell became evident, a cell made of teflon was designed. The advantage of using teflon is that it minimizes adsorption losses of ions present at very low concentrations. However, some displacement of liquid in the teflon cell was noted when the two stopcocks were opened to connect the side-arms to the central section. For this reason, an improved free-liquid electromigration cell was constructed from polished plexiglas and teflon stopcocks.

A schematic diagram of the cell is shown in Fig. 1. The central section (B, about 7 cm^3 capacity; see Tables) of the cell was filled with the solution of the radiotracer ion under investigation. The side-arms (A and C, each of about 16 cm^3 capacity) were rinsed several times until no radioactivity could be detected, and only then were they filled with the same solution as in the central section but without the radiotracer ion. This inactive solution was also placed in the cathode and anode compartments (F and G) containing platinum electrodes. The side-arms (A and C) of the plexiglas unit were connected to the electrode compartments (F and G) by means of two strips of Whatman No. 1 filter paper. The cell was attached to a d.c. power supply and to an ammeter. All parts of the cell were connected by opening the stopcocks D and E. The amount of current passed was recorded every 2 min for 30—45 min. The temperatures in the side-arms and central compartment were recorded by using thermocouples. At the end of the experiment, the stopcocks were closed, all solutions were recovered, and appropriate amounts (generally between 200 μl and 1 ml) were withdrawn for counting.

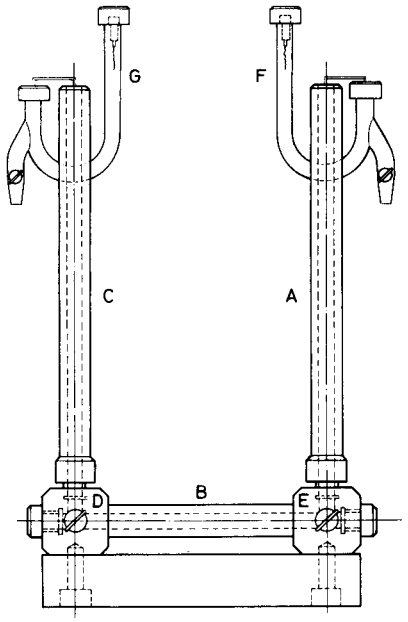

Fig. 1. Schematic diagram of the plexiglas electromigration cell.

The volume of the central compartment of each cell was measured with tracer solutions as well as with mercury. The mercury determinations were more reliable, and were therefore used in this study.

The conductivities of the test solutions were measured by using a Tacussel Electronique model CD-6N conductivity meter.

Radiotracer solutions of ^{99}Tc (as pertechnetate), ^{22}NaCl, and ^{14}C-glucose were obtained from Amersham. In order to simplify the counting process, the β-emitting ^{99}Tc nuclide was tagged in some cases with γ-emitting ^{95m}Tc (New England Nuclear).

The counting system consisted of a 7.5 cm × 7.5 cm NaI(Tl) detector coupled to a Beckman 8000 analyzer; or another 7.5 cm × 7.5 cm NaI(Tl) detector attached to a Packard Autogamma analyzer; or an Intertechnique SL30 model liquid scintillation counter.

The synthetic ground water used in this work had the typical composition of the aquifer overlying the Boom Clay, Mol, Belgium [9] which is being considered as a possible formation for HAW disposal. The concentrations of various ions in the ground water were as follows: 3.4×10^{-3} M HCO_3^-/CO_3^{2-}, 1.8×10^{-4} M Cl^-, 5.2×10^{-6} M SO_4^{2-}, 2.4×10^{-3} M Na^+, 2.0×10^{-4} M K^+, 1.3×10^{-4} M Mg^{2+}, 7.6×10^{-5} M Ca^{2+}, 1.8×10^{-6} M Fe (total). The E_h and pH were −25 mV and 8.35, respectively. This ground water was later spiked with the desired radiotracer.

The mobility values were measured under both oxic and anoxic conditions. A glove box with a purified nitrogen atmosphere was set up as described else-

where [10]. The ground water was deaerated with the same gas as in the glove box, thereby increasing its pH from 8.35 to 9.3. The concentrations of oxygen were 200—300 mg l^{-1} in the glove box, determined by a solid zirconium dioxide electrochemical cell [11], and 150—200 μg l^{-1} in the ground water, measured by a dissolved-oxygen electrode (Orion model 97-08).

RESULTS AND DISCUSSION

Preliminary experiments with pertechnetate-95m solutions by paper electrophoresis showed that the technetium activity had quantitatively migrated to the positive pole, as expected. However, with glass fibre supports a considerable portion of the technetium activity was detected near the negative pole [12]. This observation could be explained in terms of an electro-osmotic effect. There were also adsorption and spreading of radiotracer ion on the fibres. Moreover, pertechnetate solutions of very high specific activity were needed to get the counting statistics within acceptable limits in solid-support electrophoresis. In order to eliminate these problems, as well as to develop a method that could be applied directly to solutions for detecting ionic species at low concentrations, the free-liquid electromigration technique was used.

The mobility of an ion in a solution can be calculated from

$$u = v(\chi/ti)(C_0 - C)/C_0$$

where u is the ionic mobility of the radioactive species ($cm^2\ s^{-1}\ V^{-1}$), χ is the specific conductivity of the solution ($ohm^{-1}\ cm^{-1}$), i is the average current flowing through the cell (A), t is the time (s) during which current passes through the cell, C_0 is the initial concentration of the radiotracer ion in the central compartment (cpm ml^{-1}), C is the final concentration of the same ion in the same compartment after t s (cpm ml^{-1}), and v is the volume of the central part of the cell (cm^3). Although mobility values can be calculated from this equation, several factors can influence the values. These factors include adsorption, diffusion, temperature, viscosity, ionic strength, and electro-osmotic effect.

Losses from adsorption of ions, particularly those of trace elements at very low concentrations, on the walls of electromigration cells have been reported [7]. No such loss of pertechnetate for the concentration range 10^{-6}—10^{-11} M was detected in any of the three cells used in the present study.

In order to check the possible diffusion of pertechnetate from the central compartment of the cell, it was filled with a solution of $^{95m}TcO_4^-$, stopcocks were opened, and the cell was left standing undisturbed for 24 h. Sampling of the solutions in the side-arms showed no measurable diffusion.

The effect of electro-osmosis in all three cells was investigated by using ^{14}C-labelled glucose solutions; the results are shown in Table 1. This effect was most pronounced in the glass cell. The small percentage of activities detected in the side-arms of the teflon cell could very well be caused by the

TABLE 1

Measurements for studying the electro-osmotic effect with ^{14}C-labelled glucose in three cells at 24°C

Parameters	Glass cell	Teflon cell	Plexiglas cell
Activity in arm A (%)	30	5	1.2
Activity in arm C (%)	0.3	1.8	0.8
i (μA)	300	731	743
t (s)	2760	2700	2700

volume displacement when stopcocks were turned. There was practically no effect of electro-osmosis in the plexiglas cell.

The mobility of sodium-22 ion was measured for evaluating the performance as well as the reliability of the three electromigration cells. Duplicate results for each cell are given in Table 2. Considerable quantities of sodium-22 ions were detected in the anodic side of the glass cell as suspected. The combined effects of electro-osmosis and electromigration were considered to be the reasons for this behaviour which gave erroneous results. The teflon cell performed well, and only a little activity was detected in the anodic side arm. An average mobility of 4.12×10^{-4} cm^2 s^{-1} V^{-1} for sodium-22 ion in ground water (ionic strength $\mu = 3 \times 10^{-3}$ M, pH = 8.35) was obtained. It is evident from Table 2 that the plexiglas cell performed best under the experimental conditions used.

The mobility values for sodium-22 ion were measured between 10^{-2} and 10^{-3} M concentrations of sodium perchlorate (i.e., at different μ values) in the plexiglas cell. The mobilities increased almost linearly with decreased ionic strength in this range. The values were then extrapolated to zero ionic strength, giving an average mobility of 5.41×10^{-4} cm^2 s^{-1} V^{-1} at 28°C at infinite dilution. This value was further corrected for temperature by using the equation $u^0_{28} = u^0_{25}$ [1 + 0.02 (28 − 25)] to yield an average mobility at infinite dilution of 5.10×10^{-4} cm^2 s^{-1} V^{-1} at 25°C, which agrees very well with the value 5.09×10^{-4} cm^2 s^{-1} V^{-1} reported in the literature [13].

All three cells were then employed to determine the mobility of $^{95m}TcO_4^-$ ion in ground water; these results are also presented in Table 2. Again the values obtained with the glass cell were considered erroneous. The teflon cell gave slightly lower values because of the problem of volume displacement from the central compartment. An average mobility of 5.38×10^{-4} cm^2 s^{-1} V^{-1} at 24°C and 3×10^{-3} M ionic strength was obtained when the plexiglas cell was used. Assuming that the effect of temperature change on the mobility of the pertechnetate ion is similar to that for the sodium ion, so that the same temperature correction equation may be applied and also neglecting all other effects, the mobility of pertechnetate ion in 5×10^{-3} M sodium nitrate solution at 18°C measured by Shvedov and Kotegov [14] as 4.85×10^{-4} may be converted to 5.51×10^{-4} cm^2 s^{-1} V^{-1} (at 24°C) which is similar to the present value.

TABLE 2

Comparison of mobility values obtained for sodium-22 and pertechnetate-95m for the three different cells at 24°C

Parameters	Glass cell[a]		Teflon cell[a]		Plexiglas cell[b]		
	Sample 1	Sample 2	Sample 3	Sample 4	Sample 5	Sample 6	Sample 7
Mobility of sodium-22 ions							
Activity in arm A (%)	7.7	6	1.09	1.18	0.013	0.02	
Activity in arm C (%)	1.5	2.3	21.9	34.6	76.07	53.9	
Activity in compartment B (%)	85.6	89	75	65.7	22.73	45	
C_0 (cpm ml^{-1})	11240	11240	11455	11240	12912	12499	
C	9891	10435	8825	7409	2786	5553	
i (μA)	326	291	563	545	347	323	
t (s)	420	900	1860	2760	3600	2700	
χ (10^{-4} ohm^{-1} cm^{-1})	2.8	2.8	2.8	2.8	1.22	1.22	
v (cm^3)	2.63	2.63	6.6	6.6	6.98	6.74	
u (10^{-4} cm^2 s^{-1} V^{-1} at T°C)	6.45	2.01	4.06	4.19	5.35[c]	5.24[c]	
Mobility of pertechnetate-95 m							
Activity in arm A (%)	22.3	23	21.5	16.2	19	48.2	34.4
Activity in arm C (%)	0.03	—	1.8	1.2	0.4	0.25	0.2
Activity in compartment B (%)	73.2	72	74.4	82	76.7	50.8	64.7
C_0 (cpm ml^{-1})	6844	5080	5226	6865	11747	16538	6031
C	5013	3639	3891	5612	9017	8122	3827
i (μA)	262	283	622	593	458	753	732
t (s)	1200	900	1800	1200	1800	2280	1800
χ (10^{-4} ohm^{-1} cm^{-1})	2.8	2.8	2.8	2.8	2.8	2.8	2.8
v (cm^3)	2.59	2.63	6.6	6.6	6.74	6.74	6.74
u (10^{-4} cm^2 s^{-1} V^{-1} at T°C)	6.17	8.2	4.22	4.73	5.32	5.59	5.23

[a]In ground water, $\mu = 3 \times 10^{-3}$ M. [b]In $NaClO_4$ solution, $\mu = 1 \times 10^{-3}$ M, for sodium-22 measurements but in ground water for pertechnetate measurements. [c]At 28°C.

The effective diffusion coefficient D of pertechnetate in ground water was calculated from the Nernst—Einstein equation, $D = KuT/ze$, where K is Boltzmann's constant (J K^{-1}), u is the ionic mobility (m^2 s^{-1} V^{-1}), T is the temperature (K) and e is the electronic charge (C). It was assumed that the effect of ionic strength on the diffusion coefficient is negligible below $\mu = 3 \times 10^{-3}$ M so that the Nernst—Einstein equation could be applied, and a value of 1.37×10^{-5} cm^2 s^{-1} was obtained for the effective diffusion coefficient of pertechnetate ion at 24°C under oxic conditions.

The mobility of the pertechnetate ion was measured under anoxic conditions (150—200 μg l^{-1} dissolved oxygen) as well as in the presence of certain complexing agents (e.g., HCO_3^-/CO_3^{2-}, humic acid, etc.) to simulate conditions that could be encountered in potential disposal sites for HAW. Values of 5.15×10^{-4} and 5.9×10^{-4} cm^2 s^{-1} V^{-1} were obtained in ground water and near-saturated humic acid solutions, respectively. The slightly higher mobility of the pertechnetate ion in the latter solution might have been caused by a change in viscosity of the medium and not by reduction to technetium(IV), as indicated from independent measurements [10]. A combination of this electromigration method and radiochemical methods has been used to study the speciation of technetium in ground water passing through sandy clay columns and in different solutions under oxic and anoxic conditions. The application of these methods and interpretation of the results for the purpose of radioactive waste management are beyond the scope of this paper, and will be reported elsewhere [10, 15].

Conclusions

The free-liquid electromigration method is suitable for studying the physicochemical state of technetium at low concentrations in solutions. Of the three cells designed, the pyrex glass cell is not recommended for use. The teflon cell can be particularly useful in situations where adsorption of reduced species in the cell is suspected. The plexiglas cell can be reliably employed to determine mobility values under both oxic and anoxic conditions. The electromigration method can also be applied to calculate hydrated radii and hydration numbers [16], and to distinguish between microcolloids and soluble species for studying the transport of radionuclides by ground water.

The authors thank Prof. F. Girardi and Dr. A. Avogadro of the JRC, Ispra, for discussions, and Dr. U. Mazzi and F. Zorn of the CNR, Padova, for assistance.

REFERENCES

1 R. E. Wildung, K. M. McFadden and T. R. Garland, J. Environ. Qual., 8 (1979) 156.
2 E. A. Bondietti and C. W. Francis, Science, 203 (1979) 1337.
3 B. Allard, H. Kigatsi and B. Torstenfelt, Radiochem. Radioanal. Lett., 37 (1979) 223.
4 F. F. Reuss, Mem. Imp. des Naturalists des Moscou, 2 (1809) 327.
5 T. P. Makarova and A. V. Stepanov, Sov. Radiochem., 19 (1977) 103.

6 P. Benes and V. Majer, Trace Chemistry of Aqueous Solutions: General Chemistry and Radiochemistry, Elsevier, Amsterdam, 1980.
7 P. Benes and J. Glos, J. Radioanal. Chem., 52 (1979) 43.
8 H. W. Hoyer, K. J. Mysels and D. Stigter, J. Phys. Chem., 58 (1954) 385.
9 A. Bonne, SCK/CEN, Mol, Belgium, personal communication.
10 G. Bidoglio, A. Chatt, A. De Plano and F. Zorn, J. Radioanal. Chem., 79 (1983) in press.
11 C. M. Mari, S. Pizzini, T. A. Giorgi, L. Rosai and M. Borghi, J. Appl. Electrochem., 7 (1977) 215.
12 F. Zorn, Tesi di Laurea, University of Padova, Italy, 1982.
13 Handbook of Chemistry and Physics, 5th edn., CRC Press, Cleveland, OH, 1976–77, D-153.
14 V. P. Shvedov and K. V. Kotegov, Sov. Radiochem., 5 (1963) 342.
15 G. Bidoglio, A. De Plano and A. Chatt, in Proc. 1982 Int. Symp. Scientific Basis for Nuclear Waste Management, Vol. 6, Elsevier, New York.
16 R. Lundqvist, E. K. Hulet and P. A. Baisden, Acta Chem. Scand., A35 (1981) 653.

Analytica Chimica Acta, 151 (1983) 211—219
Elsevier Science Publishers B.V., Amsterdam — Printed in The Netherlands

A MECHANISTIC INVESTIGATION OF THE REACTION OF L-LEUCINE WITH TRINITROBENZENESULFONIC ACID

N. P. EVMIRIDIS and M. I. KARAYANNIS*
University of Ioannina, Chemistry Department, 30 Doboli St., Ioannina (Greece)

(Received 5th January 1983)

SUMMARY

The reaction of trinitrobenzenesulfonic acid (TNBS) with L-leucine was followed at various initial concentrations, pH values and temperatures, by measuring the change in absorbance at 420 nm. The rate at pH 9.2 was found to be expressed by k[leucine]-[TNBS]^2/(1 + [TNBS]), with an activation energy of 12.8 kcal mol^{-1}. A mechanism is proposed, in accordance with this equation, involving the formation of an intermediate product. Parallel reactions are also possible when TNBS is in large excess. Both these peculiarities impose specific conditions on rate measurements used for primary amine determinations.

A method of determination of primary amino groups with 2,4,6-trinitrobenzenesulfonic acid (TNBS) was reported in 1960 by Satake et al. [1]. The reaction is

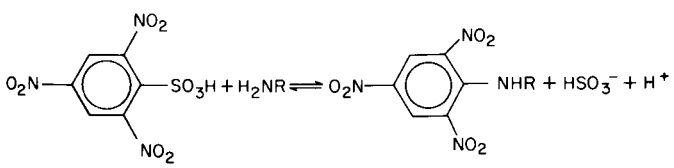

The method was based on measurement of the absorbance of the solution at 350 nm after the reaction had been quenched by acidification after 1 h. The authors at that time were studying various reagents for labelling proteins [2]. They realized the selectivity of TNBS for primary amino groups as well as its mildness. In 1966, Satake et al. [3] reported a routine method for the determination of individual amino acids in a mixture based on this spectrophotometric procedure, after chromatographic separation of the components. Fields [4] later reported a rapid method of determination based on measurements at 420 nm and Mokrasch [5] published a modified method for the determination amines, amino acids and proteins in admixture. Snyder and Sobocinski [6] reported a further modification, eliminating the quenching step used in most of the above methods.

Another group of investigators tried to use this spectrophotometric determination of primary amino groups without the quenching step, in order to

0003-2670/83/$03.00 © 1983 Elsevier Science Publishers B.V.

establish a rate relationship useful for the determination of primary amines based on kinetic measurements. Goldfarb [7] reported a kinetic study of the reaction of a large excess of TNBS with glycine, glycine peptides and acetyllysine, and found the reaction to be pseudo-first order with respect to amino concentration; Goldfarb also demonstrated the formation of sulfite complexes of trinitrophenylated amino groups. Freedman and Radda [8] investigated spectrophotometrically the kinetics of the reaction of TNBS with various amino acids, peptides and proteins, and in all cases found pseudo-first order reactions with respect to the primary amino group. They also tried to deduce mathematically the individual amino group reaction curves from the overall reaction curve of proteins containing more than one primary amino group. Recently, attempts have been made to establish a method for the determination of primary amino groups based on initial reaction rates, using either a spectrophotometer in a conventional arrangement or in a stopped flow technique [9], or a TNBS-selective electrode [10].

All the previous investigators used the initial overall pseudo-first order rate equation $r_0 = k[\text{TNBS}]\ [\text{primary amino group}] = k'[\text{primary amino group}]$ for their determinations of the amino group. A reaction mechanism is always a good guide to what is measured as part of the overall reaction rate. In multistep mechanisms, the rate is not always directly dependent on reactant concentration and this quite often produces complicated reaction curves. Consecutive reactions involve quantities and rates of formation of intermediate products which are very sensitive to small variations in conditions. Parallel reactions again involve many final products which may absorb in the same selected spectral range. Variations in concentrations of these final products may also result from small differences in reaction conditions. All these considerations, together with the evidence of sulfite complex formation of TNP—amine derivatives having maximum absorbance at 420 nm [4], show the importance of a mechanistic investigation of the reaction of TNBS with primary amines. This paper describes such an investigation of leucine with TNBS. From the results, it becomes clear how the analytical method will be affected by the reaction conditions when the method is based on initial reaction rates.

EXPERIMENTAL

Apparatus and reagents

A Pye-Unicam SP-6-200 spectrophotometer was used in conjunction with a potentiometric recorder (Varian A-25 Aerograph) to record the change in absorbance with time. The optical cell was thermostated above or below ambient temperature. The buffered solutions were checked with a pH meter (Metrohm).

All water used was double distilled and reagents were of analytical grade. Stock aqueous solutions of L-leucine (0.1 M) and TNBS (0.1 M) were prepared by dissolving 1.3120 g and 2.9320 g, respectively, in water and diluting

to 100 ml with water. The stock leucine solution was further diluted with buffer solutions to the appropriate concentration used in the experiments. The buffer solutions used were pH 8.0 (0.35 M boric acid/0.05 M sodium borate), pH 9.2 (0.05 M sodium borate), pH 10.0 (0.025 M sodium carbonate/0.025 M sodium hydrogencarbonate) and pH 11.8 (0.01 M trisodium orthophosphate).

Procedure

All solutions were thermostated before use. Unless otherwise stated the procedure and conditions were as follows: 10.0 ml of L-leucine (buffered at pH 9.2) solution was placed in a thermostated 15-ml cuvette at 25°C and 1.0 ml of TNBS solution was added. The cuvette was shaken rapidly for a few seconds and placed in the thermostated cell compartment of the spectrophotometer, and the absorbance was recorded at 420 nm against time.

RESULTS

The visible absorbance spectra of the products of the reaction of leucine with TNBS had maxima at 350 and 420 nm. There was a suspicion, derived from the spectra of the reacting mixtures discussed below, that two compounds were absorbing at 420 nm. Therefore an experiment was designed to elucidate whether the absorbance at 420 nm was from a single product or that of more than one compound. The absorption spectra of reaction mixtures nearly at equilibrium (when the rate of reaction is very slow), starting from different initial concentrations of reactants, were measured from 300 to 600 nm. Figure 1 shows series of such spectra at constant initial concentrations of leucine and differing TNBS concentrations. Both absorbance maxima (350 and 420 nm) increase as the initial TNBS concentration increases. Table 1 shows that the absorbances at the two maxima do not increase with the TNBS concentration in the same proportion. This is illustrated by the ratios of the absorbances at 350 nm and 420 nm ($A(350)/A(420)$) in each case. This ratio decreases with an increase in initial TNBS concentration when the initial leucine concentration exceeds that of TNBS, while it increases when the initial TNBS concentration becomes higher than that of leucine. Thus, depending on the initial concentrations of the reactants, it was possible, near equilibrium, to have different distributions of products contributing to $A(420)$. On leaving mixtures with excess of leucine initial concentration to equilibrate, the $A(350)/A(420)$ value again increased.

Another experiment was designed to establish if the products absorbing at 420 nm are from a reversible or an irreversible chemical reaction. For this purpose, a mixture of reactants was left to equilibrate and its spectrum was obtained. Another mixture was left only until the rate of reaction became very slow (near equilibrium). The initial reactant concentrations were chosen so that $A(350)/A(420)$ was small. The two mixtures were diluted and the absorbances were measured at both wavelengths. The results in Fig. 2 indicate

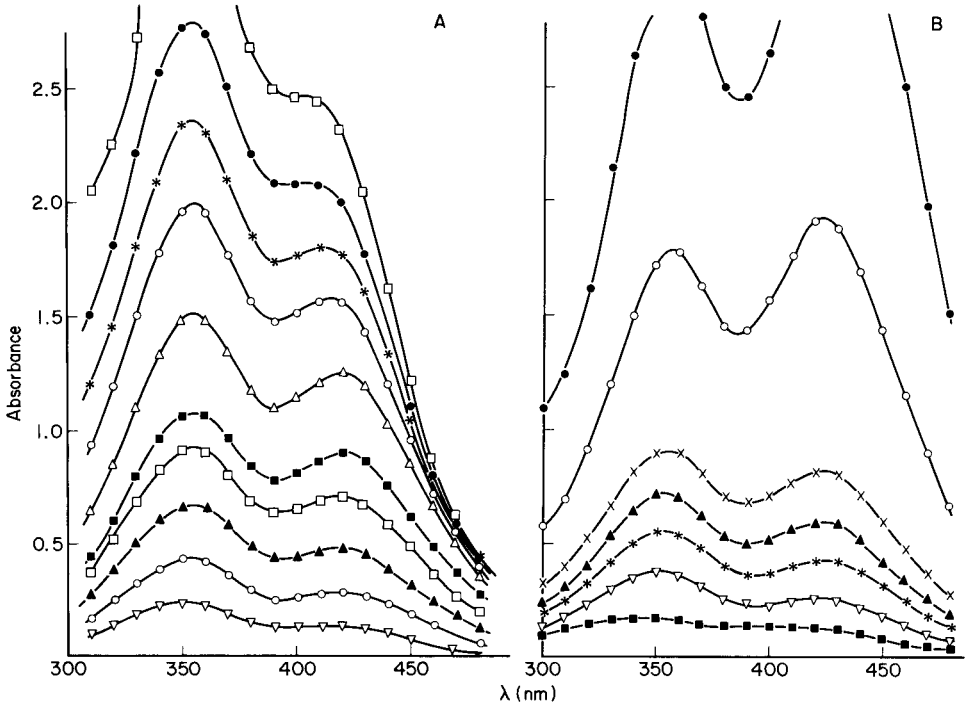

Fig. 1. Spectra of reaction mixtures of TNBS with leucine at room temperature, pH 9.2. Initial leucine concentrations: (A) 1.0×10^{-4} M; (B) 1.0×10^{-2} M. TNBS concentration: A, (▽) 2.0×10^{-5} M, (●) 4.0×10^{-5} M,(▲) 6.0×10^{-5} M, (□) 8.0×10^{-5} M, (■) 1.0×10^{-4} M, (△) 2.0×10^{-4} M, (○) 4.0×10^{-4} M, (*) 6.0×10^{-4} M, (●) 8.0×10^{-4} M, (□) 1.0×10^{-3} M; B, (■) 2.0×10^{-4} M, (▽) 4.0×10^{-4} M, (*) 6.0×10^{-4} M, (▲) 8.0×10^{-4} M, (×) 1.0×10^{-3} M, (○) 2.0×10^{-3} M, (●) 4.0×10^{-3} M.

TABLE 1

Effect of TNBS concentration on $A(350)/A(420)$ at pH 9.2

TNBS conc. ($\times 10^{-4}$ M)	$A(350)/A(420)$		
	9.1×10^{-5} M leucine	9.1×10^{-4} M leucine	9.1×10^{-3} M leucine
0.182	1.69	1.64	
0.364	1.49	1.47	1.46
0.546	1.39	1.30	1.31
0.728	1.29	1.20	1.22
0.910	1.18	1.16	1.10
1.82	1.19	0.96	0.90
3.64	1.26		<0.71
5.46	1.32		
7.28	1.39		
9.10	1.47		

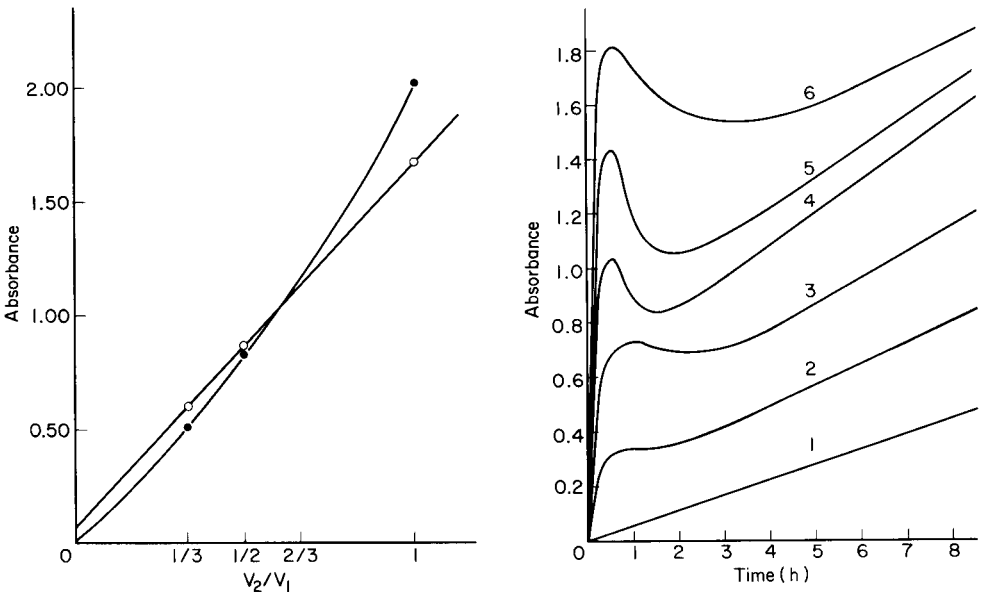

Fig. 2. Absorbance vs. dilution of a reaction mixture containing 10.0 ml of 1.0×10^{-2} M leucine buffered at pH 9.2 and 1.0 ml of 2.0×10^{-3} M TNBS at room temperature approaching equilibrium. Wavelengths: (•) 420 nm; (○) 350 nm. V_2 = initial volume, V_1 = final volume after dilution.

Fig. 3. Absorbance vs. time for the reaction of 2.0 ml of 1×10^{-2} M TNBS buffered at pH 9.2 with 10.0 ml of leucine solution of concentration: (1) 0.0, (2) 2.0×10^{-5} M, (3) 4.0×10^{-5} M, (4) 6.0×10^{-5} M, (5) 8.0×10^{-5} M, (6) 1.0×10^{-4} M.

that the mixture near equilibrium gives a linear change of absorbance with concentration at 350 nm but a more exponential change at 420 nm. Yet, the mixture at equilibrium showed linear relationships with dilution at both wavelengths.

A third experiment was done to show the relationship between absorbance change and time of reaction in the optical cell at 420 nm. The curves obtained are shown in Fig. 3. The change in initial rate of reaction with TNBS concentration at 8°C and 26°C, and with leucine concentration at various pH values, are shown in Tables 2 and 3, respectively. The temperature dependence is shown in Table 4.

DISCUSSION

The reaction profiles in Fig. 3 show the change in absorbance at 420 nm, which represents all products absorbing at that wavelength. Because the final product is the major product in a consecutive reaction mechanism, the rate of change of absorbance at 420 nm (dA/dt) represents the rate of formation of the final product ($d[P]/dt$). The shape of the curves in Fig. 3 can be

TABLE 2

Effect of TNBS concentration and temperature on the initial rate (ΔA min^{-1}) at pH 9.2 and 420 nm

TNBS conc. ($\times 10^{-4}$ M)	Initial rate (ΔA min^{-1})		
	9.1×10^{-4} M leucine[a]	9.1×10^{-3} M leucine[a]	9.1×10^{-3} M leucine[b]
0.182	0.02	0.14	0.03
0.364	0.03	0.29	0.08
0.546	0.05	0.50	0.13
0.728	0.08	0.75	0.18
0.910	0.10	1.00	0.28
1.82	0.26	2.50	0.61
3.64	0.56	6.1	1.36
5.46	1.00	11.9	2.09
7.28	1.58	15.3	3.1
9.10	2.13	21.8	4.1
18.2	4.7		8.3
36.4	9.7		14.4
54.6	12.7		

[a]At 26°C. [b]At 8°C.

TABLE 3

Effect of leucine concentration on the initial rate (ΔA min^{-1}) for 1.67×10^{-2} TNBS at 26°C and 420 nm

Leucine conc. ($\times 10^{-4}$ M)	Initial rate (ΔA min^{-1})			
	pH 8.0	pH 9.2	pH 10.0	pH 11.8
0.000	0.35×10^{-3}	1.0×10^{-3}	4.20×10^{-3}	107×10^{-3}
0.182	3.0×10^{-3}	25.0×10^{-3}	60.0×10^{-3}	287×10^{-3}
0.364	8.2×10^{-3}	47.0×10^{-3}	136×10^{-3}	400×10^{-3}
0.546	11.7×10^{-3}	97.0×10^{-3}	212×10^{-3}	640×10^{-3}
0.728	13.3×10^{-3}	113×10^{-3}	303×10^{-3}	733×10^{-3}
0.910	21.0×10^{-3}	167×10^{-3}	373×10^{-3}	

TABLE 4

Effect of temperature on the initial rate (ΔA min^{-1}) at pH 9.2 and 420 nm for 1.82×10^{-4} M TNBS and 9.1×10^{-3} M leucine

Temp (°C)	9.5	13.0	17.5	22.5	26.5
Rate	0.65	0.90	1.22	1.80	2.33

explained as follows. The ascending part after the maximum is due to a reaction taking place with TNBS alone in alkaline solutions. This behaviour of TNBS was observed in alkaline solutions without the presence of leucine during the present investigations. The hump is due to an intermediate product whose molar absorptivity at 420 nm is greater than that of the final product. Both features are superimposed on the curve for the production of the final product (TNP—leucine).

The possibility that the absorbance at 420 nm may be caused by at least two products may also be inferred from the work of Satake et al. [1] and the kinetic work of Goldfarb [7]. According to Satake et al., the molar absorptivity at 420 nm of the TNP derivative of leucine in 4% sodium hydrogencarbonate is about 40% that at 350 nm, while Goldfarb found that a sulfite complex of the TNP derivative of leucine has a molar absorptivity at 420 nm comparable to that of the TNP derivative of leucine at 350 nm. As the sulfite complex (of TNP—leucine) absorbing at 420 nm is an intermediate product, a steady-state reaction scheme can be assumed in which case $(dA/dt)_0$ is proportional to $(d[P]/dt)_0$ (initial rates). In order to ensure the above proportionality, experimental conditions must be used where TNBS decomposition in alkaline solution is minimal.

From Fig. 2 it may be realized that when the absorbance at 420 nm shows nearly equilibrium conditions (but some intermediate product is still present), the relationship between absorbance and dilution follows a composite curve with the linear contribution from the TNP derivative and an exponential contribution from the sulfite complex of the TNP derivative, thus revealing reversible behaviour associated with the intermediate product.

The data in columns 3 and 4 in Table 2 follow very similar trends (except for the negligibly small TNBS decomposition at 26°C) and both fit the equation $(dA/dt)_0 = aC_B^2/(1 + bC_B)$ where C_B is the initial concentration of TNBS, a is dependent on the leucine concentration (see below) and b is a constant. This reaction mixture has a negligible contribution from the reaction of TNBS with hydroxide ions to the absorbance at 420 nm at 26°C, because the leucine is in great excess.

The values of the constants were estimated as $a = 1 \times 10^{10}$ l^2 mol^{-2} min^{-1} and $b = 5 \times 10^4$. With these values, $(dA/dt)_0$ was calculated from the above equation for various C_B values. These values were linearly related to the experimental values (slope 1.0, correlation coefficient 0.998).

The results in Table 3 plotted against leucine concentration gave a linear relationship of the form $(dA/dt)_0 = gC_L + c$, where g and c are constants and C_L is the leucine concentraion. The value of c was dependent on the rate of reaction of TNBS with hydroxide. When this was negligible, $c \to 0$ and $(dA/dt)_0 = gC_L$. From the above equations, $(dA/dt)_0 = KC_LC_B^2/(1 + bC_B)$, where $K = a/C_L$. When $bC_B \gg 1$, this equation reduces to $(dA/dt)_0 = K'C_LC_B$, where $K' = K/b$, in agreement with Goldfarb's work [7] and that of Freedman and Radda [8] who studied the reaction in the presence of excess of TNBS. Finally, from the data in Table 4, the activation energy of the reaction is obtained as 12.8 kcal mol^{-1}.

From the data in Table 3 it can be seen that there is no linear relationship between $(dA/dt)_0$ and pH at constant TNBS concentration, in contrast to the results of Goldfarb or Freedman and Radda, but this can be justified from the extended range of pH values tested here, owing to TNBS decomposition in the presence of hydroxide. Above pH 9.5, this reaction becomes more important and contributes significantly to the absorbance at 420 nm and to $(dA/dt)_0$. The increase of the rate of reaction with pH in the range 7—9.5 is a strong indication that the active group is the unprotonated amino group of leucine [10].

From the above the following mechanism for the reaction between leucine and TNBS can be proposed:

$$L + B \underset{k_1'}{\overset{k_1}{\rightleftharpoons}} R \text{ and } R + B \overset{k_2}{\rightarrow} P$$

where L = leucine and B = TNBS; R is the sulfite complex of TNP—leucine, and P are the products, including TNP—leucine. According to this mechanism, $-dC_L/dt = k_1 C_L C_B - k_1' C_R$; $-dC_B/dt = k_1 C_L C_B - k_1' C_R + k_2 C_R C_B$; $-dC_R/dt = k_2 C_R C_B + k_1' C_R - k_1 C_L C_B$ and $dC_P/dt = k_2 C_R C_B$. Under steady-state conditions, $dC_R/dt = 0$ and $C_R = K_1 C_L C_B/[1 + (k_2/k_1')C_B]$. Hence $(dC_p/dt)_0 = k_2 K_1 C_L C_B^2/[1 + (k_2/k_1')C_B] = K C_L C_B^2/[1 + b C_B]$.

When $(k_2/k_1')C_B \gg 1$, these equations give $C_R = k_1/k_2 C_L$ and $(dC_P/dt)_0 = k_1 C_L C_B$. The last equation shows that, when TNBS is in large excess, the initial reaction rate is proportional to C_L and therefore an analytical method can be worked out for the determination of a primary amine based on the rate of reaction with TNBS.

The intermediate product interferes at wavelengths longer than 390 nm, but not at 350 nm. However, the concentration of the intermediate is negligible at low amine concentrations. Therefore, the absorbance of the intermediate does not seriously affect the absorbance at 420 nm.

This work was intended to elucidate the reaction mechanism, to give a better understanding of the reaction process, and to estimate the extent of the interdependence of variables. For instance, it could be assumed that with a larger excess of TNBS the rates obtained are closer to pseudo-first order, which is advantageous for analytical applications. However, as mentioned above, this gives rise to a parallel reaction which is very sensitive to pH and temperature variations.

Furthermore, attempts to follow the reaction at 420 nm by measuring the absorbance change at times very close to zero (i.e., before the steady-state conditions have been reached) would give a composite rate of formation, mainly of the intermediate, but partly of the final product. At 350 nm, the main contributor to the composite rate is the formation of the final product; the decay of TNBS during the reaction contributes only slightly. Finally, in order to obtain a linear calibration graph of reaction rate vs. leucine concentration, according to the above equation, it is necessary to measure the rate over the first part of the absorbance/time curves.

REFERENCES

1 K. Satake, T. Okuyama, M. Ohashi and T. Shinoda, Biochemistry, 47 (1960) 654.
2 T. Okuyama and K. Satake, Biochemistry, 47 (1960) 454.
3 K. Satake, T. Take, A. Matsuo, K. Tazaki and Y. Hiraga, Biochemistry, 60 (1966) 12.
4 R. Fields, Biochem. J., 124 (1971) 581.
5 L. C. Mokrasch, Anal. Biochem., 18 (1967) 64.
6 S. L. Snyder and P. Z. Sobocinski, Anal. Biochem., 64 (1975) 284.
7 A. Goldfarb, Biochem., 5 (1966) 2570.
8 R. B. Freedman and G. K. Radda, Biochem. J., 108 (1968) 383.
9 E. E. Sarantonis and M. I. Karayannis, Anal. Biochem., 129 (1983), in press.
10 E. E. Sarantonis, E. P. Diamandis, T. P. Hadjiioannou and M. I. Karayannis, Mikrochim. Acta, in press.

Analytica Chimica Acta, 151 (1983) 221—225
Elsevier Science Publishers B.V., Amsterdam — Printed in The Netherlands

Short Communication

HYDROLYSIS OF SOME METHYLPHOSPHONITES AND METHYLPHOSPHINATES

A. VERWEIJ*, W. H. DEKKER, H. C. BECK and H. L. BOTER

Prins Maurits Laboratory, Chemical Research Department, P.O. Box 45, 2280 AA Rijswijk (The Netherlands)

(Received 30th November 1982)

Summary. The hydrolysis of some methylphosphonites and methylphosphinates was studied in the pH range 4.5—7.5 by phosphorus-31 nuclear magnetic resonance spectrometry. For methylphosphonites, a two-step reaction mechanism was observed in which formation of the corresponding methylphosphinates was followed by production of methylphosphinic acid. Implications of the results obtained on the applicability of a verification procedure for nerve gases in surface waters are discussed.

To verify possible production of nerve gases, a method has been developed to detect compounds containing the P—CH_3 linkage in surface waters [1, 2]. As this linkage is very stable, large-scale productions of these chemical warfare agents will inevitably produce waste containing starting materials, final products and decomposition products with a P—CH_3 bond. The method involves an acidic hydrolysis to methylphosphonic acid (I) followed by methylation of the latter and gas-chromatographic detection of the dimethyl methylphosphonate (II) formed. The tervalent phosphorus compound, ethyl *N,N*-diisopropylaminoethyl methylphosphonite (III), which under its code name QL is a well-known binary precursor of the nerve agent VX, may form methylphosphinic acid (IV) on hydrolysis and consequently compound I will not be found. Thus production of QL might eventually not be detected by the verification procedure. Besides, it has been observed here that compound III transesterifies rapidly to diethyl methylphosphonite (V) and bis-(*N,N*-diisopropylaminoethyl)methylphosphonite (VI), probably because of the presence of small amounts of impurities.

It was therefore of interest to study the hydrolysis of compound III and these related methylphosphonites at various pH values in aqueous media. Phosphorus-31 nuclear magnetic resonance spectrometry (^{31}P-n.m.r.) was used to follow the formation of the hydrolysis products quantitatively.

I = $CH_3PO(OH)_2$
II = $CH_3PO(OCH_3)_2$
III = $(C_2H_5O)CH_3POCH_2CH_2N(i\text{-}C_3H_7)_2$
IV = $CH_3P(O)H(OH)$
V = $CH_3P(OC_2H_5)_2$
VI = $CH_3P[OCH_2CH_2N(i\text{-}C_3H_7)_2]_2$
VII = $CH_3P(O)H(OC_2H_5)$
VIII = $CH_3P(O)H[OCH_2CH_2N(i\text{-}C_3H_7)_2]$

0003-2670/83/$03.00 © 1983 Elsevier Science Publishers B.V.

Experimental

Materials. Ethyl hydrogenmethylphosphinate (VII) [3] and compounds IV [4] and V [5] were prepared as described in the literature. Compound III was prepared by heating a mixture of equimolar amounts of VII and *N,N*-diisopropylaminoethanol at 110°C (b.p. 49—50°C/10 Pa). Compound VI was prepared by mixing a 1:2 molar ratio of V and *N,N*-diisopropylaminoethanol in ether with excess of triethylamine. The compound was isolated by molecular distillation at 0.1 Pa. Compound VIII was prepared by heating a mixture of a 1:1 molar ratio of VII and *N,N*-diisopropylaminoethanol at 110°C (b.p. 65°C/5 Pa). Chemical structures and purities were checked by elemental analysis, gas chromatography, n.m.r., infrared spectroscopy and mass spectrometry.

Methods. The hydrolysis was initiated by adding 75 μl of the compound under test to 3 ml of the appropriate buffer solution, in which the compound dissolved slowly. The first measurement was done 90 s after the addition. A 2 M sodium citrate buffer was used for pH 4.5—6.0 and a 3 M imidazole/hydrochloric acid buffer for pH 7.5.

The ^{31}P-n.m.r. spectra were obtained with a Varian XL 100 spectrometer at 40.5 MHz and 24°C with proton decoupling, in 12-mm i.d. tubes. The final product IV was used as the internal chemical shift reference; its δ value is 25.8 ppm relative to 85% phosphoric acid. All δ values given here are relative to phosphoric acid. The reactions were followed by integration of the phosphorus peaks at 25.8, 42.7 and 45.2 ppm for compounds IV, VII and VIII, respectively, as a function of time. The spectra were obtained by using 20 pulses with 1-s acquisition time and a pulse delay of 2 s.

RESULTS AND DISCUSSION

The methylphosphonites III, V and VI reacted very rapidly with water. After dissolution, it was hardly possible to detect these compounds at their characteristic δ values at about 180 ppm. In the case of compound III, three peaks were observed at δ = 25.8, 42.7 and 45.2 ppm; these peaks are characteristic for compounds IV, VII and VIII, respectively, as verified by the use of the corresponding reference compounds. The hydrolysis of the symmetrical compounds V and VI yielded two products: V gave VII and IV, and VI gave VIII and IV. Compounds VII and VIII hydrolysed to compound IV. Figure 1 shows typical sets of consecutive ^{31}P-n.m.r. spectra obtained during the hydrolysis of III and VII.

From the compounds and their fate observed during the hydrolysis, the reaction scheme presented below is proposed. The hydrolysis of V in unbuffered systems has been described by a two-step reaction mechanism identical with that presented here [6]. Because of the extremely high rate of the first hydrolysis step in the pH range studied, it proved to be impossible to determine the rate constants k_1, k_2, k_5 and k_6. Consequently, only k_3 and k_4 could be determined. From the respective phosphorus peak areas, the ratio of the relative amounts of VII and VIII formed initially during the hydrolysis of III

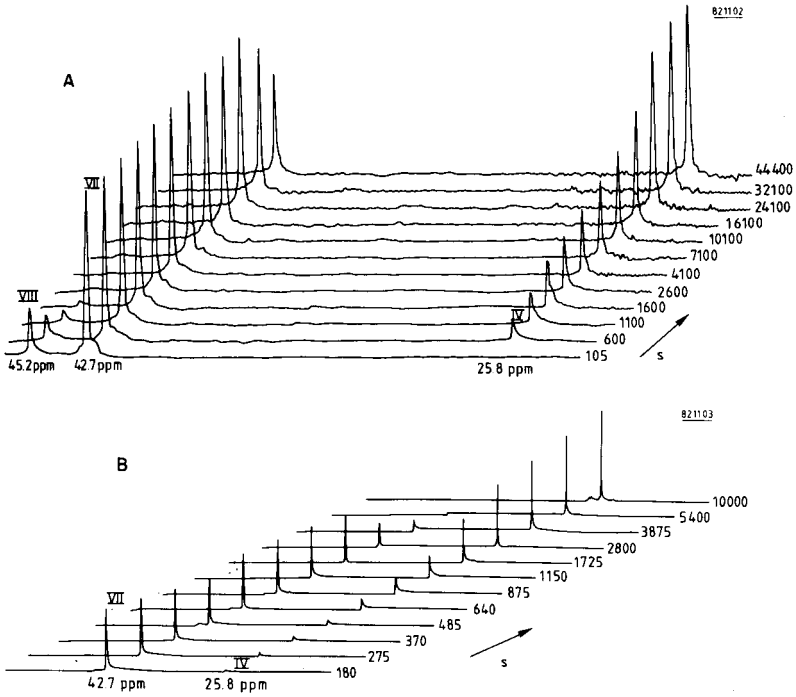

Fig. 1. Proton-decoupled ^{31}P-n.m.r. spectra recorded as a function of time: A, compound III added to sodium citrate buffer at pH 4.5; B, compound VII added to imidazole/hydrochloric acid buffer at pH 7.5. Responses are normalised to the highest peak (ppm values are relative to 85% phosphoric acid).

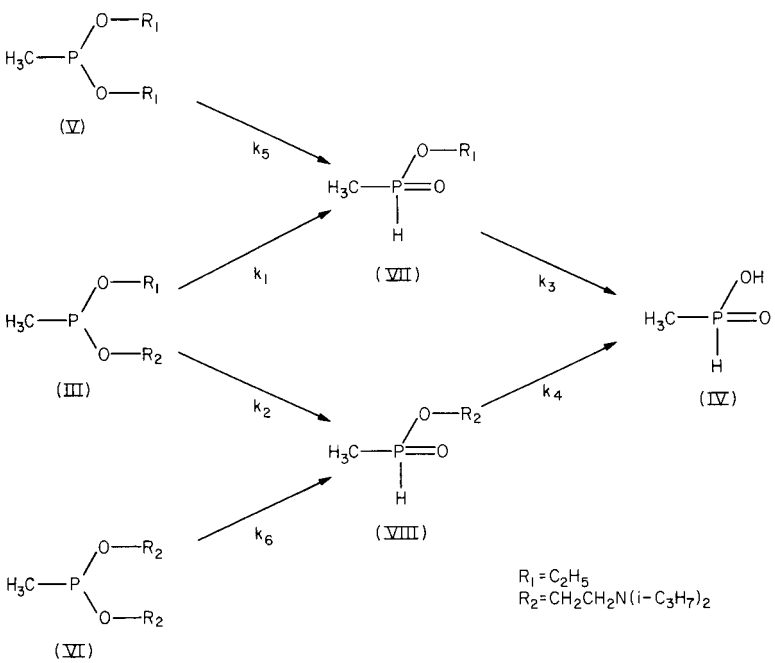

Scheme 1

were calculated to be 3.3, 2.4 and 1.7 at pH 4.5, 5.5 and 6.0, respectively. These values indicate that in the first step the *N*,*N*-diisopropylaminoethyl group is hydrolysed 2—3 times faster than the ethyl group.

In the second step the hydrolysis of VII and VIII can be described as two parallel first-order reactions producing the same product IV or

$$[IV]_t = [VII]_0 \{1 - \exp(-k_3 t)\} + [VIII]_0 \{1 - \exp(-k_4 t)\} \quad (1)$$

in which $[VII]_0$ and $[VIII]_0$ represent the initial concentrations of the compounds VII and VIII, and $[IV]_t$ is the concentration of IV at time t. From the respective phosphorus resonance peak areas, the relative amounts of compounds VII, VIII and IV were derived as a function of time. The rate constants k_3 and k_4 were obtained by fitting Eqn. (1) to a set of (IV, t) data by a least-squares method. The calculated rate constants and the corresponding standard deviations are presented in Table 1.

At pH 7.5 compound VIII hydrolysed completely within 2 min, which made the determination of rate constant k_4 impossible. In acidic medium (pH 4.5—6.0), the rate constants for compounds VII and VIII were roughly pH-independent, but the rates increased considerably in weakly alkaline medium (pH 7.5). This indicates that two reactions are involved in the hydrolysis of these methylphosphinates: (1) reaction with water in acidic medium, and (2) reaction with hydroxide in alkaline medium. A comparison of the rate constants k_3 and k_4 shows that, in the second step of the hydrolysis also, the *N*,*N*-diisopropylaminoethyl group is more susceptible to cleavage than the ethyl group.

From the half-lives of the second rate-determining step of the hydrolysis, it may be concluded that compound III, the binary precursor of the nerve

TABLE 1

Rate constants and corresponding half-lives obtained for the hydrolysis of compounds VII and VIII in the pH range 4.5—7.5

Compound	pH	k (μs)	$t_{1/2}$ (h)	Derived from the hydrolysis of
VII (k_3)	4.5	18.2 ± 0.1		VII
	4.5	17.2 ± 0.5		III
	5.5	10.6 ± 0.8	12	III
	6.0	16 ± 2		III
	6.0	20 ± 2		V
	7.5	620 ± 20		III
	7.5	440 ± 10	0.4	VII
	7.5	502 ± 9		V
VIII (k_4)	4.5	1030 ± 60		VIII
	4.5	930 ± 10		III
	4.5	1280 ± 50	0.2	VI
	5.5	850 ± 60		III
	6.0	1040 ± 90		III

agent VX, as well as compounds V and VI, possibly formed by transesterification of compound III, will hydrolyse to compound IV within a few days when present in water. Consequently, for verification purposes, the probability of finding the original compound III in waste and surface-water samples will be rather small. Nevertheless, compound IV will remain as its phosphorus-containing representative. Under the conditions of the verification procedure, this compound is methylated to methyl methylphosphinate which is detected by gas chromatography. As the signal of the latter can be differentiated from that of compound II, this provides a means of distinguishing wastes originating from classically produced VX and its binary precursor QL.

REFERENCES

1 A. Verweij, H. L. Boter and C. E. A. M. Degenhardt, Science, 204 (1979) 616.
2 A. Verweij, C. E. A. M. Degenhardt and H. L. Boter, Chemosphere, 3 (1979) 115.
3 D. Fiat, M. Halman, L. Kugel and J. Reuben, J. Chem. Soc., (1962) 3837.
4 K. A. Petrov, N. K. Bliznyuk, Yu. N. Studev and A. F. Kolimiets, Zh. Obshch. Khim., 31 (1961) 179.
5 F. W. Hoffmann, T. R. Moore, J. Am. Chem. Soc., 80 (1958) 1150.
6 K. E. Daugherty, W. A. Eychaner and J. I. Stevens, Appl. Spectrosc., 22 (1968) 95.

Analytica Chimica Acta, 151 (1983) 227—229
Elsevier Science Publishers B.V., Amsterdam — Printed in The Netherlands

Short Communication

A COBALT-59 NUCLEAR MAGNETIC RESONANCE REAGENT FOR THE DETERMINATION OF HYDROGEN/DEUTERIUM RATIOS

JOHN G. RUSSELL
Chemistry Department, California State University, Sacramento, CA 95819 (U.S.A.)
ROBERT G. BRYANT*
Chemistry Department, University of Minnesota, Minneapolis, MN 55455 (U.S.A.)
(Received 30th November 1982)

Summary. The very large chemical shift range provided by ^{59}Co-n.m.r. yields different lines for each of the nineteen species in the series of complexes ranging from $Co(NH_3)_6^{3+}$ through $Co(ND_3)_6^{3+}$. At equilibrium, the relative intensities of these lines provide a direct determination of the isotope composition of the solvent with respect to proton—deuterium ratios. Because the problem of extracting the isotope composition from the spectrum of as many as nineteen lines is heavily overdetermined, this technique provides a convenient and accurate means for determining isotopic composition over the whole isotope concentration range.

The chemical shift range for ^{59}Co-n.m.r. is so great that some very subtle effects, which have not been exploited, are reflected in the spectra [1]. For example, at high field (300 MHz for protons) a separate cobalt-59 resonance is resolvable for each species in the series of complex cations including $Co(NH_3)_6^{3+}$ through $Co(ND_3)_6^{3+}$. Because the isotope composition of the complex ion will be proportional to the isotope composition of the solvent in which it is dissolved, observation of the ^{59}Co-n.m.r. spectrum provides a direct measure of the isotope composition of the solvent, provided that the isotope exchange between the solvent and the complex cation is at equilibrium, and that the equilibrium isotope effect is taken into account. This communication describes a preliminary study indicating that the ^{59}Co-n.m.r. spectrum provides a rapid and sensitive means of quantifying the hydrogen/deuterium isotope composition in a protic solvent like water. It may be a very useful technique because the method should work equally well in mixed solvents and heterogeneous environments.

Experimental

The hexaamminocobalt(III) chloride was prepared by standard procedures [2]. Deionized water was used as delivered from a Continental deionizer system, and deuterium oxide (99.8%; Aldrich Chemical Company) was used as received.

The n.m.r. spectra were taken on a Nicolet NT-300 multinuclear n.m.r. spectrometer with an Oxford wide-bore magnet and the Nicolet multinuclear

0003-2670/83/$03.00 © 1983 Elsevier Science Publishers B.V.

midrange probe. Samples (4 ml) were contained in 12-mm sample tubes sealed with plastic caps and parafilm. The isotopic composition of the samples was determined by weight as the isotopic composition of both extremes was known. Care was required at the extremes of the isotope composition scales to make sure that the contamination of the sample by water adsorbed on the glass was either eliminated by exchange with the appropriate solvent or made insignificant by using large volumes.

Results and discussion

Representative spectra for the hexaamminocobalt(III) chloride dissolved in water that has three different deuterium/hydrogen ratios are shown in Fig. 1. If the samples have come to equilibrium with respect to D/H exchange, it is not possible to resolve all nineteen peaks in a single spectrum; however, the three spectra for the compositions chosen for Fig. 1 provide all nineteen peaks when taken together. The intensities of the different peaks for any given sample are related to the solvent isotope composition by the binomial distribution. The absolute intensities are, of course, related to the choice of complex ion concentration and other variables. However, the relative fractional intensity of a particular isotopomer line, I_y, is related directly to the solvent isotope composition by the equation

$$I_y = [n!/y!(n-y)!]\, p_H^y (1-p_H)^{(n-y)} \qquad (1)$$

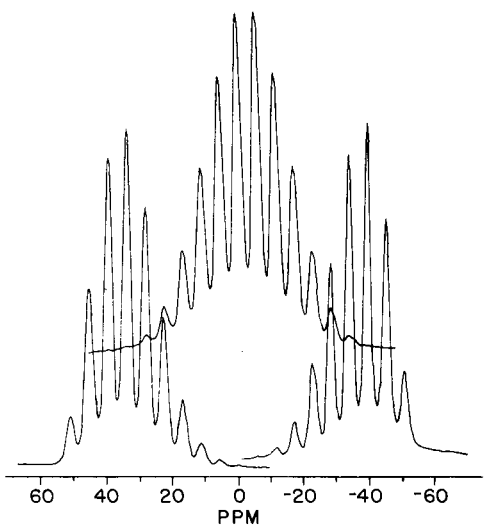

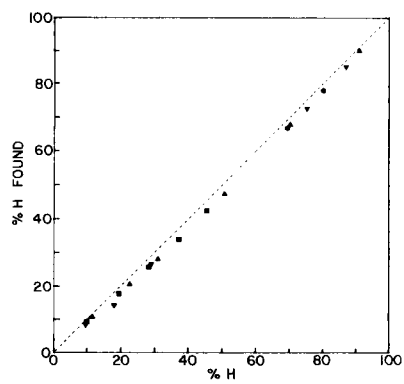

Fig. 1. The ^{59}Co-n.m.r. spectrum of $Co(NH_3)_6^{3+}$ ion accumulated at 15%, 50%, and 85% D_2O at 70.85 MHz and 298 K. The left spectrum is for the 15% D_2O sample so that the left-most resonance arises from the H_{18} complex. The middle spectrum is offset vertically for clarity.

Fig. 2. The proton fraction determined by evaluation of the ^{59}Co-n.m.r. spectrum plotted as a function of the solvent composition determined for four sample sets. The deviations from the dotted line are reproducible and include the sum of the several isotope effects that enter the problem analysis.

where n is the maximum number of protons (18 for the hexaammine complex), y is the number of protons in the particular complex, and p_H is the probability of finding a proton in the solvent, i.e., the concentration of exchangeable protons divided by the sum of the concentrations of the exchangeable protons and deuterons.

Clearly, if p_H is known, the relative intensities of the different lines can be calculated. The analytical utility is provided by extracting p_H from the measured equilibrium intensities of the ^{59}Co-n.m.r. spectrum which is best done by an iterative fit of the whole spectrum to Eqn. (1). The consequence of the equilibrium isotope effects is to shift the derived p_H slightly; however, this difficulty may be overcome by making the required calibration graph as shown in Fig. 2, which was obtained from a variety of measurements on different H_2O/D_2O mixtures. There is of course no reason why a considerable number of different compounds with large isotope shifts and exchangeable protons could not be used in the same way. The advantage of the cobalt ammines is that the large number of species provides a significant overdetermination of the problem that maintains the precision of the determination across the whole concentration range. Though the present application is in a sense trivial, extensions to mixed solvent systems and more difficult problems are easily envisioned as one has the option of controlling solubilities and charge by changing the nature of the cobalt ligand and counter ion.

This work was supported in part by the National Institutes of Health (GM-29428 and GM-25757) and by the University of Minnesota. Helpful discussions with Professor Maurice Kreevoy are gratefully acknowledged.

REFERENCES

1 R. Garth, R. J. Goodfellow, in R. K. Harris and D. E. Mann (Eds.), NMR and the Periodic Table, Academic Press, New York, 1978, pp. 225—244.
2 J. B. Work, Inorg. Synth., 2 (1946) 221.

Analytica Chimica Acta, 151 (1983) 231—235
Elsevier Science Publishers B.V., Amsterdam — Printed in The Netherlands

Short Communication

EXTRACTION EFFICIENCIES FOR ORGANIC COMPOUNDS FOUND IN AQUATIC SEDIMENTS

SIGVE SPORSTØL*, NINA GJØS and GEORG E. CARLBERG
Central Institute for Industrial Research, P.O. Box 350, Blindern, Oslo 3 (Norway)
(Received 2nd December 1982)

Summary. The extraction efficiencies for a wide range of organic compounds found in sediments were examined by comparing Soxhlet extraction with dichloromethane and ultrasonic extraction with either dichloromethane or dichloromethane containing 5% methanol. Generally Soxhlet extraction gave the highest recoveries, especially for nonpolar compounds; for compounds of medium polarity the differences were less pronounced, and for the most polar compounds the ultrasonic extraction with dichloromethane containing 5% methanol gave a somewhat better recovery than did the Soxhlet extraction. The ultrasonic extraction was most efficient when the dichloromethane contained 5% methanol.

Organic compounds often constitute a significant fraction of aquatic sediments [1]. Their concentrations are usually measured after extraction with an organic solvent. A fundamental problem in this kind of analysis is the efficiency of the recovery of the organic fraction, which will depend on extraction method [2], organic solvent [3], type of compounds to be measured [4] and type of particles in the samples [5].

Soxhlet extraction is the leading extraction method for sedimentary material [6—8]. Ultrasonic extraction is relatively new, and has been used only to a limited extent for sediments. Excellent results have, however, been reported on extraction of atmospheric particulate material, and for special groups of compounds this method is more efficient than Soxhlet extraction [9—11]. The choice of solvent for extraction will depend on the compounds to be determined. Often two or three solvents are used in sequence, but more attention has been given recently to developing fast screening methods with a one-step extraction which effectively extracts the most important classes of organic compounds. Dichloromethane is commonly used in one-step extractions. It is well suited for both nonpolar and polar compounds [3, 9] and is the recommended solvent in analyses for the EPA's "priority pollutants" [12, 13].

This communication deals with the recovery of a wide range of organic compounds from sediments. Soxhlet extraction with dichloromethane is compared with ultrasonic extraction either with dichloromethane or with dichloromethane containing 5% methanol. The samples were not spiked,

0003-2670/83/$03.00 © 1983 Elsevier Science Publishers B.V.

which may lead to an inhomogeneous distribution of compounds [4]; instead, "real world" sediments containing different groups of organic compounds served as the basis of the study.

Experimental

Samples. The marine sediment sample was collected, by use of an Eckman grab, 300 m from the effluent discharge point of a kraft pulp and paper plant. The samples were transferred to clean glass vessels and stored in frozen condition until required.

Extraction. A portion (20.0 g) of wet sediment (28.9% dry weight) was used for each extraction, and 15.9 μg of deuterated biphenyl (Stohler Isotope Chemicals) dissolved in dichloromethane was added as internal standard, prior to extraction.

For ultrasonic extraction with dichloromethane, an ultrasonic cell disruptor (Sonicator Model W-10) was used with the power source in the seventh position and a standard 4.5-in. removable titanium probe. The sediments were extracted twice with distilled dichloromethane (60 ml + 40 ml) for periods of 15 min followed by centrifugation (2300 rpm) for 15 min (Sorwall GLC-2). The dichloromethane extracts were combined, and 3 g of activated copper was added to remove sulfur. After being left overnight, the solution was dried with sodium sulfate. Ultrasonic extraction with dichloromethane containing 5% methanol was done in exactly the same way, except for addition of 5% methanol.

For Soxhlet extraction, the sediments were freeze-dried for 48 h followed by extraction with 80 ml of distilled dichloromethane in a Soxhlet apparatus for 20 h. The extraction tubes were supplied with 3 g of activated copper. The extract was dried with sodium sulfate.

All sample extracts were concentrated under a slow stream of nitrogen to a volume of 1 ml prior to gas chromatography/mass spectrometry (g.c./m.s.).

Gas chromatography/mass spectrometry. A Finnigan 9610 gas chromatograph was interfaced with a Finnigan 4021 quadrupole mass spectrometer and an Incos 2100 data system. Spectra were recorded each second at 70 eV in the electron impact mode. The gas chromatograph contained a 30 m × 0.256 mm fused silica capillary column coated with DB-5 (0.25 μm; J & W Scientific Inc.). The column was introduced via the interface oven directly into the ion chamber. Samples (2 μl) were injected splitless into a Grob-type injector with helium (40 cm^3 s^{-1} at 60°C) as carrier gas. The injector was held at 280°C, the interface oven at 240°C and the ion chamber at 250°C. The chromatograph oven was initially held at 30°C for 3 min and then programmed from 70°C to 325°C by 4°C min^{-1}, the latter temperature being held for 30 min.

Relative recoveries of the compounds were evaluated by comparing peak areas of selected ions of the compounds to peak areas of a selected ion of the internal standard (deuterated biphenyl) (Table 1). Total concentrations were calculated from one of the samples (Soxhlet/dichloromethane) by com-

TABLE 1

Comparison of recoveries by the Soxhlet and ultrasonic extractions

No.	Compound	Relative recovery[a]			$\mu g\ kg^{-1}$[b] (dry weight)	m/z[c]
		Ultrasonic/ CH_2Cl_2	Ultrasonic/ CH_2Cl_2/ 5% MeOH	Soxhlet/ CH_2Cl_2		
1	Tetradecane	0.03	0.04	1.00	1700	43
2	Pentadecane	0.05	0.06	1.00	1300	71
3	Xylene (*m*,*p*)	0.02	1.00	0.28	500	106
4	*p*-Cymene	0.12	0.56	1.00	1400	134
5	Naphthalene	0.02	0.07	1.00	160	128
6	Calamenene	0.15	0.40	1.00	80	159
7	Monoterpene	0.13	0.69	1.00	500	93
8	Sesquiterpene	0.18	0.01	1.00	300	105
9	Diterpene	0.33	0.29	1.00	2200	257
10	Tetracosanol	0.13	0.27	1.00	44000	57
11	β-Sitosterol	0.10	0.15	1.00	53000	414
12	Methylphenol	0.49	0.45	1.00	70	107
13	Nonanal	0.01	0.06	1.00	6500	57
14	Benzaldehyde	0.44	1.00	0.81	160	106
15	Dioctylphthalate	0.43	0.21	1.00	800	149
16	Tetradecanoic acid	0.47	1.00	0.28	2100	60
17	Hexadecanoic acid	0.53	1.00	0.57	2700	60

[a]Highest recovery of each compound is set to 1.00. [b]Results based on Soxhlet/CH_2Cl_2 extraction. [c]Masses used for calculation of relative recovery.

paring peak areas of peaks on the total ion chromatogram to that of the internal standard.

Results and discussion

Table 1 gives a comparison of extraction efficiencies of the three extraction methods for a selection of compounds identified in the actual sediment sample. The recovery is expressed as an index where the highest recovery of each compound is set to 1.00. Soxhlet extraction of freeze-dried sediments with dichloromethane (Soxhlet/CH_2Cl_2) gave the best recovery for most compounds. This tendency seemed to be independent of concentration, which ranged from 70 to 53 000 $\mu g\ kg^{-1}$ of dry sediment. These results are in agreement with findings reported by Kooke et al. [11], who showed that Soxhlet extraction gave the best recovery of polychlorinated dibenzo-*p*-dioxins and dibenzofurans in fly ash. They also concluded that ultrasonic extraction is less efficient for the recovery of these chlorinated compounds. Chatot et al. [9] and Golden and Sawicki [10], however, reported that polynuclear aromatic hydrocarbons were extracted more efficiently from atmospheric particulate material by ultrasonic extraction than by Soxhlet extraction.

Table 1 shows that there was a distinct difference between Soxhlet/CH_2Cl_2 and the ultrasonic methods for the hydrocarbons (compounds 1—9). The recovery of alkanes by the ultrasonic extractions was as low as 3—6% compared to Soxhlet extraction. The only exception among the hydrocarbons was *m*- and *p*-xylene, for which Soxhlet/CH_2Cl_2 extraction gave a recovery of only 28% compared to that of ultrasonic/CH_2Cl_2/5% methanol extraction. The xylenes are the most volatile of the compounds investigated, and the low recovery might therefore be due to losses during the freeze-drying process. Recovery of the alcohols (compounds 10 and 11) and the aliphatic aldehyde (compound 13) was also significantly higher by Soxhlet/CH_2Cl_2 extraction than by ultrasonic extractions. This tendency was also observed to a lesser extent for methylphenol (compound 12) and dioctylphthalate (compound 15). Interestingly, benzaldehyde (compound 14) was extracted rather more efficiently by ultrasonic/CH_2Cl_2/5% methanol extraction than by Soxhlet/CH_2Cl_2 extraction. This tendency was even more pronounced for the carboxylic acids (compounds 16 and 17) for which the ultrasonic/CH_2Cl_2/5% methanol extraction was much more effective than the other extractions.

One aspect of this investigation was to examine the effect of adding small amounts of methanol to dichloromethane during the ultrasonic extraction. Generally, dichloromethane with 5% of methanol added gave better recovery than did the pure solvent. This supports earlier findings that extraction with binary mixtures of nonpolar and polar solvents gives better recoveries than extraction with the individual solvents [3]. The only important exception was the sesquiterpene (compound 8) for which the recovery by the ultrasonic/CH_2Cl_2/5% methanol technique was much lower than would have been expected from the other terpenes (compounds 7 and 9).

The present results suggest that organic compounds found in sediments are generally extracted more effectively by the Soxhlet/CH_2Cl_2 technique than by either of the ultrasonic methods. The Soxhlet method is relatively the most efficient for nonpolar compounds. For compounds of medium polarity, the differences are less significant, and for polar compounds the ultrasonic/CH_2Cl_2/5% methanol technique is the most effective. With ultrasonic extraction, most of the compounds were extracted more efficiently with dichloromethane containing 5% methanol than with pure dichloromethane.

REFERENCES

1 J. W. Farrington, N. M. Frew, P. M. Gschwend and B. W. Tripp, Estuarine Coastal Mar. Sci., 5 (1977) 793.
2 L. R. Hilpert, W. E. May, S. A. Wise, S. N. Chesler and H. S. Hertz, Anal. Chem., 50 (1978) 453.
3 D. Grosjean, Anal. Chem., 47 (1975) 797.
4 W. H. Griest, Jr., L. R. B. Yeatts and J. E. Caton, Anal. Chem., 52 (1980) 201.
5 J. Jäger, Cesk. Hyg., 14 (1969) 135.
6 R. E. La Flamme and R. A. Hites, Geochim. Cosmochim. Acta, 42 (1978) 289.
7 T. D. Sletter, J. N. Butler and J. E. Barbash, in L. Petrakis and F. T. Weiss (Eds.),

Petroleum in the Marine Environment, American Chemical Society, Washington, DC, 1980, p. 267.
8 W. Gieger and C. Schaffner, Anal. Chem., 50 (1978) 243.
9 G. Chatot, M. Castegnaro, J. L. Roche and R. Fontages, Anal. Chim. Acta, 53 (1971) 256.
10 C. Golden and E. Sawicki, Anal. Lett., 11 (1978) 1051; Int. J. Environ. Anal. Chem., 4 (1975) 9.
11 R. M. M. Kooke, W. A. Lustenhouwer, K. Olie and O. Hutzinger, Anal. Chem., 53 (1981) 461.
12 L. H. Keith and W. A. Telliard, Environ. Sci. Technol., 13 (1979) 416.
13 B. S. Middelditch, S. R. Missler and H. B. Hines, in Mass Spectrometry of Priority Pollutants, Plenum Press, New York, 1981, p. 1.

Analytica Chimica Acta, 151 (1983) 237—243
Elsevier Science Publishers B.V., Amsterdam — Printed in The Netherlands

Short Communication

DETERMINATION OF POLYNUCLEAR AROMATIC HYDROCARBONS IN REFINERY EFFLUENT BY HIGH-PERFORMANCE LIQUID CHROMATOGRAPHY

ROBERT K. SYMONS* and IAN CRICK

Environment Protection Authority of Victoria, 240 Victoria Parade, East Melbourne, Victoria 3002 (Australia)

(Received 7th September 1982)

Summary. A study of the concentration of polynuclear aromatic hydrocarbons from laboratory water and refinery effluents by means of Sep-Pak C-18 cartridges is presented. Reversed-phase liquid chromatography with coupled ultraviolet and fluorescence detectors is applied to separate and quantify these hydrocarbons. The method is used to determine several polynuclear aromatic hydrocarbons in refinery effluents at the 0.1—50 $\mu g\ l^{-1}$ level.

Polynuclear aromatic hydrocarbons (PAH) are widely distributed throughout the environment, by natural causes (e.g., forest fires, volcanic activity, formation of petroleum) and through burning of fossil fuels, metallurgical furnaces, petroleum refining, etc. Their multi-fused ring structures may be alkylated or unsubstituted, largely depending on their temperature of formation [1, 2]. Petroleum, formed geologically at relatively low temperatures, contains a large fraction of alkylated PAH's, whereas those derived from forest fires contain a lesser amount. At the high temperatures of the internal combustion engine, the unsubstituted PAH's are formed almost entirely. The strong carcinogenic activity of several PAH isomers [3] has directed considerable attention towards their detection in a variety of matrices. High-performance liquid chromatography (h.p.l.c.) offers several advantages [4] over gas chromatography because of its ability to separate isomeric PAH's and its economy.

Extraction and preconcentration of PAH's from water systems has been widely investigated with solid adsorbents [5—8], liquid—liquid systems [9—11] and coupled-column chromatography [12—14]. As a more convenient alternative, a rapid extraction technique has been evaluated in this laboratory. The procedure involves enrichment of PAH's onto disposable Sep-Pak C-18 cartridges followed by direct injection into a reversed-phase l.c. system. The efficiency and recoveries of the method are discussed.

Petroleum refinery effluent was chosen as a real sample because of the vast amounts of water used and the likelihood of its intimate contact with PAH-containing materials within the refinery [15, 16] leading to the eventual discharge of PAH's into the sea.

0003-2670/83/$03.00 © 1983 Elsevier Science Publishers B.V.

EXPERIMENTAL

Reagents. Acetonitrile and methanol were of ChromAr grade (Mallinkrodt) specially prepared for h.p.l.c. A Milli-Q (Millipore) deionizer fitted with an Organex cartridge was used to prepare water from organic contaminants.

Standards. The PAH standards were anthracene, naphthalene, fluorene, phenanthrene, fluoranthene, pyrene, benz(a)pyrene, perylene, dibenz(a,h)-anthracene, 1-methylnaphthalene, 2-methylnaphthalene and 2,3-dimethyl-naphthalene (all from Fluka). Benz(a)anthracene was obtained from the CSIRO laboratories (Melbourne). All standards were greater than 97% purity and were used as received.

Standard PAH solutions (1 $\mu g\ \mu l^{-1}$) were prepared by dissolving 100 mg of the PAH in 100 ml of acetonitrile. In some cases, complete dissolution required ultrasonic treatment. Stock solutions and subsequent working standards were stored at room temperature in the dark [4].

Glassware. Volumetric flasks, glass syringes and sample vials were soaked in a synthetic detergent, rinsed with deionized water, dried and finally rinsed with methanol. Sample blanks confirmed that this procedure was free of PAH's and other contaminants.

Instrumentation. The modular chromatograph and chromatographic conditions used are given in Table 1.

Sample preparation and procedure. Samples were collected in 2-l brown winchesters with polytetrafluoroethylene (PTFE)—lined caps, and 20% (v/v) methanol was added. On receipt in the laboratory, the samples were extracted immediately with the Sep-Pak C-18 cartridges (Waters Associates). The Sep-Pak cartridges were previously washed with 2 ml of methanol and then 5 ml of water, and placed in the apparatus shown in Fig. 1. This arrangement allowed multiple samples, blanks and recoveries to be run simultaneously, therefore greatly reducing the time requirement. After each

TABLE 1

Chromatographic conditions for PAH detection

Pump	Constametric III, Laboratory Data Control (LDC; Riviera Beach, FL) pump
Injection device	Water Associates, autosampler WISP 710B
Column	Waters Radial Compression Module (RCM-100) housing a 10 cm × 0.8 cm, 5 μm, Rad-Pak C-18 operated at ambient temperature. N = 97,500 plates/m; k' = 6.3 (fluoranthene)
Mobile phase	75% acetonitrile/water at 2.0 ml min^{-1}.
Detectors	LDC Spectromonitor III, variable u.v. wavelength (190—400 nm)
	LDC Fluorimonitor III (λ_{ex} = 360 nm, λ_{em} = 418—700 nm)
Data collection	Hewlett-Packard HP-3388A reporting integrator with dual printer—plotters

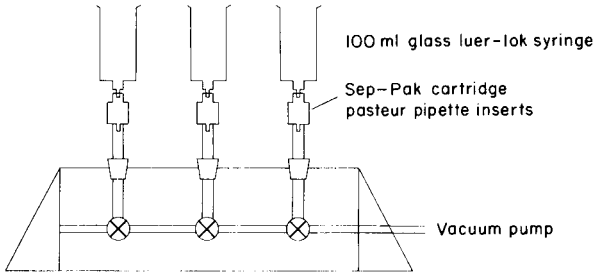

Fig. 1. Multiple sample extraction apparatus.

sample had been extracted, the compounds sorbed were eluted from the Sep-Pak with 2 ml of methanol and transferred directly into glass autosampler vials with PTFE-lined silicone self-sealing septa.

Results and discussion

Recoveries. Because of the limited solubility [17] of PAH's in water, representative spiking prior to the enrichment step proved difficult. Recovery experiments were done by adding 500 μl of a PAH mixture in acetonitrile to 500 ml of water, shaking and then passing through a Sep-Pak cartridge. Table 2 (column A) shows that the recoveries for 2- and 3-ring PAH's were acceptable, but that recoveries became increasingly worse as the number of rings increased. The relationship between the number of fused rings, de-

TABLE 2

Comparison of recoveries by liquid–liquid and Sep-Pak C-18 extraction techniques

Compound	Recovery (%)			
	Sep-Pak		Liquid–liquid	Spiking level ($\mu g\,l^{-1}$)
	A	B		
Naphthalene	92 ± 7	95 ± 6	78 ± 16	4.0
1-Methylnaphthalene	95 ± 6	96 ± 7	82 ± 12	4.0
2-Methylnaphthalene	95 ± 6	94 ± 6	84 ± 12	4.0
Fluorene	95 ± 4	96 ± 8	91 ± 6	2.0
Phenanthrene	87 ± 4	94 ± 10	90 ± 7	1.6
2,3-Dimethylnaphthalene	90 ± 5	94 ± 10	88 ± 10	4.0
Anthracene	93 ± 4	92 ± 7	92 ± 3	0.4
Fluoranthene	92 ± 7	90 ± 4	91 ± 4	2.0
Pyrene	88 ± 4	94 ± 6	94 ± 6	2.0
Benz(a)anthracene	58 ± 9	90 ± 2	94 ± 6	1.8
Perylene	58 ± 6	89 ± 9	88 ± 8	0.1
Benz(a)pyrene	53 ± 10	89 ± 9	87 ± 5	1.2
Dibenz(a,h)anthracene	45 ± 10	85 ± 10	83 ± 4	12

[a]A, spikes added to laboratory water. [b]B, spikes added to water and 20% (v/v) methanol added.

creasing solubility and adsorption [18] onto container surfaces, was considered to be the main cause of the bad recoveries for the larger PAH's. The addition of 20% (v/v) methanol [13] to the sample prior to spiking greatly improved the recoveries (Table 2, column B), which then compared well with recoveries obtained by liquid—liquid extraction [11]. Addition of 20% (v/v) methanol was therefore used for all samples prior to the sorption step.

Chromatographic separation. The isocratic separation of standard PAH's and alkylated naphthalenes, with the u.v. and fluorescence detectors, is presented in Fig. 2. Peak identification of individual RAH's, and their capacity factors are presented in Table 3. The two detectors were connected in series (u.v. first) by stainless-steel tubing (0.2 mm bore) and their signal outputs were connected via the 3388A to dual printer—plotters operated in the SYNC mode. The WISP was used to start the printer—plotters on injection.

Selective monitoring of more than one u.v. wavelength [4] allows the optimum detectability for individual PAH's to be evaluated (Table 3). Because each PAH has its own peculiar absorption characteristics, identification of PAH's is aided by comparing their relative absorbance ratios, at different wavelengths. The combination of selective wavelength monitoring with the selective and more sensitive fluorescence detector, offers a system suitable for identifying and quantifying PAH's in complex mixtures.

Application to real samples. The method was applied to samples from a treated refinery effluent before its discharge into Corio Bay (Victoria,

TABLE 3

Capacity factors, k^1, and detection limits for PAH's by u.v. and fluorescence detectors

Compound number	Compound	Detection limit (ng)[a]			k^1 [c]
		254 nm	280 nm	Fluor.[b]	
1	Naphthalene	6	4	—	2.56
2	1-Methylnaphthalene	10	2	—	3.48
3	2-Methylnaphthalene	8	4	—	3.61
4	Fluorene	1	2	—	3.97
5	Phenanthrene	0.8	3	—	4.64
6	2,3-Dimethyl-naphthalene	12	8	—	4.83
7	Anthracene	0.4	—	0.2	5.10
8	Fluoranthene	3	2	0.1	6.32
9	Pyrene	2	4	—	7.17
10	Benz(a)anthracene	1.5	0.9	0.9	9.63
11	Perylene	0.05	—	0.005	14.04
12	Benz(a)pyrene	1	1	0.05	15.93
13	Dibenz(a,h)-anthracene	25	5	5	19.55

[a]Signal-to-noise ratio = 2. A dash indicates that no significant signal was observed. [b]Fluorescence with excitation at 360 nm and measurement at 418—700 nm. [c]Capacity factors were calculated in the usual way.

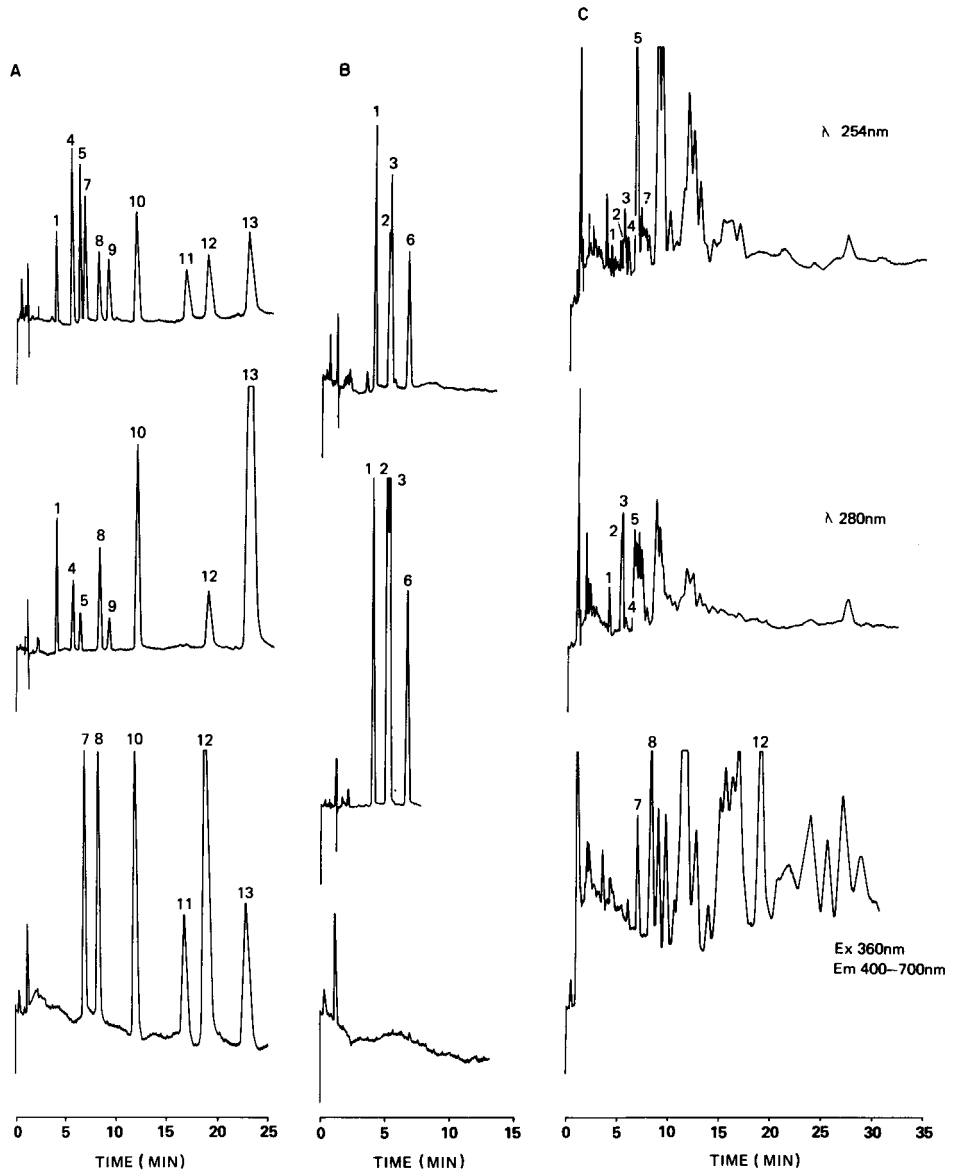

Fig. 2. Chromatograms for standard mixtures and for refinery effluent using various detection modes. Conditions are given in Table 1. Peak numbers correspond to the compounds in Table 3. The top chromatograms were obtained with u.v. detection at 254 nm, the middle chromatograms at 280 nm, and the bottom chromatograms with the fluorescence detector. (A) PAH standards; (B) alkylated naphthalenes; (C) refinery effluent after sorption (250-fold enrichment).

TABLE 4

Content of PAH's in refinery effluent sample

Compound	Found ($\mu g\ l^{-1}$)	Compound	Found ($\mu g\ l^{-1}$)
Naphthalene	15	Phenanthrene	7.1
1-Methylnaphthalene	30	Anthracene	0.26
2-Methylnaphthalene	45	Benz(a)pyrene	0.11
Fluorene	1.2	Fluoranthene	0.26

Australia). Nominally 600 ml of sample containing 100 ml of methanol was passed through a prepared Sep-Pak cartridge and the PAH's sorbed were eluted with 2 ml of methanol, affording a 250-fold concentration. Because of the saline nature of the effluent, the cartridge was washed with 2 ml of water prior to elution with methanol. Injection of the extract (10 μl) gave the chromatograms shown in Fig. 2C. The identities of the major unmarked peaks were qualitatively confirmed by g.c./m.s. as being alkylated naphthalenes and phenanthrenes, which is to be expected given the relatively low temperature of formation for crude oil.

The PAH's found were identified by comparison of their retention times and absorbance ratios with the respective standards. The reproducibilities achieved during a day's run for retention times and peak heights were 0.4% and 1.5% (relative standard deviation), respectively. Chromatography of standards along with samples was used to confirm peak identity. The concentrations of individual PAH's were calculated at each u.v. wavelength; the averages are reported in Table 4. If the agreement was poor because of peak overlap or by interference from co-eluting compounds, appropriate changes to the chromatographic conditions (e.g., mobile phase, flow rate, volume injected) were made to achieve better peak separation.

Conclusion

The Sep-Pak C-18 cartridges provide a rapid, simple means of concentrating PAH's from waters. The addition of 20% (v/v) methanol helps to minimise any adsorption of PAH onto container surfaces during sampling, storage and extraction. By avoiding the concentration of large amounts of solvent associated with liquid—liquid extractions, losses of naphthalene and its derivatives [19] are greatly reduced. The use of the reversed-phase column with coupled u.v. and fluorescence detectors provides an analytical scheme capable of reliably identifying PAH's in waters after extraction.

We thank Malcolm J. McCormick and Harry Blutstein for their critical appraisal of this manuscript.

REFERENCES

1 M. Blumer and W. W. Youngblood, Science, 188 (1975) 53.
2 R. A. Lawson, CRC Critical Reviews in Environmental Control, (Dec. 1978) pp. 197—246.
3 See, e.g., R. Freudenthal and P. W. Jones (Eds.), Polynuclear Aromatic Hydrocarbons: Chemistry, Metabolism and Carcinogenesis, Raven Press, New York, 1976.
4 R. K. Sorrell and R. Reding, J. Chromatogr., 185 (1979) 655.
5 D. K. Basu and J. Saxena, Environ. Sci. Technol., 12 (1978) 791.
6 G. A. Junk, J. J. Richard, M. D. Grieser, D. Witiak, J. L. Witiak, M. D. Argnello, R. Vick, H. J. Sver, J. S. Fritz and G. V. Calder, J. Chromatogr., 99 (1974) 745.
7 V. Leoni, G. Puccetti and A. Grella, J. Chromatogr., 106 (1975) 119.
8 P. Van Rossum and R. G. Webb, J. Chromatogr., 150 (1978) 381.
9 M. A. Acheson, R. M. Harrison, R. Perry and R. A. Wellings, Water Res., 10 (1976) 207.
10 G. A. Jungclaus, L. M. Games and R. A. Hites, Anal. Chem., 48 (1976) 1894.
11 U. S. EPA Method 610, Federal Register, 44, 233, Dec. 1979, 69514-69517.
12 A. R. Oyler, D. L. Bodenner, K. J. Welch, R. J. Liukken, R. M. Carlson, H. L. Kopperman and R. Cape, Anal. Chem., 50 (1978) 837.
13 F. Eisenbeiss, H. Hein, R. Jeoster and G. Naundorf, Chromatogr. Newsl., 6 (1978) 8.
14 W. E. May, S. N. Chester, S. P. Cram, B. H. Gump, H. S. Hertz, D. P. Enagonio and S. M. Dyszel, J. Chromatogr. Sci., 13 (1975) 535.
15 E. Katz and K. Ogan, Chromatogr. Newsl., 8 (1980) 18.
16 H. G. Preston and A. Macaluso, in C. E. Van Hall (Ed.), Measurement of Organic Pollutants in Water and Wastewater, ASTM STP686, American Society for Testing and Materials, Philadelphia, PA, 1979, p. 152.
17 R. C. Clark and W. D. MacLeod, Jr., in D. C. Mailins (Ed.), Effects of Petroleum on Arctic and Subarctic Marine Environments and Organisms, Academic Press, New York, 1977, p. 91.
18 W. E. May, J. M. Brown, S. N. Chesler, F. Guenther, L. R. Hilpert, H. S. Hertz and S. A. Weis, in H. S. Hertz and S. N. Chester (Eds.), N. B. S. Spec. Publ. 519, Trace Organic Analysis: A New Frontier in Analytical Chemistry, U.S. Dept. of Commerce, Washington, DC, 1979, p. 219.
19 C. E. Higgins and M. R. Guerin, Anal. Chem., 52 (1980) 1984.

Analytica Chimica Acta, 151 (1983) 245–249
Elsevier Science Publishers B.V., Amsterdam — Printed in The Netherlands

Short Communication

SPECTROPHOTOMETRIC OR SPECTROFLUORIMETRIC DETERMINATION OF COBALT IN STEELS BY EXTRACTION AS BIS[1-(2-PYRIDYLMETHYLENE)-2-(2-PYRIDYL)HYDRAZINE]-COBALT(III) DIMETHOXYANTHRACENESULPHONATE

D. THORBURN BURNS*, P. HANPRASOPWATTANA and S. KHEAWPINTONG

Department of Analytical Chemistry, The Queen's University of Belfast, Belfast BT9 5AG, Northern Ireland (U.K.)

(Received 21st December 1982)

Summary. The ion-pair complex formed at pH 3 is extracted into 1:9 acetone/1,2-dichloroethane. The effects of pH, diverse ions and masking are reported. The system is applied to the determination of 0.005—0.4% cobalt in various steels without prior separation of iron.

The large number of reagents and procedures for the spectrophotometric determination of cobalt is in complete contrast with the few direct or indirect fluorimetric methods available for this metal [1, 2]. Fluorimetric methods for cobalt(II) are necessarily based on quenching, owing to the paramagnetic effects of cobalt(II) [2, 3]. Cobalt(III) forms diamagnetic complexes which may be fluorescent [4] or if ionic, extractable with a fluorescent counter ion [5, 6]. The ligand 1-(2-pyridylmethylene)-2-(2-pyridyl)hydrazine [7] (pyridine-2-aldehyde-pyridylhydrazone; PAPHY) forms a non-fluorescent cationic chelate with cobalt(III) which may be extracted with eosin as the fluorescent counter ion [6]. The present work shows that lower detection limits can be achieved by using dimethoxyanthracenesulphonate as the fluorescent counter ion [8]. In addition, it is possible to clarify the chemistry of the chelation reactions involved.

Experimental

Apparatus. Absorption spectra were recorded with a Pye-Unicam SP8000 recording spectrophotometer and fluorescence excitation and emission spectra with a Baird Atomic SFR100 spectrofluorimeter. Routine absorbance measurements were made at 496 nm with a Pye-Unicam SP6-550 digital spectrophotometer and fluorescence measurements with a Perkin-Elmer 1000 fluorimeter (λ_{ex} = 396 nm, λ_{em} = 450 nm) and quartz 1-cm cells.

Reagent solution. The reagent (2-pyridinecarboxaldehyde 2-pyridylhydrazone; Aldrich) was used as supplied. A 0.1% (w/v) solution was prepared by dissolving 0.100 g of PAPHY in 5 drops of (1 + 1)hydrochloric acid and diluting to 100 ml with distilled water.

0003-2670/83/$03.00 © 1983 Elsevier Science Publishers B.V.

Sodium 9,10-dimethoxyanthracene-2-sulphonate (NaDMAS). Although this compound was used earlier [8], its preparation was not fully described. The compound was prepared by the method described by Meek et al. [9] for the synthesis of the related compound, 9,10-dimethoxyanthracene. Sodium anthraquinone-2-sulphonate (15.51 g, 0.05 mol) was ground with 5 g of zinc dust and placed in a reaction flask with 20 ml of ethanol; 200 ml of 20% (w/v) sodium hydroxide was added and the mixture was refluxed for 2 h. Methyl-*p*-toluenesulphonate was added carefully in small amounts with continual stirring until the colour was discharged. The resulting precipitate was filtered, extracted with aqueous sodium hydrogensulphite until the extracts were almost colourless, and finally recrystallised four times from water. The identity of the product was confirmed by ^{1}H-n.m.r., mass spectroscopy and elemental analysis as $C_{16}H_{13}O_5S$ Na·1/2H_2O. An 0.1% (w/v) solution was made up in distilled water.

Other solutions. A 100 ppm cobalt(II) solution was prepared by dissolving 0.2630 g of anhydrous cobalt(II) sulphate (AR grade dried to constant weight at 400°C) in 1 l of distilled water. More dilute standard solutions were prepared as required. A pH 3 buffer was prepared by mixing 81.1 ml of 0.1 M citric acid and 18.9 ml of 0.2 M disodium hydrogen phosphate. 1,2-Dichloroethane was redistilled twice and the fraction b.p. 82—83°C was used. All other reagents were of analytical grade. Twice-distilled water was used throughout.

Optimization studies

Choice of solvent. A variety of solvents including alcohols, ketones, esters, ethers, chlorinated and aromatic hydrocarbons was examined for extraction efficiency by mixing 5-ml aliquots of 1 ppm cobalt(II) solution with 0.5 ml of 0.1% PAPHY. Cobalt(II) is rapidly oxidised by dissolved oxygen in the presence of PAPHY which allows formation of the cobalt(III)—$(PAPY)_2$ complex. Next, 1-ml aliquots of NaDMAS were added and the solutions were extracted with 15 ml of the solvent. The organic phases were separated and filtered to remove excess of water, and the absorbances were measured at 496 nm against the appropriate solvent as blank. Dichloromethane and acetone/1,2-dichloroethane (1:9) were the most efficient extracting solvents. However, the latter extract was more fluorescent and less volatile and hence was used for the rest of the study.

Optimum amounts of reagents. The effects of varying the quantities of PAPHY and NaDMAS were studied for the extraction of 6 μg of cobalt into 15 ml of the solvent mixture. In each case, the absorbance of the extracts increased up to a constant value with increase in amounts of reagents. Suitable amounts were found to be 0.5 ml of 0.1% PAPHY and 2 ml of 0.1% NaDMAS for up to 6 μg of cobalt.

The effect of pH was examined on aqueous solutions containing 0, 2 or 6 μg of cobalt, and the other reagents, by addition of 1 M hydrochloric acid or 1 M ammonia solution prior to extraction. The absorbances were measured

as before. The lowest reagent blank and maximum slope for the calibration graph and hence sensitivity was at pH 3. The sensitivity changes significantly (i.e., by 20%) only outside the pH range 2—5.

Procedure for analysis of steel samples

For steel samples containing 0.05—0.4% or 0.005—0.02% cobalt, dissolve 0.1- or 1.0-g samples, respectively, in 3 or 15 ml of concentrated hydrochloric acid, followed by 1 or 5 ml of concentrated nitric acid; warm to dissolve. Boil off oxides of nitrogen and evaporate to near dryness. Add 1 or 5 ml of 100-volume hydrogen peroxide and evaporate to near dryness. Add 8 or 30 ml of distilled water, warm to dissolve, cool and, if necessary, filter through a Whatman No. 1 filter paper. Transfer to a 50-ml volumetric flask; wash the filter and precipitate with a few ml of hot 0.1 M hydrochloric acid followed by water and add the washings to the flask. Dilute to 500 ml with distilled water. A precipitate of tungstic acid is formed after initial dissolution of high-speed tool steels.

To an aliquot (10 ml) of the slightly acidic solution, containing up to 5 μg of cobalt(II), add 5 ml of distilled water and 5 ml of 40% (w/v) ammonium fluoride solution, and leave for 1 min. Add 10 ml of pH 3 citrate—phosphate buffer, 1 ml of 0.1% (w/v) PAPHY and 3 ml of 0.1% (w/v) NaDMAS. Mix thoroughly. Shake with 10 ml of 1:9 acetone/1,2-dichloroethane for 1 min to allow formation and extraction of the cobalt(III) complex. Allow the phases to separate. Filter the lower phase through a Whatman No. 1 filter paper into a 10-ml volumetric flask, and make up to volume with solvent. Determine the absorbance at 496 nm or the fluorescence at 450 nm with excitation at 396 nm in 1-cm cells. Prepare a calibration graph over the range 0—5 μg of cobalt after adding 10 ml of iron(III) nitrate (2 or 20 mg of iron) and all other reagents as for the steel sample.

Results and discussion

The composition of the complex was established spectrophotometrically and fluorimetrically by Job's method of continuous variations to have a 1:1 cobalt to DMAS ratio. The $[Co(PAPY)_2]^+$ $DMAS^-$ complex is appreciably dissociated. Earlier, Haddad et al. [6] were unable to establish the nature of the extracted complex involving eosin owing to the large excesses of PAPHY and eosin needed to ensure complete reaction. They suggested the ion-pair to be $Co(PAPHY)(PAPY)(eosin)_2$.

Linear calibration graphs were obtained over the range 0—5 μg of cobalt in the final 10-ml extract, by absorbance or fluorescence measurements. For 4 μg of cobalt the coefficients of variation estimated from 7 replicates were 1.3 and 1.5% for the absorbance and fluorescence measurements, respectively. The apparent molar absorptivity of the $Co(PAPY)_2DMAS$ ion-pair complex in the extract was 3.26×10^4 l mol^{-1} cm^{-1}. The detection limits were 0.003 and 0.004 μg Co ml^{-1} for absorbance and fluorescence measurements, respectively.

TABLE 1

Effect of diverse ions on the determination of cobalt (5 μg)
(Ions causing a change in absorbance or fluorescence of less than twice the standard deviation are regarded as non-interfering)

Ion[a]	Ratio to Co (w/w)	Change in fluorescence (%)	Change in absorbance (%)
Cr^{3+}	1000	0	0
V(V)	250	0	0
Mn^{2+}	1500	0	0
Zn^{2+}	1500	−20	−32
Cu^{2+}	1000	−26	40
	1000[b]	0	0
Ni^{2+}	50	−46	+15
	1000[c]	0	0
Fe^{3+}	1000	−14	+40
	1000[d]	0	0
Fe^{2+}	50	−86	−100
Cl^-	95000	0	0
SO_4^{2-}	5000	0	0
NO_3^-	500	0	0
ClO_4^-	250	−52	+8
HPO_4^{2-}	5000	0	0
Citrate	5000	7	14

[a]Cations added as chloride or sulphate, anions added as sodium salts. [b]In presence of thiosulphate. [c]In presence of EDTA followed by bismuth(III). [d]In presence of ammonium fluoride.

The possible interferences of a number of cations and anions on the extraction of 5 μg of cobalt were examined. The interferences by iron(III) and copper(II) were significant but could be masked by the addition of 5 ml of 40% (w/v) ammonium fluoride solution for 25 mg of iron and by addition of 30 mg of sodium thiosulphate for 5 mg of copper. Cobalt can be determined in the presence of high adverse ratios of nickel (1:5000) by using Flaschka and Speights' procedure [10] in which both metals are converted to EDTA complexes at pH 10 and cobalt is displaced with bismuth(III). This was followed by extraction of $Co(PAPY)_2DMAS$. For the steels examined it was not necessary to mask copper or nickel. At high levels of iron, a slightly enhanced extraction was noted (+4% for 2 mg and +70% for 20 mg of iron). This interfering effect in the determination of cobalt in steel and that of the blank can be allowed for by the addition of an equivalent amount of iron to the standards. The results of the interference and masking studies are summarised in Table 1.

Results for the determination of cobalt in six British Chemical Standards (six replicates on each sample) are in excellent agreement with the certified

TABLE 2

Analysis of high-purity iron and steels for cobalt

Sample type	B.S.C. no.	Cobalt, range and certified value (%)	Cobalt found (%)[a]	
			Spectrophotometric	Fluorimetric
High-speed tool steel	220/2	(0.31—0.33), 0.32	0.323 ± 0.003	0.321 ± 0.047
	481	(0.19—0.22), 0.21	0.219 ± 0.002	0.215 ± 0.064
	482	(0.21—0.27), 0.24	0.270 ± 0.010	0.267 ± 0.030
Carbon steel	456	(0.043—0.050), 0.048	0.049 ± 0.003	0.049 ± 0.017
	459	(0.073—0.080), 0.077	0.075 ± 0.005	0.075 ± 0.010
High-purity iron	260/4	(0.006—0.007), 0.007	0.0071 ± 0.0001	0.0068 ± 0.0013

[a]Mean ±95% confidence limits, 6 replicates.

values (Table 2). In common with other ion-pair extractions [2, 3], the present procedure does not require prior separation of matrix ion as is required in most other fluorimetric methods [5, 6].

REFERENCES

1 F. D. Snell, Photometric and Fluorimetric Methods of Analysis: Metals Part I, Wiley, New York, 1978.
2 D. T. Burns and P. Hansprasopwattana, Anal. Chim. Acta, 115 (1980) 389, and references therein.
3 D. T. Burns, P. Hansprasopwattana and B. P. Murphy, Anal. Chim. Acta, 134 (1982) 397.
4 G. H. Schenk, K. P. Dilloway and J. S. Coulter, Anal. Chem., 41 (1969) 510.
5 D. N. Lititsyna and D.F. Shcherbov, Zh. Anal. Khim., 28 (1973) 1203.
6 P. R. Haddad, P. W. Alexander and L. E. Smythe, Talanta, 23 (1976) 275.
7 F. Lions and K. V. Martin, J. Am. Chem. Soc., 80 (1958) 3858.
8 D. Westerlund and K. H. Karset, Anal. Chim. Acta, 67 (1973) 99.
9 J. S. Meek, P. A. Monroe and C. J. Bouboulis, J. Org. Chem., 28 (1963) 2572.
10 H. Flaschka and R. M. Speights, Microchem. J., 14 (1969) 490.

Analytica Chimica Acta, 151 (1983) 251—254
Elsevier Science Publishers B.V., Amsterdam — Printed in The Netherlands

Short Communication

SPECTROFLUORIMETRIC DETERMINATION OF ASCORBIC ACID

CHENOLI P. SHEELA,[a] ELIMBAN VIJAYAN[b] and ABBURI RAMAIAH*

Department of Biochemistry, All India Institute of Medical Sciences, New Delhi-110029 (India)

(Received 30th July 1982)

Summary. The spectrofluorimetric method described for the determination of ⩾20 nmol of ascorbic acid is based on its ability to participate in the nonenzymatic hydroxylation of tyrosine to 3,4-dihydroxyphenylalanine (dopa). The method is applied to Dulbeco's culture media.

The principal methods for the determination of ascorbic acid involve titration with a reducible dye such as 2,6-dichlorophenolindophenol or the formation of an osazone with 2,4-dinitrophenylhydrazine [1]. During the determination of tyrosinase in human skin [2] by spectrofluorimetric measurement of 3,4-dihydroxyphenylalanine (dopa) formed in the presence of the enzyme, tyrosine and ascorbic acid, it was observed that dopa was also formed nonenzymatically in significant quantities under certain conditions. The concentration of dopa thus formed was proportional to the concentrations of tyrosine and ascorbic acid. This reaction is perhaps similar to the hydroxylation of aromatic compounds in the presence of oxygen and iron(II) [3]. This communication describes a method for the determination of ⩾20 nmol of ascorbic acid based on this reaction, and shows that EDTA and iron(II) are required to maximize the hydroxylation of tyrosine to dopa.

Experimental

L-Tyrosine, L-dopa and L-ascorbic acid were obtained from the Sigma Chemical Co. All other chemicals used were of analytical-reagent grade. L-Ascorbic acid solution was always freshly made up in 0.06% metaphosphoric acid. L-Tyrosine was made up in 0.2 M phosphate buffer, pH 6.8. A Farrand manual spectrofluorimeter was used for all fluorescence measurements.

Procedure. The reaction was carried out in rimless tubes (12 mm diameter, 100 mm tall). The reaction mixture was 0.5 ml of 5 mM tyrosine in 0.2 M phosphate buffer, pH 6.8, 0.05 ml of 1.3 mM iron(II) sulphate, 0.05 ml of 6.5 mM EDTA, 0.1 ml of 2 mM ascorbic acid, 0.1 ml of 0.6% metaphos-

Present addresses: [a]Prabhalayam, Kakkad, Cannanore-5, Kerala (India); [b]Department of Physiology, University of Manitoba, Faculty of Medicine, Winnipeg (Canada).

0003-2670/83/$03.00 © 1983 Elsevier Science Publishers B.V.

phoric acid and 0.2 ml of water to make the total volume 1 ml. The pH of this solution was 6.5. The mixture was incubated at 37°C in a water bath for 30 min. At the end of the reaction, 50 μl of the reaction mixture was added to 0.90 ml of 10 mM phosphate buffer pH 6.5 containing 0.0025% zinc sulphate followed by 0.1 ml of 0.25% potassium hexacyanoferrate(III). The oxidation of dopa by hexacyanoferrate(III) was terminated after exactly 2 min by addition of 0.1 ml of a freshly made mixture of 5 M sodium hydroxide and 2% ascorbic acid (9:1 v/v). After 5 min, the fluorescence of the sample was measured at 360 nm excitation and 490 nm emission wavelengths.

The chemistry involved in the estimation of dopa by this method has been described [4]. During the experiments, the sensitivity of the instrument fluctuated slightly. The instrument was standardized periodically with a 50 ng ml^{-1} solution of quinine sulphate in 0.05 M sulphuric acid. The fluorescence obtained by a number of standard solutions of dopa (30—20,000 pmol) gave a linear calibration graph, which was used to determine the ascorbic acid originally present. Such a graph was obtained periodically, but for daily use, in every experiment the fluorescence obtained from 50 μl of freshly made 11×10^{-6} M dopa was used to calculate the amount of dopa resulting from the presence of ascorbic acid.

Results and discussion

The product formed nonenzymatically in the presence of tyrosine and ascorbic acid was shown to be 3,4-dihydroxyphenylalanine (dopa) [2]. This was determined as described originally by Bertler et al. [4] as modified by Adachi and Halprin [5] and Husain et al. [2]. The components required for the maximal rate of nonenzymatic hydroxylation of tyrosine were studied. The fluorescence arising from dopa was obtained in the presence or absence of ascorbic acid, EDTA or iron(II) sulphate or in the absence of both iron(II) sulphate and EDTA. The fluorescence from dopa in the absence of ascorbic acid is very small (2% of the fluorescence obtained in presence of 0.2 mM ascorbic acid), showing thereby that the formation of dopa is almost totally dependent on the presence of ascorbic acid. In the absence of EDTA or iron(II) sulphate, the fluorescence is decreased to 25% of its value in their presence. In the absence of both, the fluorescence was decreased by a further 15%. These results suggest that both EDTA and iron(II) sulphate are required to enhance the rate of hydroxylation of tyrosine by ascorbic acid. The addition of EDTA and iron(II) sulphate above the concentrations mentioned in the procedure did not increase the fluorescence. These experiments were done always in duplicate and the variation was less than 10%.

Effect of ascorbic acid concentration. The rates of formation of dopa at two different concentrations of ascorbic acid are shown in Fig. 1. The change in fluorescence is proportional to the ascorbic acid concentration for at least 30 min. The amount of dopa formed is directly proportional to the amount of ascorbic acid (100 nmol ascorbic acid ≡ ca. 25 nmol dopa) up to

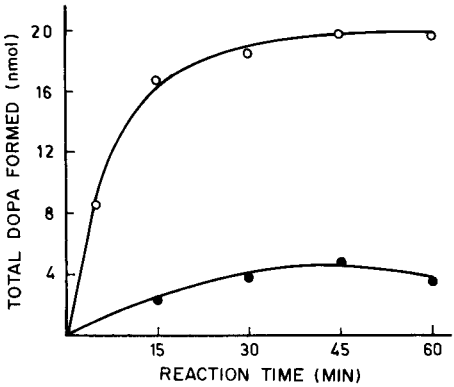

Fig. 1. Rate of formation of dopa in the presence of the following concentrations of ascorbic acid: (•) 0.02 mM; (○) 0.10 M (conditions otherwise as in procedure).

ca. 200 nmol of ascorbic acid. When the reaction was conducted in wider tubes (25 mm diameter), the dopa formed was proportional up to 400 nmol of ascorbic acid. It appears that at higher concentrations of ascorbic acid the reaction may be limited by the availability of oxygen.

Precision and recovery. The relative standard deviation for a determination of 100 nmol of ascorbic acid was 3% (n = 8).

Ascorbic acid was added to Dulbeco's Modified Eagle's Medium [6] to give a concentration of 2 mM, and five different aliquots of this medium were added to the reaction mixture described earlier to give a range of concentration of ascorbic acid from 0.02 to 0.2 mM in the reaction mixture. The recovery of duplicate determinations in each case was 98 ± 3%. The method can be applied to the determination of ascorbic acid in the range 0.02—0.2 mM in the reaction mixture. Since only 50 µl of reaction mixture was used for the determination of dopa, the reaction can equally well be conducted in a 50-µl volume and all of it can be used for the determination of dopa, in which case the method can detect as little as 1 nmol of ascorbic acid.

Mechanism of hydroxylation of tyrosine. Ascorbic acid, by its auto-oxidation in the presence of oxygen, results in the formation of hydrogen peroxide which is reduced by iron(II) complexes to form hydroxyl radicals [7]. The hydroxyl radicals hydroxylate aromatic compounds [8]. This hydroxylation is stimulated by ascorbic acid by an as yet unknown mechanism.

This work was supported by grants from the Department of Science and Technology, India (HCS/DST/971/80) to A. Ramaiah. The authors thank Miss Chaya Devi and Miss Aarti Bhatnagar for doing the reproducibility experiments.

REFERENCES

1 J. H. Roe, in P. Gyorgy and W. N. Pearson (Eds.), The Vitamins, 2nd edn., Vol. VII, Academic Press, New York, 1967, p. 27.
2 I. Husain, E. Vijayan, A. Ramaiah, J. S. Pasricha and N. C. Madan, J. Invest. Dermatol., 78 (1982) 243.
3 S. Udenfriend, C. J. Clark, J. Axelrod and B. B. Brodie, J. Biol. Chem., 208 (1954) 731.
4 A. Bertler, A. Carlsson and E. Rosengren, Acta Physiol. Scand., 44 (1958) 273.
5 K. Adachi and K. M. Halprin, Biochem. Biophys. Res. Commun., 26 (1967) 241.
6 R. Dulbeco and G. Freeman, Virology, 8 (1959) 396.
7 W. T. Dixon and R. O. C. Norman, Nature, 196 (1962) 891.
8 W. T. Dixon and R. O. C. Norman, Proc. Chem. Soc. (London), (1963) 97.

Analytica Chimica Acta, 151 (1983) 255—260
Elsevier Science Publishers B.V., Amsterdam — Printed in The Netherlands

Kurze Mitteilung

EXTRAKTION VON IRIDIUM UND RUTHENIUM MIT AUSGEWÄHLTEN 1, 3-MONOTHIODICARBONYLVERBINDUNGEN

G. RÖBISCH*, W. BANSSE, E. LUDWIG und E. UHLEMANN

Sektion Chemie/Biologie der Pädagogischen Hochschule "Karl Liebknecht" Potsdam, DDR-1500 Potsdam (D.D.R.)

(Eingegangen den 16 November 1982)

Summary. (Extraction of iridium and ruthenium with selected 1,3-monothiodicarbonyl compounds) In the presence of labilizing agents at about 85°C, iridium(III) or (IV) and ruthenium(III) form readily extractable tris chelates with monothiodibenzoylmethane, acylthioacetamides or acylthioureas in slightly acidic media. A single extraction with chloroform provides up to 92% extraction of traces of iridium and ruthenium from technical chloride solutions. Iridium can be enriched up to 30-fold with monothiodibenzoylmethane.

Zusammenfassung. Iridium(III) oder (IV) bzw. Ruthenium(III) bilden in der Hitze und in Anwesenheit von Labilisatoren mit Monothiodibenzoylmethan, Acylthioacetamiden oder Acylthioharnstoffen im schwach sauren Milieu mit organischen Lösungsmitteln gut extrahierbare Tris-chelate. Mit Chloroform lassen sich aus stark chloridhaltigen Industrielösungen Iridium- und Ruthenium-spuren in einem Extraktionsschritt mit einer Ausbeute bis zu 92% isolieren. Iridium kann dabei mit Monothiodibenzoylmethan bis zum Dreißigfachen angereichert werden.

Shome und Halder [1] setzten *N*-α-(5-Brompyridyl)-*N'*-benzoylthioharnstoff zur Flüssig—Flüssig-Extraktion und spektrophotometrischen Bestimmung von Ruthenium, Palladium und Iridium ein. Weitere Untersuchungen über die Eignung von 1,3-Monothiodicarbonylverbindungen zur Extraktion von sekundären Platinelementen sind nicht bekannt. Röbisch et al. [2] berichteten über die Bestimmung von Iridiumspuren (2 $\mu g\ l^{-1}$) mit Monothiodibenzoylmethan mittels substöchiometrischer Isotopenverdünnungsanalyse. In der vorliegenden Arbeit werden Monothio-β-diketone, Acylthioacetamide und Acylthioharnstoffe als Extraktionsmittel für Iridium- und Ruthenium-spuren aus stark chloridhaltigen Lösungen untersucht. In Tabelle 1 sind die eingesetzten Extraktionsmittel zusammengestellt. Über die Extraktion von Übergangsmetallionen mit den in Tabelle 1 aufgeführten Acylthioacetamiden und Acylthioharnstoffen wurde bereits berichtet [3, 4], ebenso über die Anwendung von Monothiodicarbonylverbindungen [5].

Experimentelles

Die radioaktive Iridium-Standardlösung ($5{,}05.10^{-5}$ M) wurde durch Mischen gleicher Volumina einer 1.10^{-4} M Lösung von Na_2IrCl_6 bzw. Na_3IrCl_6

0003-2670/83/$03.00 © 1983 Elsevier Science Publishers B.V.

TABELLE 1

Übersicht über die verwendeten 1,3-Monothiodicarbonylverbindungen

Verbindung		R'—CO—X—CS—R^2			Lit.
		X	R^1	R^2	
Monothiodibenzoylmethan	HSDBM	CH_2	C_6H_5	C_6H_5	7
Benzoylthioacetanilid	BTAA	CH_2	C_6H_5	NHC_6H_5	8
Benzoylthioacet-di-n-butylamid	BTABA	CH_2	C_6H_5	$N(n\text{-}C_4H_9)_2$	9
Acetylthioacetanilid	ATAA	CH_2	CH_3	NHC_6H_5	8
1-Piperidino-3-benzoyl-thioharnstoff	PBTH	NH	C_6H_5	NC_5H_{10}	10
1,1-Di-n-butyl-3-benzoyl-thioharnstoff	BBTH	NH	C_6H_5	$N(n\text{-}C_4H_9)_2$	10

(Ferak) in 4 M Salzsäure mit einer $1{,}1.10^{-6}$ M Lösung von $(NH_4)_2{}^{192}IrCl_6$ (Institute of Nuclear Research, Radioisotopes and Distribution Centre, Swierk, Otwock, Poland) in 4 M Salzsäure hergestellt. Die radioaktive Ruthenium-Standardlösung ($1{,}6.10^{-5}$ M) wurde durch Zugabe von 0,1 ml einer trägerfreien 2,8 M salzsauren $^{106}RuCl_3$-Lösung (UdSSR-Import) zu 100 ml einer $1{,}6.10^{-5}$ M Lösung von $RuCl_3$ (Ferak) in 4 M Salzsäure erhalten.

Die Darstellung der Liganden erfolgte nach der in Tabelle 1 angegebenen Literatur. Für die Iridium- (bzw. Ruthenium-) Extraktion fanden 5.10^{-3} M (bzw. $1{,}6.10^{-3}$ M) Ligandlösungen in 0,1 M Natronlauge Verwendung. Diese Lösungen wurden täglich frisch hergestellt.

In einem 50-ml Becherglas gibt man zu 2 ml der Iridium- (bzw. 1 ml der Ruthenium-)Standardlösung 2 ml (bzw. 1 ml) 4 M Natronlauge und dann ein abgemessenes Volumen Ligandlösung. Nach Zusatz von Ethanol und Acetatlösung wird der gewünschte pH-Wert unter Verwendung von Salzsäure und Natronlauge gegen eine Glaselektrode eingestellt und die Lösung in einem Wasserbad erwärmt. Als optimal erwies sich ein einstündiges Erhitzen auf 85°C. Nach Abkühlung auf Zimmertemperatur wird die Lösung mit Aqua bidest. für die Iridiumextraktion auf 20 ml (für die Rutheniumextraktion auf 15 ml) aufgefüllt und dann mit dem gleichen Volumen Chloroform bzw. mit den in Tabelle 2 aufgeführten Lösungsmitteln 3 Min geschüttelt. Danach wurde je 1 ml der wäßrigen und organischen Phase unter Verwendung eines Szintillationszählers mit Bohrlochmeßkopf VA-S-961 (VEB Vakutronik, Dresden) radiometrisch (Impulse Min^{-1}) vermessen.

Zur Rückextraktion schüttelten wir die beim optimalen pH-Wert erhaltene organische Phase mit dem gleichen Volumen einer wäßrigen Phase bestimmten pH-Wertes 10 Min.

Zur Prüfung der extraktiven Anreicherung wurde die wäßrige Phase vor der Komplexbildung entsprechend verdünnt und das Volumen der organischen Phase auf 3 ml verringert.

Die Flüssig—Flüssig-Extraktion führten wir in beheizten doppelwandigen Schütteltrichtern durch. Der Ligand wurde dann nicht der wäßrigen Phase zugesetzt, sondern war in der organischen Phase gelöst.

Ergebnisse

In der stark chloridhaltigen Lösung liegen Iridium(III) oder (IV) und Ruthenium(III) in Form der inerten Hexachlorometallate vor. Die Reaktion mit den Monothiodicarbonylverbindungen läuft erst bei etwa 90°C mit optimaler Geschwindigkeit ab, es reicht dann einstündiges Erhitzen. Deshalb ist es günstig, die Komplexbildung in der Hitze im Einphasensystem und erst dann die Extraktion mit dem organischen Lösungsmittel bei Zimmertemperatur durchzuführen. Das Verteilungsgleichgewicht stellt sich schnell innerhalb von 3 Min ein. Am Beispiel der Reaktion von Ruthenium mit Thiodibenzoylmethan haben wir gefunden, daß diese (experimentell einfachere) Arbeitsweise zu denselben Ergebnissen führt wie eine unter sonst gleichen Reaktionsbedingungen vorgenommene (in der Hitze experimentell aufwendigere) Flüssig—Flüssig-Extraktion.

Während die Reaktion des Hexachloroiridat-ions mit Thiodibenzoylmethan in Wasser durch Zusatz von Ethanol nicht beeinflußt wird, beschleunigt dieser die Reaktion des Hexachlororuthenat-ions mit dem Reagens erheblich (Abb. 1). Insgesamt wirken sich Zusätze solcher potentieller Labilisatoren wie Ethanol

TABELLE 2

Extraktionsparameter für die Extraktion von Iridium(III) oder (IV) (c_{Ir} = 2,5 nmol ml^{-1}, Erhitzungsdauer 60 min, 85°C, organische Phase Chloroform)

Ligand	$pH_{1/2}$	pH_{max}	R_{max} (%)	D_{max}	$u_{Eth.}$ (%)	c_{Ac^-} (mol l^{-1})	Mindest-ligand-überschuß	Möglichkeit der Anreicherung	
								$V_W:V_O$	ΔR (%)
HSDBM	4,7	6,0—6,5	92,0	11,74	—[a]	0,25 (5,5%)	20	2	0
								10	0
								20	—2,9
								30	—6,4
ATAA	3,7	5,8—6,2	86,4	6,35	—[a]	0,25 (26%)	100	2	—10,2
								10	—25,5
								20	—25,6
BTAA	5,0	7,0	90,0	9,44	33 (24,8%)	0,25 (30,5%)	100	5	—0,6
								10	—1,5
								20	—3,0
								30	—15,5
BTABA	4,0	5,5—6,5	87,4	6,93	33 (69,9%)	0,25 (20,6%)	60	5	—7,0
								10	—25,9
								20	—49,9
								30	—57,3
PETH	4,6	6,0	91,1	10,12	—[a]	—[b]	100	2	—0,5
								10	—20,0
								20	—38,0
BBTH	4,4	5,8—6,2	86,9	6,67	33 (31,6%)	0,25 (39,7%)	40	10	—2,0
								20	—5,4
								30	—15,8

[a] Ethanol ohne Einfluß. [b] Acetationen ohne Einfluß.

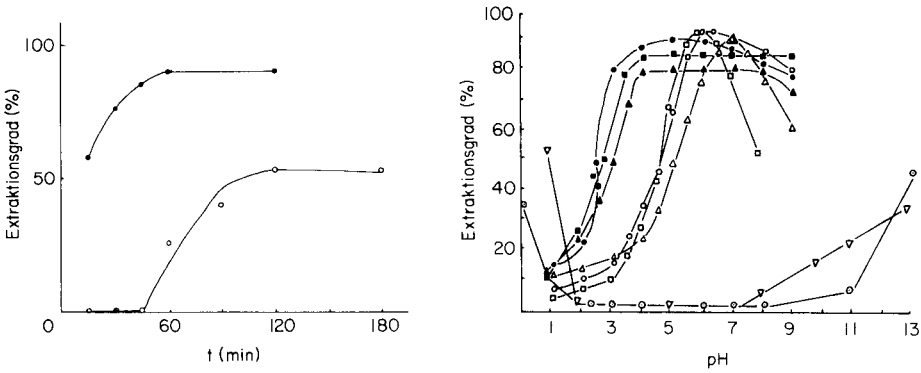

Abb. 1. Einfluß der Reaktionszeit auf die Komplexbildung von Ruthenium(III) mit HSDBM ohne (○) und mit (●) Ethanol. c_{Ru} = 1,07 nmol ml^{-1}, c_{HSDBM} = 107 nmol ml^{-1}, pH 5, 85°C.

Abb. 2. pH-Abhängigkeit der Bildung der Iridium- und Ruthenium-chelate. c_{Ir} = 2,5 nmol ml^{-1}, c_{Ru} = 1,07 nmol ml^{-1}, c_M:c_L = 1:100, $u_{Eth.}$ = 33%, c_{Ac^-} = 0,25 mol l^{-1}, 1 h, 85°C. Kurven: (○) Ir—HSDBM; (△) Ir—BTAA; (□) Ir—PBTH; (●) Ru—HSDBM; (▲) Ru—BTAA; (■) Ru—PBTH. pH-Abhängigkeit der Rückextraktion der bei pH 6 gebildeten Ir—(HSDBM)-Komplexe (⊙) und Ir—BTAA-Komplexe (▽).

und Acetationen [11] in Abhängigkeit vom vorgegebenen Element (Ir oder Ru) und vom eingesetzten Liganden unterschiedlich aus (Tabellen 2 und 3). Eine überzeugende Deutung dieser unterschiedlichen Einflüsse, die über die allgemeine Vermutung hinausgeht, daß der Labilisator die Bildung eines weniger inerten Intermediär-Komplexes fördere, bedarf weiterer Untersuchungen. Da die verwendeten Monothiodicarbonylverbindungen bei längerem Erhitzen (>2 Stunden) im Reaktionsmilieu deutlich hydrolytisch abgebaut

TABELLE 3

Extraktionsparameter für die Extraktion von Ruthenium(III)
(c_{Ru} = 1,07 nmol ml^{-1}, Erhitzungsdauer 60 min, 85°C, organische Phase Chloroform)

Ligand	$pH_{1/2}$	pH_{max}	R_{max} (%)	D_{max}	$u_{Eth.}$ (%)	c_{Ac^-} (mol l^{-1})	Mindest-ligand-überschuß	Möglichkeit der Anreicherung	
								V_W:V_O	ΔR (%)
HSDBM	2,5	4,0—6,0	91,0	10,11	33 (65%)	0,25 (14%)	100	2	—11,5
								5	—12,5
								10	—39,6
BTAA	3,0	4,0—7,0	80,3	4,07	33 (6,4%)	0,25 (8,7%)	100	2	0
								5	—8,9
								10	—14,3
PBTH	2,7	4,0—9,0	85,3	5,80	33 (24,3%)	0,25 (15%)	100	5	0
								10	—7,5
								20	—11,5

werden, wirkt sich die reaktionsbeschleunigende Wirkung der Labilisatoren auch günstig auf die überhaupt erzielte Extraktionsausbeute aus. In den Tabellen 2 und 3 ist dieser Effekt in den Spalten, die den optimalen Volumenanteil an Ethanol ($u_{Eth.}$) bzw. die optimale Acetationenkonzentration (c_{Ac^-}) im Reaktionsmedium angeben, mit ΔR als Differenz der ohne und mit Labilisator erzielten Extraktionsausbeuten aufgeführt.

Der Einfluß des organischen Lösungsmittels auf die Extraktionsausbeute der unter optimalen Bedingungen gebildeten Komplexe ist aus Tabelle 4 zu entnehmen.

Die verwendeten Monothiodicarbonylverbindungen reagieren mit dem Chlorokomplex des Ruthenium(III) bei niedrigeren pH-Werten ($pH_{1/2}$ = 2,5—3,0) als mit dem des Iridiums(III) oder (IV) ($pH_{1/2}$ = 3,7—5,0), wie aus der Abb. 2 und den Tabellen 2 und 3 ersichtlich ist. Der pH-Bereich für optimale Extraktion ist beim Ruthenium viel breiter als beim Iridium. Zwischen den ermittelten $pH_{1/2}$-Werten und den Aciditäten der Liganden [12] besteht kein einfacher Zusammenhang.

Der zur Erzielung der optimalen Komplexbildung notwendige Mindestüberschuß der Liganden (Tabellen 2 und 3) gestattet qualitativ eine Abstufung der Stabilitäten der gebildeten Trischelate. Eine größere Stabilität als die übrigen zeigen $Ir(HSDBM)_3 > Ir(BBTH)_3 > Ir(BTABA)_3$.

Der Verlauf der Rückextraktion der Chelate in eine wäßrige Phase (Abb. 2) läßt ihre relativ hohe Stabilität gegenüber Säuren und Basen erkennen. Im Gegensatz zur kinetisch gehemmten Bildungsreaktion erfolgt die Reaktion der Trischelate mit Protonen und Hydroxidionen im Zweiphasensystem in wenigen Minuten bei Zimmertemperatur.

Die Zusammensetzung der Komplexe wurde in Lösung nach Job und durch Elementaranalyse der isolierten Chelate bestimmt. In beiden Fällen wurde das Verhältnis Metall:Ligand = 1:3 gefunden. Die Oxydationsstufe +3 für Ruthenium und auch für Iridium, unabhängig davon, ob ursprünglich Chloroiridate(III) oder(IV) eingesetzt wurden, konnte mittels ESCA-Untersuchungen an den Festkomplexen gesichert werden [6].

TABELLE 4

Abhängigkeit des Verteilungskoeffizienten D und der Extraktionsausbeute R für $Ir(HSDBM)_3$ und $Ir(BTAA)_3$ vom Lösungsmittel

Lösungsmittel	$Ir(HSDBM)_3$		$Ir(BTAA)_3$	
	D	R (%)	D	R (%)
Chloroform	11,74	92,0	9,44	90,0
Chloroform/Ethanol (1:1)	12,03	92,3	9,74	90,7
Tetrachlorkohlenstoff	0,46	31,5	3,10	75,6
Trichlorethen	0,67	40,1	3,18	76,1
Toluen	0,21	20,6	3,02	75,2
Xylen	0,50	33,2	2,54	71,8
Heptan	1,49	59,8	0,91	47,7

Für die Verwendung der hier untersuchten 1,3-Monothiodicarbonylverbindungen in der Spurenanalyse bieten sich wegen der niedrigen Erfassungskonzentration, der guten Anreicherungsmöglichkeit und der breiten pH-Stabilität der Komplexe für Iridium insbesondere BTAA sowie HSDBM (12 pmol ml^{-1}) [2] an, für Ruthenium PBTH (0,2 nmol ml^{-1}). Trotz der für die Rutheniumextraktion niedrigeren $pH_{1/2}$-Werte sind die untersuchten Reagenzien für die anreichernde Isolierung und Bestimmung von Iridiumspuren besser geeignet als für Rutheniumspuren. Die kinetische Trägheit der Komplexbildung kann sehr günstig zur Erhöhung der Selektivität durch Vorextraktionen bei Zimmertemperatur genutzt werden. Zur Trennung von Ruthenium und Iridium durch gezielte pH-Einstellung bei der Komplexbildung reichen die $pH_{1/2}$-Differenzen nicht aus.

LITERATUR

1 S. C. Shome und P. K. Halder, Int. Solvent Extraction Conf., Liège, 1980, S.80, Association des Ingénieurs sortis de l'Université de Liège, Liège.
2 G. Röbisch, W. Bansse und E. Ludwig, Anal. Chim. Acta, 117 (1980) 313.
3 K. Gloe, E. Ludwig, P. Mühl und E. Uhlemann, DDR-WP B 01 D/217 376.
4 P. Mühl und K. Gloe, 5. Int. Symp. Reinstoffe in Wissenschaft und Technik, Dresden 1980, Proceedings I, S. 203 Zentralinstitut für Festkörperphysik und Werkstofforschung der AdW der DDR, Dresden.
5 E. Uhlemann und R. Morgenstern, Z. Chem., 17 (1977) 405.
6 G. Röbisch, W. Bansse, E. Ludwig und R. Szargan, Z. Allg. Anorg. Chem., 493 (1982) 26.
7 E. Uhlemann und H. Müller, Angew. Chem., 77 (1965) 172.
8 E. Ludwig und E. Uhlemann, Z. Chem., 15 (1975) 234.
9 W. Schroth, D. Schmidt und A. Hildebrandt, Z. Chem., 14 (1974) 93.
10 L. Beyer, E. Hoyer, H. Henning, R. Kirmse, H. Hartmann und J. Liebscher, J. Prakt. Chem., 317 (1975) 829.
11 V. M. Savostina, O. A. Spigun, V. A. Parmenova, A. A. Valschin und V. M. Peschkova, Zh. Anal. Chim., 31 (1976) 2154; 32 (1977) 556.
12 E. Ludwig, E. Uhlemann, K. Gloe und P. Mühl, Anal. Chim. Acta, 140 (1982) 171.

Analytica Chimica Acta, 151 (1983) 261—263
Elsevier Science Publishers B.V., Amsterdam — Printed in The Netherlands

Short Communication

SPECTROPHOTOMETRIC DETERMINATION OF BENZIDINE BY EXTRACTION OF AZO DYE INTO 3-METHYL-1-BUTANOL

PRATIMA VERMA and V. K. GUPTA*
Department of Chemistry, Ravishankar University, Raipur, 492 010 (India)
(Received 26th August 1982)

Summary. The method is based on diazotization, coupling with α-naphthol in acidic medium, and extraction of the violet dye formed in alkaline solution into 3-methyl-1-butanol. Beer's law is obeyed up to 0.25 μg ml^{-1} at 535 nm. The molar absorptivity and the Sandell sensitivity are $6.6 \pm 0.02 \times 10^4$ l mol^{-1} cm^{-1} and 0.0028 μg cm^{-2}, respectively. A detailed interference study is reported.

Benzidine is an important product in the dye industry and is a common constituent of several hair dyes, despite its well-known carcinogenic effects particularly with regard to bladder tumours [1, 2]. The chloramine-T method [1] based on the oxidation of benzidine and it subsequent spectrophotometric measurement is said to be selective and sensitive, but the colour formed is unstable in strong sunlight and there are interferences from other phenols and aromatic amines. Other methods [3—6] that might be used for the determination of benzidine are inselective and are mostly designed for determining aromatic amines in general. In the present communication, a novel extractive—spectrophotometric determination of benzidine is described. The method is based on diazotization and coupling of diazonium ion with α-naphthol in acidic medium. The violet dye formed on addition of sufficient alkali [6] can be extracted into isoamyl alcohol (3-methyl-1-butanol). The dye shows maximum absorption at 535 nm, and the method provides excellent sensitivity.

Experimental

Apparatus. An ECIL Model GS 865 spectrophotometer and a Carl-Zeiss Spekol were used with 1-cm glass cells, for spectral measurements. An ECIL Model 821 pH meter was used to check pH.

Reagents. A 1×10^{-2} M stock solution of benzidine in aqueous 20% ethanol containing a few drops of concentrated hydrochloric acid was stored in an amber glass bottle. The stock solution, which was stable for 15 days, was diluted appropriately to give a solution containing 10 μg ml^{-1} benzidine. An aqueous 0.1% (w/v) stock solution of sodium nitrite was prepared in deaerated water. A 200 μg ml^{-1} solution of sodium nitrate was prepared by appropriate dilution. A 1×10^{-2} M solution of α-naphthol (recrystallized

0003-2670/83/$03.00 © 1983 Elsevier Science Publishers B.V.

from ethanol) was prepared in aqueous 20% ethanol.

All solutions were prepared from analytical-reagent grade chemicals, and twice-distilled water was used throughout.

Procedure. An aliquot (about 100 ml) of aqueous sample containing 5—25 μg of benzidine was mixed in a separatory funnel with 1 ml of diluted sodium nitrite solution and 5 ml of concentrated hydrochloric acid. After occasional shaking for 2 min, 1 ml of aqueous 3% (w/v) sulphamic acid solution was added to destroy the excess of nitrite, followed by 10 ml of the α-naphthol solution. After 2—3 min, the solution was made alkaline with 5 M sodium hydroxide, and the violet azo dye was extracted with two 5-ml portions of 3-methyl-1-butanol. The purple extract was dried over anhydrous sodium sulphate and the absorbance was measured at 535 nm against a reagent blank. The amount of benzidine was calculated from a calibration graph prepared from similar measurements.

Results and discussion

The absorption spectrum of the violet azo dye showed maximum absorption at 535 nm. The absorbance was stable for about 24 h and remained constant in the temperature range 20—40° C.

The effect of acidity on the diazotization reaction was studied; at least 0.2 M hydrochloric acid was necessary for complete diazotization and constant results were obtained over the range 0.2—5.0 M HCl. Diazotization was complete in 1 min but times up to 1 h did not affect the absorbance. The minimum time required for coupling with α-naphthol was 2 min; again, reaction times up to 1 h did not affect the final absorbance. The colour started to develop at pH 9 but full colour development was observed only above pH 11. At least a 1:1 mole ratio of benzidine and nitrite was needed for full colour development but the absorbance remained the same up to 1:10 mole ratios. Maximum absorbance was obtained at 1:50 to 1:100 molar ratios of benzidine and α-naphthol.

Beer's law, molar absorptivity, sensitivity and reproducibility. The colour system was found to obey Beer's law in the range 0—25 μg of benzidine per 100 ml of sample solution at 535 nm. The molar absorptivity and the Sandell sensitivity were $6.6 \pm 0.02 \times 10^4$ l mol^{-1} cm^{-1} and 0.0028 μg cm^{-2}, respectively. The reproducibility of the method was checked by replicate determinations

TABLE 1

Spectral characteristics of the dye in various solvents

Solvent	ϵ^a (10^4 l mol^{-1} cm^{-1})	Stability (h)	Solvent	ϵ^a (10^4 l mol^{-1} cm^{-1})	Stability (h)
Water	6.0	6	n-Hexanol	5.8	12
n-Butanol	5.5	24	n-Octanol	5.6	10
3-Methyl-1-butanol	6.6	24			

[a] At λ_{max} = 535 nm in all cases.

TABLE 2

Tolerance limits in the measurement of 0.1 μg ml^{-1} benzidine

Tolerance limit[a] (μg ml^{-1})	Substance
700	Toluene
500	Methanol, benzene
300	Phosphate
200	F^-, I^-, NO_3^-, SO_4^{2-}, Mn^{2+}, Ca^{2+}[b], Sr^{2+}[b]
150	Ba^{2+}[b], Pb^{2+}[b], Fe^{3+}[c], pyridine
100	Mg^{2+}[b], Co^{2+}, nitrobenzene, chlorobenzene, dichlorobenzene, *o*-, *m*-, *p*-nitrotoluene
80	Cr(VI)
50	Cu^{2+}, aminopyridine, diphenylamine
30	Aniline, *o*-nitroaniline, formaldehyde
25	Phenol
10	*p*-Nitronaphthylamine, 1-amino-2-naphthol
5	*m*-Nitroaniline

[a]The amount causing an error of $\leqslant 2\%$. [b]With 1 ml of 10% EDTA solution added. [c]With 1 ml of 10% sodium potassium tartrate added.

on a standard solution (0.2 μg ml^{-1}) of benzidine over a period of 7 days. The standard deviation and relative standard deviation of the absorbances were 0.0043 and 1.2%, respectively.

Extraction of the dye. Higher alcohols such as n-butanol, 3-methyl-1-butanol, n-hexanol and n-octanol were tested for the extraction. 3-Methyl-1-butanol was most satisfactory. Complete phase separation was not possible with benzene or chloroform, and the solution became turbid with n-propanol. Spectral characteristics of the dye in various solvents are given in Table 1.

Interferences. The effects of possible interferences commonly present in polluted waters were studied, and known amounts of substances commonly found in dye industry effluents were added to standard benzidine solutions. The tolerance limits are listed in Table 2. Some amines, which are also toxic, interfered with this method in high concentrations. They changed either the spectral characteristics or the molar absorptivity. *p*-Nitroaniline and toluidine caused positive interferences with a sharp change in the wavelength of maximum absorption.

The authors thank the Head of this Department for providing laboratory facilities.

REFERENCES

1 W. Leithe, The Analysis of Air Pollutants, Ann Arbor Science, Ann Arbor, MI, 1971.
2 F. A. Patty, Industrial Hygiene and Toxicology, Vol. 2, Interscience, New York, 1963.
3 G. Norwitz and P. N. Keliher, Anal. Chem., 53 (1981) 56, 1238.
4 Yun-Xiang Li, Huan Ching K'Oh-Such, 6 (1979) 29 (in Chinese); Chem. Abstr., 92 (1980) 185577j, p. 227.
5 J. T. Stewart, T. D. Shaw and A. B. Ray, Anal. Chem., 41 (1969) 360.
6 J. W. Daniel, Analyst, 86 (1961) 640.

Analytica Chimica Acta, 151 (1983) 265—269
Elsevier Science Publishers B.V., Amsterdam — Printed in The Netherlands

Short Communication

DETERMINATION OF CALCIUM, BARIUM AND STRONTIUM IONS BY DIFFERENTIAL PULSE STRIPPING VOLTAMMETRY AT A HANGING ELECTROLYTE DROP ELECTRODE

VLADIMÍR MAREČEK* and ZDENĚK SAMEC

J. Heyrovský Institute of Physical Chemistry and Electrochemistry, Czechoslovak Academy of Sciences, UTováren 254, 102 00 Prague 10 — Hostivař (Czechoslovakia)

(Received 2nd December 1982)

Summary. A hanging electrolyte drop electrode is used in the determination of $1—4 \times 10^{-6}$ M concentrations of calcium, barium and strontium ions by differential pulse stripping voltammetry. The method is based on the transfer of these ions from water to nitrobenzene facilitated by the complex formation with the macrocyclic polyether diamide, 7,19-dibenzyl-2,3-dimethyl-7,19-diazo-1,4,10,13,16-pentaoxacycloheneicosane-6,20-dione.

Recently, it has been demonstrated [1, 2] that electrolysis at the interface between two immiscible electrolyte solutions can be used for determination of the ions that participate in a simple ion-transfer reaction at the water (w)/oil (o) interface: $M^z(w) \rightleftharpoons M^z(o)$, where z is the charge on ion M. In order to avoid interference from charge-transfer reactions of the base electrolyte ions, the free energy of the transfer reaction in which the ion to be determined participates, should be close to zero. Thus, in the above simple ion transfer, mainly semi-hydrophobic ions can be determined, e.g., choline [3], acetylcholine [1, 3], tetramethylammonium [4] or tetraethylammonium [2] cations, and picrate [5, 6], octoate [6], dodecylsulfate [6] or perchlorate [6] anions.

The transfer of a strongly hydrophilic ion from water to an oil phase can be facilitated by the presence of a substance L in the oil phase which forms a complex ML at the interface and acts as an ionophore [7]: $M(w) + L(o) \rightleftharpoons ML(o)$. In this case, the negative value of the free energy of the complex formation compensates for the positive value of the free energy of ion transfer, so that the free energy of the total transference to the oil phase may be close to zero. Facilitated transfer of alkali metal cations across the water/nitrobenzene interface was observed in the presence of the valinomycin, nonactin and dibenzo-18-crown-6 [7—9]. Recently [10, 11], the similar effects of acyclic and cyclic ligands derived from 3,6-dioxaoctane—dicarboxylic acid on the transfer of proton, alkali and alkaline-earth metal cations were reported. The cyclic ligand, 7,19-dibenzyl-2,3-dimethyl-7,19-diazo-1,4,10,13,16-pentaoxacycloheneicosane-6,20-dione (I), exhibits the selectivity for calcium ions [12]. The stoichiometry of its complexes formed at the interface was found to be 1:1 or 1:2 for monovalent or divalent cations, respectively [11].

0003-2670/83/$03.00 © 1983 Elsevier Science Publishers B.V.

The present communication deals with the possibility of using differential pulse stripping voltammetry (d.p.s.v.) at a hanging nitrobenzene electrolyte drop electrode for the determination of calcium ion in the presence of ligand I.

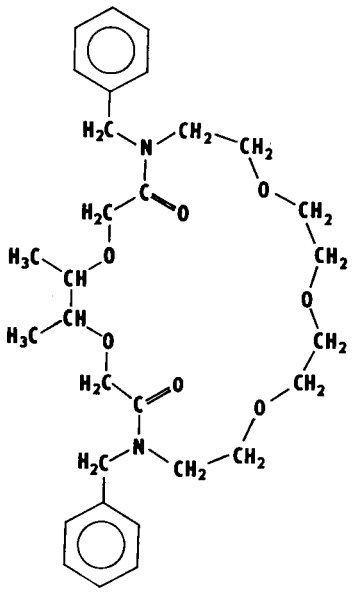

(I)

Experimental

The chemicals used were of analytical-reagent grade, except for tetrabutylammonium tetraphenylborate (TBATPB) which was prepared in this laboratory [2]. Nitrobenzene (analytical-reagent grade) and twice-distilled water were used for preparation of the base electrolyte solutions, 2.5 mM magnesium chloride in water and 5 mM TBATPB in nitrobenzene. The concentration of ligand I in the nitrobenzene phase was 1 mM. The ligand was generously donated by Dr. O. Ryba and Dr. J. Petránek, Institute of Macromolecular Chemistry, Prague.

The assembly for the hanging nitrobenzene electrolyte drop electrode (HEDE), the electronic circuit and the procedure were as described previously [1, 2]. A staircase voltage pulse (1 mV/20 ms) was applied to the HEDE at an initial potential E_i towards the potential of pre-electrolysis, E_e. During the time of pre-electrolysis (60 s), the aqueous test solution was stirred (1000 rpm). The ion which has been concentrated into the nitrobenzene drop, was stripped by application of potential pulses of 20-mV amplitude, superimposed on a potential ramp (cf. [2]). The sensitivity of the d.p.s.v. was increased by reducing the pulse duration and the time interval between pulses to 20 ms each. The current was sampled at the end of each time interval and the difference of the sampled currents was stored in the computer memory.

Potential E is the potential difference $\Delta_n^w\phi = \phi(w) - \phi(nb)$ between the aqueous and nitrobenzene phases related to the formal potential difference for the tetrabutylammonium cation, $\Delta_n^w\phi^\circ_{TBA^+}$ [2]: $E = \Delta_n^w\phi - \Delta_n^w\phi^\circ_{TBA^+}$.

Results and discussion

Figure 1A shows the d.p.s.v. curves of the calcium ion transfer. The initial potential E_i, at which the transfer of Ca^{2+} to the nitrobenzene phase is negligible, and the potential of pre-electrolysis E_e were 0.180 V and 0.380 V, respectively. The current signal is symmetric with a peak potential, E_p, of 0.262 V and a peak half-width, $\Delta E_{p/2}$, of about 80 mV. Strontium and barium ions exhibit similar behaviour (cf. Fig. 1B), the corresponding peak potentials being 0.315 V for both ions. In Fig. 2, peak heights are plotted against the concentrations of Ca^{2+}, Sr^{2+} or Ba^{2+} in the aqueous phase; linearity is good for micromolar concentrations of these ions.

The position of the peak in d.p.s.v. is controlled mainly by thermodynamic factors while the peak height depends on the transport and kinetic parameters of the ion-transfer reaction. For a reversible reaction [13, 14], $E_p = E^{rev}_{1/2} \pm (\Delta E/2)$, where $E^{rev}_{1/2}$ is the half-wave potential of the reversible polarographic wave and the pulse height ΔE is 20 mV; in the present case, the plus sign is applicable. When the concentration of the ligand in the oil phase c^o_L is consi-

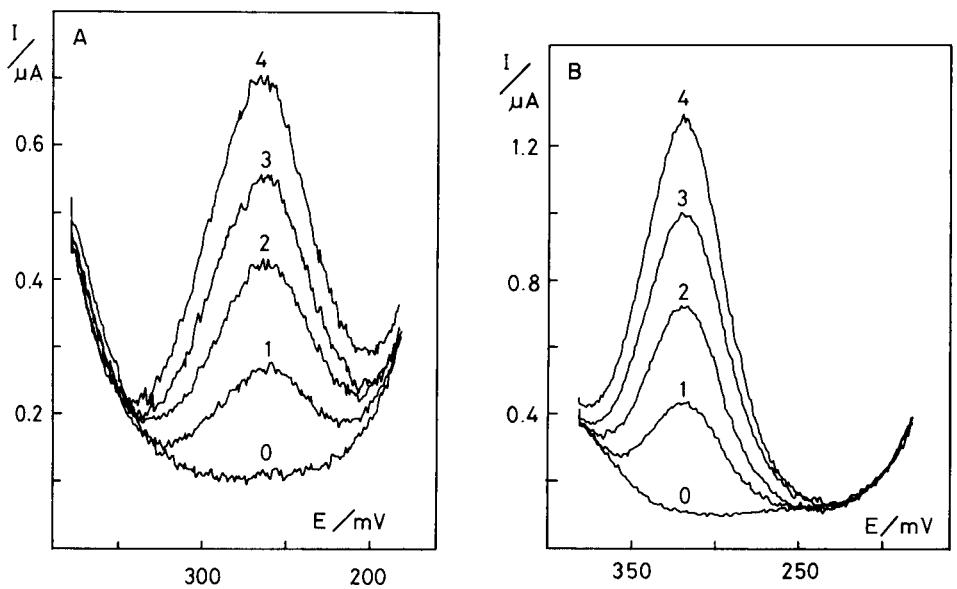

Fig. 1. Differential pulse stripping voltammograms of (A) calcium and (B) barium ion transfer at the HEDE. Concentrations (μM) of metal ion in the aqueous phase are indicated on the curves. Base electrolytes were 2.5 mM $MgCl_2$ in water and 5 mM TBATPB in nitrobenzene, with 1 mM ligand I in the nitrobenzene. The ohmic drop compensation was 6 kohm.

derably higher than that of the alkaline earth-metal cation M^{2+} in the aqueous phase, the reversible half-wave potential for the charge-transfer reaction

$$M^{2+}(w) + 2L(o) \rightleftharpoons ML_2^{2+}(o) \quad (1)$$

is given by [11]

$$E_{1/2}^{rev} = E_M^o + (RT/4F) \ln[D_M(w)/D_{ML}(o)] - (RT/2F) \ln K(o) [c_L^o]^2 \quad (2)$$

where E_M^o is the formal potential of the ion-transfer reaction at the interface, D indicates the diffusion coefficient of M^{2+} and ML^{2+} in the aqueous and oil phase, respectively, and $K(o)$ is the stability constant of the complex ML_2^{2+} in the oil phase.

Table 1 summarizes the thermodynamic parameters of the transfer reactions $M^z(w) \rightleftharpoons M^z(o)$ and $M^{2+}(w) + 2L(o) \rightleftharpoons ML_2^{2+}(o)$ for the alkaline earth-metal ions at the water/nitrobenzene interface and the apparent rate constants, k_i^o of the facilitated ion transfer. The reversible half-wave potentials were evaluated from Eqn. (2) for $c_L^o = 1$ mM, $D_{ML}(o) \simeq D_L(o) = 1.5 \times 10^{-10}$ m^2 s^{-1} and $D_M(w) \simeq D_{Ca}(w) = 1.2 \times 10^{-9}$ m^2 s^{-1} [11]. There is fairly good agreement between these values and those inferred from the peak potentials and pulse height (0.252, 0.305 and 0.305 V for Ca^{2+}, Sr^{2+} and Ba^{2+}, respectively). Obviously, the peak heights and half-widths reflect the difference in the apparent rate constant of reaction (1). In fact, I_p decreases in the sequence $Ba^{2+} > Sr^{2+} > Ca^{2+}$ (cf. Fig. 2), while $\Delta E_{p/2}$ increases in the same sequence

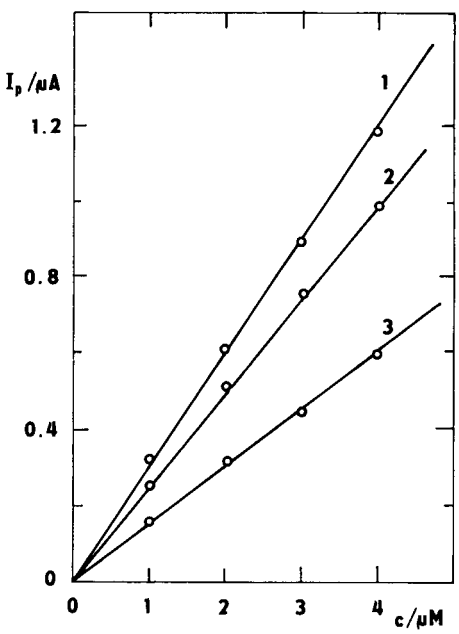

Fig. 2. Plots of the peak heights for (1) Ba^{2+}, (2) Sr^{2+} and (3) Ca^{2+} vs. their concentration in the aqueous phase.

TABLE 1

Standard Gibbs energies of transfer from water to nitrobenzene $\Delta G^{o,w\rightarrow nb}_{tr,X}$, the corresponding formal potentials E^o_M for the alkaline earth-metal ions and the stability constants K of their 1:2 complexes with ligand I in nitrobenzene, and the reversible half-wave potentials $E^{rev}_{1/2}$ and apparent rate constants k^o of the facilitated alkaline earth-metal ion transfer [11]

Ion	$\Delta G^{o,w\rightarrow nb}_{tr,X}$ (eV)[a]	E^o_M (V)[b]	$E^{rev}_{1/2}$(V)[c]	$log\ K$[d]	k^o_{ML}/k^o_{CaL}
Mg^{2+}	0.722	0.609	0.446	12.0	3.2
Ca^{2+}	0.698	0.597	0.247	18.3	1
Sr^{2+}	0.684	0.590	0.281	16.9	4.8
Ba^{2+}	0.640	0.568	0.298	15.6	25

[a]From extraction data [15], cf. [11]. [b]Relative to the formal potential of the tetrabutylammonium cation, $\Delta^w_n\phi^o_{TBA^+}$ = 0.248 V [16]. [c]c^o_L = 1 mol m^{-3}. [d]Stability constant K expressed in M^{-2}.

from $\Delta E_{p/2} \approx 55$ mV for barium ion (cf. Fig. 1B), through 70 mV for strontium ion to about 80 mV for calcium ion. The peak half-width for barium is close to the value required for a reversible charge transfer, 45.2 mV [13, 14].

At present, the analysis of samples containing alkali and alkaline earth-metal cations can be done most easily by means of ion-selective electrodes [17]. Electrolysis at the interface between immiscible electrolytes offers an alternative approach. Based on the present results, the determination of calcium ion is possible in the presence of a large amount of magnesium (about 1:2500), but other alkaline earth-metal ions and alkali metal ions may interfere. Extension of the method is under investigation.

REFERENCES

1 V. Mareček and Z. Samec, Anal. Lett., 14 (1981) 1241.
2 V. Mareček and Z. Samec, Anal. Chim. Acta, 141 (1982) 65.
3 P. Vanýsek and M. Behrendt, J. Electroanal. Chem., 130 (1981) 287.
4 Z. Samec, V. Mareček, J. Weber and D. Homolka, J. Electroanal. Chem., 99 (1979) 385.
5 D. Homolka and V. Mareček, J. Electroanal. Chem., 112 (1980) 91.
6 P. Vanýsek, J. Electroanal. Chem., 121 (1981) 149.
7 D. Homolka, L. Quoc Hung, A. Hofmanová, M. W. Khalil, J. Koryta, V. Mareček, Z. Samec, S. K. Sen, P. Vanýsek, J. Weber, M. Březina, M. Janda and I. Stibor, Anal. Chem., 52 (1980) 1606.
8 A. Hofmanovà, L. Quoc Hung and M. W. Khalil, J. Electroanal. Chem., 135 (1982) 257.
9 J. Koryta, Electrochim. Acta, 24 (1979) 293.
10 D. Homolka, V. Mareček, Z. Samec, O. Ryba and J. Petránek, J. Electroanal. Chem., 125 (1981) 243.
11 Z. Samec, D. Homolka and V. Mareček, J. Electroanal. Chem., 135 (1982) 265.
12 J. Petránek and O. Ryba, Anal. Chim. Acta, 128 (1981) 129.
13 R. L. Birke, Anal. Chem., 50 (1978) 1489.
14 I. Ružič, J. Electroanal. Chem., 75 (1977) 25.
15 M. Pivoňková and M. Kyrš, J. Inorg. Nucl. Chem., 31 (1969) 175.
16 J. Koryta, P. Vanýsek and M. Březina, J. Electroanal. Chem., 75 (1977) 211.
17 See, e.g., J. Koryta, Anal. Chim. Acta, 61 (1972) 329; 91 (1977) 1; 111 (1979) 1; 139 (1982) 1.

Analytica Chimica Acta, 151 (1983) 271—274
Elsevier Science Publishers B.V., Amsterdam — Printed in The Netherlands

Short Communication

DETERMINATION OF THE AQUEOUS SOLUBILITY OF 4-CHLOROBIPHENYL

THOMAS R. STOLZENBURG* and ANDERS W. ANDREN
Water Chemistry Program, University of Wisconsin, Madison, WI 53706 (U.S.A.)

(Received 30th November 1982)

Summary. The generator-column technique for quantifying aqueous solubilities of hydrophobic substances by liquid chromatography was modified by using a detachable extractor column. This modification allowed the collection of halogenated solutes such as polychlorinated biphenyls and their detection by electron-capture gas chromatography. The technique was evaluated with 4-chlorobiphenyl. Determined aqueous concentrations depend on flow rate through the generator column below 0.4 g min^{-1}. Aqueous solubility was determined at four temperatures in the flow-rate-independent region. At 298 K the solubility of 4-chlorobiphenyl in water is 1.41×10^{-7} mole fraction.

The importance of solubility data for environmental studies is to provide fundamental information necessary to make predictions of transport pathways in aqueous systems. Water solubility is the key chemical property affecting the partitioning of a chemical to any other phase in contact with water. By itself, aqueous solubility has been used to predict bio-accumulation [1—5]. Together with vapor pressures and adsorption coefficients, water solubilities are essential parameters for whole-system models of solid/solution and solution/air transport.

The determination of aqueous solubilities in subnanomolar regions is difficult. Traditional batch techniques, wherein excess of solute is dissolved in an aliquot of water, suffer from several limitations. Detection limits become a problem for slightly soluble organics. If large quantities of water are used to compensate for low solute concentrations, the prospect of losses from the aqueous phase during any transfer and concentration steps is likely. Wall adsorption usually occurs. Finally, operational constraints in the separation of truly dissolved from suspended solid solute must be considered in a stirred system. Equilibration times of solid solutes with water can be in the order of days or longer in unstirred solutions.

May et al. [6] introduced a convenient method for determining aqueous solubilities of several polynuclear aromatic hydrocarbons (PAHs). The method eliminates several limitations inherent in batch techniques and offers hope for accurately determining aqueous solubilities for a variety of slightly soluble, nonionizable compounds. Because detection problems for a variety of compounds still exist, the method was modified so that halogenated compounds sensitive to electron capture detection by gas chromatography could

0003-2670/83/$03.00 © 1983 Elsevier Science Publishers B.V.

be measured. Briefly, the technique allows one to saturate water very quickly by passing it through a temperature-controlled generator column packed with inert material of small diameter coated with the compound of interest. In this study, the modified method was tested by using different generator column flow rates and temperatures. 4-Chlorobiphenyl was used as the test compound.

Experimental

The water used in this study was high-performance liquid chromatographic grade (Baker, Phillipsburg, NJ). Commercial-grade hexane was purified by passage through a column of sodium sulfate and activated alumina gel. The 4-chlorobiphenyl was 99% pure (Analabs, North Haven, CT).

The equipment consisted of a water reservoir attached to the generator column, with the effluent going either to waste or to an extractor column. The stainless steel generator column (15 cm long, 2.1 mm i.d.) was packed with either 60—80 mesh glass beads or sand. The packing was held in place by 2-μm pore size stainless steel frits set in fluorocarbon rings (Alltech Assoc., Deerfield, IL). A mass of compound equivalent to 0.1—1.8% of the mass of packing was dissolved in dichloromethane. The solution was added to the packing material in a beaker and the solvent was driven off by nitrogen. Several columns were tested with a variety of percentage coatings in the described range on both sand and glass beads. No measurable trends in the generated aqueous concentration were observed.

The generator column was thermostated to $\pm 0.1^{\circ}C$ in a water jacket connected to a constant-temperature water circulator (Model 90T, Polyscience, Niles, IL). Approximately 6 g of water was pushed through the system for each determination. Flow was controlled by a gas regulator attached to pressurized nitrogen (<50 psi) which forced water from a glass reservoir. The generator column remained in-line between test runs so that pre-equilibration with water was unnecessary. As a precaution, however, approximately 10 ml of water was pumped through to waste at the test flow rate before each run.

The extractor column used in this study was a Sep-Pak C_{18} cartridge (Millipore, Bedford, MA). To quantify the amount of water extracted during each test, a vial was attached to the outlet of the extractor column and weighed before and after. Following a test run, the Sep-Pak was dried by passing nitrogen through it for 30 min. Then the compound was eluted with three 1-ml aliquots of hexane delivered with a syringe. The hexane solution was injected directly into the gas chromatograph for quantification by standard curve. It was found that no additional 4-chlorobiphenyl was eluted by using more than 3 ml of hexane.

Results and discussion

Aqueous concentrations of 4-chlorobiphenyl at 25°C were measured at generator column flow rates ranging from 0.024 to 1.32 g min^{-1}. Figure 1 shows a steep dependence of aqueous concentrations on flow rates below

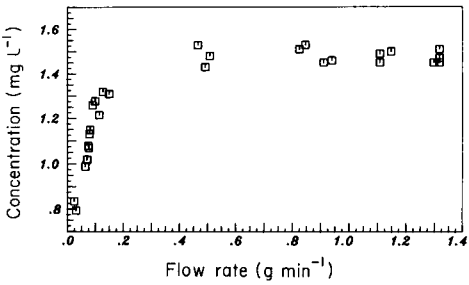

Fig. 1. Concentration of 4-chlorobiphenyl vs. flow rate at 25°C.

about 0.4 g min^{-1}. For the 14 data points above 0.4 g min^{-1}, the best-fit regression line was calculated giving a slope of −17.1 ± 60 at the 95% confidence level. A slope of zero falls well within the 95% confidence limits of the slope. Hence, the 0.4—1.3 g min^{-1} region is independent of flow rate. The effect of flow above 1.3 g min^{-1} was not studied. These results and subsequent experience showed that it is necessary to check the dependence of concentration on flow rate for any particular set of column dimensions or packing configuration. The mechanism causing depressed aqueous concentrations with lower flow rates will be studied further.

Orientation with respect to flow may be important for short, straight columns. Manually packed columns may exhibit channeling through loosened packing if the flow is from bottom to top. Generator column path length for some of the water under these conditions may be too short for solution equilibration to occur. Results are irreproducible. Longer coiled columns are not expected to be as sensitive to orientation.

The solubility of 4-chlorobiphenyl was measured in the region of flow-rate independence. At 25°C, a value of 1.41 (±0.03) × 10^{-7} mol fraction was measured. Reported values by the batch technique range from 0.86 × 10^{-7} [7] to 1.11 × 10^{-7} mol fraction [8, 9]. A predicted value of 1.78 × 10^{-7} mol fraction [10] has been reported from a regression analysis of all reported polychlorinated biphenyl congener solubilities against molecular surface area and melting points.

TABLE 1

Aqueous solubilities of 4-chlorobiphenyl at four temperatures

Temperature (°C)	Solubility (10^{-7} mol fraction ± s)[a]	Number of determinations
4.0 (±0.1)	0.631 (±0.027)	17
20.0 (±0.1)	1.15 (±0.05)	11
25.0 (±0.1)	1.41 (±0.03)	14
32.0 (±0.01)	2.03 (±0.05)	12

[a] s = standard deviation.

Solubility measurements were also conducted at 4, 20 and 32°C. Table 1 lists the aqueous solubilities and standard deviations for 4-chlorobiphenyl. Solubility increases with temperature as expected.

The technique described above is presently being used with higher chlorinated biphenyl congeners. Other improvements are being explored. Because the cost of pure compound may be prohibitive, low-volume generator columns are desirable. Other packing materials may prove to be more suitable than glass beads. For instance, Chromosorb W binds the compound more efficiently, possibly eliminating the need for column frits to prevent sloughing off of solid material.

This work was funded by the University of Wisconsin Sea Grant College Program under grants from the Office of Sea Grant, National Oceanic and Atmospheric Administration, U.S. Department of Commerce, and from the state of Wisconsin (Federal Grant NA800-AA-D-00086, Project R/MW-21).

REFERENCES

1 R. L. Metcalf, J. R. Sanborn, P.-Y. Lu and D. Nye, Arch. Environ. Contam. Toxicol., 3 (1975) 151.
2 C. T. Chiou, V. H. Freed, D. W. Schmedding and R. L. Kohnert, Environ. Sci. Technol., 11 (1977) 475.
3 W. Ernst, Chemosphere, 11 (1977) 731.
4 E. E. Kenaga, Environ. Sci. Technol., 14 (1980) 552.
5 C. T. Chiou, D. W. Schmedding and M. Manes, Environ. Sci. Technol., 16 (1982) 4.
6 W. E. May, S. P. Wasik and D. H. Freeman, Anal. Chem., 50 (1978) 175.
7 O. Hutziner, S. Safe and V. Zitko, The Chemistry of PCBs, CRC Press, Cleveland, OH, 1974, p. 269.
8 P. R. Wallnofer, M. Koniger and O. Hutzinger, Analab Res. Notes, 13 (1973) 14.
9 L. Weil, G. Dure and K. E. Quentin, Z. Wasser Abwasser Forsch., 7 (1974) 169.
10 D. Mackay, R. Mascarenhas, W. Y. Shiu, S. C. Valvani and S. H. Yalkowsky, Chemosphere, 9 (1980) 257.

Analytica Chimica Acta, 151 (1983) 275—277
Elsevier Science Publishers B.V., Amsterdam — Printed in The Netherlands

Announcement

WORKING PARTY ON ANALYTICAL CHEMISTRY (WPAC), FEDERATION OF EUROPEAN CHEMICAL SOCIETIES (FECS)

EUROPEAN ANALYTICAL COLUMN 6

In January 1983 the WPAC consisted of 27 national chemical societies of 22 European countries represented by 24 delegates. Among the FECS member societies, only the PanCyprian Union of Chemistry and the Turkish Chemical Society are not represented in the WPAC. Egypt, Israel and IUPAC are observers.

The 13th meeting of the WPAC was held in München, April 26, 1982, on the occasion of "Biochemische Analytik—Analytika". At this meeting the following items were discussed.

Euroanalysis IV, 1981, Helsinki

The proceedings of this European Conference on Analytical Chemistry including the plenary and keynote lectures are now available in the series Review on Analytical Chemistry (Series editors: H. Malissa, Vienna, and W. Fresenius, Taunusstein). The 250-page volume is edited by L. Niinistö and is available from the publishers (Akademiai Kiado, Budapest and Association of Finnish Chemical Societies, Helsinki 26, Finland). The former publishers are taking care of distribution in communist countries only.

Euroanalysis V, August 26—31, 1984, Cracow, Poland

After the successful meetings in Heidelberg (1972), Budapest (1975), Dublin (1978) and Helsinki (1981), the next event in this well-established series of European broad-spectrum conferences will take place at the Jagellonian University and the Technical University of Cracow. There will be two special sessions: Computer-Based Analytical Chemistry (COBAC III) and Speciation in Trace and Environmental Chemistry. The main programme will include 4 plenary and 12 keynote lectures besides the presentation of discussion papers and posters. The conference president is Prof. Dr. A. Hulanicki, Institute of Fundamental Problems in Chemistry, University of Warszawa, Pasteura 1, PL-02093 Warszawa, and the conference secretary is Prof. Dr. Z. Kowalski, Academy of Mining and Metallurgy, Institute of Materials Science, Al. Mickiewicza 30, PL-30059 Cracow.

Euroanalysis VI, 1987, Paris (France)

Prof. Dr. E. Roth has been nominated as chairman of this conference.

Rules for the organization of Euroanalysis Conferences

The 13th General Assembly of the FECS (June 17/18, 1982, Rome) agreed to the following wording as proposed by the WPAC at its 13th meeting.

(1) The Euroanalysis conferences shall be broad-spectrum conferences with preference given to European speakers as invited lecturers. No person shall be offered a plenary or keynote lectureship at two successive Euroanalysis conferences.

(2) The venue for the next but one Euroanalysis conference shall be decided at the WPAC meeting held during a Euroanalysis conference, i.e. six years ahead. Venues should be rotated between all European countries. In voting, each country may cast only one vote (Directive IX(i)).

(3) The Chairman or Secretary shall, in writing, invite member Societies to tender for the Euroanalysis conference at least 9 months ahead of the WPAC election meeting, informing the Societies of the conditions attached to the conference. A copy of the letter of invitation shall be sent to all delegates of WPAC for information.

(4) The praesidium of Euroanalysis conferences shall consist of the Chairman of WPAC, a representative of the previous organizing group, a representative of the next group and a representative of the host country, who shall be chairman.

(5) The plenary and keynote lectures should be published as soon as possible after the Euroanalysis conference (title: Euroanalysis: Review on Analytical Chemistry). This responsibility should be undertaken by the Chairman of the organizing committee in conjunction with an editor appointed by the Praesidium. This volume should be available throughout the member countries at reasonable cost.

(6) It shall be a condition for the organizing of a Euroanalysis conference that every interested scientist shall be able to attend without hindrance. The organizing country shall accept to provide the necessary entry/exit documents for all Euroanalysis delegates without undue delay.

Other meetings

Scientific Session on Electrochemical Detection in Flow Analysis, October 17—20, 1982, Matrafüred (55th event of FECS). There were 60 participants, 4 plenary and 5 keynote lectures, 19 discussion papers. For further details, contact the conference chairman, Prof. Dr. E. Pungor, Institute for General and Analytical Chemistry, Technical University Budapest, Gellért-tér 4, H-1502 Budapest XI.

Scientific Symposium on Pattern Recognition in Analytical Chemistry (56th event of FECS). There were 50 participants and 13 lectures. Discussions emphasised the possibilities and limitations of the practical applicability of pattern recognition (for details, contact Prof. Dr. E. Pungor).

Symposium series on Computer-based Analytical Chemistry. COBAC II, April 28—29, 1982, München, and COBAC III, August 1984, Cracow. It was felt that because of the success of COBAC II (see H. Malissa, Fresenius Z. Anal. Chem., 313 (1982) 449), this conference series should be continued as a special session during Euroanalysis V (COBAC III) The chairman will be Prof. Z. Hippe, Department of Physical Chemistry, I. Lukasiewicz Technical University, PL-35959 Rzeszow. Scientists interested in this rapidly expanding branch of analytical chemistry are welcome to contribute to this event.

Pending FECS sponsorship for WPAC activities. 4th Symposium on Ion Selective Electrodes, October 15—17, 1984, Matrafüred, and Regional Student Competitions in Analytical Chemistry, 1983, Budapest. The latter will comprise Mini-olympic Games on a regional basis with expected participants from Austria, Bulgaria, Czechoslovakia, Hungary, Italy, Rumania, Yugoslavia, etc., in the tradition of the successful student competitions formerly organized by Prof. V. Vajgand in Belgrade.

Education in Analytical Chemistry

As required by a decision of WPAC at its 13th meeting, a standardized questionnaire for the evaluation of the situation in the field of education in analytical chemistry was prepared and distributed to all major European Universities. More than 100 responses have been received so far from 15 European countries and form the basis for the first statistical evaluation in this field in Europe. Interested colleagues are kindly requested to contact the secretary of WPAC (address below).

Standard Reference Materials (SRM)

Work is proceeding towards the establishment of a system for the preparation and use of reference materials in cooperation with European specialists in the field.

Next (14th) meeting of the WPAC

The Royal Netherlands Chemical Society has invited WPAC to hold the 14th meeting in Amsterdam in connection with the 9th ISM '83 on August 28, 1983.

PROF. DR. ROBERT KELLNER (Secretary of WPAC)
Institut für Analytische Chemie,
Technische Universität Wien,
A-1060 Wien, Getreidemarkt 9,
Austria

Analytica Chimica Acta, 151 (1983) 279
Elsevier Science Publishers B.V., Amsterdam — Printed in The Netherlands

Errata

S. Angelova and H. W. Holy, Optimal Speed as a Function of System Performance for Continuous Flow Analyzers.

Anal. Chim. Acta, 145 (1983) 51—58.

On p.53 of this paper, lines 15, 17 and 18, and in the legend to Figure 1, please note that

$2t_s + t_w$ should read $t_s + t_w$. corrected A.H. 26/11/30

Saswati P. Bag and H. Freiser, Liquid Distribution in the Copper(II)-7-(1-vinyl-3,3,6,6-tetramethylhexyl)-8-Quinolinol System.

Anal. Chim. Acta, 135 (1982) 319—325.

Various errors occurred in this paper. The title should read:
Distribution in the Copper(II)-7-(1-vinyl-3,3,5,5-tetramethylhexyl)-8-Quinolinol System.

Other errors are as follows:

Page	Line	Error	Correction
320	31	7-(1-vinyl-3,3,6,6-tetra...	7-(1-vinyl-3,3,5,5-tetra...
322	6	$(\epsilon_{HL}T_L - A)(A - \epsilon_L T_L)$	$(\epsilon_{HL}T_L - A)/(A - \epsilon_L T_L)$
324	2	$10^{22.9} \times 10^{-9.9}$	$10^{22.9} \times (10^{-9.9})^2$
324	3	$10^{13.0}$	$10^{13.1}$
324	4	13.4	23.9
324	6	$10^{9.5}$	$10^{9.0}$
324	12	9.5	9.0

Corrected A.H. 26/11/30

Vol. 151, No. 1

ACA announcements

ANNOUNCEMENTS OF MEETINGS

FACSS X – THE FEDERATION OF ANALYTICAL CHEMISTRY AND SPECTROSCOPY SOCIETIES 10th ANNUAL MEETING, PHILADELPHIA, PA, U.S.A., SEPTEMBER 25–30, 1983

In 1983, the FACSS meeting will be celebrating its 10th anniversary. Over the past decade, FACSS has consistently been a forum for the presentation of research results of the highest quality. At the 1983 meeting, papers will be presented in the following categories: atomic spectroscopy, infrared and Raman spectroscopy, n.m.r. spectroscopy, mass spectroscopy, chromatography (gas, liquid, ion, etc.), electrochemistry, thermal analysis, particle/surface analysis, data processing/computerization/laboratory automation, biological/clinical/forensic analysis, environmental analysis, and new analytical techniques. Within these categories, symposia on special topics are also being prepared.

Workshops and short courses. As in previous years, workshops and short courses will be offered prior to, during, and after the conference. Details of these will be available soon.

Equipment exhibits. Centrally located at the meeting will be an exhibition of scientific equipment and services. This exhibition can afford an excellent opportunity for suppliers and users of scientific equipment to meet and discuss mutual interests. For exhibit information contact: Peter Keliher, Exhibits Director, P.O. Box 96, Collegeville, PA 19426, U.S.A.

Preliminary programme. If you wish to receive a copy of the preliminary program please write to: FACSS X Program Chairman, John O. Lephardt, Philip Morris Research Center, P.O. Box 26583, Richmond, VA 23216, U.S.A.

WORKSHOP ON LOW DISPERSION LIQUID CHROMATOGRAPHY, AMSTERDAM, THE NETHERLANDS, JANUARY 19–20, 1984

"Microbore", "miniature" and "high speed" are words that are appearing more and more frequently in references to high-performance liquid chromatography. The trend that they reflect is a reduction in volume of all the components in a chromatographic system. The critical implication is that the dispersive contributions of all instrument factors external to the column have to be kept to a minimum. Therefore these techniques are grouped under the name: low dispersion liquid chromatography (LDLC). There are obvious benefits to be gained by applying LDLC: savings in stationary phase and solvent, reduced analysis time, improved absolute detection limit, enhanced separation efficiency, easier compatibility with hyphenated systems, etc.

The forthcoming LDLC workshop will address this topic in detail, with special emphasis on miniaturized columns and particle dimensions, high speed separations, systems for the generation of low flows, small volume injectors, miniaturization of system elements, detectors with small detection volumes and fast response and measurements of dispersion effects.

The workshop will be held at the Free University in Amsterdam. The workshop language will be English (no simultaneous translation will be offered). The proceedings will be published by Elsevier Science Publishers B.V. as a special issue of the *Journal of Chromatography*, after the usual refereeing procedure. Besides regular lectures, instrument demonstrations and applications will be offered and discussed. A short course on "Low Dispersion LC" will be held at the Free University on January 17 and 18. The deadline for registration is December 15, 1983.

Further information may be obtained from: LDLC Workshop Office, Dept. of Analytical Chemistry, Free University, De Boelelaan 1083, 1081 HV Amsterdam, The Netherlands.

BIOCHEMISCHE ANALYTIK 84 – INTERNATIONAL CONFERENCE ON BIOCHEMICAL AND INSTRUMENTAL ANALYSIS, MUNICH, G.F.R., APRIL 10–13, 1984

The 9th Conference on Biochemical Analysis will be held in 1984 at the Münchener Messegelände. The breadth of the scientific themes will be considered in 16 half-day symposia. The themes selected by the Scientific Committee may be supplemented by poster demonstrations. Besides the provision of information during the course of the scientific programme, more time than is usual will be allowed for discussion in individual scientific meetings. The conference will be broadened in the direction of the technical development and field of application by the "Analytica Forum München", at which novelties of industrial development by the technical exhibition will be presented.

Further information may be obtained from: Dr. Rosmarie Vogel, General Secretary, Abteilung für Klinische Chemie und Klinische Biochemie in der Chirurgischen Klinik Innenstadt der Universität München, Nussbaumstrasse 20, D-8000 München 2, G.F.R. Tel: (089) 15 30 32; telex 5 216 018 bird d.

ANALYTICAL CHEMISTRY IN DEVELOPMENT, COLOMBO, SRI LANKA, AUGUST 21–24, 1984

The above conference is being organized as a result of the increased interest and importance of analytical chemistry in resolving problems in areas such as agriculture, mineral and natural resources, environment, medicine, raw materials, etc. It is hoped that the conference will promote more interaction between chemists in developed and developing countries. Details can be obtained from either the Centre for Analytical Research and Development, Department of Chemistry, University of Colombo, Sri Lanka; or, the Trace Analysis Research Centre, Chemistry Department, Dalhousie University, Halifax, N.S. B3H 4J1, Canada.

THIRD WORKSHOP ON LC–MS AND MS–MS, MONTREUX, SWITZERLAND, OCTOBER 24–26, 1984

The above-mentioned workshop is being organized by the International Association of Environmental Analytical Chemistry and sponsored by instrumental companies and national bodies and will include an exhibition.

The topics will include technical developments in LC–MS and MS–MS with on-line and off-line aspects and applications of these techniques in environmental analysis, clinical analysis and other areas. Subtopics will be introduced by plenary lectures, followed by brief research presentations and posters, and by panel discussions on the state-of-the-art of LC–MS and MS–MS. The proceedings will be published in a special issue of the *Journal of Chromatography*.

For further information on attendance and submission of papers contact: Professor Dr. R.W. Frei, Department of Analytical Chemistry, Free University, De Boelelaan 1083, 1081 HV Amsterdam, The Netherlands.

© Elsevier Science Publishers B.V., 1983

0003-2670/83/$03.

All rights reserved. No part of this publication may be reproduced, stored in a retrieval system or transmitted in any fo or by any means, electronic, mechanical, photocopying, recording or otherwise, without the prior written permission the publisher, Elsevier Science Publishers B.V., P.O. Box 330, 1000 AH Amsterdam, The Netherlands.
Submission of an article for publication implies the transfer of the copyright from the author(s) to the publisher a entails the author(s) irrevocable and exclusive authorization of the publisher to collect any sums or considerations copying or reproduction payable by third parties (as mentioned in article 17 paragraph 2 of the Dutch Copyright Act 1912 and in the Royal Decree of June 20, 1974 (S. 351) pursuant to article 16b of the Dutch Copyright Act of 191 and/or to act in or out of Court in connection therewith.
Special regulations for readers in the U.S.A. — This journal has been registered with the Copyright Clearance Cent Inc. Consent is given for copying of articles for personal or internal use, or for the personal use of specific clients. This consent is given on the condition that the copier pay through the Center the per-copy fee stated in the code the first page of each article for copying beyond that permitted by Sections 107 or 108 of the U.S. Copyright Law. T appropriate fee should be forwarded with a copy of the first page of the article to the Copyright Clearance Center, In 21 Congress Street, Salem, MA 01970, U.S.A. If no code apears in an article, the author has not given broad cons to copy and permission to copy must be obtained directly from the author. All articles published prior to 1980 may copied for a per-copy fee of US $2.25, also payable through the Center. This consent does not extend to other kinds copying, such as for general distribution, resale, advertising and promotion purposes, or for creating new collecti works. Special written permission must be obtained from the publisher for such copying.
Special regulations for authors in the U.S.A. — Upon acceptance of an article by the journal, the author(s) will asked to transfer copyright of the article to the publisher. This transfer will ensure the widest possible dissemination information under the U.S. Copyright Law.

Printed in The Netherlands.

ıtinued from outside back cover)

CONTENTS

(Abstracted, Indexed in: Anal. Abstr.; Biol. Abstr.; Chem. Abstr.; Curr. Contents Phys. Chem. Earth Sci.; Life Sci.; Index Med.; Mass Spectrom. Bull.; Sci Citation Index; Excerpta Med.)

(Continued on inside back c